De Montfort University- Leicester

Faculty of Health and Life Sciences

SIMULTANEOUS REMOVAL OF ALKYLPHENOLS AND OILS IN SIMULATED PRODUCED WATER BY UV/MW/FENTON-LIKE PROCESS USING A NOVEL SURFACE FUNCTIONALISED HETEROGENEOUS PAN CATALYST

A thesis submitted for the degree of Doctor of Philosophy (Ph.D.) in Environmental Technology

Emmanuel Ushie Ushie

Supervisor

Prof. Katherine Huddersman

April 2018

Dedication

This thesis is dedicated to my best friend, Stella E. Ushie for the love, support, patience and understanding especially during the course of this research.

Abstract

Owing to post treatment challenges of managing $Fe(OH)_3$ sludge associated with classical Fenton catalysis, this research applies a heterogeneous Fenton-like catalysis for the treatment of produced water from oil mining. The catalyst is a surface functionalized fibrous heterogeneous polyacrylonitrile (PAN) catalyst developed at De Montfort University. This catalyst has been used in the decontamination of simulated produced water (PW) for the oxidative degradation of alkylphenols and oils. In addition to being endocrinal disruptors, alkylphenols (AP) constitute the most toxic component of PW. They are primarily of petroleum origin and are thought to partition into the water phase during petroleum mining. Out of about 116 million m^3 of PW discharged into the Norwegian sector of the North Sea, APs account for 323 tons of which 90% are C1 to C3 short chain alkylphenols (SCAPs). These SCAPs are amongst the most stable constituents of PW and are responsible for PW toxicity. Batch and continuous flow experiments using the PAN catalyst in a hydrogen peroxide system, PAN catalyst assisted by ultraviolet (UV) radiation, PAN catalyst assisted by microwave (MW) and PAN catalyst assisted by both UV and MW in a Fenton-like system was used for the oxidative decomposition of synthetic PW. Parameters monitored were; loss of 3,5-dimethyl phenol (DMP) which is a model alkylated phenolic compound, COD removal, and oil-in-water removal. A catalytic oxidative reaction of 200 mL simulated PW was carried out in batch mode, while 900 mL was used in a rotating disc flow reactor for the continuous flow experiments, where the influence of initial H_2O_2 concentration, catalyst concentration, bubbling air flow rate, variation in UV flux density, effect of competing inorganic anions, etc. were investigated. Results for the unassisted Fenton-like catalysis of PW in batch

mode at optimum conditions showed 94% AP removal and up to 30% COD removal after 4 h, while oil- in- water concentration was reduced by 85.8%, although 50.3% of the lost oil was absorbed onto the catalyst. The UV- assisted catalytic oxidation (irradiance of 2.66 mW/cm^2) resulted in > 99% AP degradation after 40 min, and 59% COD removal after 4 h, while the oil- in- water concentration was reduced down to non-detectable levels, with 8.78 mg/L oil (which constitutes 5.67% of initial concentration) adsorbed on the catalyst. The results of the unassisted Fenton-like continuous flow experiments at optimum conditions showed ~ 10% COD removal, ~ 90% average DMP degradation, and about 50% average OIW removal in 4 h retention time. The UV/MW/Fenton-like assisted continuous flow process at optimum experimental conditions, recorded an average of 31% COD removal, >99% OIW removal and >99% DMP degradation. Thus, assisting the reaction with UV/MW resulted in a more extensive as well as a quicker decontamination of produced water. Intermediate oxidation products tentatively determined from the catalytic oxidation of DMP include benzoquinones, hydroquinones, benzaldehydes, formic and acetic acids. The cause of catalyst deactivation after about 30 days of reaction was suspected to be due to loss of Fe through leaching and catalyst poisoning. The reaction is thought to be 87% heterogeneous route (including adsorbed component), as leached Fe contributed about 13% to the loss of DMP through a homogeneous route.

List of Conference Papers

This research has informed a paper presented in a conference;

- Recent Advances on the Treatment of Produced Water from Oil Mining Using UV- Assisted Heterogeneous Fenton-Like Catalysis. Proceedings of IChemE catalysis and reaction engineering symposium. Sheffield University, England United Kingdom. May 31st 2017.

Acknowledgement

I offer my sincere appreciation to my supervisor, Professor Katherine Huddersman, for her painstaking supervision and guidance throughout the course of this program. This research would never have been possible without her astute support and encouragement.

I am grateful to the government of Nigeria for providing funding for this research through the award of the Niger Delta Development Commission (NDDC) scholarship.

I could never repay the debt of gratitude owed my family. Stella, Claire and Junior, thank you for all the sacrifices and love, which made all the difference during the course of this research. Mum, Mathias, Ukongzi, Franca, Akomaye, and all my uncles and cousins; I am grateful for the financial and material support availed me during the course of this research, I could never thank you all enough. Thank you!

To my friends and colleagues especially members of the wastewater research group too numerous to mention, I am grateful for the friendships and useful criticisms which was an essential ingredient during the years of this research. I am also very grateful to the technical team in the analytical laboratory; Umesh, Nazmin and Janit who were kind enough to grant me unscheduled access to analytical equipment used for this research.

Finally, I am eternally grateful to God for His steadfastness, which has kept me.

Table of Contents

List of Figures

List of Tables

1 Introduction

1.1 Background

Although water constitutes about 70% of the earth, fresh water accounts for only 2.5%, some of which occurs as glaciers, while most of it occurs as ground water, with only about 0.3% making up fresh surface water (Ragheb, 2018). The 21st century industrial growth, which has led to increased economic activities has resulted in commensurate impacts on water and air quality (Murakami and Fujishima, 2010).

The oil and gas industry has not been insulated from this growth. There has been tremendous increase in oil prospecting activities especially in the United States where shale oil and gas (otherwise called tight oil or gas) has generated so much interest within the oil and gas sector (US EIA, 2016). These activities heightened in early 2015 (US EIA, 2016) and has contributed to the glut in the industry due to massive production, culminating in the current fall in the price of the commodity. These heightened oil and gas development activities have been accompanied by huge production waste, also called exploration and production waste -E&P Waste.

E&P waste is grouped into three, namely; produced water, drilling waste (drill cuttings, drilling and well completion chemicals) and associated waste (API, 2000). The most significant of these three classes of waste is produced water, owing to its sheer volume and toxicity (Viel et al., 2004; Stephenson, 1991; Krause, 1995). It is estimated that in 2014, about 201 billion barrels of produced water was generated around the globe, only 65billion barrels was re-injected for enhance oil recovery (EOR) processes, while 136.9 billion was disposed of into the sea (Future Market Insight, 2014).

Produced water (PW), also known as associated formation water, is water that is trapped in the formation and exported to the surface with oil and gas during exploration and production (E&P) activities (Viel et al., 2004; Viel, 2015).

It is by far the most challenging and most voluminous waste stream associated with E&P activities in terms of cost and management (Stephenson, 1991; Krause, 1995). In offshore fields, produced water especially presents a particularly distinct challenge whereby frequent discharge into the sea is a commonplace and considered an acceptable management strategy after certain environmental considerations (O&G, 2005).

The characteristics of any produced water are a function of the geological location and geology of the formation upon which crude oil extraction is taking place. In addition, the operational condition, the age of production, as well as additives used in the extraction process and the drilling environment are responsible in shaping the characteristics and composition of any produced water (Ahmadun et al., 2009). Enhanced oil recovery techniques and the proliferation of new production wells has altered the dynamics of common oil to water ratios (1:2-10) - where the range of 2 to 10 vary according to the age and the type of well (Henderson et al., 1999; Sumi, 2005; Benko and Drewes 2008; Igannu and Chen 2012). In spite of this seeming shift in dynamics, this waste stream remains significant. For instance, in the United States, Viel, (2015) reported an increase in the production of oil and gas by 29% and 22% respectively, but an increase of less than 1% of produced water between 2007 and 2012, through enhanced oil and gas recovery techniques. However, the rise of less than 1% of produced water volumes has

been projected to increase steadily through 2020. Although, 1% might seem small, in reality however, this is still huge because the volumes involved are very large. Due to the size of this waste stream, the global produced water treatment systems market has been forecasted to grow at a compound annual growth rate (CAGR) of 6.1% between 2014 and 2020.

The perception of risks resulting from produced water discharges is based mainly on three descriptors, namely; Toxicity, bioavailability and effect on ecosystem or community (Ekins et al., 2004). The risks or otherwise associated with produced water discharges have been marred in controversy owing largely to the difficulty involved with identifying and scientifically verifying what component of produced water poses harm (Ekins et al., 2005). The relationship between these descriptors have been further elaborated in Figure 1.1, to show the inter-relationship between these risk descriptors. According to Ekins et al., (2005), produced water constituent has to be bioavailable (that is available in a form that it can be taken up by living organisms), toxic (available in concentrations levels capable of causing harm) before it can have consequences (effect), leading to harm.

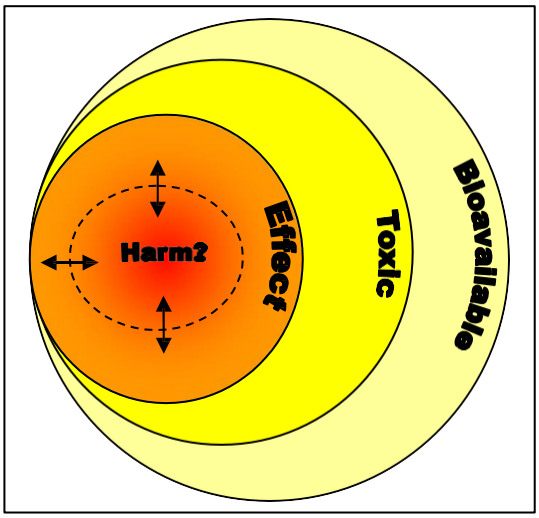

Figure 1.1: Relationship between risk indicators and perceived harm (Ekins et al., 2005)

As a result of this, produced water discharge quality criteria differs slightly from one country to the other, although it is almost unanimous in the discharge criteria for the oil-in–water (OIW) parameter, following Oslo Paris (OSPAR) Convention 2001.

There is hardly any doubt about the potential relative toxicity of most components of produced water especially the aromatic fraction, however, this depends largely on the concentrations they occur in produced water stream. Central to the toxicity of this waste stream is the presence of phenolic compounds, especially the alkylated phenols. The most abundant phenolic compounds in produced water are the ones with short side chains, the C1 –C5 which are mainly phenols, methyl phenols and dimethyl phenols (Røe and Johnsen, 1996; Neff et al., 2011). This group of compounds are distinguished by the marked variation in chemical properties across the homologous series. Their significance in produced water is their low oil/water partition coefficient and high attraction for solid sorption (Later and Bennett, 2011). They exhibit high mobility due to their varied solubilities in polar and non-polar solvents and can penetrate lipid membranes once

they are able to get into the tissues of aquatic organisms (Boitsov et al., 2004). Their occurrence in produced water can be small due to possible biodegradation in the reservoir during long-range secondary migration, (Larter and Bennett, 2011), and this is responsible for their small occurrence in produce water even though they occur in high concentrations in petroleum. Long range secondary migration of hydrocarbon entails the movement of hydrocarbon from the source rock (usually fine grained shale), through fissures and fault lines towards reservoir rock (usually sandstone), while primary migration is the movement or "squeezing" of hydrocarbon out of the source rock. The process and duration of this oil travel is sometimes long enough for biodegradation and other attenuations to reduce the concentrations of these alkylphenols in oils and by implication, in PW.

The partition coefficient of components of produced water is very important in assigning risk factors to various constituents of Produced water. According to Frost et al., (1998), of all the stable aromatic compounds in crude oil, alkylphenols and polycyclic aromatic hydrocarbons (PAHs) are the components of gravest concern and hence the most potentially harmful constituents of produced water owing to their toxicity. According to Frost et al., (1998 section 5.2), "it is now generally accepted within the scientific community that the water-soluble fraction of PAHs and alkylphenols contribute most to the acute and chronic toxicity of produced water". However, PAHs are partitioned into the oil phase and less likely to be found in harmful concentrations in produced water because of their low aqueous solubility (Faksness et al., 2004; Johnsen et al., 2004), regardless of this, both PAH and alkylphenols are considered in literature as the

dissolved components of produced water as shown in Figures 1.2 and 1.3. Some of them are thought to be toxic, mutagenic, and carcinogenic (Sun et al., 2009).

In their study of the effect of storage conditions on the produced water chemistry and toxicity, Binet et al., (2011) stored produced water which was diluted with sea water (to simulate discharge into ocean environment) for a maximum of 96 hours and determined the toxicity afterwards, using Microtox® bacterial bioassay. They found that most PW constituents were readily degraded by up to 90% due mainly to volatilization of benzenes toluene, ethylbenzene and xylene (BTEX) and photodegradation of BTEXs, PAH, napththelene, ammonia and Total Petroleum Hydrocarbons (TPHs) of C10 to C28. They also found that despite these huge loss of constituents, there was only a slight change in toxicity for both the closed and open storage tests. They concluded that toxicity was not caused by any of ammonia, naphthalene or BTEXs, but was caused by phenols, TPH of C10 to C14 and production chemicals.

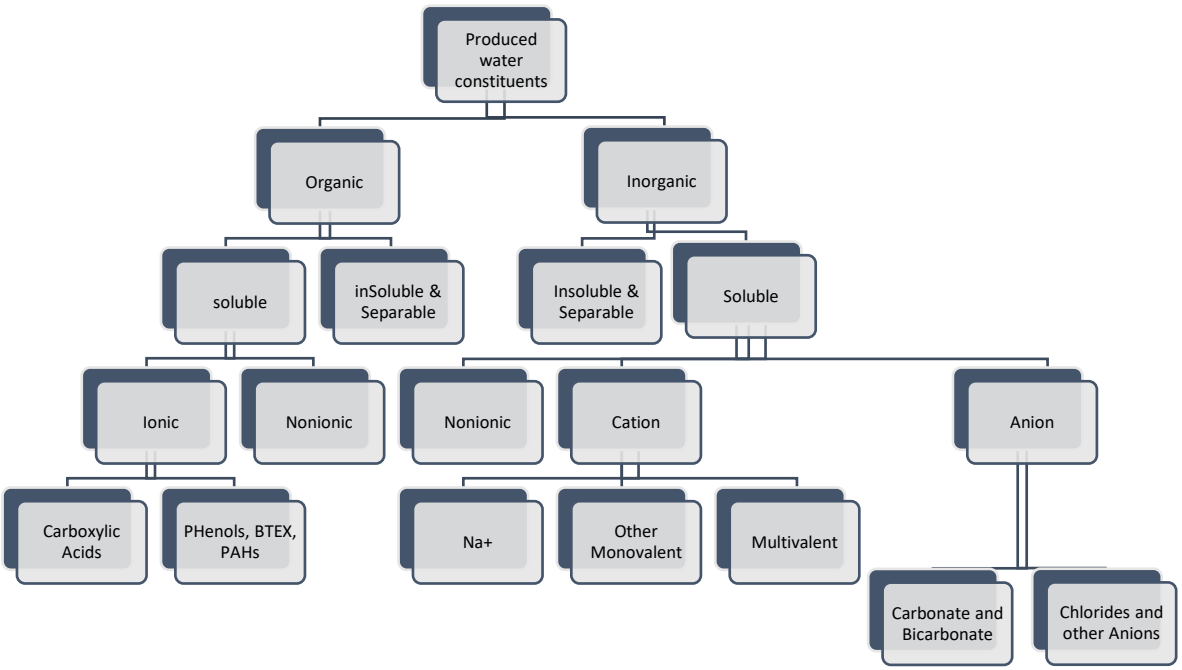

Figure 1.2: Overview of produced water constituents (Reproduced from Hayes & Arthur, 2004)

Faksness et al., (2004) reported about 85% alkylphenols and 80% 2-6 rings PAHs in produced water (these were found mainly in the dispersed oil fraction) as shown in Table 1.1 below. In Table 1.1, there is no correlation between the variation in the % reduction of C4-C5 phenols and the % reduction of oil-in-water. For example, when the oil-in-water was reduced by 50% (from 40 to 20 mg/L), there is only 7% reduction (155 to 143 mg/L) of C4- C5 phenols. Burns and Codi, (1999) also reported 5 to 10% PAH in produced water mainly as dissolved oil in the water fraction, which indicates that, most of the PAHs are in the oil phase.

Although the one ring aromatic hydrocarbons; (BTEXs) are adjudged the most abundant hydrocarbons in Produced water (Table 1.2), sometimes in concentrations of about 600 mg/L, they are for most part unstable (Neff et al., 2011). This is due to their extreme volatility, which results in the rapid loss of these compounds by air striping during treatment and during mixing of produced water with the ocean (Terrens and Tait, 1996).

Table 1.1: Overview of average concentrations of PAHs and phenols at various concentrations of dispersed oil in produced water from some oil fields. Reproduced from Faksness el al., (2004)

Dispersed oil	**40 mg/l**	**20 mg/l**		**5 mg/l**		
% reduction OIW	***0%***	***50%***		***87.5%***		
						% in dispersed
component	*µg/l*	*µg/l*	*% reduction*	*µg/l*	*% reduction*	*oil*
2-3 ring PAH	205	122	40%	60	71%	81%
4-6 ring PAH	3.17	1.77	44%	0.71	78%	89%
PAHs	208	124	41%	61	71%	81%
C4-C5 phenols	153	143	7%	136	11%	13%
C6-C9 phenols	2.47	1.37	45%	0.55	78%	89%

Figure 1.2 above shows an overview of produced water constituents. According to Myhre, (2004), short-chained alkylphenols (C1-C3) are the most common ones in produced water as shown in Table 1.2 and this view is also shared by Roe and Johnsen (1996). From Table 1.1, it is observed that as the concentration of oil-in-water is halved, the concentration of C4 and C5 phenols remains almost unchanged, with a corresponding reduction of only 7%, and only about 13% in dispersed oil, whereas C6-C9 phenols show 45% reduction when OIW concentration is halved. All other constituents of PW in Table 1.1 show over 80% composition in the dispersed oil indicating their final sink in the E&P waste stream. The C6 to C9 alkyl phenols, although most toxic, they are however rare in produced water, while Johnsen, et al., (1994), in Boitsov et al., (2004) opined that the phenolic fraction in produced water is responsible

for its toxicity and are thought to be suspected endocrinal disruptors. These views are shared by Boitsov et al., (2004), Yang et al., (2007) and Thomas et al., (2009). OLF, (2001) in Boitsov et al., (2004) reported about 116 million m^3 of produced water discharge into the Norwegian sector of the North Sea with alkylphenols accounting for mass of 323 tons, of which 90% are C1 to C3 short chained alkylphenols (SCAPs) and are likely to remain dissolved in the water fraction.

Table 1.2: Selected Groups of Organic Compounds in Produced Water (Source: Norsk Olje and Gass environmental report 2015) Discharged In Produced Water (Kg)

Constituent	2005	2006	2007	2008	2009	2010	2011	2012	2013	2014
Alkylphenols C1-C3	257 668	335 937	341 254	324 626	310 191	310 217	298 324	300 662	295 596	399 079
Alkylphenols C4-C5	13 273	15 571	12 513	12 473	12 949	10 258	14 360	15 892	13 177	12 846
Alkylphenols C6-C9	302	132	173	198	184	294	219	124	146	231
Others	8 131 449	7 519 086	7 959 150	8 838 787	7 814 585	7 905 978	8 611 126	8 424 293	7 971 565	9 063 413
BTEX	1 479 637	1 644 661	1 826 674	1 803 998	1 902 925	1 818 173	1 675 059	1 855 037	1 920 150	1 963 541
EPA 16	44 392	66 968	52 567	48 312	51 512	1 541	1 863	1 794	2 255	2 448
Phenols	170 118	179 405	212 822	207 560	185 041	166 660	179 546	206 564	503 045	653 851
Oil in water	2 097 498	1 057 837	1 178 851	947 549	1 156 501	1 200 078	1 235 608	1 325 326	1 689 917	1 560 328
Organic acids	34 711 299	34 838 267	35 818 064	31 263 700	27 204 909	24 752 275	22 251 835	22 144 558	53 788 966	31 606 050
PAH	121 454	89 899	73 776	81 157	101 664	140 867	155 915	166 366	156 528	169 764

* Naphthalene and phenanthrene were removed from EPA-PAH in 2010

1.2 Alkylphenols: Origin, Occurrence and Environmental Significance

These are a family of organic compounds formed from the alkylation of phenols (Lorenc et al., 2001) They occur mainly in crude oil and are natural constituents of crude oil and coal liquefaction products (OSPAR, 2010; Licha et al., 2002) and depending on the quality and origin, their concentration in crude oil vary considerably (Tailor et al., 1997).

The abbreviation SCAP (short chain alkyl phenols) has been used to differentiate these alkyl phenol homologues from other phenols. They have carbon chains ranging from C1 to C5 (Figure 1.3) and are the most abundant in produced water and drill cuttings which have been contaminated by SCAPs. (Bekins et al., 2001, Baedecker et al., 1993). According to Sauter and Licha, (2002), there are about 34 C1-C3 SCAPs and phenol, made up of; phenol (C0), cresols (C1) which has 3 isomers, dimethylphenols (C2) which has 6 isomers, ethylphenols (C2), which has 3 isomers and trimethylphenols (C3) which has 6 isomers. Others are; ethyl methylphenols (C3) with 10 isomers, n-propylphenols (C3) with 3 isomers, and isopropylphenols (C3) with 3 isomers. This has been represented in Figure 1.3, with each group representative. They are highly soluble in aqueous solutions.

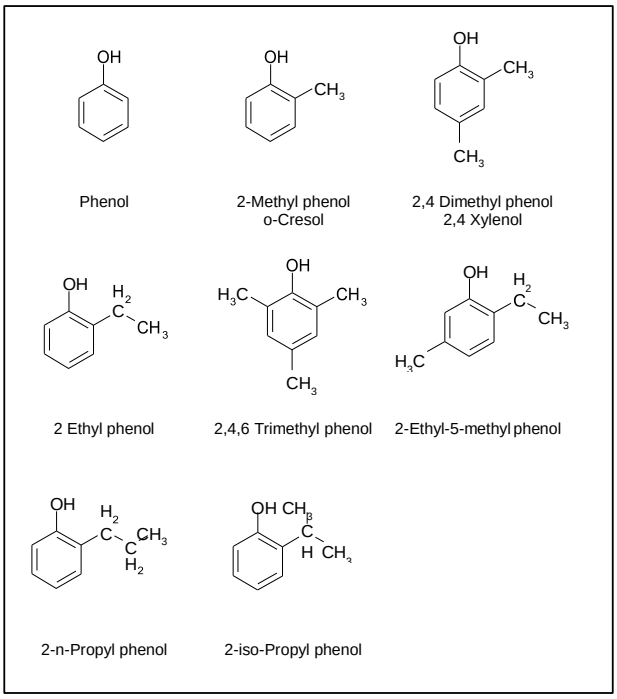

Figure 1.3: Chemical formula of representatives of each of the eight SCAP subgroups (Reproduced from Sauter and Licha, 2002).

In terms of environmental significance, alkylphenols were first reported as oestrogenic as far back as 1930. Recent studies have thrown more light on the implications of these findings and it is therefore not surprising that three alkylphenolic compounds are listed as priority pollutants namely; nonylphenol (NP), octylphenol (OP) and 2,4,6-tri-tert-butylphenol (OSPAR 2010), because they meet the OSPAR criteria for bioaccumulation and persistency. Their toxicity is known to increase with increase in length of their chains (Warhurst, 1995). C1-C3 are predominant in produced water, however, only a small amount of the long chain alkyl phenols are found in produced water (Tailor et al., 1997; Boitsov et al., 2007).

From the foregoing, the following deductions can be made:

- There is a growing need to better manage existing water resources, which have come under stress from industrialization in most regions of the world.
- Produced water is a major waste stream due its sheer volume and potential toxicity and is likely to increase in volume over the next 5 years.
- The main toxicants in produced water are the alkylphenols which require treatment or removal before disposal to forestall potential bioaccumulation and toxicity to marine biota.
- In terms of market share, there is a need for the development of a robust produced water treatment system, which has capacity to deal with environmentally significant constituents of produced water especially the short chained alkylphenols. (Existing treatment methods have been appraised in the next chapter under the review of previous literature).
- Although alkylphenols are currently routinely monitored in some oil installations. For example, the North Sea, not many oil producing countries of the world monitor this parameter routinely

The treatment of wastewater has gained more prominence over the years, however current efforts are aimed at the removal of dispersed oils in produced water, which in effect addresses only part of the problem relating to the toxicity arising from PAHs (as these are in the oil fraction). The alkylphenols which partition into the water phase are not effectively addressed under most current treatment strategies. In the present study, attempts have been made to address these issues using advanced oxidative processes (AOP) in coupled systems.

1.3 General Aims & Objectives

The Aim of this study is to establish the mineralization potentials of short chained alkyl phenols in produced water by a novel heterogeneous PAN catalyst of De Montfort University Leicester, England in an advanced oxidation process utilizing a Fenton-like reaction. The optimised oxidation conditions are subsequently applied to a simulated produced water sample.

The following are the objectives to achieve the above aim:

1. To determine possible reaction intermediates and kinetics of reaction and propose an oxidation mechanism for the degradation of DMP.
2. To carryout batch optimization for the following parameters; catalyst concentration, H_2O_2 concentration, temperature and pH of catalytic reaction.
3. To carry out a dynamic flow reaction of the catalytic system by scaling up the optimised batch reactor system and evaluate same with the DMP in both water and in simulated produced water.
4. To couple the optimised system to simultaneous UV and microwave radiations and evaluate the performance of the assisted system in a continuous process.
5. To investigate the activity of the catalyst.

1.4 Overview of Dissertation

Chapter 1 provides the introduction and the objectives of the research.

Chapter 2 presents a critical review of previous literature for both general and specific applications of oxidative decomposition for produced water treatment. It also outlines the principles of some of these applications.

Chapter 3 presents the results for the batch decomposition of DMP in water using the PAN catalyst and kinetic data analysis of the process.

Chapter 4 presents the catalytic decomposition of DMP in water in a continuous plug-flow system. It also presents the proposed mechanistic pathway for the oxidation of DMP in heterogeneous catalytic system.

Chapter 5 presents the degradation of simulated produced water in both batch and continuous flow processes using the modified PAN catalyst in normal Fenton-like process, monitoring the loss of DMP, COD, oil-in-water and H_2O_2.

Chapter 6 presents UV/microwave assisted Fenton-like reaction of the degradation of simulated produced water in continuous flow process, monitoring the loss of DMP, COD, oil-in-water and H_2O_2.

Chapter 7 presents the conclusion, perspectives and further work.

2 Literature Review

2.1 Introduction

This review chapter has been approached through three sections; appraisal of current produced water treatment methods, the principle of Fenton oxidation, and the potential for the application of a novel heterogeneous catalyst in a coupled Fenton-like process for the simultaneous removal of alkylated phenols and oils in oil-field produced water.

2.2 Review of Existing Produced Water Treatment Technologies

Over the years, a large number of treatment methods have been adopted to treat produced water (Ekins et al., 2005). A typical composition of produced water is given in Table 2.1. The focus of the present study however is to advance a treatment method with potentials to simultaneously remove both the dispersed and dissolved oils, and alkylated phenols from produced water (Table 2.2). The selection of a suitable produced water treatment method is largely dependent on whether the component is a dispersed or a soluble constituent. This is also guided by the existing risk assessment regime by regulatory bodies. As it stands today, the focus of all regulatory bodies is the dispersed oil in water, even though most other constituents of concern in produced water are dissolved in the water phase (Ekins et al., 2005). The good news however is that some operators have taken the initiative to effect “zero harmful discharges” of produced water to the marine environment by 2020 (Ekins et al., 2005), which supports this work in the need for the development of a system with potentials to simultaneously remove both the dissolved and dispersed organic components. This initiative is being sustained by the introduction of discharge risk assessment and management tools by OSPAR decision 2000/2, such as the CHARM (Chemical Hazard Assessment Risk Management)

model. The model output known as the hazard quotient (HQ) gives the ratio of the predicted environmental concentration (PEC), to the no effect concentration (NEC). According to Johnsen et al., (2000), others models such as DREAM (Dose Related Risk and Effect Assessment Model) have been deployed in this regard. This review will therefore focus on the major treatment methods that emphasize the removal of oils as well as those that emphasize the removal of dissolved organics, which is the focus of the present study. Ekins et al., (2005) and Arthur et al., (2005) reviewed currently used methods for produced water management. Mastouri et al., (2010), have more recently comprehensively reviewed methods applied for the removal of oils as follows;

Table 2.1: Typical material composition of produced water discharged from oil fields in the Norwegian sector of the North Sea (Adopted from Frost et al., 1998; E&P 1994 in Ekins et al., 2005)

Sources		Seawater			Produced water			Ratio Produced water: seawater (mid)
		Range	Mid	Unit	Range	mid	Unit	
Sources: Frost 1998, Section 1.2	Dispersed oil	-	-	-	15-60	44	mg/L	-
	BTEX	-	-	-	1-67	6	mg/L	-
	NPD	9-185	88	ng/l	0.06-2.3	1.2	mg/L	0.014
	PAH	1-45	22	ng/l	130-575	468	µg/L	21.273
	Organic Acids (<C6)	-	-	-	55-761	368	mg/L	-
	Phenols(C0-C4)	-	-	-	0.1-43	8	mg/L	-
	Barium (Ba)	22-80	29	µg/l	0.2-228	87	mg/L	3.0
	Cadmium (Cd)	4-23	10	ng/l	0.5-5	2	µg/L	0.2
	Copper (Cu)	20-500	240	ng/l	22-82	10	µg/L	0.042
	Mercury (Hg)	1-3	2	ng/l	<0.1-26	1.9	µg/L	0.95
	Lead (Pd)	20-81	31	ng/l	0.4-8.3	0.7	µg/L	0.023
	Zinc (Zn)	0.3-1.4	0.6	µg/l	0.5-13	7	mg/L	11.666
	Iron (Fe)*	1.8	1.8	µg/l	0.1-15	4.3	mg/L	2.389
Source: E&P 1994, p.4					4.5-6	5.25	mg/L	2.889
	Radium (^{226}RA)				1.66	1.66	Bq/L	Seawater concentrations not available
	Radium (^{228}RA)				3.9	3.9	Bq/L	
	Manganese (Mn)				0.1-0.5	0.45	mg/L	
	Berllium (Be)				0.02	0.02	mg/L	
	Nickel (Ni)				0.02-0.3	0.14	mg/L	
	Cobalt (Co)				0.3-1	0.35	mg/L	
	Vanadium (V)				0.02-0.5	0.24	mg/L	

* Second row set of rows below Iron (Fe) is from E&P 1994, while the top rows are from Frost 1998. Note: The medians for the produced water numbers and the mid points for the seawater concentrations were provided in the source. Bq (Becquerel, and 1 Bq = 1 s^{-1})

*NPD is Naphthalene, Phenanthrene and Dibenzothiophene

2.2.1 Hydrocyclones

Also called static oil-water separators, hydrocyclones were first developed in Southampton University, United Kingdom in 1978 (Sinker, 2007) and are some of the most commonly used produced water management techniques especially in the UK (Ekins et al., 2005). The principle of its operation is based on centrifugal forces and the

difference in the specific gravity of oil and water. This is achieved by the rotating motion of produced water, initiated by the hydrocyclones being fed oily water tangentially, thereby intensifying the effect of gravity by several orders of magnitude leading to the separation of oil from the water (Mastouri et al., 2010). This force pushes the oils which are lighter to the core of the cones, while the heavier water is pushed in a vortex outwards, which continues downwards and exits through the narrow end (Figure 2.1). Because there is multi-cone modules, there is high oil recovery with small footprints (Arthur et al., 2005). Residence time is between 2-3 seconds (Mastouri et al., 2010), with free oil removal of 50 to 70 mg/L, however this works only under high pressures and high flowrates (Knudsen et al., 2004; Sinker, 2007). This technique separates oil from water, but the dissolved organic constituents are not removed (Ekins et al., 2005).

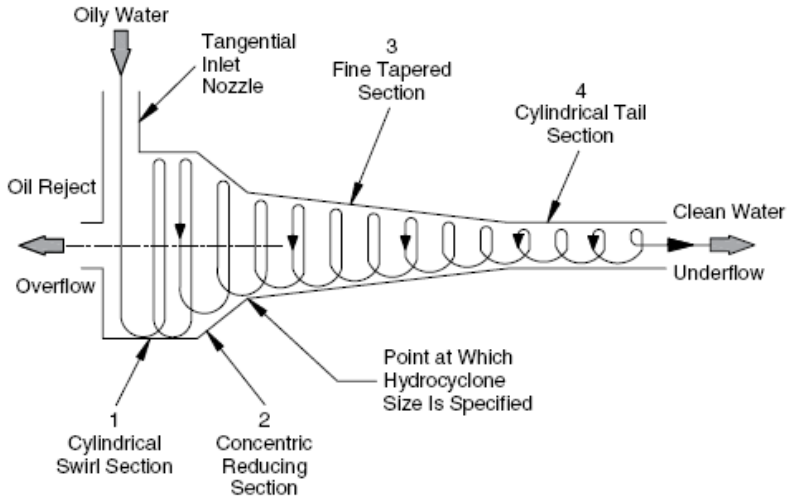

Figure 2.1: Schematic of a Hydrocyclone (Mastouri et al., 2010)

2.2.2 Centrifuges

There is no major difference in principle between centrifuges (Figure 2.2) and hydrocyclones. Both work under the same basic principle however, the centrifugal force in the centrifuges is generated by moving parts, whereas in hydrocyclone, it is generated by the tangential inlet feed. Centrifuges are also able to separate smaller droplets of oils and consume much higher energy than the hydrocyclones (Ekins et al., 2005). In addition to this, centrifuges also operate at lower pressures than the hydrocyclones (Mastouri et al., 2010). Centrifuges find fewer applications due to their operational costs (Arnold and Stewart, 2008).

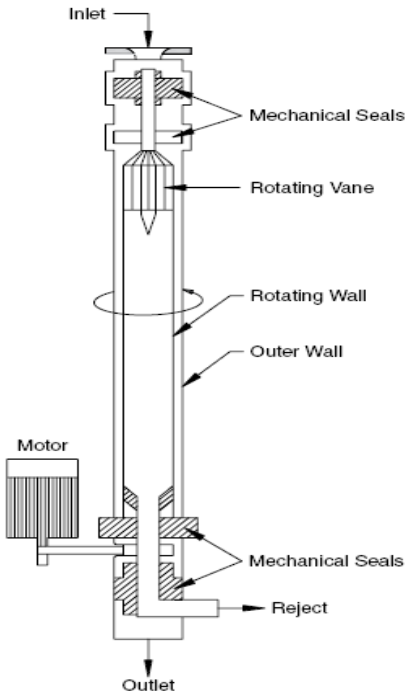

Figure 2.2: Schematic of a Centrifuge (Arnold and Stewart, 2008)

2.2.3 Corrugated Plate Separators

Developed in 1950, corrugated plate separators (Figure 2.3) can remove oil droplet sizes of 40µm and above. It uses gravity separation and works by providing longer paths for oil to travel through, thereby enhancing coalescence to form larger droplets before being collected into skim tanks (Arthur et al., 2005; Mastouri et al., 2010).

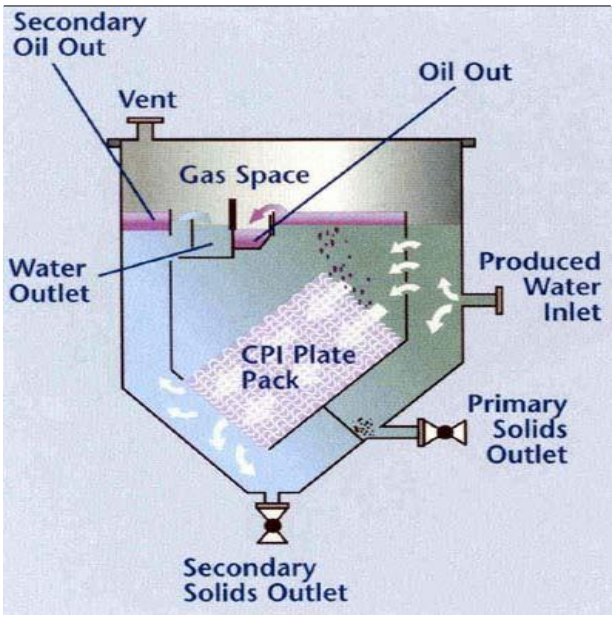

Figure 2.3: Schematic showing flow pattern of a typical down-flow CPS design (Source: NATCO Group)

2.2.4 American Petroleum Institute (API) Gravity Separator

According to Mastouri et al., (2010), it is the most frequently used gravity separation method used, removing up to 99% free oil of particle size > 150 microns in produced water. It is commonly a concrete rectangular basin (Figure 2.4), which provides a surface for detention of oily water where separation of oil takes place by gravity, with lighter pollutants separating from the heavier ones. The lighter oil separates as floating scum and is removed by a device for floating oil removal (API, 1990). This is not effective with

small dispersed oil droplets and oil emulsions. With smaller oil droplets, the separation time increases significantly. The efficiency depends a lot on the additives; the flocculants, coagulants and the separation times (Arthur et al., 2005).

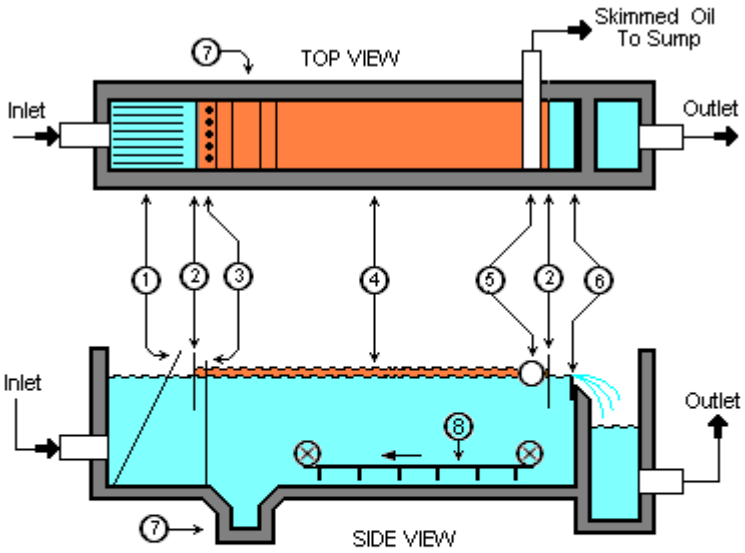

1 Trash Tap (inclined rods)

2 Oil retention baffles

3 Flow distributors

4 Oil layer

5 Slot pipe skimmer

6 Adjustable over flow wier

7 Sludge sump,

8 Chain and flight scraper

Figure 2.4: Schematic of an API oil separator. Source: (Baychoke M., 2007)

2.2.5 Flotation Separation

This works in two different methods; induced air or gas and pressurised air or gas flotation. It works by the introduction of charged gas bubbles, which are generated by

electrification into the produced water. These gas bubbles acquire charges, which are opposite to the negative charge on the surface of the oil droplets (Frankiewicz and Walsh, 2017), thus causing an attraction between the oils and the air or gas bubbles. Because the density of the oil is reduced when it is attached to air bubbles the oil rises along with the gas bubbles to the surface as the gas bubbles rise, making it easy for oil to be floated off (Arthur et al., 2005; Arnold and Stewart, 2008; Bradley, 1990). Although it has a high throughput and low retention time, the setback of this treatment method is however the limited size of recoverable oil droplet of not smaller than 25 microns (Arthur et al., 2005). It finds application as a polishing step in produced water treatment (Ekins et al., 2005). This has been presented in Figure 2.5.

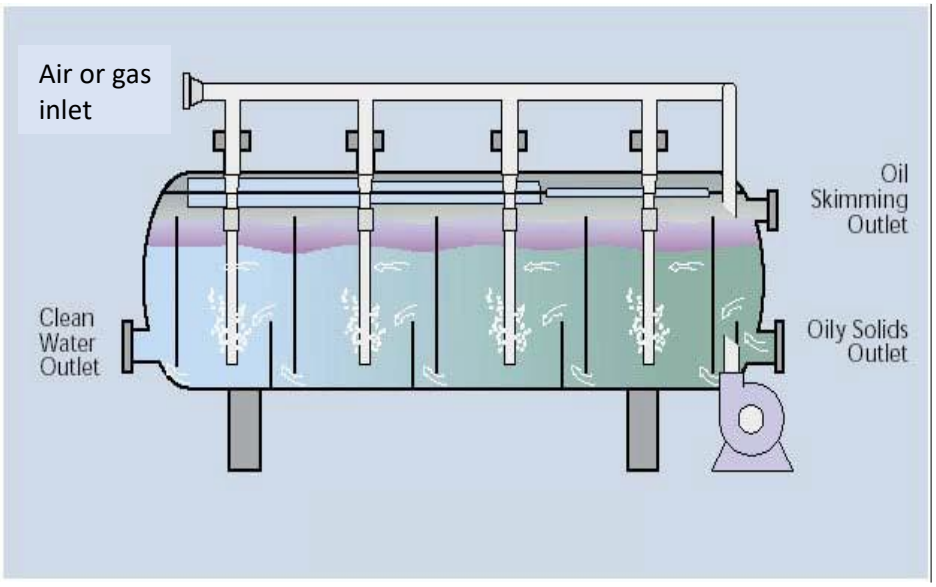

Figure 2.5: Induced gas floatation cell (Source NATCO Group in Arthur et al., 2005)

2.2.6 Adsorption

Adsorbent materials are those that exhibit hydrophobic – oleophilic properties (Arthur et al., 2005). These materials have been effectively used to remove oils from produced

water when inlet concentrations are below 10 mg/L (Owens and Lee, 2007 in Arthur et al., 2005). Some of these materials have capacity to remove organic constituents of wastewaters as well. According to Ekins et al., (2005) and Glimmerman, (2006), absorbent materials can be grouped into two main categories; regenerative adsorbents, such as Macro Porous Polymer Extraction (MPPE) materials that can be reactivated and reused. Insitu regeneration is possible with low-pressure steam, which volatilizes the hydrocarbons (Ekins et al., 2005). Non-regenerative adsorbents on the other hand, are replaced after use and transported to disposal sites. Their applications span both natural and synthetic materials. The problems stem from the environmental issues created by the use of non-biodegradable synthetic materials for absorption purposes. Although natural equivalents exist in the form of wood chips, coconut and rice husks, cotton wool, activated carbon, etc. there is still the problem of having to deal with spent absorbent materials, which becomes waste in itself especially those that cannot be regenerated. In terms of the economy of re-use or re-generation of adsorption media, it is thought to be possible with acid backwash and solvent treatments; however, suspended particles are to known to clog the interstices of the adsorption media, diminishing their efficiency, which can generate additional wastes (Ahmadun et al., 2009). Commercial applications have been found with zeolites, activated carbon, organoclay, sand filters and others (Arthur et al., 2005).

2.2.7 Membrane Filtration

Membranes are able to remove most aliphatic and aromatic compounds in produced water, which effectively constitutes both the dissolved and the dispersed oils in water by filtration (Ekins et al., 2005). The membrane pore sizes are usually about 0.1-0.2 µm

(micro filtration), so the build-up of filter cake is prevented by cross flows and turbulent flows on membrane surface. It is possible to use chemicals (coagulants) to increase particle sizes of the oil-in-water droplets and achieve better separation with larger pore sized membranes. Cleaning is achieved through a pressure pulsed system and the use of chemicals (Ekins et al., 2005). The trapped aliphatics and aromatics are channelled to a settling tank where oils are separated. The main disadvantage of these membranes is that, its expected lifetime is lower than all other treatment methods (Martin, 2014). Periodic fouling by suspended solids often leads to blockage, requiring regular tending. There are micro, ultra, and nano filtration membrane systems in addition to reverse osmosis Table 2.2 (Mastouri et al., 2010). In most cases if emulsions (slightly viscous oil-water mixture in the oil/water boundary) are formed as a result of the mixing of incompatible oil types, such as asphaltic crude oil and paraffinic crude oil, resulting in the precipitation of asphaltenes are not pre-treated with demulsifiers, membranes are inefficient and hence not good for oil removal. The main advantage of membranes is that they have capacity to remove dissolved oil in water of up to 0.01 µm (ultrafiltration drop sizes); however, this comes at a huge cost.

Table 2.2: Applications of advanced membrane filtration technologies (Mastouri et al., 2010)

Membrane Filtration	Separation Specifications	Applications
Microfiltration (MF)	>100,000 Daltons 5 - 0.1 µm	bacteria, viruses, suspended solids, oils etc
Ultrafiltration (UF)	10,000 to 100,000 Daltons 0.1- 0.01 µm	proteins, starch, viruses, colloid silica, organics, dyes, fats, paint solids etc
Nanofiltration (NF)	1,000 to 100,000 Daltons 0.01-0.001 µm	starch, sugar, pesticides, herbicides, divalent ions, organics, BOD, COD, detergents etc
Reverse Osmosis (RO)	salts especially 0.001 -0.0001 µm	metal ions, acids, sugars, aqueous salts, dyes, natural resins, monovalent salts, BOD, COD, ions etc
Gas Liquid Membrane	CO_2, H_2S	decarbonation, hydrogen sulfide removal

2.2.8 Electrodialysis (ED)

Suitable for produced water with low total dissolved solids, this technique involves placing membranes namely; cation exchange membranes (CEM) and anion exchange membrane (AEM) between a pair of electrodes (anode and cathode) in a solution of produced water containing charged ions (Figure 2.6). These ion exchange membranes contain a series of charged functional sites, which function to remove charged substances from the wastewater. Positively charged membranes allow the flow of anions, while negatively charged ones allow only the flow of cations through it. Since charged ions, which are mainly dissolved salts are in solution they are able to flow through these membranes and get attached to the electrodes, which bear opposite charges from the ions in solution (Mastouri et al., 2010; Ahmadun et al., 2009). This

technique's ability to remove non-charged organic molecules and other non-charged constituents is limited.

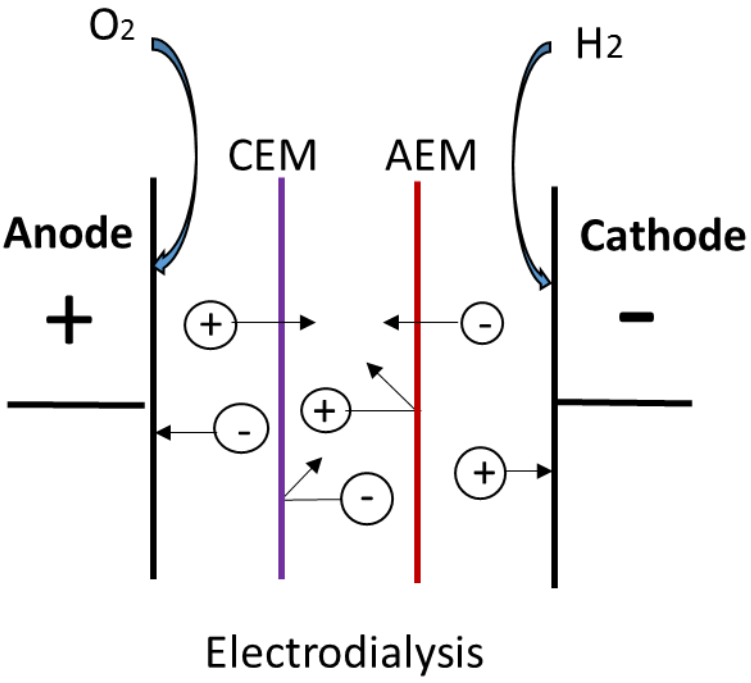

Figure 2.6: Schematic of Electrodialysis process. Redrawn from Igunnu, (2014)

2.2.9 Steam Stripping

Although not suitable for produced water from oil operations, it is able to remove hydrocarbons generated from gas production platforms where there is condensed water derived from glycol generation in gas fields. Produced water is brought into contact with steam, in and intense fashion, in a packed column in a process known as stripping (Ekins et al., 2005). This is able to remove both dispersed and some dissolved oils. The vapours of the stripped compounds are then condensed and separated in much smaller volumes of water.

2.2.10 Freeze Thaw-Evaporation (FTE)

B.C Technologies (BCT) has successfully applied this technology for the treatment of produced water. It involves taking advantage of natural temperature changes resulting from the presence of natural salts and other dissolved components of produced water, to concentrate dissolved constituents, by alternately freezing and thawing produced water, thereby resulting in large volumes of uncontaminated water. The freezing point of the produced water is lowered below the freezing point of pure water due to the presence of these salts. When produced water solution is cooled below zero ^{0}C pure ice crystals are formed in addition to unfrozen solution of produced water containing high concentrations of the dissolved constituents. The pure ice, which is essentially uncontaminated, is then separated from the unfrozen solution by density difference, and thawed (Boysen et al., 1997). Although this technique has capacity to remove over 90% of metals, dissolved and suspended solids and TPH, water recovery is mostly only during the winter (Boysen et al., 1999).

2.2.11 Biological Technologies

The use of biological treatment methods such as the activated sludge systems, trickling filtration units, sequencing batch reactors, aerated lagoons etc., have been used for the treatment of produced water and is well documented (Ahmadun et al., 2009; Fahkru'l-Razzi et al., 2009). Although some are easy to operate and use solar energy, however its demerits is in the sheer size and weight of these systems which makes their applications offshore impracticable (Mastouri and Nadim, 2010). This has also been faced with challenges, ranging from resistance of some refractory compounds like the fulvic and humic acids to biodegradation (Wang et al., 2012), alteration of microbial organisms by

inorganic compounds as well as long retention periods makes offshore applications impracticable (Mastouri and Nadim, 2010).

A comparison of current treatment technologies for oil and gas produced water by Arthur et al., (2005), cited in Ahmadun et al., (2009) and has been presented in Table 2.3, and some of these techniques have already been discussed. A critical look at the treatment methods, which are capable of removing dissolved organic compounds highlighted on Table 2.3, exposes treatment gaps, associated with these treatment methods. The few techniques which are capable of simultaneously removing both free and dissolved oils as well as other dissolved organic compounds of concern in produced water have various limitations which make their application challenging. For instance, the application of Extraction technique leads to the generation of solvent waste, which requires further management/treatment. Ozonation on the other hand, which is an advanced oxidation process, has high energy requirements in addition to high cost of chemicals, and side reactions with bromides to form bromates ($Br^- + O_3 \rightarrow BrO_3^-$) which is a suspected carcinogen. Absorption as noted earlier requires effective management/disposal of spent absorbents and regeneration wastes. Membranes are expensive and replete with fouling and blockages, requiring frequent regeneration and sometimes, outright replacements, leading to high cost implications. In the light of the foregoing, an advanced oxidation system, is being proposed, which involves the release of an unselective hydroxyl (OH) radical with broad spectrum for the oxidation of most organic compounds.

Table 2.3: Comparison of current technologies for oil and gas produced water treatment (Arthur et al., 2005, cited in Ahmadun et al., 2009)

Treatment	Description	Advantages	Disadvantages	Waste stream	Oil and gas produced water
Corrugated plate separator	Separation of free oil from water under gravity effects enhanced by flocculation on the surface of corrugated plates	No energy required, cheaper, effective for bulk oil removal and suspended solid removal, with no moving parts, this technology is robust and resistant to breakdowns in the field	Inefficient for fine oil particles, requirement of high retention time, maintenance	Suspended particles slurry at the bottom of the separator	Oil recovery from emulsions or water with high oil content prior to discharge. Produced water from water-driven reservoirs and water flood production are most likely feedstocks. Water may contain oil and grease in excess of 1000 mg/L.
Centrifuge	Separation of free oil from water under centrifugal force generated by spinning the centrifuge cylinder	Efficient removal of smaller oil particles and suspended solids, lesser retention time high-throughput	Energy requirement for spinning, high maintenance cost	Suspended particles slurry as pre-treatment waste	
Hydrocyclone	Free oil separation under centrifugal force generated by pressurized tangential input of influent stream	Compact modules, higher efficiency and throughput for smaller oil particles	Energy requirement to pressurize inlet, no solid separation, fouling, higher maintenance cost		
Gas floatation	Oil particles attach to induced gas bubbles and float to the surface	No moving parts, higher efficiency due to coalescence, easy operation, robust and durable	Generation of large amount of air, retention time for separation, skim volume	Skim off volume, lumps of oil	
Extraction	Removal of free or dissolved oil soluble in lighter hydrocarbon solvent	No energy required, easy operation, removes dissolved oil	Use of solvent, extract handling, regeneration of solvent	Solvent regeneration waste	Oil removal from water with low oil and grease content (<1000 mg/L) or removal of trace
Ozone	Strong oxidizers oxidize soluble contaminant and easy operation, efficient for primary treatment of soluble constituents remove them as precipitate	Easy operation, efficient for primary treatment of soluble constituents	On-site supply of oxidizer, separation of precipitate, by-product CO_2, etc.	Solids precipitated in slurry form	Quantities of oil and grease prior to membrane processing. Oil reservoirs and thermogenic natural gas reservoirs usually contain trace amounts of liquid hydrocarbons.
Adsorption	Porous media adsorbs contaminants from the influent stream	Compact packed bed modules, cheaper, efficient	High retention time, less efficient at higher feed concentration	Used adsorbent media, regeneration waste	
Lime softening	Addition of lime to remove carbonate, bicarbonate, etc. hardness	Cheaper, accessible, can be modified	Chemical addition, post-treatment necessary	Used chemical and precipitated waste	These technologies typically require less power and less pre-treatments than membrane
Ion-exchange	Dissolved salts or minerals are ionized and removed by exchanging ions with ion-exchangers	Low energy required, possible continuous regeneration of resin, efficient, mobile treatment possible	Pre- and post-treatment require for high efficiency, produce effluent concentrate	Regeneration chemicals	Technologies. Suitable produced waters will have TDS values between 10,000 and 1000 mg/L. Some of the treatments remove oil and grease

Rapid spray evaporation	Injecting water at high velocity in heated air evaporates the water which can be condensed to obtained treated water	High quality treated water, higher conversion efficiency	High energy required for heating air, required handling of solids	Waste in sludge form at the end of evaporation	Contaminants and some of them require oil and grease contaminants to be treated before these operations.
Freeze–thaw evaporation	Utilize natural temperature cycles to freeze water into crystals from contaminated water and thaw crystals to produce pure water	No energy required, natural process, cheaper	Lower conversion efficiency, long operation cycle	Ditto Rapid spray evaporation	
Treatment	**Description**	**Advantages**	**Disadvantages**	**Waste stream**	**Oil and gas produced water**
Microfiltration	Membrane removes micro-particles from the water under the applied pressure	Higher recovery of fresh water, compact modules	High energy required, less efficiency for divalent, monovalent salts, viruses, etc.	Concentrated waste from membrane backwash during membrane cleaning,	Removal of trace oil and grease, microbial, soluble organics, divalent salts, acids, and trace solids. Contaminants can be targeted by the selection of The membrane.
Ultrafiltration	Membrane removes ultraparticles from the water under the applied pressure	Higher recovery of fresh water, compact modules, viruses and organics, etc. removal	High energy, membrane fouling, low MW organics, salts, etc	concentrate stream from the filtration operation	
Reverse osmosis	Pure water is squeezed from contaminated water under pressure differential	Removes monovalent salts, dissolved contaminants, etc., compact modules	High pressure requirements, even trace amounts of oil and grease can cause membrane fouling	Ditto micro filtration	Removal of sodium chloride, other monovalent salts, and other organics. Some organic species may require pre-treatment. While energy costs increase with higher TDS, RO is able to efficiently remove salts in excess of 10,000 mg/L.
Activated sludge	Using oil degrading microorganisms to degrade contaminants within water	Cheaper, simple and clean technology	Oxygen requirement, large dimensions of the filter	Sludge waste at the end of the treatment	Removal of suspended and trace solids, ammonia, boron, metals, etc. Post-treatment is normally required to separate biomass, precipitated solids, dissolved gases, etc.
Constructed wetland treatment	Natural oxidation and decomposition of contaminants by flora and fauna	Cheaper, efficient removal of dissolved and suspended contaminants	Retention time requirement, maintenance, temperature and pH effects	Ditto activated sludge	

2.3 Advanced Oxidation Processes (AOP)

The mention of AOP was first made by Glaze in 1987. It describes the various processes and methods used to generate hydroxyl radical (which is the main oxidizing intermediate) and other reactive intermediates used for oxidation of a broad spectrum of oxidizable organic and inorganic compounds especially in water treatment (Ibhadon and Fritzpatrick, 2013). Oxidation refers to the transfer of electrons from the reductant, which is an electron donor, to the oxidant, which has a hunger for electrons. This chemical process, results in the transformation of the oxidant and the reductant, forming very reactive species called radicals, which have an unpaired valence electron(s). These radical species formed from a redox reaction are very reactive due their unpaired valence electron and hence unstable. They are able to participate in the secondary reaction and initiate the oxidation of other organic compounds in a reaction system, up to the point of thermodynamic equilibrium. The reaction of a reactive radical species such as a hydroxyl radical which has an oxidation potential of 2.8 V (Table 2.4), with organics in a reactive system is what is called advanced oxidation process (AOP) (Glaze et al., 1987).

Table 2.4: Standard oxidation potential of some oxidants in volts (V). (Legrini et al., 1993; Parsons, 2004).

Oxidant	Standard Oxidation potential (V)
Fluorine (F_2)	3.03
Hydroxyl radical ($^{\bullet}OH$)	2.80
Ozone (O_3)	2.07
Hydrogen peroxide (H_2O_2)	1.77
Perhydroxyl radical ($HO^{\bullet}_2$)	1.70
Potassium permanganate ($KMnO_4$)	1.67
Chlorine dioxide (ClO_2)	1.50
Chlorine (Cl_2)	1.36
Bromine (Br_2)	1.09

Advanced Oxidation Processes have generated huge interest in both fundamental and applied works and are well documented (Herrmann et al., 1999; Laine and Cheng, 2007; Tarr, 2003), owing to their potential to completely transform or degrade contaminants, use of environmentally benign reagents, absence of secondary waste and small footprints.

Several varieties of AOPs (Table 2.5), which involve the *in-situ* generation of OH radicals using different processes such: chemical, photochemical, electrochemical and sonochemical means are well documented (Gumus and Akbal, 2016; Mehmet and Jean-Jacques, 2014; Babuponnusami and Muthukumar, 2013; Stasinakis, 2008). The oldest and arguably the most applied chemical AOP is the classical Fenton method, which involves the use of Fe^{2+} catalyst in aqueous solution, the presence of H_2O_2 at acidic pH for the oxidation of organic compounds (Tarr, 2003; Gogate and Pandit, 2004). The down

side of this application is in the narrow pH range associated with classical homogeneous Fenton processes and the sludge produced from the process.

Table 2.5: Examples of methods classified as AOPs. Source: (Stasinakis, 2008; Munter, 2001; Mota et al., 2008)

Dark AOP	**Light Driven AOP**
Fenton(Fe^{2+} + H_2O_2)	UV/H_2O_2
Fenton-like systems (Fe^{3+} + H_2O_2)	UV/TiO_2
Ozonation (O_3)	O_3/UV
Ozone +H_2O_2	Photo-Fenton (Fe^{2+} or Fe^{3+}/H_2O_2/UV)
Electrolysis (Electrodes + Current)	O_3/H_2O_2/UV
Sonolysis (Ultrasounds)	
Wet air oxidation (WAO)	

2.4 Homogeneous and Heterogeneous Catalysis

Fundamentally, a catalyst functions by thermodynamically lowering the activation energy requirement, and achieves this by providing alternative reaction pathways which unlike an un-catalysed reaction, increases reaction rate by circumventing the slow rate determining step (Michael, 2000). Depending on the stage of aggregation, catalysts can be described as either homogeneous or heterogeneous (Michael, 2000). The term homogeneous is used if the catalyst and the reactants are in the reacting phase, whereas heterogeneous is used if the reactants and the catalyst are in different phases. In conventional homogeneous Fenton reactions, insoluble ferric ion complexes, build up in the system owing to the slow regeneration rate of ferrous iron and with increase in pH,

there is increased sludge formation, which poses a challenge to system. A lot of research has been focused on surmounting these challenges posed by homogeneous processes, such as the heterogeneous Fenton-like process. This involves the use of insoluble oxides of iron or immobilized iron, such as ferric iron on a solid support, such as has been adopted in this study. Homogeneous reactions, initiate faster reactions because they are intimately diffused within the medium at a molecular level as are the pollutants but the challenge of separation of the treated effluents from the catalyst after a treatment cycle does exist, which in turn makes the reuse of catalyst challenging, and expensive. In addition, there are regulatory issues involved with the discharge limits for some homogeneous catalysts. Heterogeneous catalysis has the advantage of clear effluents, catalyst reuse/recycling, which results in low operating cost. There is however a challenge of mass transfer limitations and slow initial rates of reactions.

There have been variations to the traditional Fenton oxidation aimed at improving efficiency, giving rise to hybrid or coupled techniques such as ultraviolet (UV-Fenton) or Photo-Fenton (which involves irradiating/exposing the Fenton reactions with/to electromagnetic irradiations of wavelengths between 190 to 390 nm and between 400 and 700 nm for UV and Photo-Fenton respectively). Recently, others involve the coupling of conventional Fenton reactions to microwave radiations as well as UV in a homogeneous system (Barros et al., 2013; Gromboni et al., 2007). The application of UV-H_2O_2 for wastewater treatment using solution phase UV reagents such as H_2O_2 is well known, however, this is disadvantaged by the fact that there is relatively high-energy demand and the persistent fouling and subsequent lamp sleeve cleaning requirements.

2.5 Applications of UV/Photocatalysis

The growth in industrialization in the 21st century especially in China, India and Brazil has resulted in water pollution and air pollution and bringing to the fore a relatively new phenomenon known as global warming (Murakami and Fujishima, 2010). Consequently, access to safe water has become a more serious challenge in most parts of the planet. The effect is even worse in developing countries, where little importance is placed on environmental planning and this trend is not expected to abate with the increasing population. As a result of this, and for good ecological health, there has never been a more urgent need to treat wastewater than now. According to UNESCO Water Corporation (2013), about 780 million people lack access to clean water. Ibhadon and Fitzpatrick (2013) however put this value at over 1 billion, while over 2.5 billon people mostly from Asia, Africa, central and southern America have challenging sanitary conditions. The report also predicted an increase of 2 to 3 billion of world population growth over the next 40 years, with an accompanying 70% increase in food demand, which is expected to lead to increased agricultural activities, resulting in about 19% increase in the demand for agriculture alone by 2030.

Several water treatment methods have been in use over the decades, however applications of these water treatment methods is a function of factors such as legislation, efficiency, suitability and cost.

UV/TiO2 application in water treatment has however gained prominence and was first reported as far back as 1977 (Pelaez et al., 2012). The activation of TiO_2 surface by UV radiation results in two distinct events; the promotion of an electron from the valence

band to the conduction band, resulting in electron deficiency in the valence band (otherwise called an electron hole h^+) and excess negative charge in the conduction band (e^-) (Ohama and Van Gemert, 2011). Because these two outcomes have oxidizing and reducing properties respectively, they can participate in redox reactions. However, the disadvantage is that, the recombination of the electrons and holes is a very slow process. Apart from this, the energy requirement for the photon to promote an electron from the valence to the conduction band is high (E_g of TiO_2 in anatase phase is 3.2 Ev, and corresponds to UVA photons at 388 nm) (Ohama and Van Gemert, 2011). In addition to these, post treatment requirements such as separation of catalysts from waste water/slurry is also a setback. Notwithstanding, TiO_2 catalyst is highly stable in both acidic and alkaline solutions.

UV/H_2O_2 has found applications in both industrial and domestic water treatment systems. This is because; photocatalysis has been proven to oxidize refractory organics, which are otherwise not susceptible to biological treatment methods (Machulek Jr. et al., 2012). However, most research into the application of photocatalysis for water treatment have ended with laboratory scale trials, with a few commercial applications. This is due to problems with effective photocatalytic designs, related to poor reaction kinetics, mass transfer, light absorption etc (Ray, 1999; Ray and Beenackers, 1996).

Companies that have commercialised include: RayWox solar photocatalysis, (Observatory NANO 2010), Zentox Corporation (ozonation), Matrix Photocatalytic Inc. (UV/TiO_2), Clearwater Industries (solar oxidation system), Photox Bradford Ltd. (TiO_2), Lynntech Inc. (ozonation), Purifics Environmental Technologies Inc, (TiO_2 in slurry) etc.

(Gervens et at., 2007). Apart from purifics, the others appear to be small companies mostly in the product developmental stage. In addition, Clearwater Industries and Photox Bradford Ltd are offshoots of researches originally done at universities of Florida and Bradford respectively. In terms of environmental impact, photocatalysis especially for heterogeneous systems, results in lower impact on the environment owing to its versatility, the absence of sludge, absence of biofouling agents and reusability of catalyst. Although like most other systems, there is a potent risk of toxic by-products formation (Ibhadon and Fitzpatrick, 2013; Pueh, 2010), photocatalysis has found wide application in several other fields, some of which have found commercialization (Observatory NANO, 2011). Table 6.3 shows a summary of the various applications of photocatalysis, fields of application, effects and practical examples as given by Murakami and Fujishima, (2010).

Table 2.6: Applications of Photocatalysis (Akira et. al., 2000; Murakami and Fujishima, 2010; Observatory NANO, 2011).

Function	Basic Application	Primary effect	Practical examples
Oxidative decomposition	Air Cleaning	Deodorization VOC elimination NOx Elimination	Air cleaners, air conditioning, Road asphalt, crosswalk brick Blinds, curtains, wallpaper
	Water decontamination	Elimination of harmful substances, Elimination of persistent biological substances Eliminating Bacteria Degradation of organics.	River water, Ground water, Industrial wastewater, Nutrient solution cleaning, systems for hydroponic agriculture, Water cleaning device for lakes etc.
	Antibacterial applications and sterilization	Eliminating viruses, Sterilization and antibacterial action, Mold prevention, Elimination of hazardous substances	Walls and floors of hospital, operating rooms, interiors etc. Catheters Clothing such as uniforms, masks warfare chemicals
Super-hydrophilic properties	Anti-soiling, antifogging applications	Oil contamination elimination Prevention of fogging Self-cleaning	Buildings (tiles and paint) Tent films, Glass windows Automobile slide mirrors Sound barriers, cover glass, etc.
Water Cleaving	Power and Energy	Splitting of water molecule	Hydrogen production as clean energy

The focus of the present study is on oxidative photocatalytic decomposition potentials with respect to wastewater, highlighted in Table 2.6 above.

2.6 Application of Microwave (MW) Radiation in Advanced Oxidation Processes

The application of microwave radiation in AOP for the treatment of wastewater in less turbid wastewater streams is well documented (Sun and Pignatello, 1993; Herrmann et al., 1999; Remya and Lin, 2011; Baros et al., 2013). The details of the principle and mechanism of activation is discussed in detail in chapter six. It has found application in several organic synthesis reactions (Mohammadi, 2013) and in the acceleration of organic chemical reactions and in most cases, performed better than the conventional heating (Abramovitch, 1999; Strauss and Trainor, 1995). Gromboni et al., (2007) reported the coupling of MW to photo-Fenton reaction for the degradation of chlorfenviphos and cypermethrin where residual carbon content was monitored. Results showed over 98% removal in 4 min. The reaction parameters included 950 W MW power, Cadmium low pressure special lamps were used, In the reaction, microwave radiation was used to activate UV radiation, using special UV lamps developed by Florian and Knapp Germany. The lamps emission wavelengths was 228 nm. Reagent concentrations were as for a variable wastewater volume of 9 to 30 mL is as follows: 0.5–6.0 mL of H_2O_2 30% (m/v), and 1.0–4.0 g L^{-1} of Fe(II).

Remya and Lin, (2011) made a compilation of MW coupled processes at different experimental conditions and substrates with varying results as shown in Table 2.7 below.

Table 2.7: Studies of coupled MW with other AOPs. (Remya and Lin, 2011)

Contaminant and its type	Type of AOP	Reaction condition/chemical oxidation scheme	Degradation efficiency, % (time. min)	Mineralization efficiency, % (time. min)	Remarks
Residual water with clofenvinphos and cypermethrin	MW-photo-Fenton process	Waste water composition – 400:1 (v/v) of water and pesticide (13.8% (m/v) clofenvinphos and 2.6% (m/v) cypermethrin), volume – 10 mL, Fe(II) solution – 2.1×10^{-3} mol/L and H_2O_2 1.1 mol/L, MW output power – 950 W, temperature – 140 °C.	–	95	Without MW, only 86% of degradation was observed after 5 h of photo-Fenton process.
Pharmaceutical waste water	MW-Fenton like	Initial COD loading – 49912.5 mg/L, volume – 50 mL, H_2O_2 dosage – 1300 mg/L, $Fe_2(SO_4)_3$ dosage – 4900 mg/L, MW output power – 300 W, temperature – 28 °C, pH – 4.42.	–	57.53	1. MW-Fenton process improved the degradation efficiency and the settling of sludge. 2. In addition, it reduced the yield of sludge and improved the biodegradability of effluent.
Atrazine (organic compound with an s triazine-ring)	MW/UV (EDLs)	Initial concentration – 50 mg/L, volume – 50 mL, EDLs A – 254, 297, 313, 365, 405, 436, 546, 577 and 579 nm, light intensity – 9–10 mW/cm^2, MW output power – 900 W.	100	–	Dechlorination–hydroxylation mechanism is one of the main degradation mechanisms of atrazine.
Bromophenol blue (triphenyl methane	MW/UV (EDLs)	Initial concentration – 100 mg/L, volume – 50 mL, EDLs A – 400–760 nm, light intensity – 440 cd/m^2, MW output power – 900 W, temperature – 100 °C.	100		MW/UV could cause benzene ring open to generate aliphatic intermediates.
Acid orange 7 (AO7) dye)	MW/UV (EDLs)/H_2O_2	Initial concentration – 100 mg/L, volume – 750 mL, air – 0.15 m^3/h, MW output power – 700 W (continuous mode), temperature – 38 ± 1 °C.	~95	30	MW/EDL/H_2O_2 process was 32% more than H_2O_2/TEL (traditional electrode lamp) process in the degradation of AO7.
Phenol	MW/UV/H_2O_2	Initial concentration - 200 mg/L, volume – 300 mL, MW output power – 1 kW, temperature – 50 °C, low pressure Hg lamp 8W	90	95	MW irradiation increased both phenol conversion and TOC removal efficiency above 50%.

Phenol, chlorobenzene, nitrobenzene, 4-chlorophenol (4-CP), and	MW/UV/H_2O_2	Initial concentration – 10^{-3} mol/L (except PCP with concentration – 6×10^{-6} mol/L), H_2O_2 concentration – 5×10^{-3} mol/L, MW output power – 900 W, conventional high-pressure Hg discharge lamp – 400W, temperature – 20 °C.	–	–	1. Simultaneous MW/UV/H_2O_2 remediation was more efficient than MW/H_2O_2 and UV/H_2O_2 based treatments. 2. The degradation of phenol and chlorobenzene were increased respectively by a factor of 21 and 6 for MW/UV/H_2O_2 based treatment compared to the sum of degradation from MW/H_2O_2 and UV/H_2O_2 remediation. 3. Combined effect of MW and UV showed modest enhancement in the degradation of nitrobenzene, 4-CP and PCP.
2,4-Dichlorophenox (chlorophenoxyacetic herbicide)	MW/UV (EDLs)/TiO_2	Initial concentration – 0.04 mM, TiO_2 loading – 50 g/10 ml of 2,4-D solution, light irradiance – 2 mW/cm^2 with a wavelength of 314, 366, 405, 436, 546 and 577 nm, MW output power – 700 W, temperature – 200 °C, pH – 4.9.	100	–	The rate of degradation (2×10^{-3} mM/min) showed that the MW/UV/TiO_2 was 10 times more efficient than photocatalytic method.
Methylene blue (MB) (heterocyclic aromatic compound)	MW/UV (EDLs)/TiO_2	Initial concentration – 100 mg/L, volume – 50 mL, TiO_2 loading – 0.1 mg, EDLs A – 250–760 nm, MW power – 900 W, temperature – 100 °C, pH – 7.	96	50	The decomposition of MB could be by the enhanced production of active radicals.
Bisphenol A (BPA) (endocrine disruptor)	MW/UV (EDLs)/TiO_2	Initial concentration – 0.1 mM, volume – 30 mL, TiO_2 loading – 60 mg, light irradiance – 0.9 mW/cm^2, MW output power – 1.5 kW, temperature – 150 °C, pressure – 1 MPa, pH –6.7	–	100	MWPC two-fold faster mineralization compared to the photocatalysis method because of the accelerated generation of the highly oxidizing OH.

2.7 Application of AOPs in Oily Wastewater or Produced Water Treatment

AOP is considered an emerging technology in produced water management because not much work has been undertaken in this field. Most studies done so far have not gone beyond pilot scale trials. The application of conventional Fenton reagent for the treatment of refinery waste at laboratory scale, where total petroleum hydrocarbon (TPH) was monitored has been reported by Hasan et al., (2014). TPH reduction rate of 36.47% was recorded. Further reduction of TPH by 73.07% was achieved by dilution, with the addition of 40 mL water per gram of the oily sludge under optimized conditions.

Conventional Fenton reaction has also been applied at laboratory scale for the remediation of simulated produced water for the removal of PAH – Naphthalene (Ma et al., 2014), where 98% removal was recorded at optimum experimental conditions after 60 minutes.

At industrial scale, ESCO international recently applied AOP using ozone and UV at pilot scale for the treatment of produced water, which lowered the COD from 300 mg/L to acceptable levels of less than 50 mg/L, with oil concentrations dropping from 20 mg/L to less than 0.1 mg/L. After what they described as successful trials, they are now involved with the design of an AOP treatment plant, capable of handling flowrates of 900 m^3/h produced water effluents (ESCO International, 2014). However, they did not study the dissolved organics such as alkyl phenols. UV disinfection using TiO_2 as catalyst has also currently been applied at industrial scale to deal with common oil production environment bacteria, such as sulphate reducing bacteria, acid producing bacteria and

slime forming bacteria, which can cause H_2S intrusion in oil wells and corrosion (ATG UV Technologies, 2017).

The use of heterogeneous Fenton catalysis for the treatment of produced water is not reported, save for refinery wastewater, whose characteristics mirrors that of produced water but which is clearly different in composition. No attempts at simultaneous application of UV-Fenton-MW in a heterogeneous Fenton-like process for the degradation of produced water from oil and gas production been done to the author's knowledge and this forms the focus of the present study.

The disadvantages of AOPs include high operating costs resulting from the cost of reagents for poorly optimised processes, slightly high capital costs reduced efficiency (depending on the type of process; mainly homogeneous or heterogeneous). There is also a problem of the formation of potentially toxic recalcitrant reaction intermediates, reduced efficiency from turbid wastewater (as with photochemical systems), etc.

2.8 Modified Heterogeneous Polyacrylonitrile (PAN) Catalyst

Due to the merits associated with the application of heterogeneous catalysis over the homogeneous, such as: easy separation from reaction effluent, low cost, ease of preparation, ease of regeneration, and a potentially extended pH range, there has been tremendous interest focused on the synthesis of heterogeneous Fenton like catalysis. This interest has been directed mostly at modification of fibres especially PAN (Li et al., 2013; Han et al., 2011; Vitkovskaya et al., 2003), owing to its durability and structural strength such as elastic resistance to most oxidants, mineral acids and heat (Choudhury 2006; Dong et al., 2010). This modification process involves the impregnation of

catalytically active transition metal complexes on the functionalized surface of PAN fibres. Transition metals are preferred in this application because of their partially filled d orbitals making them highly reactive (Hagen, 2000).

Studies at De Montfort University has led to further development of a novel fibrous heterogeneous PAN catalyst, through the immobilization of a catalytically active Fe^{3+} on the surface of the functionalized polymer. The presence of chemically highly reactive nitrile groups on the polymer, allowed functionalisation with a mixture of hydroxylamine and hydrazine salts in alkaline solution to form chelating ligands (carboxylilate, amins and oxime) (Ishtchenko et al., 2003; Vitkovskaya et al., 2003). This indigenous catalyst has been successfully tested for the oxidative decomposition of several waste effluents from pharmaceutical, textile, agrochemical, etc., and other model compounds at laboratory scale in a heterogeneous Fenton-like process using H_2O_2 as oxidant (Chi et al., 2013; Chi & Huddersman, 2011; Chi and Huddersman, 2007). Pilot scale trials on oestrogen removal from municipal waste stream and remediation of landfill leachate has also been reported. A Recent pilot trial in the application of the fibrous material (before impregnation with the Fe_3^+ catalyst) allowed its use as an ion exchange material, which has also been hugely successful for metal uptake (Upreti et al., 2016). The present study focuses on the application of this modified PAN catalyst for the simultaneous removal of alkylated phenols and oils from oil and gas produced water, in a Fenton-like oxidation process and in a UV/microwave assisted Fenton oxidation process as a potential technique for produced water treatment.

2.9 Fenton/Fenton-like Reactions

Fenton reaction involves the use of Fenton's reagent, which is an aqueous solution of hydrogen peroxide and ferrous iron (Fe^{2+}), for the decontamination of organic pollutants. This was first reported by Henry John Fenton in 1894 (Machulek Jr. et al., 2012). Fenton-like processes as described earlier involves the use of other transition metals or some form of adaptation or modification of the catalyst source. The mechanism of the classic Fenton reaction according to Fenton, H. J. (1894), is based on advanced oxidation process, which has already been discussed. However, the species responsible for oxidation in the classic Fenton reaction has remained a subject of controversy; whether this reaction is based on a radical pathway or a ferryl route. The number of reaction equations as well has been a subject of this controversy. Some reactions that best describe possible reactions occurring in Fenton or Fenton-like processes have however been generally accepted by most studies and these few reactions have been divided into three groups (Hasan et al., 2014; Hermosilla et al., 2009; Pignatello et al., 2006; De Laat and Gallard, 1999) as follows

i. Reactions of inorganic species which include Fe^0, Fe^{2+}, Fe^{3+}, H_2O_2 , $^{\bullet}OH$ and $HO_2^{\bullet}$. The equations in this category are;

$$Fe^0 + H_2O_2 + 2H^+ \rightarrow Fe^{2+} + 2H_2O \text{ (not used in this work)} \quad (2.1)$$

$$Fe^{2+} + H_2O_2 \rightarrow Fe^{3+} + OH^- + {}^{\bullet}OH \quad (2.2)$$

$$Fe^{3+} + H_2O_2 \rightarrow Fe^{2+} + HO^{\bullet}{}_2 + H^+ \quad (2.3)$$

$$Fe^{2+} + {}^{\bullet}OH \rightarrow Fe^{3+} + OH^- \quad (2.4)$$

$$Fe^{3+} + HO^{\bullet}{}_2 \rightarrow Fe^{2+} + O_2 + H^+ \quad (2.5)$$

ii. Reactions of reactive species in equations (2.6 to 2.10) with organic substrates, which include contaminants and by-products. These include;

$$RH + {}^{\bullet}OH \rightarrow R^{\bullet} + H_2O \quad (2.6)$$

$$R^{\bullet} + Fe^{3+} \rightarrow R^{+} + Fe^{2+} \quad (2.7)$$

$$R^{\bullet} + Fe^{2+} + H^{+} \rightarrow RH + Fe^{3+} \quad (2.8)$$

$$R^{\bullet} + H_2O_2 \rightarrow ROH + {}^{\bullet}OH \quad (2.9)$$

$$R^{\bullet} + O_2 \rightarrow ROO^{\bullet} \quad (2.10)$$

iii. The Third set of reactions according to Hasan et al., (2014) and Kusic et al., (2006) are reactions which are otherwise known as the side reactions or scavenging reactions. These are;

$$H_2O_2 + {}^{\bullet}OH \rightarrow HO^{\bullet}{}_2 + H_2O \quad (2.11)$$

$$HO^{\bullet}{}_2 + {}^{\bullet}OH \rightarrow H_2O + O_2 \quad (2.12)$$

$${}^{\bullet}OH + {}^{\bullet}OH \rightarrow H_2O_2 \quad (2.13)$$

2.10 Summary of Literature Review and Literature Gaps

Several established techniques for wastewater treatment currently in use at industrial scale are well documented; however, there is limited literature on the application of Fenton/Fenton-like oxidation for the treatment of produced water or related waste stream. Most of the current techniques are able to remove suspended or dispersed oils through physical means (absorption, separation and gravity methods). The use of filtration membranes has been useful for the removal of chloride and other dissolved organic compounds; however, cost and frequent fouling have hindered the application

of this technique. In addition, most of the techniques capable of removing dissolved organic components and suspended oils are mere phase transfer processes and not mineralization.

The application of a Fenton-like technique appears to be a promising technique and its efficiency can be enhanced by the use of coupled technologies such as UV and microwave radiations. The next chapter, (chapter three) deals with the catalysis of DMP in water using the PAN heterogeneous catalyst in H_2O_2 system both in batch and in continuous flow regime.

3 Catalytic Degradation of 3,5-Dimethyl Phenol (DMP) Using a Modified Heterogeneous PAN Catalyst in a Fenton-Like Process – *Reaction Process Optimization*.

3.1 Introduction

This chapter focuses on the catalytic degradation of DMP in both batch and continuous flow modes. It presents the reaction optimization process using the one-factor-at-a-time model (OFAT), in batch mode, and the optimised conditions from the batch process are further applied in a continuous flow mode, where the effects of process parameters on the treatment process have been investigated. In addition, it details the source, type and quality of the materials used for the study of the Fenton-like catalytic degradation of hydrogen peroxide and DMP, which has the structural formula shown in Figure 3.1.

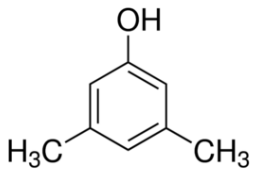

Figure 3.1: Structural formula of DMP

Furthermore, this chapter documents and justifies the choice of the analytical methods employed in monitoring the reaction process and the experimental procedures adopted. The process optimization of the decomposition of hydrogen peroxide and DMP which represents a model alkylphenol found in produced water, catalysed by a PAN heterogeneous catalyst is intended to establish the best conditions for this process which would form a basis for scaling up the reaction process.

3.2 Aims

- To establish the optimum reaction conditions in batch mode for the process parameters such as concentration of H_2O_2, amount of catalyst, temperature, pH of reaction solution, concentration of substrate.
- To scale-up the batch process in a continuous flow system.
- To make inferences on the oxidation route (radical or ferryl) by incorporating a known radical scavenger in the reaction solution.
- To draw significant conclusions and make recommendations.

3.3 Experimentation

Alkyl phenols generally have high polarity and low volatility (Yang Bai-Juan et al., 2007). However, their chemical properties in water vary as the substituent on the aromatic ring changes (Burin et al., 2011). This makes analysis of this class of compounds challenging for analytical chemists. According to Lee, (2000) and Burin et al., (2011), HPLC is the most reliable analytical method for the analysis of phenols in water, using C18 reverse-phase columns, UV detection systems and polar organic solvents. Bravo et al., (2006) reported the use of both reverse phase and normal phase chromatography in the analysis of phenols in water where he noted that separation in the reverse phase was based mainly on the hydrophobicity. Accordingly, the longer the carbon chains of the alkyl groups of phenols, the longer the retention time for the analyte. For normal phase however, he maintained that separation was based on geometry and polarity, making it

easy for separations between isomers. He also noted that peak overlap was a common phenomenon to both reverse and normal phase columns.

3.3.1 Instrumentation for Batch Work

3.3.1.1 High Performance Liquid Chromatography (HPLC)

Chromatography in general terms is an analytical method which involves the separation of the constituents of a mixture by passing the mixture of compounds (either in liquid or gaseous matrix) through a chromatographic column of immobilized stationary phase, aided by a mobile phase usually a solvent (HPLC) or a combination of gases (GC) (Kupiec, 2004). Separation is achieved by selective interaction between the constituents of the mixture and the stationary phase.

A Perkin Elmer series 200 HPLC with a UV detection system was used for monitoring DMP degradation using the following instrumental parameters; the column was a C18 250 mm x 4.6 mm with internal packing of 5 µm aggregates purchased from Phenomenex. Isocratic gradient mobile phase of acetonitrile and water (40:60 v/v) in 1 L solvent bottle was used. The injection volume was 40 µL, with a loop volume of 20 µL. The detection wavelength was 210 nm and flow rate was 1 mL/min with a total run time of 6 min.

3.3.1.2 DMP Calibration Using HPLC

Equipment calibration was carried out as follows: 25 mg/L of DMP was used for preliminary studies. 1000 mg/L standard stock solution was prepared in double distilled water by first dissolving 0.1 g of DMP in 100 mL volume. The DMP standard was carefully weighed out into a 100 mL volumetric flask and made up to mark with double distilled

water. The solution was then sonicated for 60 min to achieve faster and complete solubilisation. Working standards of 5, 10, 15, 20, and 25 mg/L were prepared in triplicates by serial dilution from the standard stock and analysed in the HPLC using the instrument conditions specified in section 3.3.1. The calibration graph is as shown in Figure 3.2.

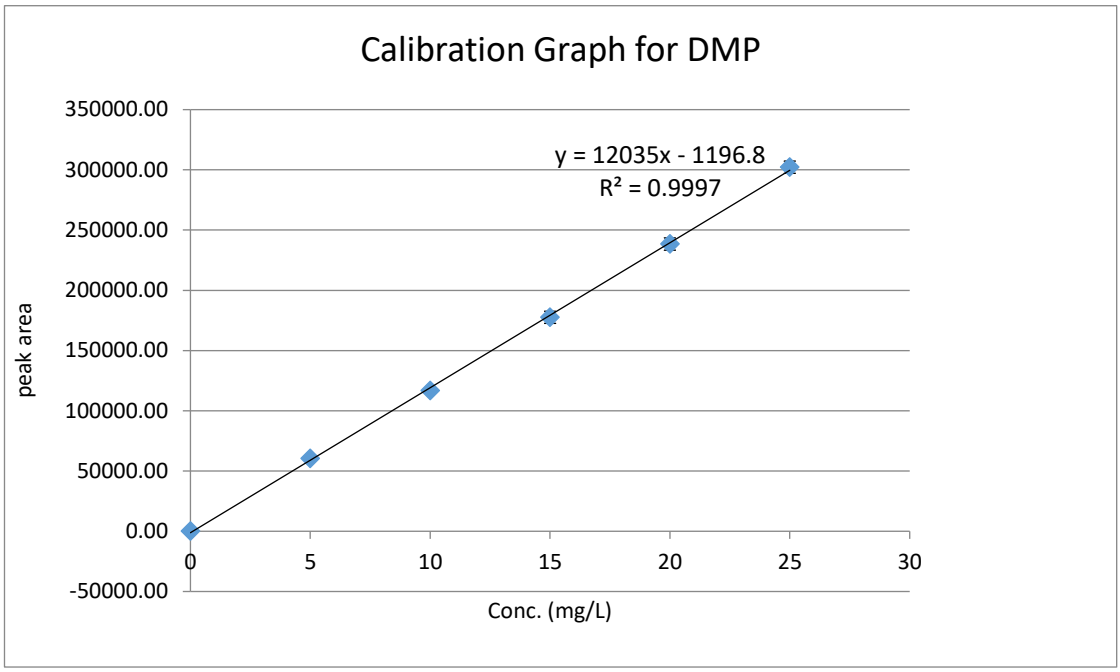

Figure 3.2: Calibration graph for DMP analysed by HPLC-UV detection method

3.3.1.3 Hydrogen Peroxide Calibration using HPLC

Equipment calibration for H_2O_2 was done using 30% w/v H_2O_2 solution purchased from Fisher scientific UK. The seven- point calibration spanned from 25 mg/L to 1500 mg/L made up in double distilled water, averaged from duplicate injections in the HPLC. The instrument parameters and chromatographic conditions used in the HPLC for H_2O_2 determination/quantification are same as those described in section 4.3.1.1. Peak retention time was 2.5 min. The calibration graph is as shown in Figure 3.3.

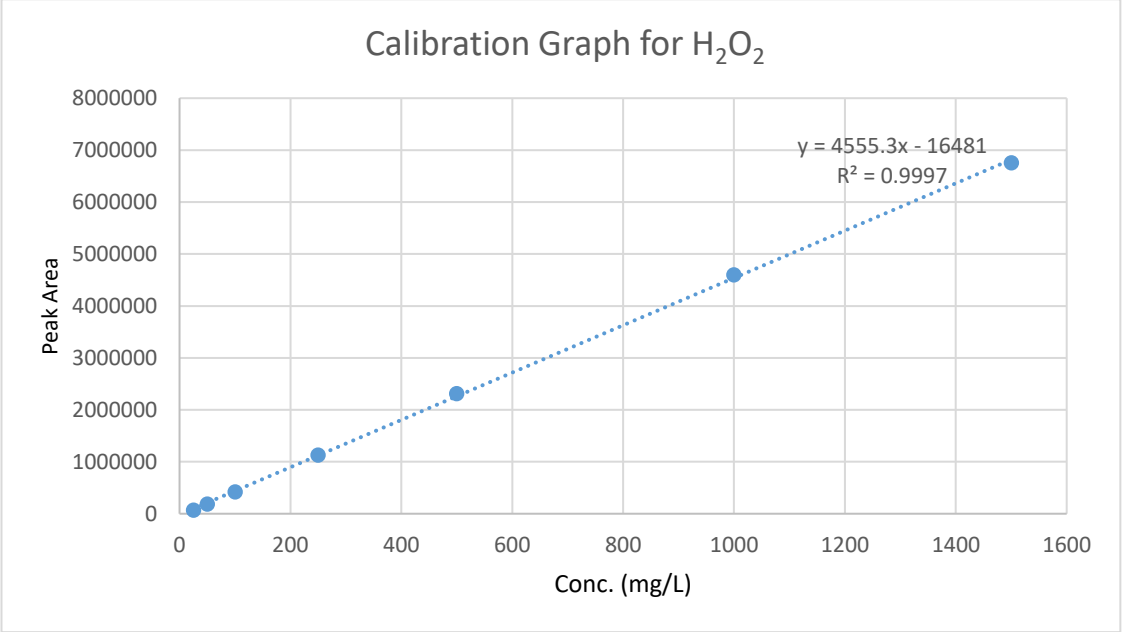

Figure 3.3: Calibration Graph for H_2O_2 using HPLC. Calibration standards were prepared as per section 3.3.1.2

3.3.1.4 Analysis of Chemical oxygen Demand (COD) Using Spectrophotometry

The chemical oxygen demand COD, was monitored using spectrophotometry reference method –COD cuvette test ISO 15705 with cuvette vials product code LCI 400, measuring range 0 – 1000 mg/L for DMP in water. 2 mL of sample was pipetted into the specified vial after shaking the vial for proper mixing of constituents. This was again agitated after sample introduction to enable proper mixing of the sample with the constituents of the vial. The vial was then placed in a Hach Lange LT200 heating block, pre-set for COD analysis (148 ^{o}C for two hours). The solution was cooled to room temperature and COD was measured directly on a DR 3800 Hach Lange spectrophotometer. To compensate for H_2O_2 interference in the COD values, contribution of H_2O_2 to COD was done. This was achieved by HPLC determination for residual H_2O_2. The concentration of H_2O_2 determined by HLPC was applied in the calibration graph equation of H_2O_2 Vs COD. The

determined value (which is equal to the H_2O_2 contribution to COD) was then subtracted from the measured COD in reaction solution, to get the actual COD. A calibration graph of the contribution of H_2O_2 to COD is presented in Figure 3.4.

The HPLC method was evaluated and compared with the colorimetric method for the determination of H_2O_2 using titanium sulphate and similar results were obtained. The calibration graph for the colorimetric method and H_2O_2 method have been presented in Figure 3.5. The results were validated by plotting H_2O_2 calibration by HPLC against, H_2O_2 calibration absorbances determined by UV-Visible titanium sulphate method and the R^2 of the graph which is expected to be 1, was 0.99, suggesting a reasonable goodness of fit (Figure 3.6).

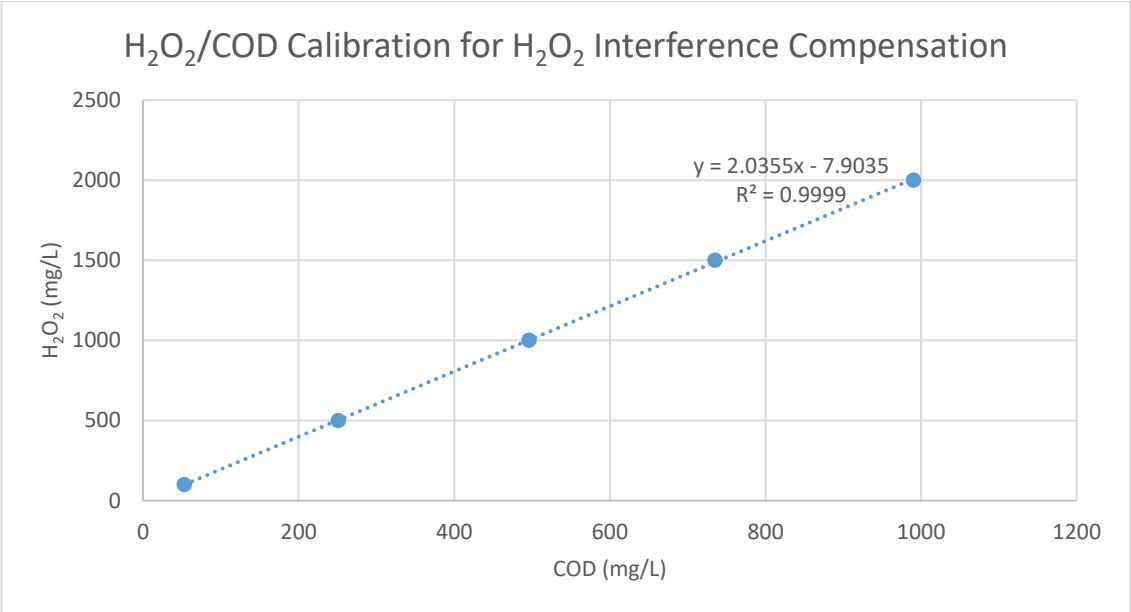

Figure 3.4: Calibration curve for the contribution of H_2O_2 to COD. H_2O_2 standards prepared in double distilled water, ranging between 50 and 1000 ppm were analysed in DR 3800 Hach Lange spectrophotometer.

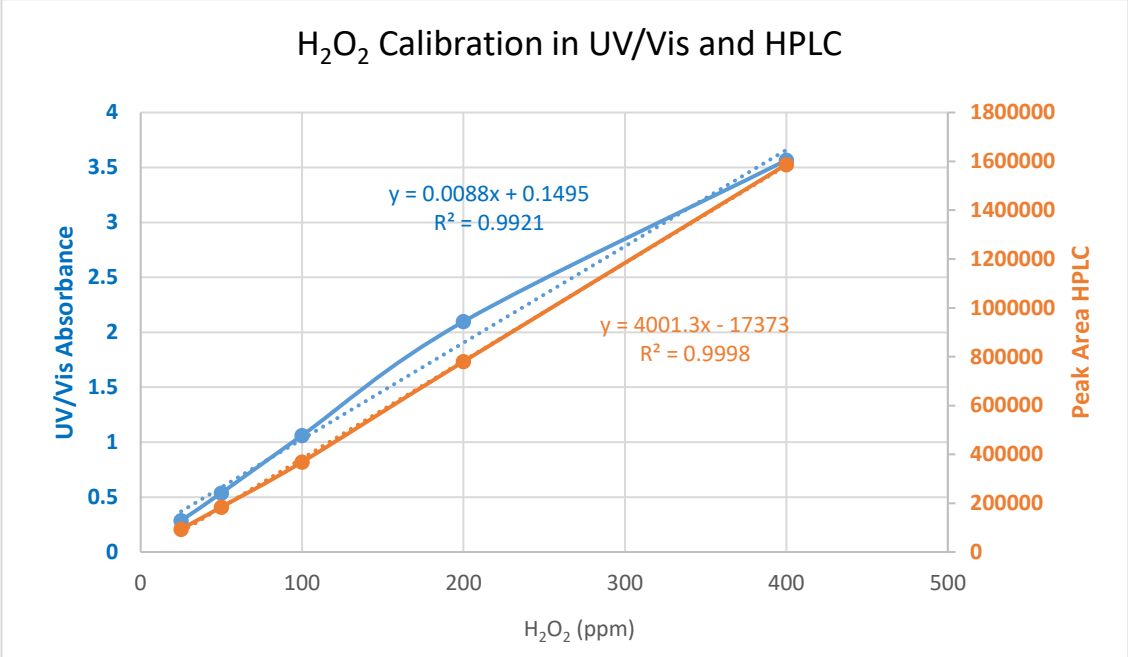

Figure 3.5: Calibration graph for both colorimetric and HPLC determination of H_2O_2

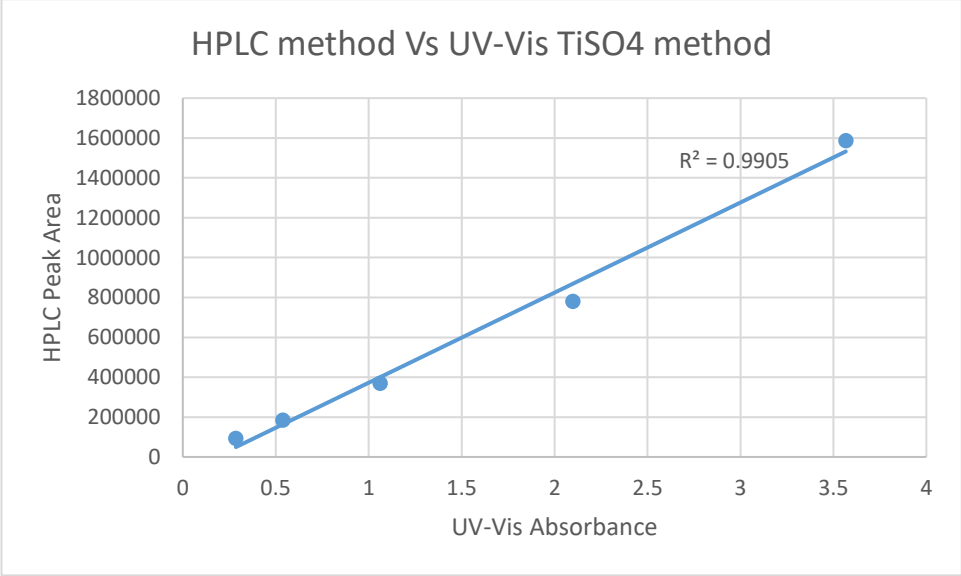

Figure 3.6: Validation plot with respect to the UV-Vis $TISO_4$ method for the use of HPLC analytical method in the determination of H_2O_2.

The calorimetric method was first reported by Eisenberg in 1943. Essentially, the $Ti(SO_4)_2$ colorimetric method is based on the photoelectric measurement of the intense yellow

colour intensities, resulting from the formation of pertitanic acid, which is a product of the reaction between H_2O_2 and titanium sulphate reagent according to equation 3.1 below. The reagent solution was prepared according to the protocol described by Eisenberg, (1943).

Briefly, 1 g of anhydrous titanium dioxide was digested in 100 mL of sulphuric acid for 16 hours at a temperature of 150 ^oC. The cooled solution was diluted four folds using double distilled water. This was then filtered using qualitative filter paper (150 mm) before use. The same calibration standards used for the HPLC H_2O_2 calibration were used to calibrate the UV-Vis spectrophotometer and the calibration graphs are presented in Figure 3.5 above.

$$Ti^{4+} + H_2O_2 + 2H_2O \rightarrow H_2TiO_{4\ (pertitanic\ acid)} + 4H^+ \quad \ldots (3.1)$$

3.3.2 Analytical processes for Continuous flow experiments

For the continuous flow experiments, loss of DMP and H_2O_2 were monitored on the HPLC and leached iron from the catalyst was measured by AAS. The conditions for these analytical techniques have been described in more detail previously and below.

3.3.2.1 HPLC Analysis

A Perkin Elmer series 200 HPLC with a UV detector was used for monitoring of DMP loss using instrumental parameters previously described in section 3.3.1.1.

3.3.2.2 Analysis of Total Iron Leached into Reaction Solution and on the Catalyst

The leached iron concentration for the reaction process was monitored using a PerkinElmer flame atomic absorption spectrometer (AAS) AAnalyst 200 model. The calibration showed a good linearity between 0.25 and 10 mg/L using a 1000 mg/L standard stock, from which working standards between 0.25 and 10 mg/L were made up in double distilled water and used for the calibration. A six-point calibration on this instrument gave an R^2 value of 0.996 as presented in Figure 3.7. This calibration range was chosen after preliminary tests showed that iron leached from the catalyst during the reaction fell within the concentration range and that the range was linear.

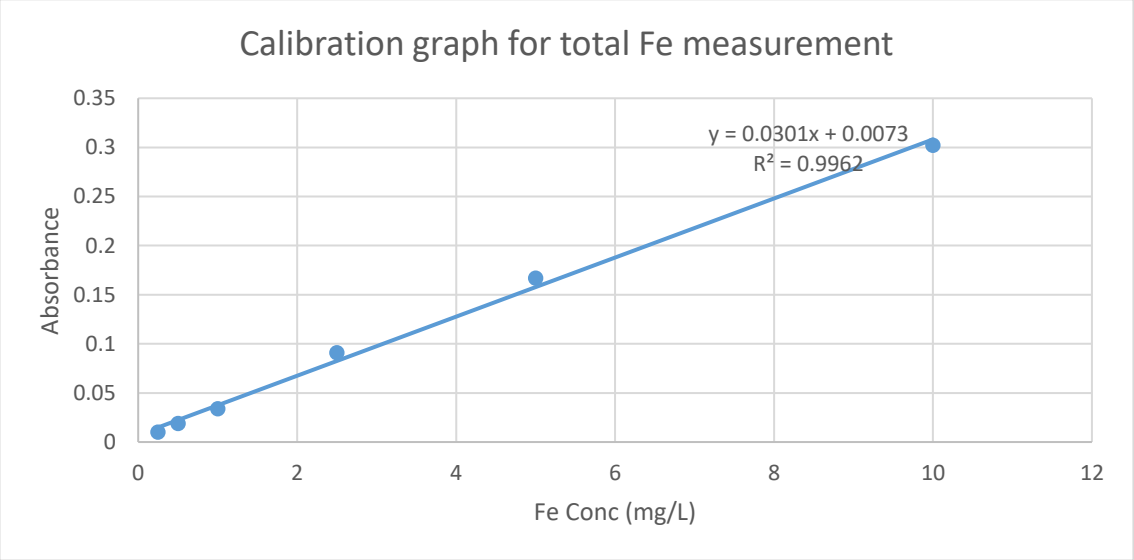

Figure 3.7: Calibration graph for the determination of total Fe using AAS

Table 3.1: Chemicals, Reagents and materials

Chemical/reagent	**Chemical Formula**	**Molar mass (g)**	**% Purity**	**Source**
Acetonitrile	CH_3CN	41	>99	Sigma Aldrich
Double distilled water	H_2O	18		DMU-Fistreem Cyclon: WSC044
Hydrochloric acid	HCl	36	35	Sigma Aldrich
3,5-Dimethyphenol	$(CH_3)_2C_6H_4$	122	>99	Sigma Aldrich
Sodium Hydroxide	NaOH	40	98	Sigma Aldrich
Acetic Acid	CH_3COOH	60	99	Sigma Aldrich
Hydrogen Peroxide	H_2O_2	34	30	Fisher scientific
Dichloromethane	CH_2Cl_2	85	99.9	Sigma Aldrich
Methanol	CH_3OH	32	99	Sigma Aldrich
Titanium dioxide	TiO_2	79	99.5	Sigma Aldrich
Sulphuric acid	H_2SO_4	98	95-98	Sigma Aldrich
Qualitative filter paper			QL 100	Fisher scientific

Other materials are Marlow series 101U peristaltic pump, Clark Boxer compressor pump and P1000 Gilson pipette. A Jenway-350 portable pH meter was used for pH monitoring while a Kern PLJ 2100-2M weighing balance was used to weigh out PAN catalytic mesh and substrate.

3.4 Experimental Methodology

3.4.1 Substrate Preparation:

500 mg/L stock solution was prepared by carefully weighing out 100 mg of DMP pure standard, into 200 mL flask and making it up to mark with double distilled water. 200 mL of 25 mg/L solution of the model organic pollutant (DMP) was then prepared from the 500 mg/L stock solution by carefully measuring out 10 mL from DMP stock into a 200 mL volumetric flask and making up to mark with double distilled water. 200 mL of DMP was prepared to enable duplicate catalytic runs and the average results were reported.

3.4.2 Catalyst Normalisation

About 50 g of PAN catalytic mesh was carefully cut and washed gently with water to remove loose material (including loosely held iron) and air-dried at room temperature. The catalyst mesh was then immersed in a 1000 mL beaker filled with double distilled water, which was then gradually adjusted to desired pH using 0.1M HCl and /or 0.1 M NaOH. The mesh was then removed from solution and air-dried after the pH was observed to be stable over one hour.

3.4.3 Experimental Procedure for Catalysis of 3,5-DMP with H_2O_2 in Batch Mode

The normalised PAN catalyst mesh was cut and weighed out to predetermined weights of between 2 g to 6 g (1 g of yarn contains 0.272 mmol/g of PAN mesh). From 200 mL of 25 mg/L DMP solution, 100 mL each was transferred into two 250 mL reactors (thermostatted Radley carousel). The catalytic reaction was then initiated by the addition of 400 ppm H_2O_2 into the reactor vessels containing the substrate solution and the catalyst. The initiation reaction step is as shown in equation (2.3).

Samples were taken at predetermined intervals of 15 min to monitor the loss of both DMP and the H_2O_2. The first sample (0 min) was taken before the introduction of catalyst, subsequently, the required amount of catalyst was introduced into the 100 mL DMP solution, the pH of the solution (catalyst and substrate) was checked and adjusted to desired pH and H_2O_2 was introduced. Stirring was achieved by using a stirring bar (flea) in the reactor, set to 400 rpm to ensure proper mixing. The reaction was timed to ensure regular sampling intervals. The effect of temperature was investigated between 10 and 40 ^oC, and the effect of H_2O_2 concentration was investigated between 0 and 600 ppm. The effect of pH was also investigated from pH3 to pH9, while the effect of substrate concentration was examined between 25 and 100 mg/L. The effect of a hydroxyl radical scavenger on the reaction was investigated by the addition of tertiary butyl alcohol at concentrations between 20 and 2500 mg/L. Finally, the effect of catalyst concentration was investigated by loading between 2 g and 6 g of catalyst.

3.4.4 Experimental Procedure for Continuous Flow Experiments

The experimental rig for this process is as presented in Figures 3.8a and 3.8b (photograph of reactor set up and sketch of reactor set up respectively). In total, two continuous flow experiments were conducted for the oxidation of DMP using the modified PAN heterogeneous catalyst. The initial experiment was designed for process optimization to get the best conditions for the treatment process (Pinheiro and Wagner, 2001). The optimised conditions were then scaled up, and applied in the second continuous flow experiment.

The reactor used for the continuous flow experiments was a cylindrical borosilicate glass reactor, stacked vertically using clamps, and measuring 20 cm in length with an internal diameter of 1.5 cm. It consisted of an outlet and an inlet at the top and bottom of the reactor for treated effluent and influent respectively. The structure of this reactor was consistent with a plug-flow reactor system, but unlike conventional plug-flow reactor systems, mixing was in the axial direction (one end to the other or back to front) not radial, using a Clark Boxer compressor pump, delivering air at a rate varied between 6 and 10 cm^3/min from the bottom of the reactor.

Most catalytic reactor systems operate as plug-flow processes, where the concentration of reactants varies throughout the tube length, and hence the reaction rate also varies except for zero order reactions (Rosen, 2014). Where the catalyst is impregnated on a solid support as in this case and interacting with fluid phase reagents, the rate of catalytic reaction is proportional to the exposed area, efficiency of diffusion of reagents and the degree of turbulent mixing (Ibragimov, 2011; Bird et al., 2002; Fogler, 2006; Forni, 1999).

For the first experiment, 12.5 g of catalyst was cut into round discs and stacked centrically, in a vertical fashion along the column of the reactor. Baffles were created using perforated plastic material cut into the same round shape as the catalysts discs but of slightly larger diameter, which fitted tightly into the reactor. These were held in place by a plastic string, fixed centrally in the reactor.

The feedstock (substrate solution) made up of 50 mg/L DMP and oxidant solution – 800 ppm H_2O_2, was delivered from separate influent tanks into the 300 mL capacity reactor,

via silicone tubing of outside diameter, 4.8 mm and inside diameter of 2 mm. The reaction volume was 200 mL. The solutions of DMP and H_2O_2 were delivered into the reactor via peristaltic pumps at a variable flow rate of 0.3 to 0.82 mL/min to achieve a variable residence time, giving a reacting substrate concentration of 25 mg/L of DMP and 400 mg/L H_2O_2 after combination in the reactor.

Fresh feedstock was replenished as required, while the process parameters (flow rate or residence time, H_2O_2 concentration and air flow rate) were monitored and optimised for the first continuous flow reaction, to get the optimum conditions which were then used for the repeat experiment.

Figure 3.8a: Photograph of continuous flow reactor set up for DMP degradation

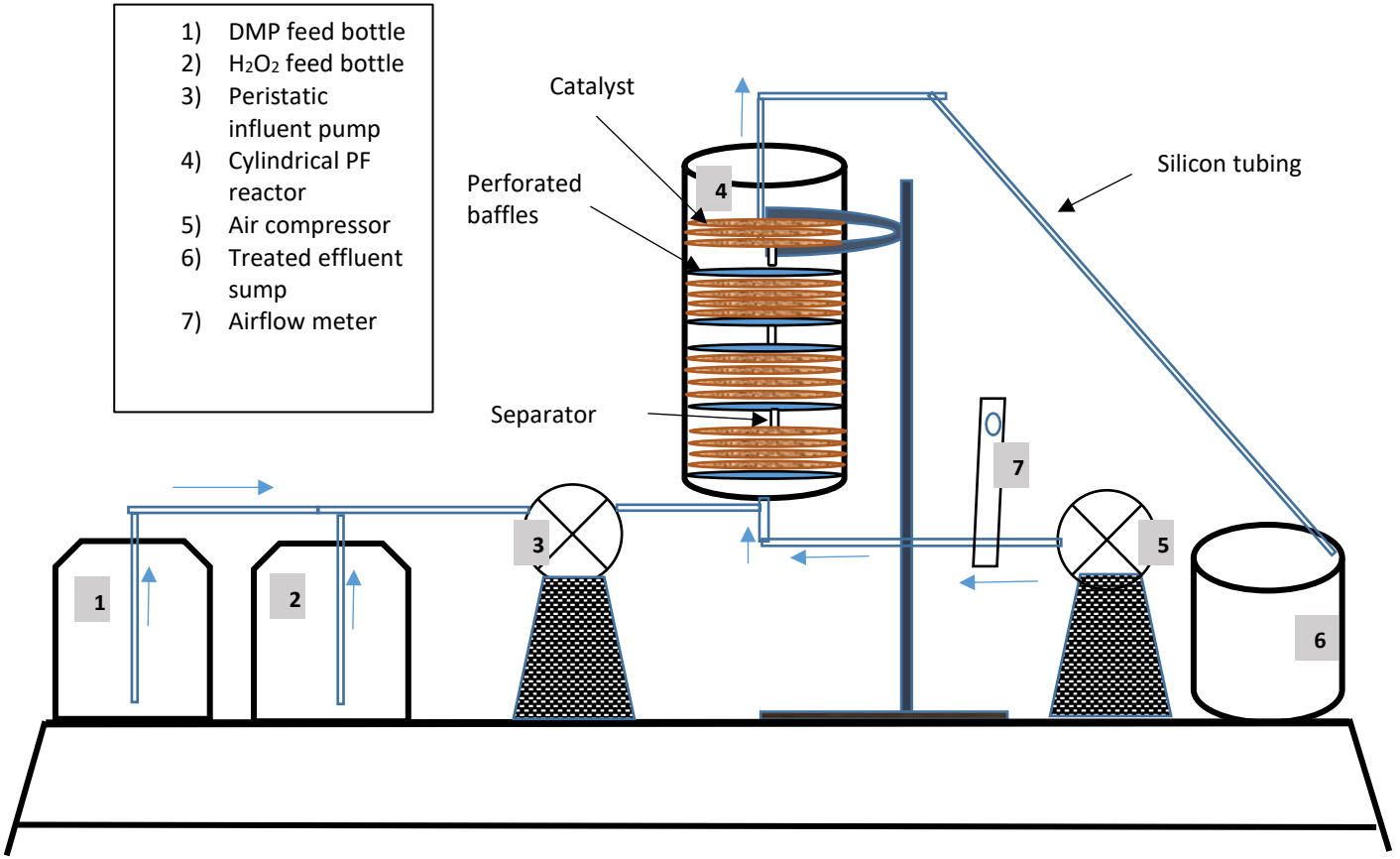

Figure 3.8b: Continuous flow reactor set up for DMP degradation

3.4.5 Experimental procedure for the Determination of Leached Iron and amount of iron on Mesh

To determine the iron leached into the reaction solution, sample volumes of 20 mL were collected in plastic bottles, from treated effluent, acidified to pH 2, and analysed on the AAS to get the leached iron into reaction solution.

The amount of Iron held on the mesh was determined as follows; 0.1 g of yarn was carefully untwined and digested in 25 mL vials to which 10 mL of concentrated HCL was carefully transferred (in 4 replicates). All four vials were tightly stoppered, placed on a digestion-heating block and heated at 150 ^{o}C for two hours. This was allowed to cool down to room temperature and the contents of each of them was transferred into a 100 mL volumetric flask by passing the contents over a glass funnel fitted with quantitative filter paper and the residue was rinsed with 10 mL of 2 M HCl. The filtrates were made up to mark with double distilled water in the 100 mL volumetric flask. 1 mL of filtrate solution was withdrawn into a 10 mL volumetric flask using an auto pipette and made up to mark. This was then analysed on the AAS.

3.4.6 Evaluation of the Extent of Homogeneous Contribution by Leached Iron

Extent of homogeneous contribution to the heterogeneous system was investigated. To do this, at the end of the experiment (after two hours), the catalyst was removed from the solution and both the main and duplicate reaction solutions were mixed together and agitated. 0.45 µm syringe filter was used to filter out 15 mL solution to test for total iron leached using the AAS. The solutions were then acidified and tested for total iron content. This procedure was repeated as duplicate.

The experimental procedure was repeated under the same conditions but this time, at the end of the experiment, the catalyst was removed from solution and the solution was reconstituted to 25 mg/L of DMP and pH, adjusted to 3.0. The total loss of peroxide from the reacting solution was determined by HPLC and calculated to be 35% which corresponds to 140 mg/L and which is equivalent to the theoretical peroxide demand for the complete oxidation of 25 mg/L of DMP (section 3.4.5 below). 42 µL of 30% by weight H_2O_2 was then carefully measured out into the same solution to initiate a fresh catalytic reaction where the only catalyst present was the leached iron (this formed the post-run reaction solution).

A similar reaction solution using freshly prepared $Fe_2(SO_4)_3.7H_2O$, of concentration 0.8 mg/L, equivalent to the measured iron leached into solution from the catalyst to evaluate the contribution of homogeneous leached iron to the catalytic oxidation reaction.

3.5 Results and Discussions for Batch Reactions

3.5.1 Theoretical Peroxide Demand for Mineralization of 25 mg/L DMP

The amount of H_2O_2 in moles, theoretically required to completely oxidize a mole of an organic compound in this case DMP (Figure 3.8, RMM 122 g/mol) is the theoretical peroxide demand. This was calculated mathematically as shown to serve as a guide.

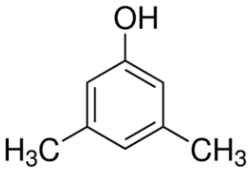

Figure 3.8: Chemical Structure of 3,5-DMP

For 25 mg/L DMP in 100 mL reaction volume, = 25 mg/L, = 2.5 mg/100 mL

$C_8H_{10}O + 10O_2 \rightarrow 8CO_2 + 5H_2O$ … (3.2)

$2H_2O_2 \rightarrow 2H_2O+O_2$ … (3.3)

2 moles $H_2O_2 \rightarrow$ 1 mole O_2 + 2 moles H_2O … (3.4)

25 mg DMP/122= 0.205 mmoles/L DMP

0.205 mmoles/L DMP ∴ requires 0.205 x 20 x 34 mg/L H_2O_2

H_2O_2 =139.4 mg/L

3.5.2 Effect of pH on the Decomposition of 3,5-DMP

Hydrogen ion potential (pH) is the most important process parameter in Fenton reaction (Bishop et al., 1968). It plays a crucial role in Fenton chemistry reactions and accounts for the catalyst's stability, reactivity, solubility (for homogenous), type of radicals

formed and as a consequence, the efficiency of the degradation process (Pignatello et al., 2006; Petri et al., 2011).

The catalytic degradation of 3,5-DMP and H_2O_2 at various pH values over time is as shown in Figures 3.9 and 3.11 respectively. The fastest rate of loss of DMP was observed at pH3 as shown in Figure 3.9 and this is in agreement with Gulkaya et al., (2006), Tamimi et al., (2008), and Emami et al., (2010). In their case, however, Fe^{2+} was used as catalyst in a homogeneous system.

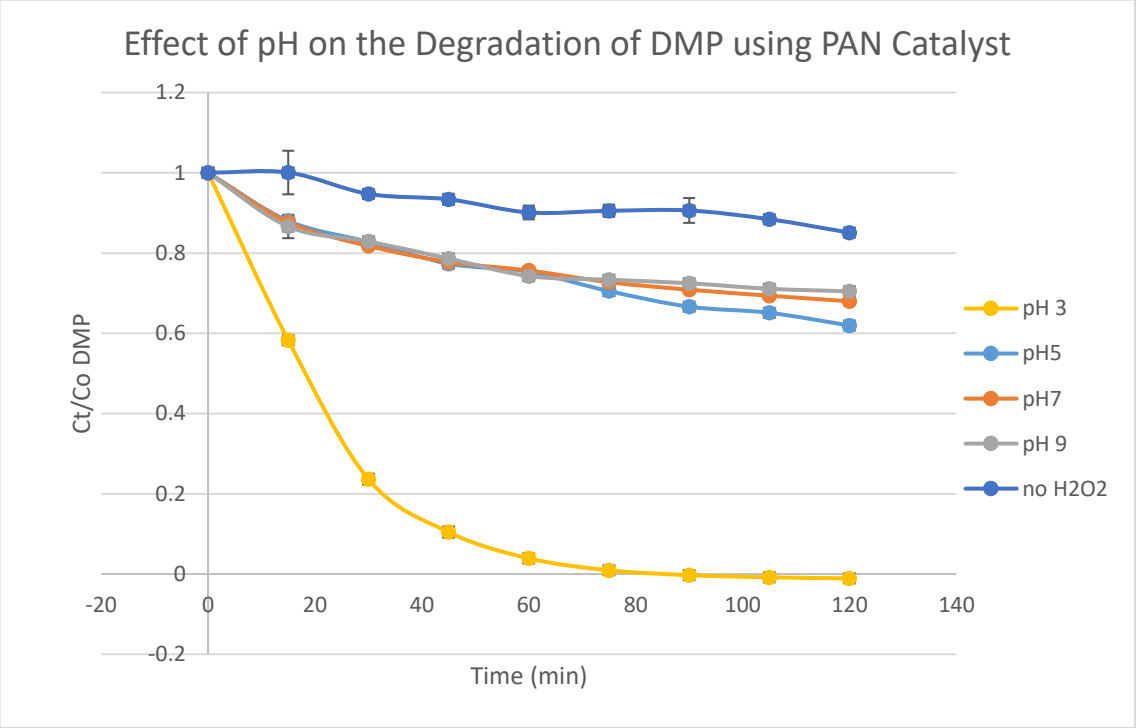

Figure 3.9: Degradation of DMP at different pHs under the following conditions; 5 g catalyst, 400 mg/L H_2O_2, pH 3, 5, 7 and 9 at a temperature of 25 $^oC\pm1$

Other workers (Pignatello et al., 2006; Bautista et al., 2007; Homem et al., 2010) have documented slightly different optimums for pH in homogeneous Fenton reactions with a range between pH2.5 and 4.5. Kanel et al., (2003) while working on soil

decontamination held a different view on the optimum pH for Fenton-like catalytic decomposition of phenanthrene, using Geothite (ferric oxyhydroxide, Figure 3.10) as a catalyst in a heterogeneous system. They documented an increase in the degradation of phenanthrene as pH was increased from 3 to 7. This view is shared by Watts, (1999), who also used Geothite and silica as catalyst in insitu soil remediation at neutral pH with unstabilized H_2O_2 as oxidant. They contended that the increase in oxidation rate as pH was increased from 3 towards 7, was due to contribution of hydroxylated form of iron ($Fe(OH)^+$), which is 10 times more reactive than Fe^{2+} (Pignatello et al., 2006). $Fe(OH)^+$ reacts faster with H_2O_2 to yield $^{\bullet}OH$ according to equation (3.5) and this must have contributed to the oxidation process, and hence increased the rate of oxidation of organic compounds.

$$H_2O_2 + Fe(OH)^{2+} \rightarrow Fe(OH)_2^+ + {}^{\bullet}OH \qquad ...(3.5)$$

Figure 3.10: Chemical structure of Goethite

Although there was no significant difference in the rate of loss of DMP between pH 5, 7 and 9 which is clearly distinguishable from sorption in the present study, the order of the rate of loss was 3>>5 >7>9, indicating a reduction in the rate of loss of substrate with rise in pH. The reason for this is not very clear. Salgado et al., (2013), suggested that the type of reactive species produced during Fenton reactions and hence the reactivity is pH dependent. They further explained that the reactivity of Fenton reaction at pH 3 is

directly related to the speciation of Fe^{3+}, and its stability at various pH. They contend that, although both $[Fe(OH)]^{+}$ and Fe^{3+} are both involved in Fenton reaction, the main specie is the Fe^{2+} especially at low pH, because it more solution, however, the $[Fe(OH)]^{+}$ is far more reactive than the Fe^{2+}. As the pH is increased, soluble species of iron are not stable and hence the limited reaction. The reactivity of the $[Fe(OH)]^{+}$ is because its ligands are able to exchange H_2O for H_2O_2 to form a peroxo-complex $[Fe(OOH)]^{+}$, which is thought to be an intermediary of the Fenton reaction (Szulbinski, 2000).

Walling, (1975) on the other hand, linked the loss of reactivity at weakly acidic pH to what was termed, "dilute acid solution" during the decomposition of H_2O_2 by Fe^{3+} to the formation of H_2O and O_2 according to the following equation (3.6).

$$2H_2O_2 \rightarrow 2H_2O + O_2 \quad \ldots (3.6)$$

3.5.3 Effect of pH on the Degradation of H_2O_2 Using PAN Catalyst

The effect of the pH on the reaction is being considered in terms of its effect on both the degradation of the substrate (DMP) and its effect on the H_2O_2, which has an indirect effect on the reaction.

Loss of H_2O_2 at pH 3 and 5 was about 28 and 30% respectively (Figure 3.11), and almost at the same rate. The experiments for the assessment of loss of H_2O_2 at pH5 were repeated (Figure 3.12) using a different H_2O_2 quantification method (colorimetric method) for validation and the results were similar. These experiments were repeated using a different H_2O_2 calibration method for comparison. Some studies have also reported a rapid loss of H_2O_2 at pH above 4 (US Peroxide 2016), although in homogeneous systems, the present study is in agreement with this. There was a

significant increase in the rate of loss of H_2O_2 as the solution pH was raised above 5, suggesting an increase in the rate of H_2O_2 degradation with increase in pH. Several reasons have been advanced for an increased rate of degradation H_2O_2 and in general these include; temperature, solution pH, and the presence of impurities (Yazici et al., 2010; Evonik Industries, 2016).

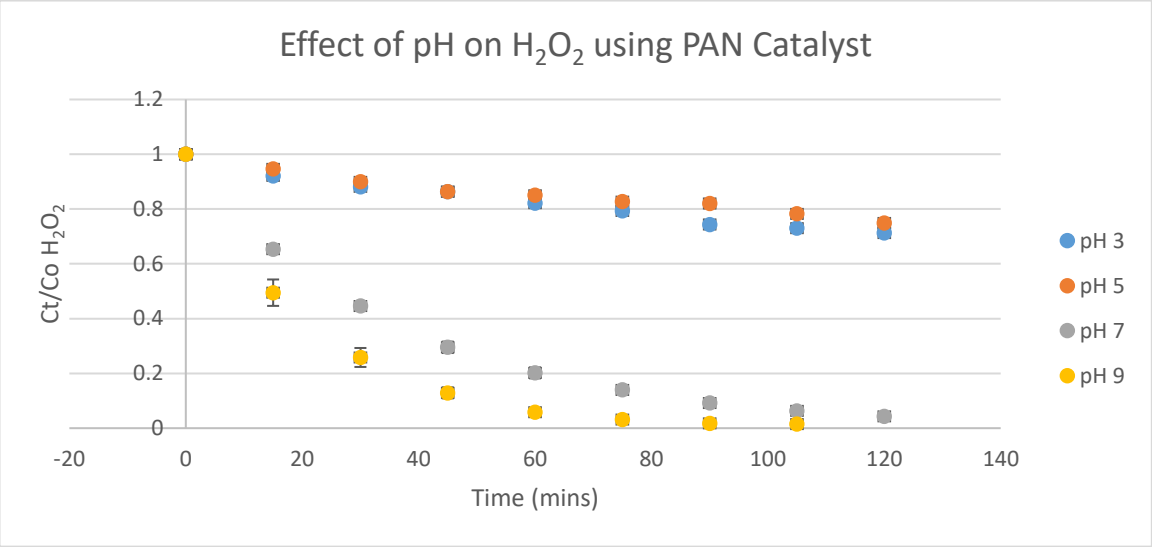

Figure 3.11: Loss of H_2O_2 over time at pH 3,5,7 and 9, with 5 g catalyst, 400 mg/L initial H_2O_2 concentration, 25 mg/L of DMP at 25±1 °C in 100 mL of reaction solution.

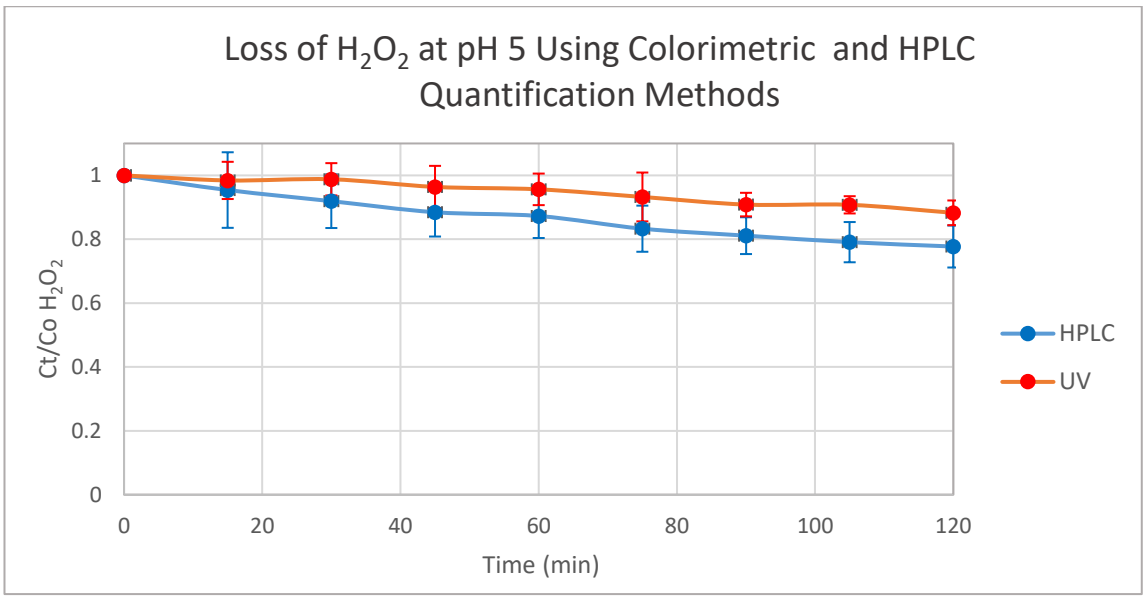

Figure 3.12: Loss of H_2O_2 at pH 5 using colorimetric and HPLC quantification methods (for analytical method comparison)

This has further been explained in terms of the stability of iron species with respect to pH. Bishop et al., (1968), while working with ferric salts in Fenton oxidation of refractory organics in municipal wastewater, observed a trend similar as reported in the present study, in the loss of both substrate (as COD) and H_2O_2. They reported a better substrate removal at pH 3, from an initial COD of 126 mg/L down to 40 mg/L and from 126 down to 54 mg/L for pH5 (for what they termed Loveland waste) as shown in Figures 3.14 and 3.15 respectively, all marked with broken red lines. Stumm, (1964) explained that below pH3, the predominant soluble ferric species are the hydrated ferric ion $[Fe(H_2O)6]^{+3}$, while between pH3 and 4, the iron specie is hydrated ferric complex $[Fe(OH)(H_2O)_5]^{+2}$. Above pH 4, the soluble ferric specie changes to $[Fe(OH)_2(H_20)_4]^{+}$ and with further increase in pH, ends up as $Fe(OH)_4^{-}$. This means that the total concentration of insoluble ferric species increases as the pH is increased. This suggests that, at the transition or switching boundary between pH4 and 5, the species of ferric iron, is likely to be low

amounts of hydrated ferric ion $[Fe(H_2O)6]^{+3}$ and equally low amounts of hydrated ferric complex $[Fe(OH)(H_2O)_5]^{+2}$. These are responsible for the slow degradation of H_2O_2 at pH5 as shown in Figure 3.11 above. However, beyond this transition boundary, the rapid loss of H_2O_2 indicates a change in degradation mechanism of H_2O_2 from a soluble ferric species driven mechanism, to a base-catalysed mechanism on the surface of the flocculated $Fe(OH)_3$ (Bishop et al., 1968).

Table 3.2 (unless otherwise stated, all solutions were acidified before analysis). pH9 had the highest leached total iron concentration (1.6722 mg/L), while the filtered solution of pH 9 reaction (before acidification) had less total iron concentration (0.2025 mg/L). This suggests that the stability of the different ferric species at different pH (as listed by Stumm, 1964) bond differently to the ligands at different pH, with the $Fe(OH)_4^-$ held loosely by the ligands at pH9, while $[Fe(OH)_2(H_20)_4]^+$ appears to be held tightly at pH 7. The colloidal or flocculated iron is thought to have been responsible for the rapid catalytic decomposition of H_2O_2 at pH 9 to H_2O and O_2, as shown in equation 3.6 (Bishop et al., 1968; Watts et al., 1993; Khan et al., 1994; Salgado et al., 2013; US Peroxide 2016; Kanel et al., 2003).

Table 3.2: Leached iron in solution at various pH from 5 g of catalyst and 400 mg/L of H_2O_2 in 100 mL. (pH was monitored throughout the experiments)

Solution pH	**3**	**5**	**7**	**9 (Filtered, unacidified)**	**9**
Total Iron Conc. (mg/L)	0.8060	0.0322	ND	0.2025	1.6722

*ND = below detection

From Table 3.2, pH 7 had undetectable amounts of leached iron in reaction solution followed by pH 5 (0.0322 mg/L).

Overall, the order of leached iron in solution was pH7 < 5 < 3 < 9 . The reaction solutions before acidification were filtered and the residue showed variation in colour at different pH. The residue on the filter is as shown in Figure 3.13.

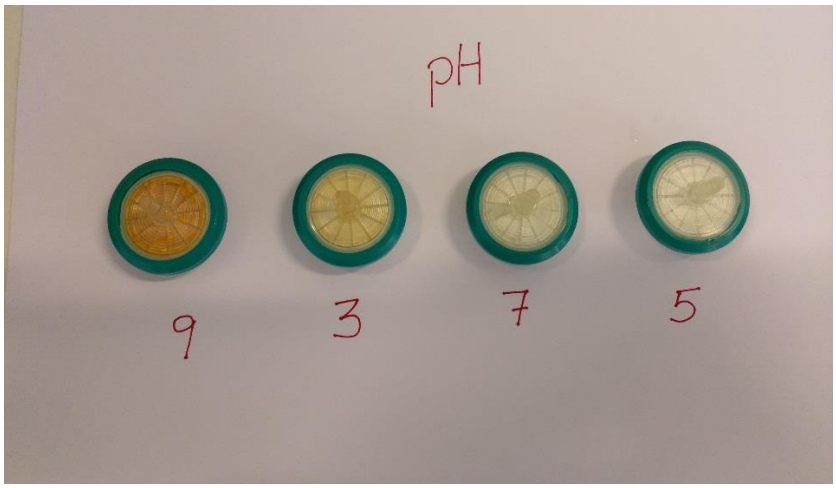

Figure 3.13: Photograph of residues of filtered reaction solutions after 2 h reaction using 0.45 µm syringe filter.

Bishop et al., (1968) has also linked this rapid breakdown of H_2O_2 at higher pH to the production of organic acids, oxidation products and the potential for chelation and complexing ferric ions in the reaction system, although no proof was provided for this.

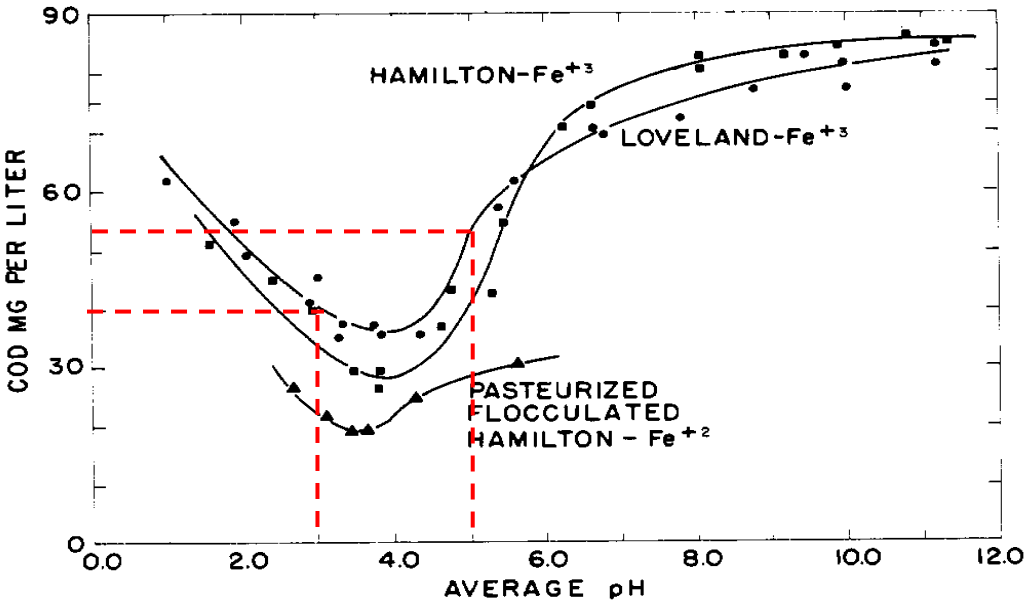

Figure 4. Reduction of COD at various pH

Solid phase. Ferric hydroxide
Total catalyst concentration. 0.001264 eq. per liter
Initial H_2O_2 concentration. 0.01251 to 0.01264 eq. per liter
Temperature. 65° C.
Reaction period. 22 hours

Figure 3.14: Rate of loss of COD according to similar studies by Bishop et al., (1968)

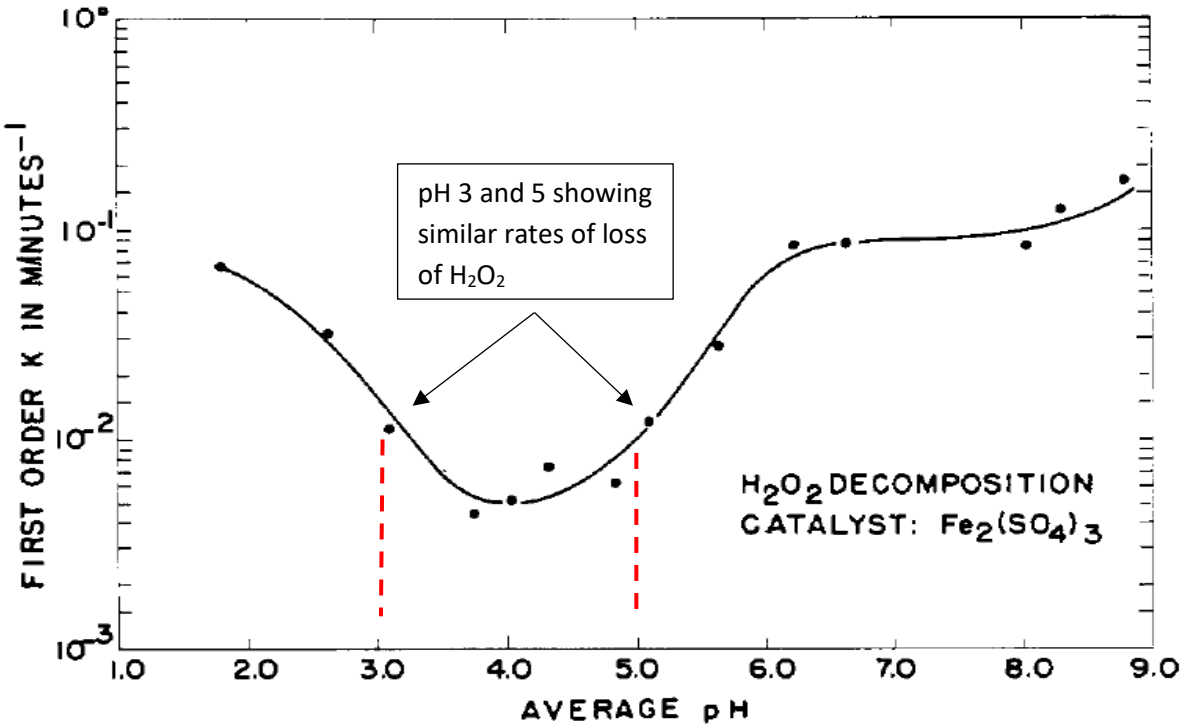

Figure 3. Decomposition constant at various pH

System. Heterogeneous above pH 2.5
Solid phase. Ferric hydroxide
Total ferric concentration. 0.001264 eq. per liter
Temperature. 65.8° C.
Initial H_2O_2 concentration. 0.01125 to 0.01267 eq. per liter

Figure 3.15: Rate of loss of H_2O_2 according to similar studies by Bishop et al., (1968)

3.5.4 Effect of H_2O_2 Concentration on the decomposition of 3,5-DMP

The use of H_2O_2 as an oxidant for disinfection, water treatment purposes and other industrial applications is well documented. Used separately, iron salts and H_2O_2 are not efficient oxidation agents against most complex organic compounds (Bishop et al., 1968). This claim has been supported in this work by control experiments (0 mg/L H_2O_2) as shown on Figure 3.16 below. There was a 15% loss of DMP, and this is likely due to sorption on the catalytic mesh.

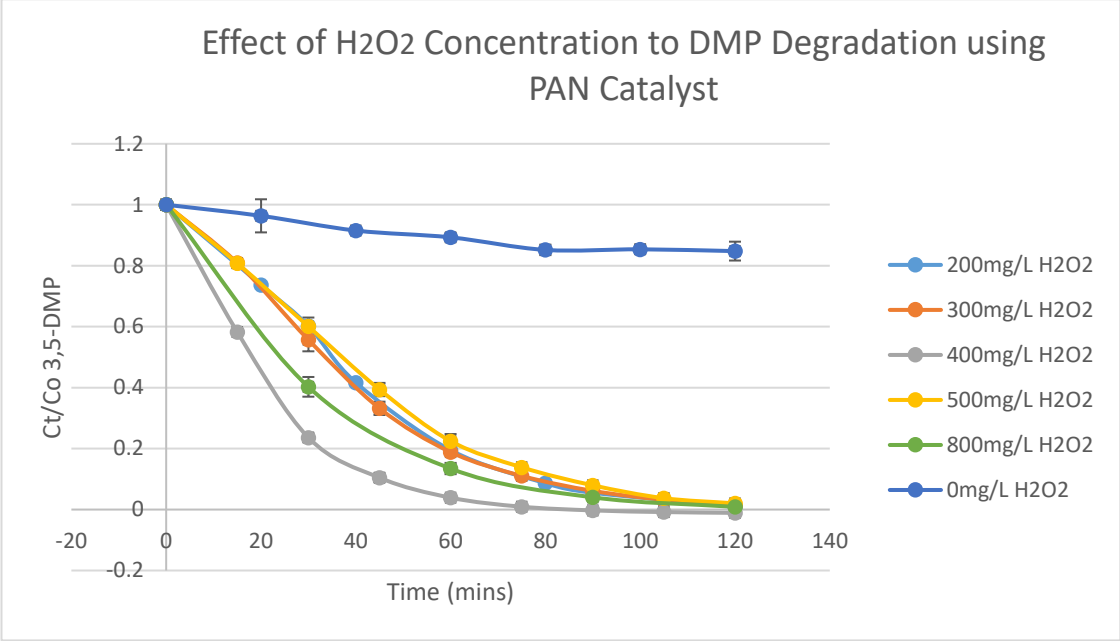

Figure 3.16: Effect of initial H_2O_2 concentration on the degradation of DMP. Reaction parameters were; pH3, 25 mg/L DMP, 25^{o}C±1, 5 g catalyst, 100 mL reaction volume.

Figure 3.16 above shows the effect of H_2O_2 concentration on the rate of degradation of the model pollutant used for this study, DMP. The rate of loss in 120 min of reaction with respect to variation in the concentration of H_2O_2 under the following experimental conditions; 5 g catalyst, pH3, 25±1^{O}C, 100 mL reaction volume, 25 mg/L initial concentration of 3,5-DMP is stratified into four defined bands. These are; 0 mg/L, which showed a loss of about 15% substrate due to sorption on the surface of the catalyst, 500, 200 and 300 mg/L which together forms a second band with a relatively gentle loss of DMP. In addition, 800 mg/L, which is the third band, showed a better rate of loss of DMP, compared to the second band. Lastly, 400 mg/L H_2O_2 yielded the fastest rate of loss of substrate. Interestingly, for an initial 400 ppm H_2O_2 concentration, the peroxide degradation of 30% (Figure 3.16) coincided with the calculated theoretical peroxide demand value for the oxidation of 25 mg/L of 3,5-DMP which was 139.4 mg/L, however,

complete mineralization may not have been achieved as evident in the formation of organic acids (section 4.3.4.4 Chapter four).

As shown in Figure 3.16, there is a corresponding increase in reactivity with increase H_2O_2 until a threshold of 400 mg/L after which a further increase no longer had a positive effect on the reactivity of the system. This trend is in agreement with previous studies by Zhang et al., (2005), Jiang et al., (2010), Gulsen and Turan, (2004) and Beltran et al., (1995). In their study of the effect of H_2O_2 on Fenton-like reactions, Jiang et al., (2010) showed that increase in the concentration of H_2O_2 enhanced the degradation of phenol but noted that excess H_2O_2 resulted in decrease in the decomposition of H_2O_2, and by extension, the phenol. They attributed this to "scavenging" of the hydroxyl radical by the excess H_2O_2. Their position is strengthened by Kavitha and Palanivelu, (2005) who also believe that the reduction in the rate of loss of substrate beyond "optimum concentration of H_2O_2" could be as a result of scavenging of OH radical. They argued that the excess H_2O_2 reacts with $^{\bullet}OH$ to form hydroperoxyl radical ($HO_2^{\bullet}$) as shown by equation (3.7) which is a weaker free radical species (Torrades et al., 2003; Chamarro et al., 2001; Lu et al., 1999 Kavitha and Palanivelu, 2005).

$$^{\bullet}OH + H_2O_2 \rightarrow HO_2^{\bullet} + H_2O \quad \ldots (3.7)$$

3.5.5 Effect of Catalyst concentration on the degradation of H_2O_2

The rate of loss of H_2O_2 in Fenton type reactions has also been looked at by several workers. Hermosilla et al., (2009) looked at factors other than pH that influence the loss of H_2O_2 in Fenton oxidation reactions. They suggested that the consumption of H_2O_2 in Fenton type reactions also depends on the concentration of catalyst in the reaction.

They showed that the higher the catalyst concentration, the faster the rate of loss of H_2O_2 under the same experimental conditions. Although marginal, the present study follows a similar pattern as shown in Figure 3.17 below. 5 g and 6 g catalysts show the same rate of loss. This suggests that, the rate had become limiting most likely by the rate of diffusion of H_2O_2 to the catalyst. There was about 30% loss of H_2O_2 in two hours for 5 g catalyst and a corresponding loss of > 99% DMP (see Figure 3.18).

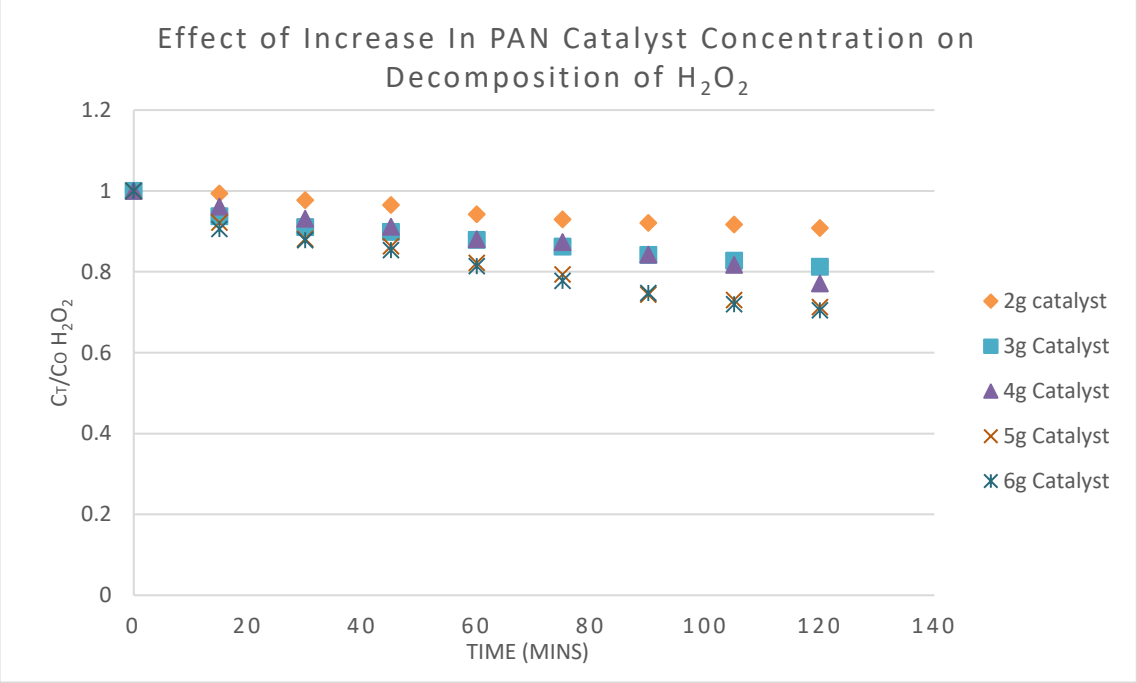

Figure 3.17: Relative rate of loss of H_2O_2 with respect to change in concentration of catalyst. Conditions: pH3, 25 mg/L DMP, 400 mg/L H_2O_2, temp 25 ^oC in 100 mL reaction volume.

3.5.6 Effect of Catalyst Concentration on Degradation of DMP

In heterogeneous Fenton-like processes, the effect of iron catalyst dosing follows a similar pattern to that of the homogeneous system except that, in the homogeneous reaction, excessive dosing of iron salts increases both the overall total dissolved solids in the treated effluents and the conductivity which may require further treatment

(Hermosilla et al., 2009). The effect of increased concentration of catalyst was examined over a range of 0 g to 6 g of catalyst. (1 g of catalyst = 0.272 mmol Fe/g of PAN mesh). Figure 3.18 shows that H_2O_2 alone is unable to decompose DMP over an 80 min period, after which it slowly begins to decompose DMP. There was a corresponding increase in the rate of loss of DMP with increase in the concentration of catalyst from 2 g to 5 g and no increased reactivity beyond 5 g. This conforms to the views of Lu et al., (1999) and Torrades et al., (2003). They contended that in excess concentration of Fe^{3+}/Fe^{2+} catalyst, there is a possibility of $^{\bullet}OH$ scavenging according the equations 3.8.

$$^{\bullet}OH + Fe^{2+} \rightarrow HO^{-} + Fe^{3+} \quad \ldots(3.8)$$

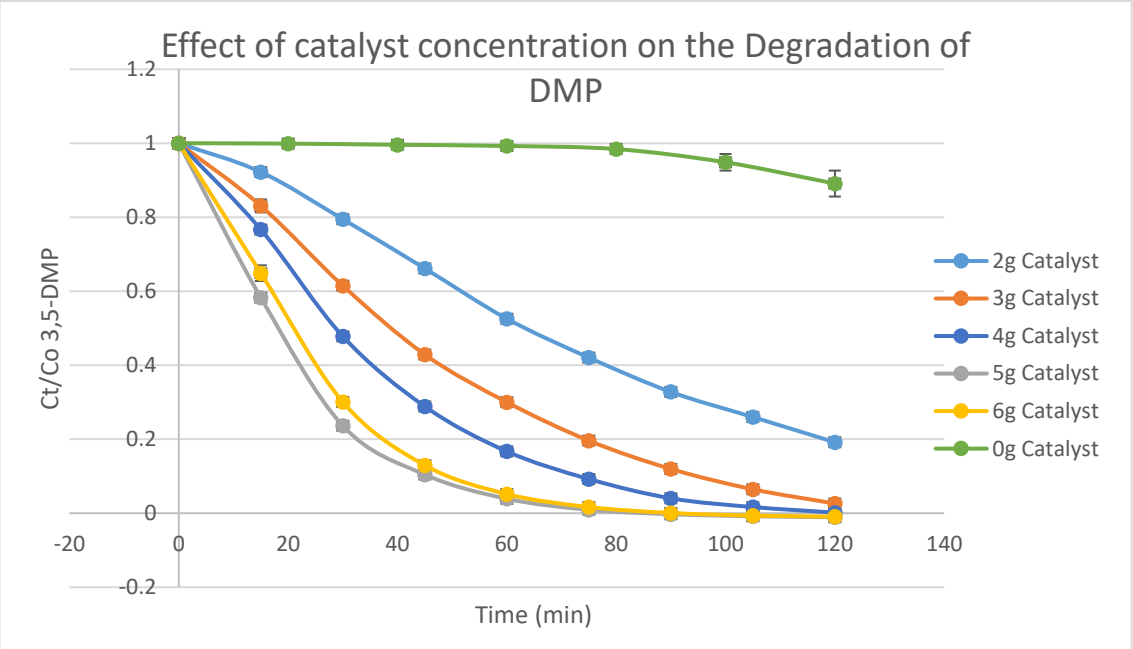

Figure 3.18: Degradation of DMP as a function of catalyst concentration and H_2O_2 concentration of 400 ppm, DMP of 25 mg/L, at pH3, and temperature of 25±1 °C, 100 mL reaction volume. *1 g of catalyst =0.272 mmol Fe/g of PAN mesh.

The reaction of 5 g and 6 g catalyst in DMP degradation ties with the H_2O_2 degradation graph for 5 g and 6 g catalyst in Figure 3.17, while a similar trend is followed by 2, 3 and 4 g catalyst (Figure 3.18), with respect to H_2O_2 degradation in Figure 3.17.

3.5.7 Effect of Homogeneous Fenton Catalysis Contribution

The degree/extent of influence of homogeneous catalysis on the rate of conversion of DMP was investigated according to the procedure described in section 3.4.6, following the confirmation of leached iron in solution (Table 3.2). The catalyst was removed after catalysis and a fresh feed introduced into the catalysed solution. The results are as presented in Figure 3.19. The homogeneous catalytic activity in the reaction contributed to about 13.5% loss of DMP.

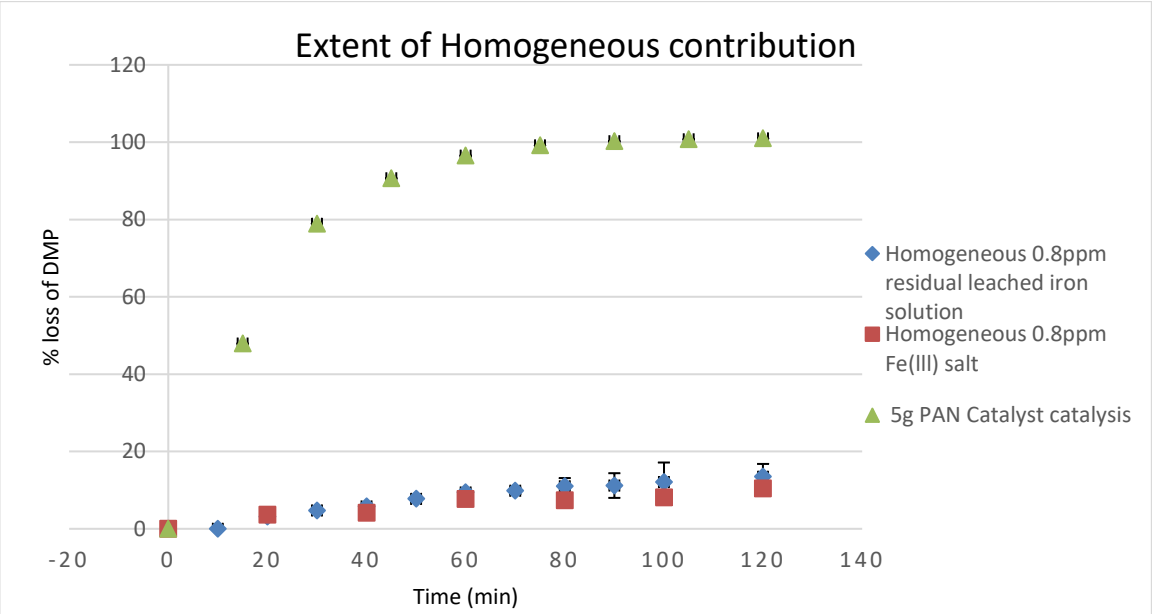

Figure 3.19: Effect of homogeneous Fenton contribution to catalytic system. Reaction condition; pH3, 5 g catalyst for heterogeneous process, 0.8 mg/L $Fe^{2}(SO_4)_3{\cdot}5H_2O$ as Fe^{3+} used for homogenous catalysis, leached iron 0.8 ppm, 400 mg/L H_2O_2, 25° C±1.

A Similar experiment was conducted using the same concentration of Fe ($Fe_2(SO_4)_3 \cdot 5H_2O$) as the amount of iron (lll) leached from the catalyst at the end of the 2 hour reaction. A similar result of 10.4% loss of DMP after 2 hours was observed in comparison. The heterogeneous system achieved a DMP degradation > 99%. This result would suggest that the reaction process was mainly catalysed in the heterogeneous phase with about 13.5% contributions from the homogeneous processes.

Apart from the low absolute concentration of soluble iron in solution after the reaction, the poor performance of the homogeneous system could also be due to the molar ratios of the main constituents of the Fenton reagent. Most authors have suggested a molar ratio ($Fe:H_2O_2$) of between 1:5 to 1:95 as optimums for homogeneous Fenton oxidation depending on the type and specie of iron (Hermosilla et al., 2009; Khamaruddin 2011). Hence, with a ratio of 1: 823 (0.8:400 Fe: H_2O_2) in the present system described in Figure 3.18 above, there was a possibility of scavenging by excess H_2O_2.

Finally, the amount of iron on the mesh was determined according to the procedure previously described in section 3.4.5, and assayed on the AAS. The iron on the mesh was calculated as follows:

Measured concentration on the AAS was 3.038 mg/L.

Hence, 3.038 mg/L x DF = 30.379 mg/L

(Where DF is dilution factor = 10)

That is, 3.038 mg of Fe in 100 mL (equivalent to 30.38 mg in 1000 mL)

If 3.038 mg of Fe was digested from 0.1 g of yarn

∴ 1 g of yarn would have 30.38 mg of Fe = 0.544 mmol/g of yarn = 0.272 mmol/g of PAN mesh

3.5.8 Effect of Temperature

Figure 3.21 shows the rate of removal of DMP over time at different temperatures. The rate of removal of DMP was monitored at 10, 25 and 40 ^{o}C. 10 ^{o}C was achieved by using a refrigerating circulator as shown in Figure 3.20, in a 300 mL jacketed open reactor which was covered with a cling film. The reacting mixture was stirred by a flea and magnetic stirrer, set at 350 rpm. Quality control was maintained by testing the reaction temperature with an external digital temperature probe at regular intervals.

Figure 3.20: Reaction system set-up for effect of temperature on the degradation of DMP

There was a corresponding increase in the rate of removal as the temperature was increased from 10 through 25 to 40 ^{o}C as shown on Figure 3.21. Expectedly, the reaction

of 10 °C at 40 min of reaction showed about 19% loss of DMP, while the reaction run at 25 °C showed 85% loss of DMP at 40 min. The 40 °C reaction had the fastest rate and was completed in less than 40 min. The temperature range was chosen to reflect cold, temperate and warm climatic conditions. The results are in agreement with US Peroxide, (2016), but they however reported a decline in efficiency beyond 40-50 °C which was attributed to the instability of H_2O_2 at high temperatures. They held that, at high temperatures H_2O_2 decomposes quickly to O_2 and H_2O according to equation 3.6.

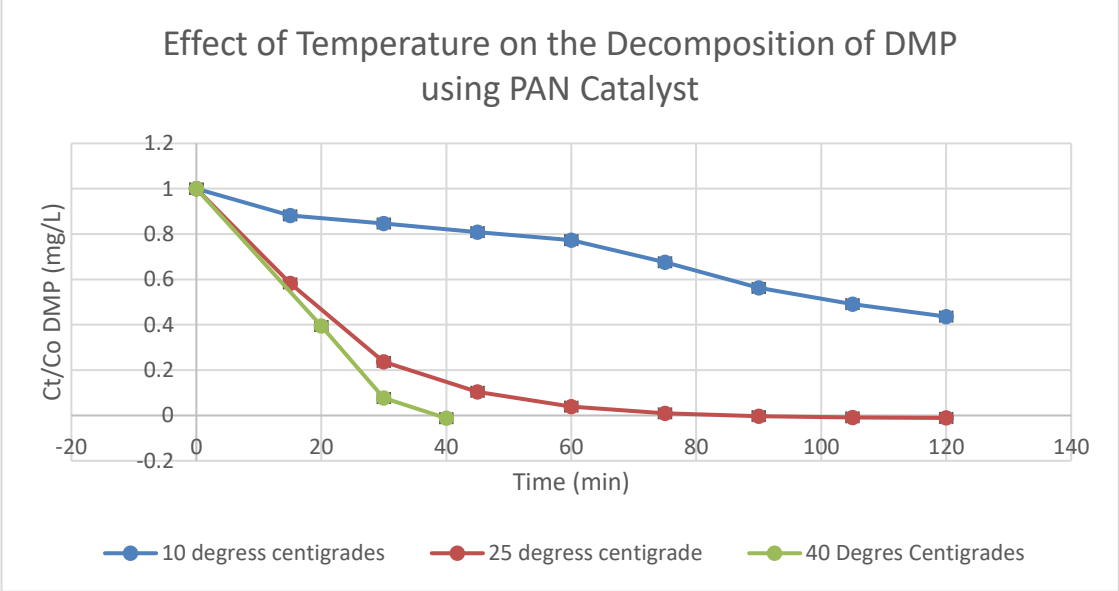

Figure 3.21: Effect of temperature on the degradation of DMP with time. DMP 25 mg/L, H_2O_2 400 ppm, pH3, 100 mL reaction volume and 5 g catalyst.

According to Zhang et al., (2005), organic compound conversion in Fenton and Fenton-like reactions tend to increase with rise in temperature as reflected in the increased removal of COD with increased temperature. In their study on the effect of temperature on the Fenton oxidation of landfill leachate, Aygun et al., (2012), also found a direct

correlation between temperature increase and improvement in degradation and COD removal. Hermosilla et al., (2009) also indicated that there was a slight increase in COD removal with temperature increase however, it was not significant when temperature was increased from 25 to 35 and then to 45 ^{O}C, giving an average COD loss of 64% in all, using conventional Fenton in a homogeneous system in the treatment of Landfill leachate.

3.5.9 Effect of Tertiary Butyl Alcohol

Several compounds have been identified as radical scavengers and this is well documented. Joshi et al., (2001) reported the successful use of folic acid as a hydroxyl radical scavenger due to its anti-oxidant properties. Tertiary butyl alcohol (TBA) has also been used by Jiang et al., (2010), to demonstrate the reaction pathway of Fenton and Fenton-like processes. According to them, the high reaction rate constant recorded in the reaction of TBA and hydroxyl radical is a pointer to its radical scavenging properties.

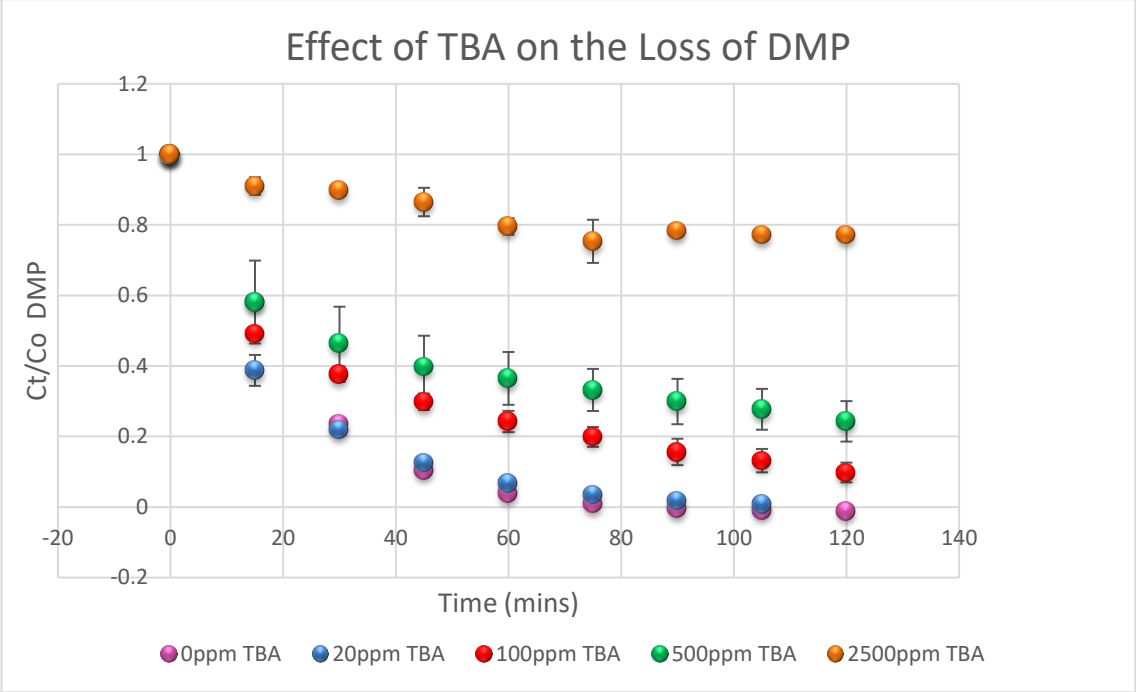

Figure 3.22: The degradation of DMP over time in the presence of TBA. pH3, H_2O_2 400 ppm, temp 25 ^oC±1, 5 g catalyst and 100 mL reaction volume.

The results from Figure 3.22 above shows decrease in the reaction rate as the concentration of TBA increases at 25±1 ^oC. At 120 min, DMP was least degraded when TBA concentration was 2500 ppm. For 20 ppm TBA, there was an insignificant effect on the rate of degradation of DMP which suggests that the rate of reaction of $^{\bullet}OH$ with TBA at that concentration is similar to the reaction rate of DMP with $^{\bullet}OH$. Therefore, the effect of TBA takes effect only when the concentration of TBA is high (2500 ppm), resulting in the slow degradation of DMP. The rate-limiting factor therefore was the TBA. According to Teton et al., (1995), the reaction rate constant for the reaction of TBA and $^{\bullet}OH$ is very high and varies with temperature, which makes TBA a $^{\bullet}OH$ scavenger as exemplified in Figure 3.21 above. They recorded a rate constant k for the reaction of $^{\bullet}OH$ and TBA of 1.07± 0.08 X 10^{12} molecule^{-1} s^{-1} at 298 K (24.9 ^oC), while Wallington et al., (1988), reported a higher k value of 3.3 ± 1.6 X 10^{12} molecule^{-1} s^{-1} at 310 ± 150 K

(36.9 ± -123 ^{o}C). Figure 3.22 therefore suggests that this reaction (equation 3.9 below) was likely a radical type reaction at pH3 although further laboratory studies are required to fully verify this.

$$^{\bullet}OH + (CH_3)_3COH \rightarrow CH_2(CH_3)_2OH + H_2O \quad \ldots (3.9)$$

3.5.10 Effect of Initial Concentration of Substrate

The effect of the initial concentration of DMP was investigated and the results for the relative and absolute loss of DMP with increase in concentration are presented in Figure 3.23 and 3.24. The results from Figure 3.23 shows 99.3% removal at 25 mg/L initial concentration of DMP, 85.8% removal at 50 mg/L initial DMP concentration and 82% removal at 100 ppm initial DMP concentration. This indicates that the initial DMP concentration is an important factor in the extent of degradation. The higher the initial concentration, the lower extent of degradation and the slower the disappearance of DMP. The total amount of DMP degraded per unit time at 60 minutes was 30 mg/L for 50 mg/L initial concentration of DMP (equivalent to 60% loss) and 58 mg/L for 100 mg/L initial concentration of DMP. This observation is in agreement with Asim et al., (2005). In their study of phenol and chlorinated phenol degradation using Fenton's reagent, they reported that the solutions containing higher concentrations of both phenols and chlorinated phenols recorded slower relative degradation, but higher amount of conversion and no explanation was given for this. The slow loss of DMP at higher initial concentrations may be due to increased competition for OH radicals between the intermediates and the DMP molecules as a result of increased initial concentration of DMP. Belattar et al., (2012) also made similar observation while studying the effect of

initial concentration on the decomposition of DMP, and suggested similar reasons. The saturation of catalyst active sites as a result of higher concentration of DMP can also lead to slower reactions and could be responsible for the slower loss of DMP in this case, where the ratio of H_2O_2:DMP was constant.

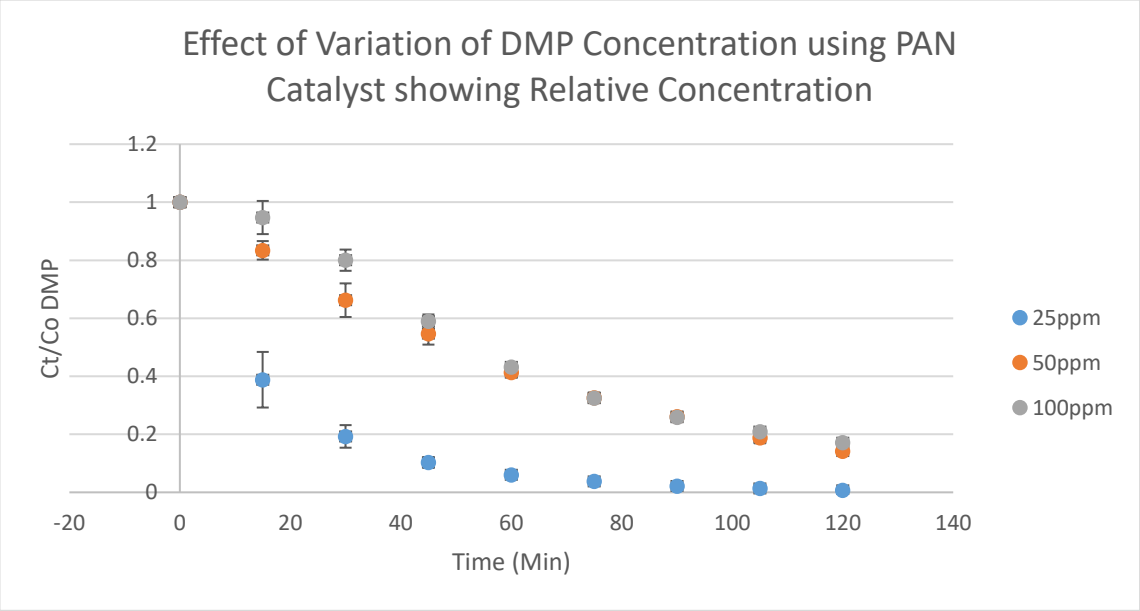

Figure 3.23: Effect of concentration on the degradation of DMP showing relative concentrations. Reaction volume of 100 mL, 400 mg/L H_2O_2, 5 g catalyst, pH3 and 25 ^oC ±1.

The rate of removal of DMP is shown in Figure 3.24 below, using the absolute concentrations plots. In terms of rate in relative loss; 25 mg/L > 50 ~ 100 mg/L (Figure 3.24), while in terms of absolute loss of , rate of loss was 100 mg/L > 50 mg/L > 25 mg/L (Figure 3.24).

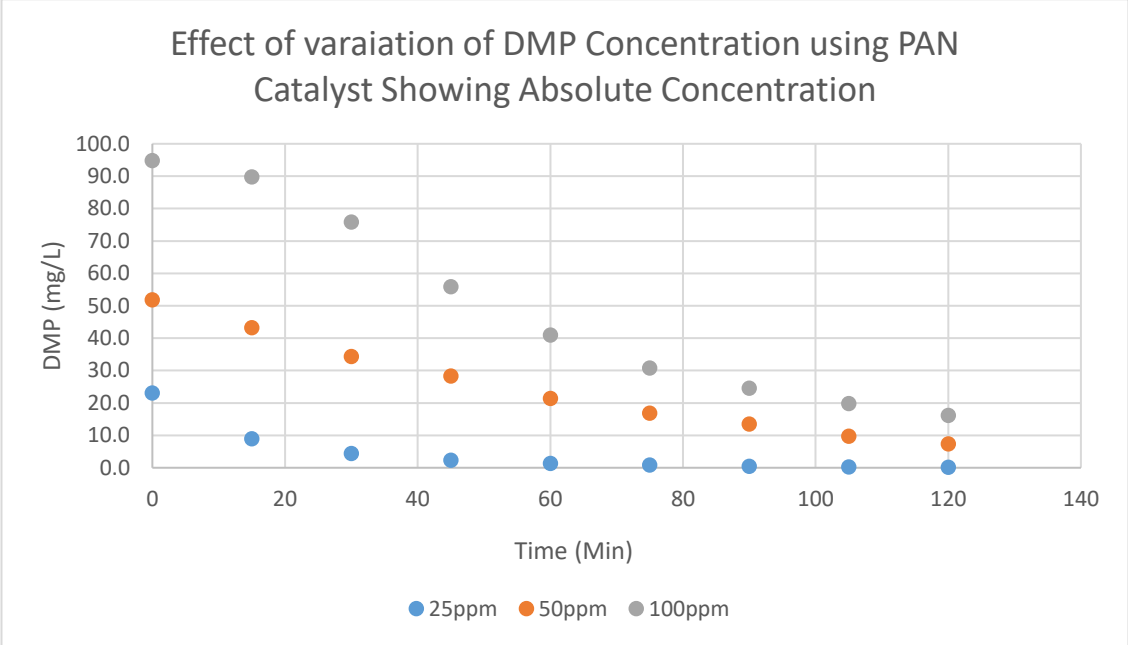

Figure 3.24: Effect of concentration on the degradation of DMP showing absolute concentrations. Reaction volume of 100 mL, H_2O_2 400 mg/L, 5 g catalyst, pH3 and 25 ^oC ± 2.

3.6 Results and Discussions for Continuous Flow Reactions

The results of the continuous flow experiments for the heterogeneous degradation of DMP at room temperature are presented in Figure 3.25. The rate of loss of DMP, peroxide, and leached iron were monitored. In addition, the effect of H_2O_2 concentration, effect of variation of retention time, effect of variation in airflow rate on and the amount of leached iron and the loss of DMP were also investigated.

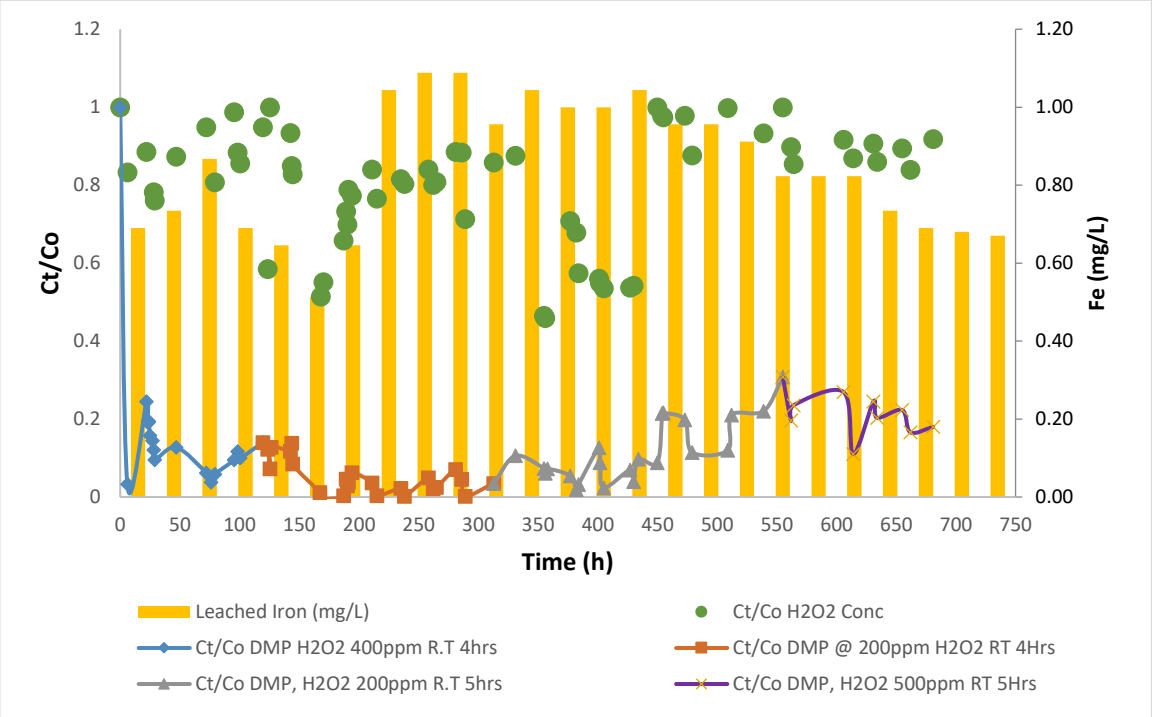

Figure 3.25: Effect of various process parameters on the loss of DMP, H_2O_2 and leached iron at pH3, ambient temperature, 12.5 g catalyst (production roll 3) 200mL reaction volume, Initial DMP of 25 mg/L, initial H_2O_2 of 200, 400, and 500 mg/L, RT of 4 h (0.83 mL/min) and 5 h (0.66 mL/min).

3.6.1 Effect of Air flow rate on the rate of Loss of DMP

Control experiments were carried out in Radley carousel reactor in batch mode to evaluate the possible oxidizing effect of oxygen from air (or stripping effect of air) on DMP before an air compressor was used to achieve mixing in the continuous flow experiments. This experiment was done in other to evaluate the possibility of the loss of DMP through the sparging effect of the air pump, which could have a possible volatilization effect on DMP. The results are presented in Figure 3.25a. The results showed a 20% loss of DMP with only air as oxidant, after five hours reaction time. The reaction conditions for the control experiment was as follows: 25 mg/L DMP, 5 g of catalyst, pH3 at ambient temperature and airflow rate 10 cm^3/min. This result is in agreement with sorption experiments (catalyst without peroxide) presented previously in Figure 3.9 where about 13% loss of DMP was reported to be due to sorption at 120 min. The total loss of DMP in the present control experiment was about 20% (Figure 3.5a); however, the duration was 5 hours. It is likely that the extra loss of about 7% resulted from further sorption over the extended reaction time, as DMP is relatively stable, with a boiling point of 219 ^oC, and a low vapor pressure of 0.0405 mm Hg @ 25 ^oC, which makes it less volatile (International chemicals safety cards 2017).

This suggestion is corroborated by the chromatograms for the control experiment where bubbled air was used to effect mixing. These have been presented in Figure 3.26 and show no indication of degradation products, suggesting that, in addition to sorption, the extra loss of DMP may not have been due to catalytic activity. Loss from stripping or oxidation would have continued, not tailed off.

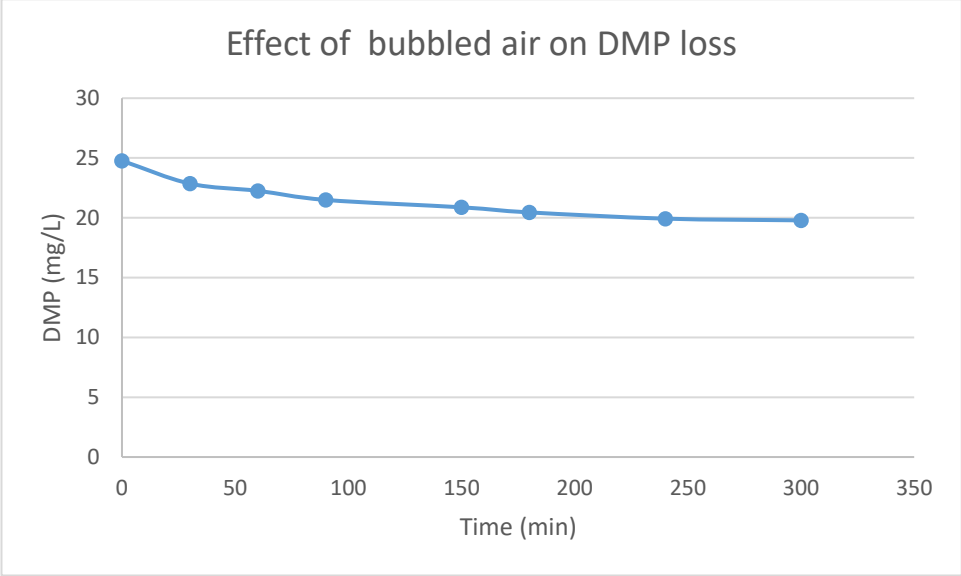

Figure 3.25a: Loss of DMP using air as oxidant at pH3, 5 g catalyst, 25 mg/L DMP, 10 cm^3/min airflow rate, ambient temperature and 100mL reaction volume.

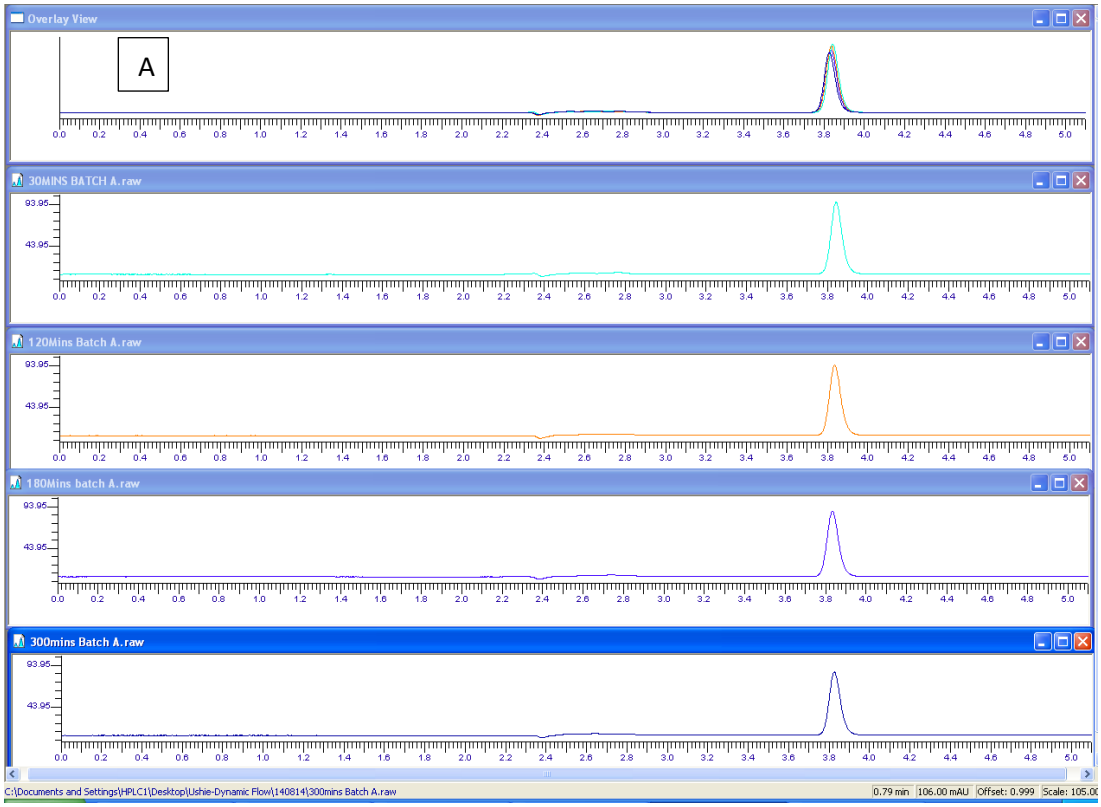

Figure 3.26: Snap shot of chromatograms at 30, 120, 180 and 300 min of bubbling air into reaction system in the presence of 5 g catalyst, at pH3, 25 mg/L DMP, 10 cm^3/min airflow rate, ambient temperature and 100 mL reaction volume ("A" are staked chromatograms).

The rate of loss of DMP in the continuous flow experiment was investigated by sampling and analysis at regular intervals throughout the duration of the experiment. The airflow was varied between 6 cm^3/min and 10 cm^3/min (t_0 to t_{350} for 6 cm^3 and t_{351} to t_{681} for 10 cm^3 respectively). In the first 24 h, the flow was transient as can be seen in Figure 3.27 and steady state flow was attained subsequently. There was no significant difference between 6 cm^3/min and 10 cm^3/min airflow rates, but higher flow rates slightly reduced the rate of loss of DMP. This is presumably due to possible break-through of DMP molecules under increased agitation (Logsdon, 1987; Wagner and Pinheiro, 2001) but it is also possible that the catalyst was beginning to deactivate. Apart from possible breakthrough of substrates, there is also a possibility of partial concentration of the reaction system, through evaporation caused by high airflow rates leading to loss of water and increased residual substrates concentration (General Electric Power and Technology, 1997).

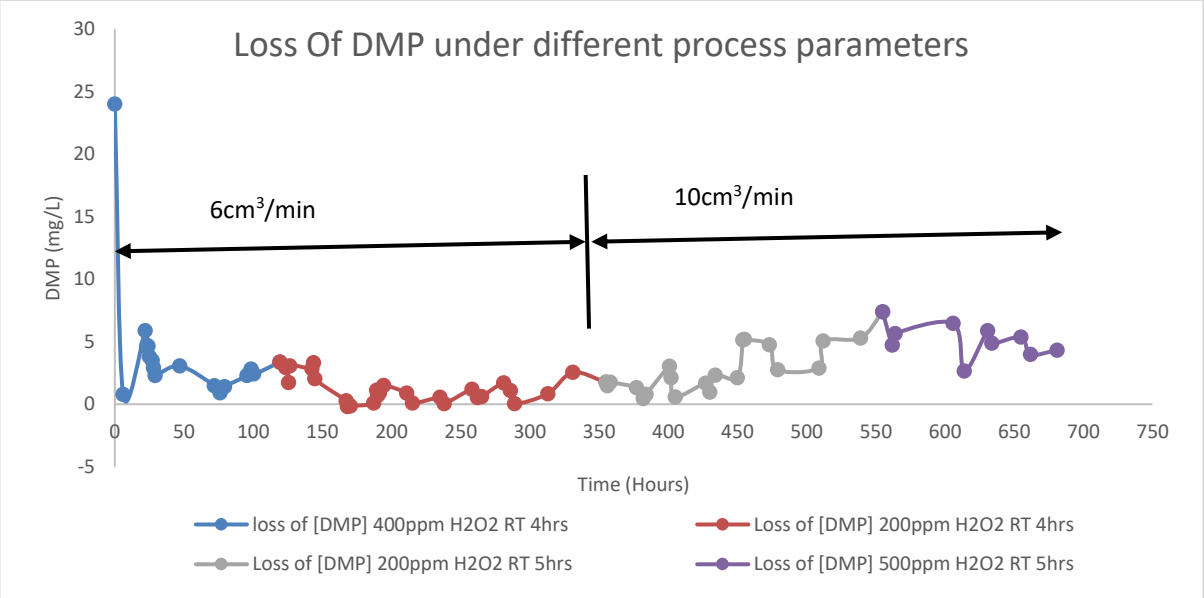

Figure 3.27: Loss of DMP under varied process parameters: at pH3, ambient temperature, 12.5 g catalyst (production roll 3) 200 mL reaction volume, Initial DMP conc of 25 mg/L, initial H_2O_2 of 200, 400, and 500 mg/L, RT of 4 and 5 h.

Cases of volatilization in tank reactors resulting from aeration in aerated stirred tank reactors have also been reported. Under these circumstances, the substrates were volatile and unstable (Libra, 1991; Truong and Blackburn, 1984; Roberts et al., 1984).

3.6.2 Effect of Initial H_2O_2 Concentration on the Loss of DMP

The effect of initial H_2O_2 concentration was investigated in the continuous flow experiment by varying the initial concentration of H_2O_2 used in the treatment system while keeping other parameters constant. This was varied between 400, 200 and 500 ppm initial H_2O_2 concentration at the beginning, middle and final stages of the experiments respectively.

In the first phase of H_2O_2 dose regime of 400 ppm, the retention time was 4 h (0.8 mL/min) and an average H_2O_2 consumption of about 10%. In molar concentration terms, 10% H_2O_2 consumption is equal to 1.176 mM H_2O_2 /L, used as shown below;

400 ppm $H_2O_2 = \frac{400}{34} = 11.76$ mM H_2O_2/L. Therefore, 10% consumption = 1.176 mM H_2O_2 /L.

The low consumption of H_2O_2 in the system is likely due to mass transfer limitations in continuous flow processes and a possible scavenging reactions. Following the same calculations for the second phase of H_2O_2 dose regime of 200 ppm with an average consumption of 25%, means that 1.47 mM of H_2O_2 was used, which is similar to the amount of H_2O_2 consumed in the first phase, and both phases had the same retention times of 4 h. In the third phase, where the concentration of H_2O_2 was maintained at 200 ppm, and retention was increased to 5 h, there was 2.35 mM of H_2O_2 consumed.

Therefore, 25% increase in retention time resulted in 60% increase in the consumption of H_2O_2 (4 →5 h, resulted in 1.47 →2.35 mM H_2O_2/L), which suggests that increasing the retention time, resulted in increased breakdown of H_2O_2, which should result in increased breakdown of DMP under the right pH conditions.

However, in the fourth phase of H_2O_2 dose regime, an increase in the H_2O_2 concentration from 200 to 500 ppm whilst keeping the retention time at 5 h, showed an average H_2O_2 consumption of only about 10 – 12%. This is about 1.47 mM H_2O_2 consumption, suggesting loss of catalytic activity, evidenced in the reduced conversion of DMP after 550 h of continuous flow experiment (Figure 3.25a and 3.27).

The results from Figures 3.25 and 3.27 suggest that 200 mg/L in continuous flow had the best outcome for the loss of DMP during the experiment, even though the experimental optimum H_2O_2 concentration in batch mode was 400 mg/L (Figure 3.16, section 3.5.4).

3.6.3 Effect of Increasing Mass of Catalyst

Optimised conditions such as H_2O_2 concentration and airflow rate at initial concentration of 200 mg/L and 6 cm^3/min respectively were adopted for use for the second experiment, while the catalyst load was increased to 20 g, to examine the effect of increasing the mass of catalyst on the decomposition of DMP and H_2O_2. The results are presented in Figure 3.28a.

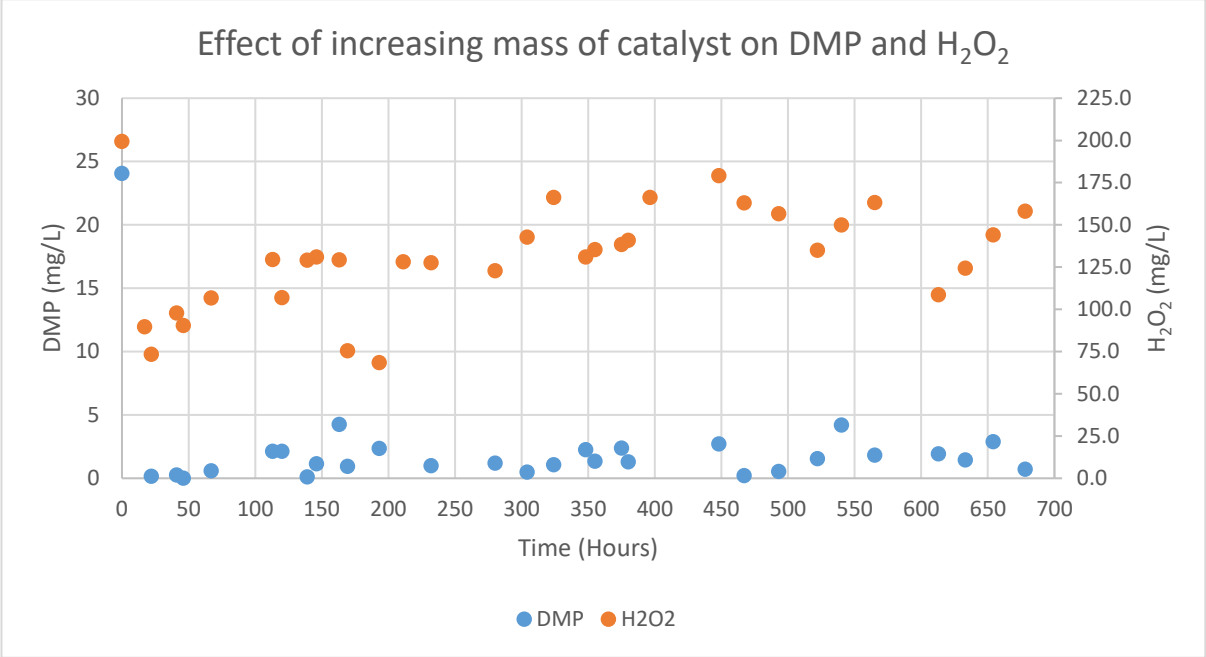

Figure 3.28a: Effect of increasing the amount of catalyst on the oxidation of DMP. Initial H_2O_2 concentration of 200 mg/L, airflow rate of 6 cm^3/min at pH3, with 20 g catalyst, and ambient temperature.

The results of the optimised reaction (Figure 3.28a) showed a better decomposition at an average of about 90% DMP over 678 h, thus, suggesting that the excess H_2O_2 used in the previous experiments was not necessarily required. The loss of DMP is as shown in the superimposed chromatogram for initial reading (black), 17 h (blue) and 678 h (green) of the continuous flow reaction in Figure 3.28b below. Between 0 →80 h H_2O_2 consumption was about 100 ppm, between 100 → 300 h there was about 75 ppm H_2O_2 consumption while between 300 → 678 h, there was only about 50 ppm H_2O_2 consumption. Therefore, H_2O_2 consumption reduced as the continuous flow experiment persisted with a reduction of 50% in its decomposition between the start and the end of the experiment. This suggests a possible reduction in catalytic activity in the reaction system; however, the activity in the system was still sufficient to decompose the DMP as shown in Figure 3.28a. This corroborates the views of Bartholomew and Argyle,

(2011), that optimization of reaction conditions can extend the life of a catalyst and increase its activity, owing to the decline of unwanted side reactions.

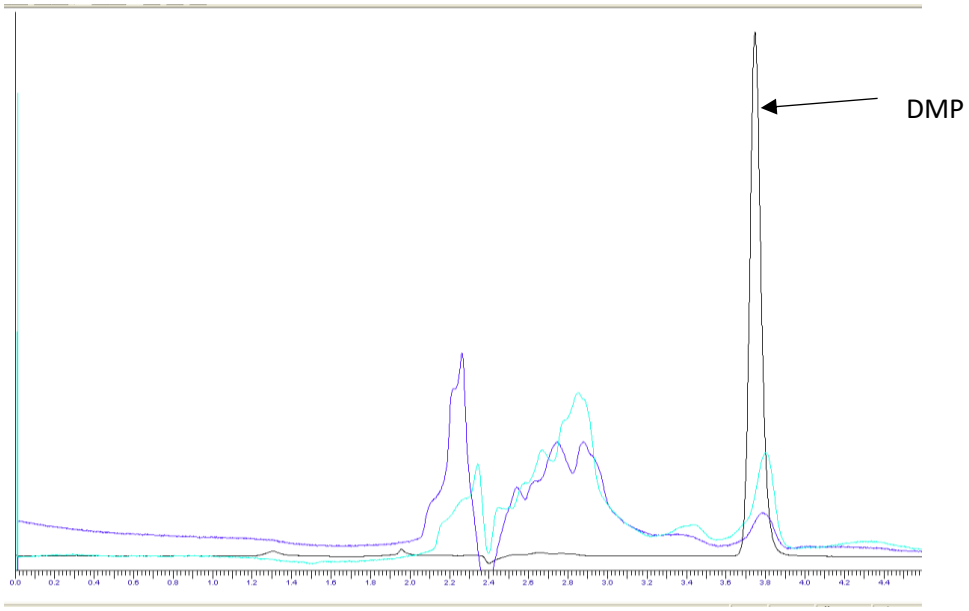

Figure 3.28b: HPLC chromatograms of initial reading (black), 17 h (blue), and 678 h (green) of continuous flow reaction.

3.6.4 Effect of Retention time on the Loss of DMP

The influence of reaction retention time was evaluated by varying the flowrate in the preliminary study (Figure 3.25) for the reaction system between 0.82 mL/min and 0.6 mL/min, corresponding to 4 and 5.55 h retention times respectively. There was no significant difference in the rate of loss of DMP with increase in retention time from 4 to 5.55 h, however, this appeared to have reversed the apparent catalyst deactivation process as is shown between ≈ 610 and ≈ 680 h in Figure 3.25, where there are indications that the catalyst was starting to deactivate. Toet et al., (2005), and Merino-Solís et al., (2015) reported an improvement in pollutant removal with increase in hydraulic retention times. Increased retention time provides more time for reactants

interaction and provides time for more effective mass transfer and the opportunity for further oxidation of recalcitrant pollutants and other oxidative intermediates, which would have otherwise been responsible for catalyst deactivation through poisoning, clogging or blocking of reactive sites (Argyle and Bartholomew 2015; Spivey et al., 2001).

3.6.5 Leached Iron from Catalyst

During continuous flow heterogeneous catalytic reactions, the catalyst tends to lose its catalytic efficiency over time due to several factors, which could be mechanical or chemical (Argyle and Bartholomew, 2015; Nauman, 2002). There was no indication that the H_2O_2 dose or the airflow rate had a direct correlation with leached iron as shown in Figure 3.27, however, this could have been due to the more acidic pH3. The leached iron from the catalyst used for this study was estimated from Figure 3.29 using the trapezium rule computation in Microsoft Excel spreadsheet 2013, given as;

$$\mathrm{A} = \frac{1}{2}(a + b)h \qquad \text{... (3.10)}$$

Where A is area of individual trapezoids, a and b are concentrations at times t_1 and t_2 respectively, and h is the volume at v_1 and v_2 in liters, based on the flowrate at the sampling time, calculated as h_2-h_1 in liters.

Volume (liters) = (FR x 60 x 24 x No of days)/1000

Where reaction flow rate FR in mL/min was taken as 0.82 mL/min from t = 0 to t = 313 and 0.6 mL/min from t = 314 to t = 678 h.

Total iron leached which corresponds to the area under the dynamic curve was calculated as 24.99 mg, using Microsoft Excel 2016 and is presented in Table 3.3.

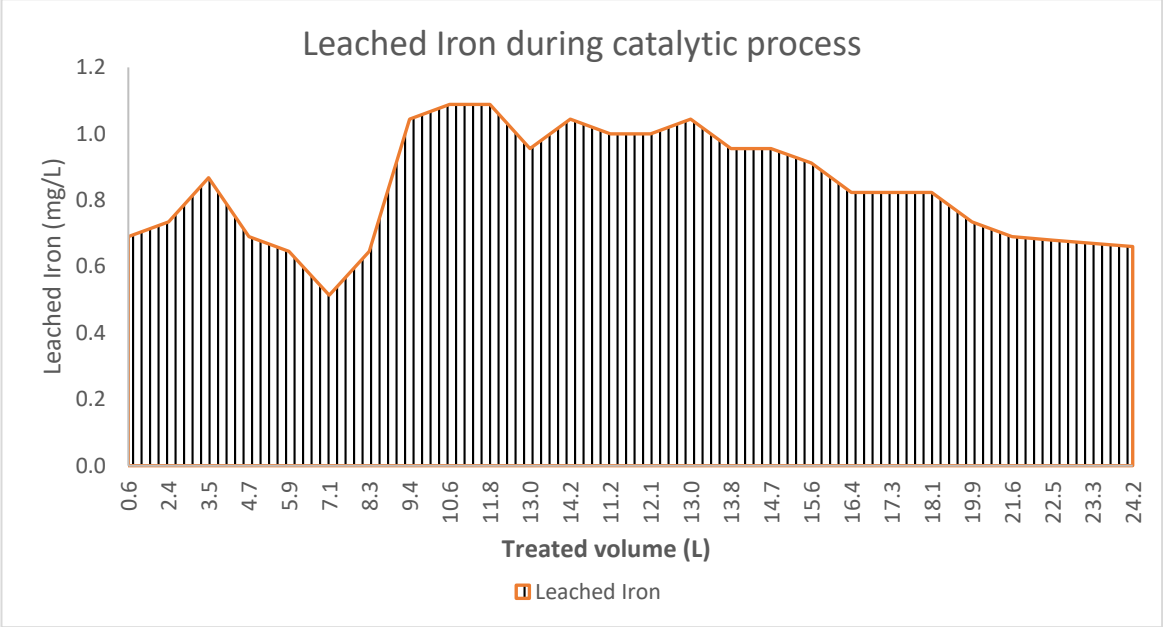

Figure 3.29: Estimated leached iron from area under the dynamic curve, using calculated volume (litres/day) used as the x-axis for the excel calculations. Experimental conditions: pH3, ambient temperature, 12.5 g catalyst (production 3) 200 mL reaction volume, Initial DMP of 25 mg/L, initial H_2O_2 of 400 ppm, RT of 4 h.

As shown on Table 3.3, the total percentage of iron leached from the catalyst was 13.77%, thus indicating that only an insignificant amount of iron was leached out from the catalyst. In addition, there was no direct correlation between leached iron and the rate of or extent of loss of DMP as seen in Figure 3.25. In Figure 3.29, the curve for leached iron appeared to form a dumbbell shape going from an initial value of ~ 0.6 mg/L, peaking at a maximum concentration of 1.1 mg/L and returning to about 0.6 mg/L leached iron concentration. Although there was starting to be a tailing of the DMP degradation at 500 h of use. This tailing of activity may not have been a result of leached iron from the catalytic system, but presumably, due to unavailability of catalyst active sites, otherwise known as poisoning, which shall be discussed in more details in the next chapter. However, it is also possible that not all the iron on the mesh was active.

The average leached iron per day was calculated as a weighted average because there was variation in flow rate of from 0.60 mL/min to 0.82 mL/min at 313 h (after 15.35 L flow) to 4 h retention time and 5.55 h retention times respectively.

To calculate weighted average leached iron per day (WA), we have that:

$$\mathrm{WA} = \frac{(\text{measured conc X } d_2 - d_1) + (\text{measured conc X } d_3 - d_2) + \cdots}{\text{sum of days}} \quad \ldots(3.11)$$

Where d_1, d_2, and d_3 are the days in ascending order.

Table 3.3: Calculated amount of Leached Iron during continuous flow of Figure 3.29.

Total catalyst amount on discs (g)	Fe per gram of PAN Mesh (mM/g)	Total Iron on catalyst in reactor (mg)	Weighted Average of leached Fe per day (mg/L)	Total Fe leached from catalyst (mg)	Fe left on catalyst after experiment (mg)	Fe loss (%)
12.50	0.272	189.87	0.93	24.99	162.17	13.16

3.6.6 Yield Degree and Mass of DMP Decomposed

The mass of substrate decomposed during the duration of the continuous flow experiment and the yield degree of substance (α) were computed and it is given as;

$$\alpha = S/[\left(\frac{Ct}{Co}\right) * t] \quad \ldots (3.12)$$

Where S is the area above the dynamic curve (Figure 3.30), and is also equal to the mass of DMP decomposed. It is given by; the total area of graph minus the area below the curve, while Ct/Co is 1 and t is duration of the experiment (in hours) (equation 3.12).

The total area of the graph was calculated as area of the rectangle (xmax * ymax) Figure 3.30, i.e 25 mg/L x 24.19 L which equals 604 mg and which is equal to the mass of DMP supplied into the system. The area under the curve, was calculated from Microsoft excel 2013, applying the sum of the areas of trapezoids (equation 3.10) was 75.0 mg. By subtracting this value (75.0 mg) from the area of the graph, the area above the dynamic curve S, was obtained as 529.75 mg, which is equal to the mass total mass of DMP decomposed. This is so when the residual values of substrate (DMP) is plotted against volume as shown in Figure 3.30 below.

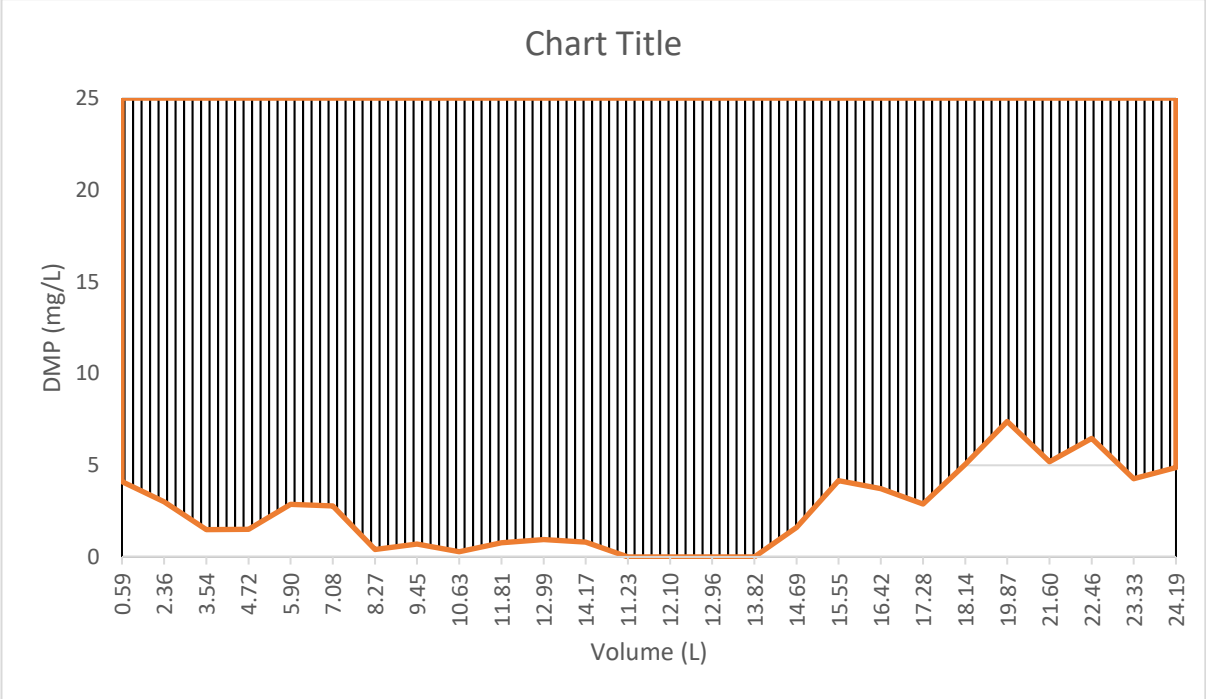

Figure 3.30: Determination of area above the dynamic curve as mass of DMP decomposed. Reaction conditions: pH3, ambient temperature, 12.5 g catalyst (production 3) 200 mL reaction volume, Initial DMP conc of 25 mg/L, initial H_2O_2 conc of 200, 400, and 500 mg/L, RT of 4 and 5.55 hours.

We have that, the degree of yield α:

$$\alpha = \frac{529.75\ Hours}{1 * 678\ Hours}$$

The degree of Yield = 0.8588 calculated from equation (3.12) and presented in Table 3.4 below.

Table 3.4: Parameters used for the determination of yield degree of DMP

S Area above the curve	C_0 Initial [DMP] (mg/L)	C_t/C_0	t Duration of reaction (Hours)	α Yield degree of DMP	Mass of DMP supplied in reactor (mg)
529.75	25	1	678	0.8588	604

S which is the mass of DMP decomposed (mg) was calculated as 529.75 mg. This is as presented in Table 3.5.

Table 3.5: Parameters used for the determination of mass of DMP decomposed

α Yield degree of DMP	Q Avg. Flow rate (mL/hr)	t time (hr)	Co Initial [DMP] (mg/L)	S Mass of DMP decomposed (mg)	Mass of DMP supplied in reactor (mg)
0.8588	42.6	678	25	529.75	604

Overall, almost all the DMP was decomposed as shown in Figure 3.30. The mass of DMP decomposed by the catalyst during the continuous flow experiment of 529.75 mg shows variation from the mass of DMP decomposed in the presence of other competing anions and other organics under similar conditions as seen in the next chapter, which is likely due to the influence of competing side reactions of BTEX, aliphatic hydrocarbons, bicarbonates and sodium salts.

3.7 Summary

Process parameters such as catalyst concentration, initial H_2O_2 concentration, pH of reaction solution, temperature and presence of radical scavengers have been evaluated and successfully defined for the decomposition of DMP under defined conditions and optimum conditions established for the heterogeneous oxidation process using the one factor at a time (OFAT) approach. Like most other Fenton and Fenton-like processes, the optimum reaction pH under the given experiment condition is 3. In addition, the reaction appears to follow the $^{\bullet}OH$ reaction mechanism.

The application of the modified PAN heterogeneous catalyst for the oxidation of DMP in the presence of H_2O_2 in continuous flow mode has proved successful, with a good yield degree of DMP, of 0.8588. The total mass of DMP decomposed in 678 h was 529.75 mg with about 13.16% iron loss from the catalyst, which indicates the durability of the catalyst system. However, the inability of the reaction system to completely oxidize the acetic acid can lead to catalyst poisoning and possible deactivation, resulting from blockage of catalyst reactive sites, which has been discussed in more detail in chapter 5. The next chapter focuses on the degradation intermediates formed from the catalytic decomposition of DMP using the PAN heterogeneous catalyst.

4 Oxidation Scheme for the Degradation of 3, 5-Dimethylphenol Using a Modified PAN Heterogeneous Catalyst

4.1 Introduction

According to Boitsov et al., (2004), the focus of most studies on alkylphenol (AP) has been on the long chain APs, (C8, and C9) which are degradation products of Alkyl phenol ethoxylates (APE). The catalytic degradation of DMP to my knowledge has been studied by Belattar et al., (2012). However, no attempt was made to propose a degradation pathway, or identify the oxidation intermediates.

Common analytical protocols used for the determination of these compounds and their oxidation products are high performance liquid chromatography (HPLC) and gas chromatography (GC). However, because most alkyl phenols are both very polar, thermally labile and occur in very low concentrations in the natural environment, a sample preparation step known as derivatization is commonly carried out before analysis by GC (Yang et al., 2007).

This chapter therefore describes the procedures and methodology used, including sample preparation and analytical procedures to attempt the determination of a tentative oxidation scheme of the Fenton-like heterogeneous degradation of DMP.

4.2 Aims and Objectives

The aim of this chapter is to carry out experiments in batch mode leading to a possible determination and identification of reaction intermediates of DMP degradation and propose a tentative oxidation scheme for the catalytic degradation of DMP, using the PAN catalyst.

The Objectives are as follow:

- To design a suitable sample preparation procedure and carry out solid phase extraction for analysis and hence, the determination of oxidation intermediates.
- To use analytical techniques such as HPLC, GCMS, LCMS and IC to attempt the identification of reaction intermediates, and propose an a tentative oxidation scheme
- To identify the fragmentation ions formed in GC- mass spectrum, and track their evolution.

4.3 Materials and Methods

4.3.1 Reagents, Chemicals and materials

The chemicals, reagents and materials used are as shown in Table 4.1.

Table 4.1: Materials used study

Reagents/chemicals/materials	Molecular formula	Source	Purity%
Dichloromethane	CH_2Cl_2	Sigma Aldrich	98
Methanol	CH_3OH	Sigma Aldrich	99
3,5-Dimethyphenol	$C_6H_3(CH_3)_2OH$	Sigma Aldrich	99
Double distilled water	H_2O	DMU-Fistreem Cyclon: WSC044	-
Acetonitrile	CH_3CN	Sigma Aldrich	99
Acetone	CH_3COCH_3	Sigma Aldrich	98
Hydrochloric acid	HCl	Sigma Aldrich	35
Acetic acid	CH_3COOH	Sigma Aldrich	99.85
Formic Acid	HCOOH	Sigma Aldrich	96

The following materials were also used for the study; PAN heterogeneous catalyst (production 3), C18 Strata–X-CW, 500 mg, 6 ml solid phase extraction (SPE) cartridges purchased from Phenomenex UK, 6 ml and 50 ml syringes and a plastic connector

tubing. Other materials used for the study include; Radley carousel, flea, magnetic stirrer, analytical balance.

4.3.1.1 Experimental Procedure for Catalysis of DMP and Determination of Oxidation intermediates

The concentration of substrate was first made to 25 mg/L and catalysed in a heterogeneous batch process following the procedure in section 3.4.1, chapter three. From the optimization studies, it was observed that the onset of intermediate formation as seen on the HPLC chromatograms in Figure 4.10 was 10 minutes with the most intermediates formation at 30 minutes (Figure 4.10). Accordingly, the whole reaction volume was extracted at 30 minutes by solid phase extraction process (SPE). The SPE procedure has been described in 4.3.3.1.1. This resulted in the oxidation products being transferred from the aqueous phase to an organic phase of 1:1 DCM: methanol (v/v). The organic eluent from the SPE process was then pre-concentrated using a rotavapour model R210 at 800 psi at 50 ^{o}C for 10 min to near dryness. This was then reconstituted in 1.5 mL of dichloromethane DCM and methanol (1:1 v/v) and analysed on the GCMS as required.

For the LCMS analysis, the reaction solution was sampled directly from the reactor at predetermined time interval 30 min and analysed on the LCMS. Identification of intermediates was by analysis of mass spectrum of the various peaks and comparison with literature. Ion chromatography was used to test for the presence of low molecular weight organic acids, which are thought to be the products of the breakdown of organic compounds before the final mineralized products of CO_2 and H_2O (Chi and Huddersman

2007). This was done by matching unknown compounds with the retention time of analytical standards of pure compounds. The concentration of these acids was determined from calibration plots (Figure 4.0). Control experiments were performed by reacting H_2O_2 and the catalyst, in the absence of the substrate to investigate any possibility of organic acid release from the catalytic mesh.

4.3.2 Instrumentation

Analytical equipment used for this study included the following; Perkin Elmer HPLC series 200 fitted with a UV detection system, PerkinElmer Flame Atomic Absorption Spectrometer AAnalyst 200 model, Bruker 430 gas chromatograph coupled to a Bruker 320 mass spectrometry detecting system. Others are Metrohm Modular MIC-2 advanced ion chromatography system, coupled to a conductivity detector and Agilent Technology 1260 Infinity Liquid Chromatograph coupled to a 6120 quadrupole mass spectrometer detector.

4.3.3 Methodology for the determination of oxidative intermediates

To monitor oxidative intermediates in the heterogeneous catalysis of DMP in the presence of H_2O_2, the reaction was first monitored in the HPLC as described previously, followed by GCMS and LCMS analysis for a possible, positive identification of oxidation intermediates using their characteristic ion or fragmentation patterns (Sheldon et al., 2009; Milman, 2005; Stein, 1994; Sanders, 1999). Ion chromatography was also employed for sample analysis-post treatment to test for the presence of organic acids in the reaction system, which were identified by matching their retention times with those of the analytical standards of pure compounds. The details of the analytical protocols including sample preparations have been described in more details in the next section.

4.3.3.1 Sample Preparation Procedure

4.3.3.1.1 Solid phase extraction (SPE) procedure for GCMS

Strata-X 33u polymeric reverse phase 500 mg/6 mL SPE cartridges were conditioned by passing 3 mL of methanol through the 500 mg packing bed as described in Yang et al., (2007). This was done to remove residual bonding agents. Following this, the SPE cartridges were then equilibrated by passing 6 mL of double distilled water at a flow rate of 2 mL/min. Care was taken to make sure that the packing material in the cartridge was not exposed to air. Subsequently, the cartridge was exposed to the reaction solution, by flowing the solution through the cartridge under suction using a 50 mL syringe. The analytes sorbed on the C18 extraction cartridge were eluted using 20 mL dichloromethane/methanol solution 1:1 v/v. This procedure was repeated but this time the elution was done with a weak solution of formic acid in methanol (Boitsov et al.,

2004) for comparison. A mixed solvent- methanol/dichloromethane was chosen to ensure the elution of both polar and less polar analytes. Yang et al., (2007) had used a combination of dichloromethane/hexane or acetone and had similar recoveries while Boitsov et al., (2004), used a solution of formic acid in methanol with success. The eluent was concentrated by evaporating to near dryness using a Rotavapour model R210 at 800 psi for 10 min and temperature of 50 ^{o}C. This was reconstituted in 1.5 mL dichloromethane/methanol and analysed in the GCMS.

4.3.3.2 Gas chromatographic Analysis (GCMS)

A Bruker-430 gas chromatograph coupled to a Bruker-320 mass spectrometry detector (GCMS) system was used for the qualitative analysis. The stationary phase was a Zebron ZB-5MSi (5%-diphenyl-95%-dimethyl polysiloxane copolymer) with dimensions 30 m x 0.25 mm x 0.25 µm (packing), purchased from Phenomenex UK and the carrier gas (helium) was flowed at the rate of 1 mL/min. Injection temperature was 270 ^{o}C, volume was 1 µl injected in spilt mode at 5:1. The oven temperature program started at 100 ^{o}C for 3 min to 270 ^{o}C ramped at 5 ^{o}C/min giving a total run time of 42 min. The ionization source was the electron impact ionization (EI) at 70 eV, transfer line temperature of 270 ^{o}C and the mass range from 50 to 300 amu.

4.3.3.3 Liquid Chromatography Mass Spectroscopy (LCMS)

The following instrument parameters were set for liquid chromatograph: Injection volume 10 µL, at a draw speed of 200 µL/min, in standard injection mode. All solvents used were MS grade. The mobile phase was acetonitrile and water 45:55 v/v, in 0.1% formic acid at a flow rate of 1 mL/min using a C18 reverse phase column, of 4.6 mm ID,

5 µm packing, and 250 mm length. For scan mode, the mass spectrometer was set to a scan range of 50 to 500 amu and a fragmentation voltage of 70 ev using the atmospheric pressure ionization electrospray (API-ES) on positive polarity. On the selected ion monitoring (SIM) mode, the following ions were monitored: 122, 138, 136, 150, and 166 (such as were seen in GCMS). The gas temperature was 350 ^{o}C, drying gas flow rate was 10.0 L/min. There was no rigorous sample preparation, except for filtration using 0.45 µm filter cartridge attached to a 5 mL syringe, to prevent the catalyst fibrils from blocking the ionization source and needle. All solvents used where MS grade. The catalytic reaction was sampled at predetermined intervals of 10 min starting from zero minutes up to 60 min. Total method run time was 10 min and DMP retention time was 8 min under the stated conditions.

4.3.3.4 Ion Chromatographic Analysis

The ion chromatography was based on the method previously described by Chi and Huddersman (2007). Metrohm Modular MIC-2 advanced system, coupled to a conductivity detector, with a stationary phase comprising a metrosep 6.1005.200 organic acid analytical column, of length 250 mm and diameter 7.8 mm, particle size of 10 µm, made of polystyrene/divinylbenzene copolymer packing material was used for the analysis of liquid samples to determine the presence of organic acids. The isocratic mobile phase was perchloric acid ($HClO_4$), heptafluorobutyric acid (HFBA) and sulphuric acid. The mobile phase flow rate of 0.5 mL/min was used, while the detector was operated in positive mode, at a scale of 1.0 µs. The samples were filtered through a 0.45 µm Whatman filter paper to remove catalyst fibrils in order to forestall any blockage of

the sample aspirator. Identification of peaks was achieved by comparison with retention times of known organic acids standards.

Calibration graphs of acetic acid and formic acids were plotted over a range of 0.5 to 10 mg/L each using pure acetic and formic acids. 500 mg/L standard stock of acetic acid (specific density of 1.052 g/mL) was prepared by carefully pipetting 95 µL of acetic acid into 200 mL volumetric flask and making it up to mark with double distilled water. Working standards of 0.5 to 10 mg/L were prepared from the 500 mg/L standard stock by dilution. For 10 mg/L for instance, 2 mL of the standard stock solution of acetic acid was pipetted into 100 mL volumetric flask and made up to mark with double distilled water. This process was repeated for other working standards of acetic acid of various concentrations. For formic acid (specific density of 1.220 g/mL), 500 mg/L standard stock was prepared by carefully pipetting 82 µL of formic acid into 200 mL volumetric flask and making it up to the mark with double distilled water. The calibration graph has been presented in Figure 4.0 below.

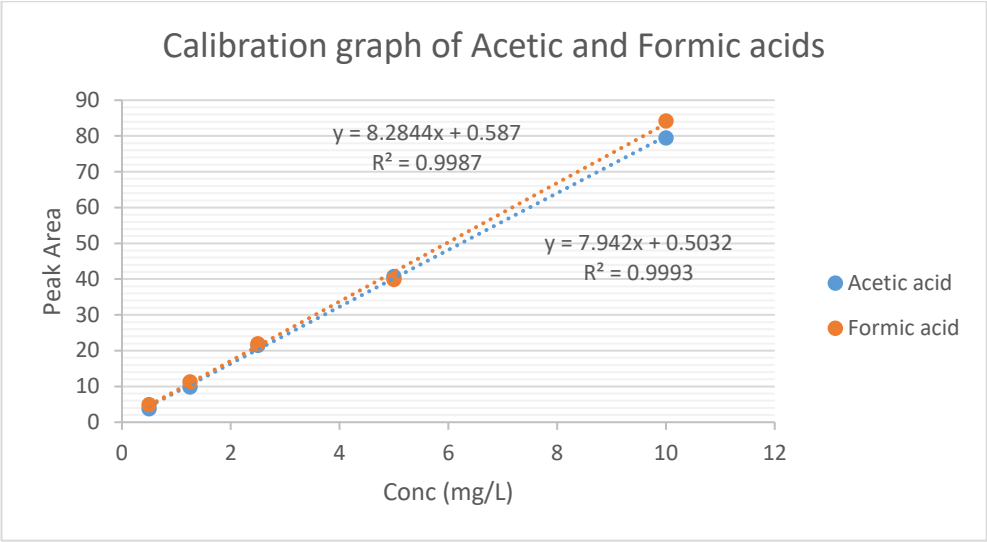

Figure 4.0: Calibration graph for acetic and formic acids

4.4 Oxidation Intermediates In the Degradation of 3,5-DMP in Heterogeneous Catalysis

The oxidation of oxidizable or refractory organic compounds to their final products is known to proceed through various oxidative intermediaries before reaching mineralization, which is CO_2 and H_2O (Chi and Huddersman 2007). Oxidation will also lead to easily biodegradable simpler molecules, or other substituted compounds called reaction intermediates (Catrinescu et al., 2011). The process of oxidation of most organic compounds can often lead to the formation of intermediates or end-products with more toxic properties than even the starting compounds (Chi and Huddersman 2007). The need to identify these intermediates, with a view to proposing the degradation pathway for DMP cannot be over emphasised.

The decomposition or transformation reactions that come about as a result of catalytic chemical activities will vary given different starting materials. The decomposition of

DMP has been reported by Belattar et al., (2012), where goethite (Fe^{3+} hydroxide) was used as catalyst, leading to the removal of about 60% DMP of 1.5 g/L initial concentration, without an oxidant after 100 h of irradiation with low pressure mercury UV lamp - Philips 125 W at a wavelength of 365 nm. About 85% removal was however achieved after 5 h, using 1 g/L H_2O_2 as an oxidant at pH9, and 70% removal at pH3 under the same conditions. The oxidation scheme was not disclosed and to my knowledge, there has been no report of the oxidation scheme of DMP.

4.5 Results, Discussions and Tentative Oxidation Schemes from Qualitative Analysis.

The use of chromatographic techniques in the determination and possible identification of unknown components of samples or reactions is well known owing to their robustness, reproducibility, sensitivity and selectivity (Chi and Huddersman 2007; Milman, 2011). The use of more than one instrument with different detector capabilities for the purpose of identifying unknown components of the reaction is so as to complement each other and make up for the individual limitations of the respective instruments.

The results from HPLC-UV, GCMS, LCMS and Ion Chromatography have all been presented to corroborate the findings and propose a tentative scheme for the catalytic decomposition of DMP in the presence of H_2O_2 in a heterogeneous system.

4.5.1.1 HPLC-UV Analysis Results and Discussions

The loss of DMP in the heterogeneous catalytic system was routinely monitored on the HPLC with UV detector, throughout the duration of the experiments, at predetermined intervals as earlier mentioned. The loss of the starting compound (DMP) was monitored,

as well as the intermediates over time. The chromatograms are as shown in Figure 4.1 while the separated compounds are shown in Figure 4.2.

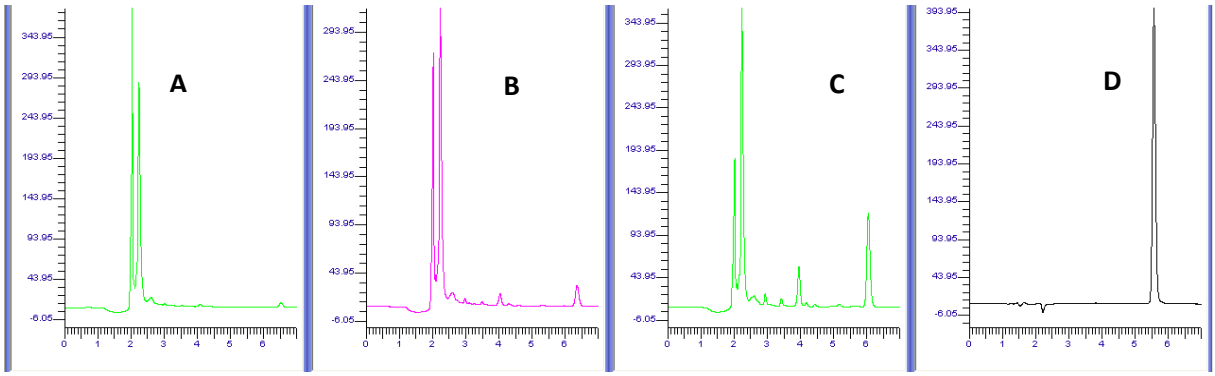

Figure 4.1: Chromatograms at different reaction times. A= 120 min, B=60 mins C= 30 mins D 0mins. Batch reaction at pH3, 400 mg/L H_2O_2, 5 g catalyst, 25 mg/L DMP, temperature of 25±1 ^oC, and 100 mL reaction volume.

A snapshot of results from the HPLC analysis, at different reaction times has been presented as A to D on Figure 4.1. A, shows the chromatogram after 120 minutes of reaction time, C and B is a snapshot of the chromatograms showing intermediates at 30 minutes and 60 minutes respectively, while D shows the initial reaction at zero minutes. The peaks and their respective retention times are presented in Table 4.2 below.

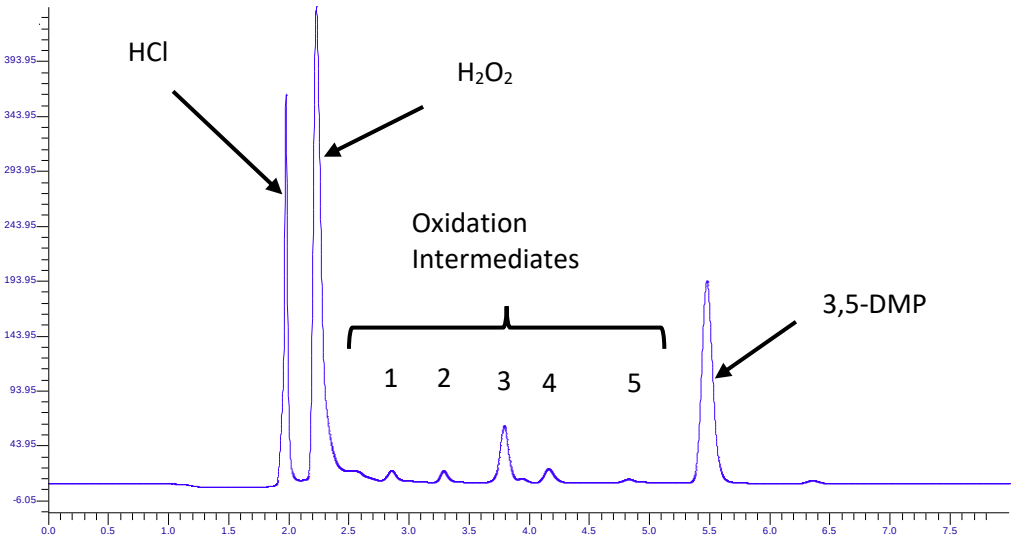

Figure 4.2: Chromatogram from HPLC-UV detector at 30 min reaction time showing intermediates in batch reaction at pH3, 400 ppm H_2O_2, 5 g catalyst, 25 mg/L DMP, temperature of 25±1 ^oC, and 100 mL reaction volume.

Table 4.2: Retention times of the reaction intermediates obtained from HPLC analysis of the catalytic oxidation of DMP shown on chromatogram in Figure 4.2.

Intermediate Peak Number	Retention time (min)
1	2.95
2	4.49
3	3.45
4	3.98
5	5.20
DMP	5.50

As shown on Figure 4.2, the reaction proceeded with the formation of intermediates and terminated with the disappearance of the intermediates. The starting compound (DMP), H_2O_2, HCl (used for pH adjustment) and the intermediates, have been labelled as

shown on Figure 4.2, while the appearance and disappearance of oxidation intermediates have also been plotted out as shown on Figure 4.3.

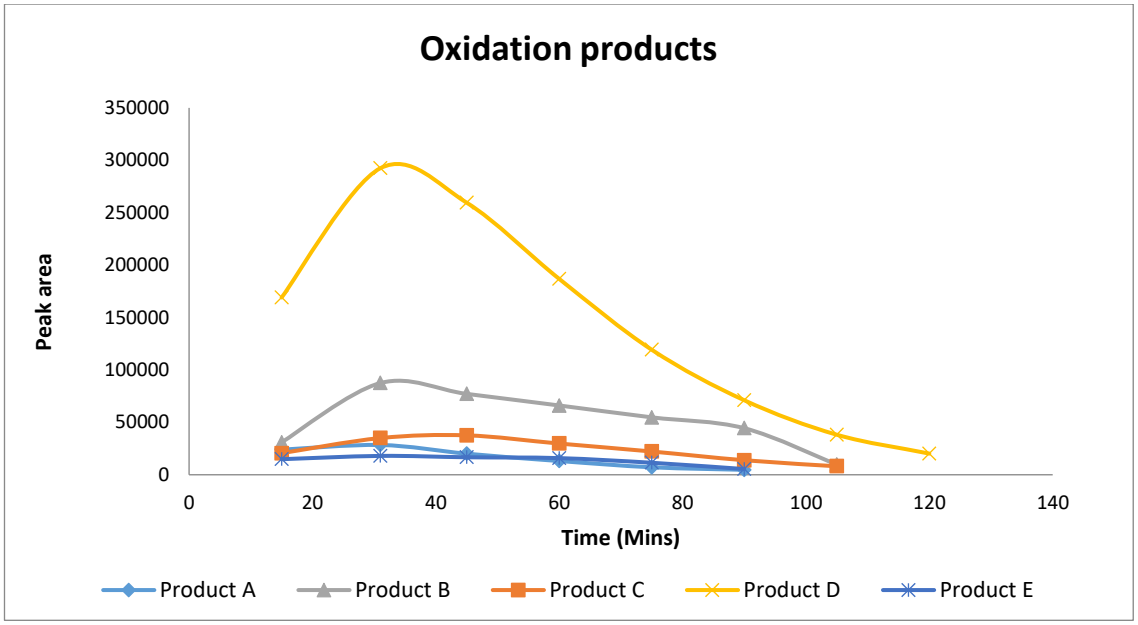

Figure 4.3: A plot of oxidation intermediate peak areas as monitored on HPLC-UV in batch mode catalysed at pH3, 400 ppm H_2O_2, 5 g catalyst, 25 mg/L DMP, temperature of 25±1 ^oC 100 mL reaction volume.

The different products on Figure 4.10, shows that reaction intermediates did not accumulate in the system, but had different reaction rates owing to differing susceptibility to oxidation. In addition to this, there appeared to be selective reactivity of these compounds to the oxidizing species in the reaction. Product D was least susceptible to the oxidising species and hence there was build up until after 40 min.

Although it is possible to identify reaction intermediates by matching the retention times using the HPLC data, however, the technique is very subjective owing to co-elution of some compounds due to poor separation ability of analytical technique. Attempts

were however made to match retention times of suspected intermediates, but this was not successful. In addition, not many suspected oxidation intermediates were commercially available. Other more selective separation/identification techniques were used to further investigate the oxidation intermediate of DMP.

4.5.1.2 GCMS Analysis Results and Discussions

Gas chromatography analysis was further undertaken using a mass spectrometer detector to increase sensitivity and selectivity/specificity. When a given molecule in a sample is impacted upon by a beam of electron, it results in the formation of a 'family' of ion fragments, wherein the mass distribution of the fragments are unique to the original parent molecule. This is the principle of mass spectrometry detection system and the basis for its application for the positive identification of unknown compounds (Skoog et al., 1992; Chi and Huddersman 2007; Moldoveanu and Kiser 2007; Sheldon et al., 2009; Milman 2011).

The results presentation and discussion for GCMS data is based on the individual peaks on the GCMS total ion chromatogram, which has been presented in Table 4.3. Each individual peak (Figure 4.4) with the corresponding mass spectrum (showing fragments) has been highlighted and attempts have been made to account for most of the prominent mass fragments of the compounds on the chromatogram. The evolution of tentative reaction intermediate from either the parent compound (DMP) or from other intermediates has also been done.

Figure 4.4 shows a GCMS total ion chromatogram (TIC) in the scan mode which was obtained from the heterogeneous catalytic decomposition of DMP, sampled at 30 min.

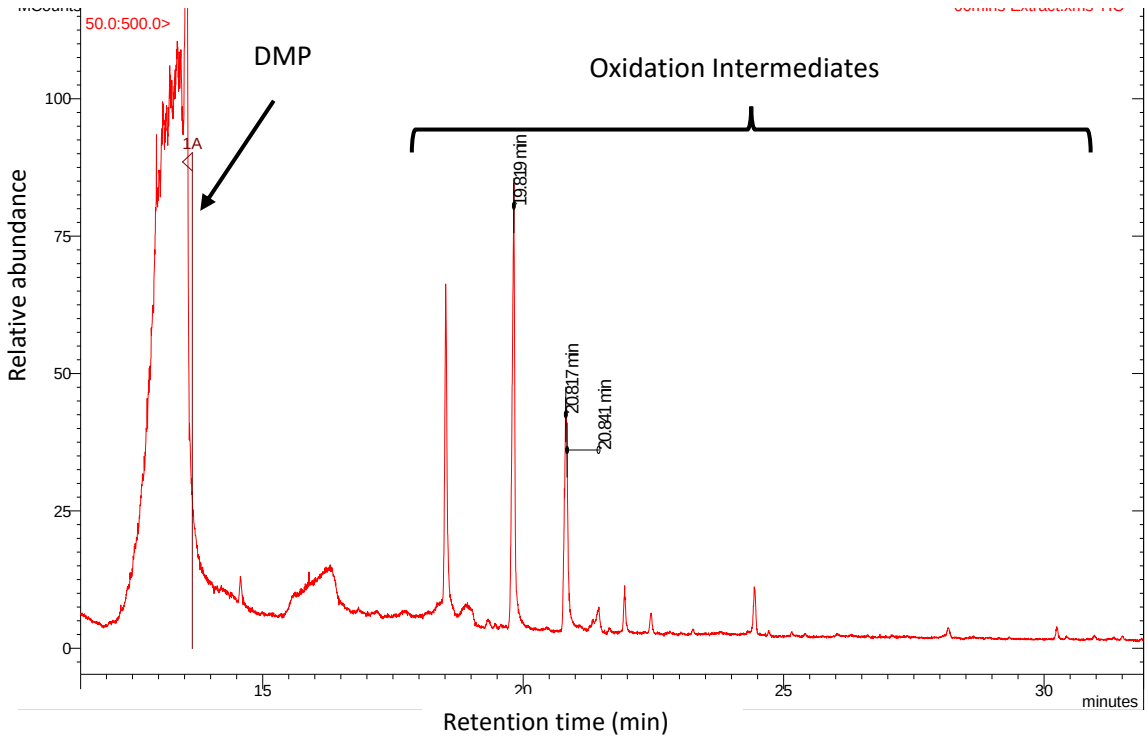

Figure 4.4: TIC of 30 min sample of DMP catalysis at pH3, 400 ppm H_2O_2, 5 g catalyst, 25 mg/L DMP, temperature of 25±1 ^oC and 100 mL reaction volume.

After 30 minutes reaction, the sample was prepared for GC-MS analysis according to the protocol described previously. The results showed about ten intermediate compounds on the GCMS. The mass spectrum data of six of the most prominent peaks were analysed. The results for peak 1 are as shown on Figures 4.5 and 4.6.

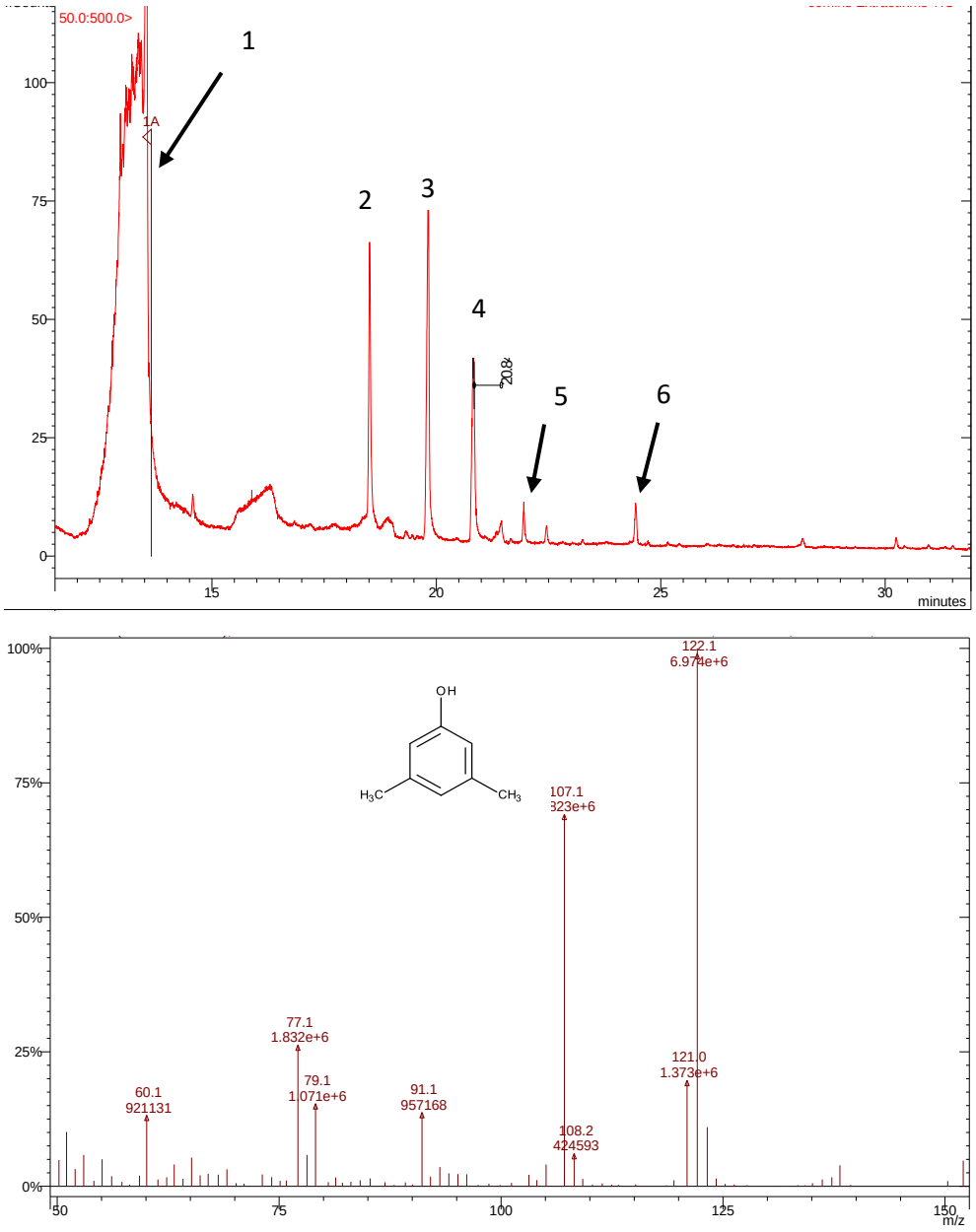

Figure 4.5: TIC and the mass spectrum of peak 1 on the chromatogram for the oxidation of DMP at 30 min reaction.

Other peaks were also analyzed and their characteristic ion (m/z) or fragmentation patterns for most obvious peaks whose fragments had a relative abundance of 25% and over, are presented in Table 4.3. Peaks with few fragments such as M= 122 (the peak associated with the starting compound) however had all fragments above 10% relative abundance analyzed and reported.

Table 4.3: Fragmentation patterns in the GCMS analysis of possible intermediate compounds, including the parent ion showing retention times and molecular ions

Peak No	Retention time (min)	M^+	Characteristic ions (m/z)	Figure No
1	13.64	122	122, 121, 107, 91,79, 77, 60	Figure 4.5
2	18.7	138	138, 137, 136, 123, 107, 91, 77, 60	Figure 4.8
3	19.8	138	138, 136, 123, 107, 77, 51	Figure 4.9
4	20.8	138	138, 123, 120, 109, 107, 92, 91, 79, 77, 65 53	Figure 4.11
5	21.9	166	166, 138, 123, 122, 121, 109, 107, 95, 92, 91, 78, 77, 65, 60, 53, 50	Figure 4.13
6	24.5	149.9	149.9, 121 122, 107, 91, 71, 60, 57	Figure 4.16

Peak 1

The fragmentation of the parent compound (DMP), is as shown in Table 4.3 as peak 1, while its chromatogram with mass spectrum is presented in Figure 4.5. The base peak M = 122 corresponds to the molecular ion (M^+). A possible loss of hydrogen H atom could have resulted in 121 ion fragment. There is also a possible loss of a methyl CH_3 group, from the molecular ion, resulting in 107 m/z ion fragment, which shows a high abundance of 70% and is presumably a hydroxytropylium (Silverstein et al., 2005). There is a 91 m/z fragment, which is likely to be a tropylium ion, that could have resulted from

a loss of a methoxy radical from the molecular ion – 122 m/z (Figure 4.6 below). Most 91 m/z ions in aromatic hydrocarbons fragmentations are thought to be a tropylium ion rather than a benzylic cation (Silverstein et al., 2005; Budzikiewicz et al., 1964; Grubb and Meryerson, 1963). This is said to be responsible for the ease of the loss of a methyl group from xylenes, except for toluene (Silverstein et al., 2005).

Looking at the fragmentation of toluene, which has a similar structure to DMP (except for the OH group in DMP), the elimination of hydrogen from toluene molecular ion also results in 91 m/z fragment and this has always been thought of, as a benzyl cation (C_7H_7). However, studies from deuterium labeling experiments suggest that, the tropylium structure is a plausible fragment for the ion (Johnstone, 1972). They argued that if the toluene molecular ion first rearranged to a hydrotropylium ion, a loss of hydrogen could likely result in a tropylium ion at m/z 91.

Silverstein and his co-workers also suggested that the presence of a characteristic cluster of some ions which include 77 ($C_6H_5^+$), 78 ($C_6H_6^+$) and 79 m/z ($C_6H_7^+$) is a common feature of aromatic hydrocarbons fragmentations and is due to an α cleavage (one of the fragmentation pathways for radical molecular ions) and hydrogen migration which is a common feature of monoalkylbenzenes. This explains the presence of a phenyl cation at m/z 77 and 79 in the fragmentation of M^+ = 122 molecular ion peak. The evolution of 60 m/z is not very clear.

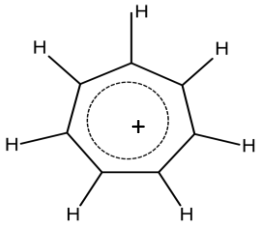

Tropylium ion 91m/z

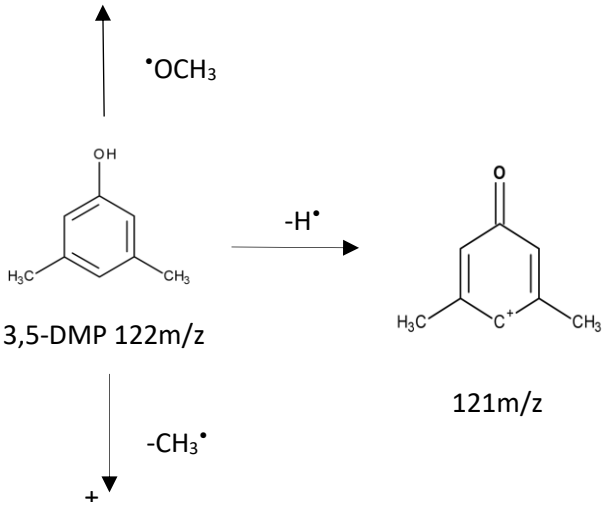

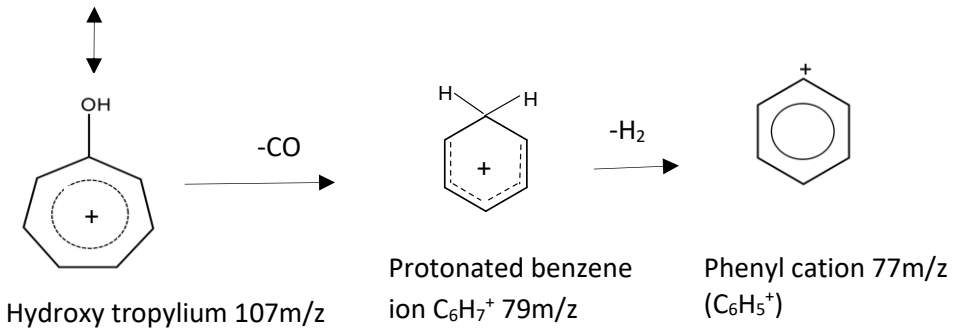

Figure 4.6: Observed fragmentation pathway for 3,5-DMP (peak 1) and proposed evolution of the fragments shown in Table 4.6.

Peak 2

Peak number 2 on Table 4.3 had a molecular ion of 138. This molecule is likely to be a product of the sequential hydroxylation of the parent compound after a possible hydrogen atom abstraction, resulting to three possible isomers: 3,5-dimethyl hydroquinone, 3,5-dimethyl catechol and 3-hydroxymethyl-5-methylphenol as shown in Figure 4.24. These propositions are in agreement with Zazo et al., (2005) and Palacio et al., (2009). Zazo et al., reported about 90% conversion of phenol after 30 min, following the hydroxylation of the aromatic ring, resulting in dihydroxybenzenes.

The fragmentation pathway for peak 2, M = 138 was mainly by elimination in most part and rearrangement (for the formation of tropylium ion from benzyl cation). A loss of a hydrogen atom could result in the 137 m/z ion. While a loss of a methyl group (-15) from peak 2, M = 138 could result in m/z 123 ion. The 107 m/z ion could have resulted from the loss of an oxygen radical (-16), same for the 91 m/z ion (Kim et al., 2003). Further elimination of another methylene group (-14) could have resulted in 77 m/z fragment, which corresponds to a phenyl cation $C_6H_5^+$ which further fragmented to give 60 m/z mass fragment. The chromatogram and mass spectrum are as shown in Figure 4.8.

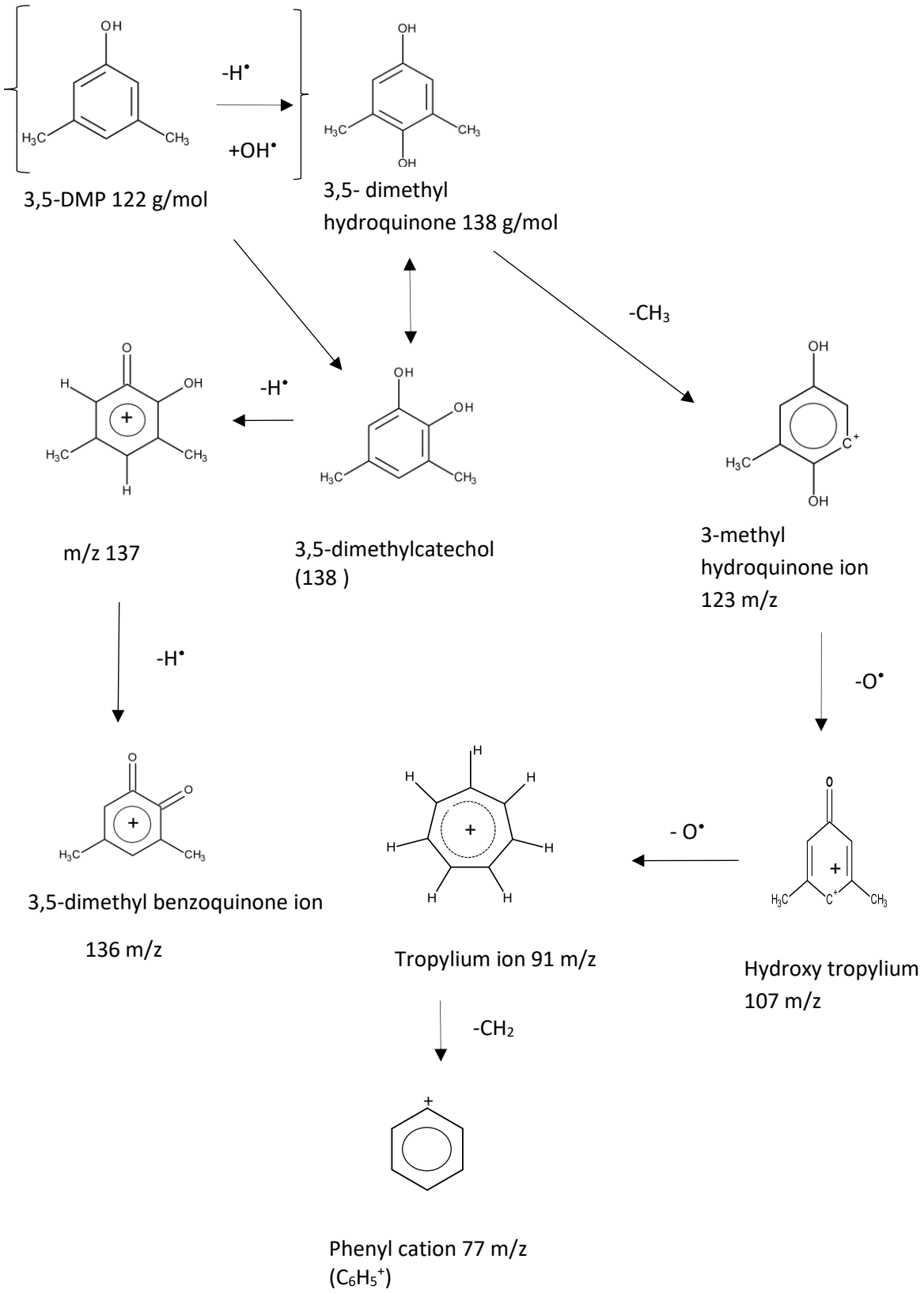

Figure 4.7: Proposed pathway for the formation of M =138 (peak 2) tentative molecule from 3,5-DMP and evolution of the fragments of this molecule previously shown in Table 4.3.

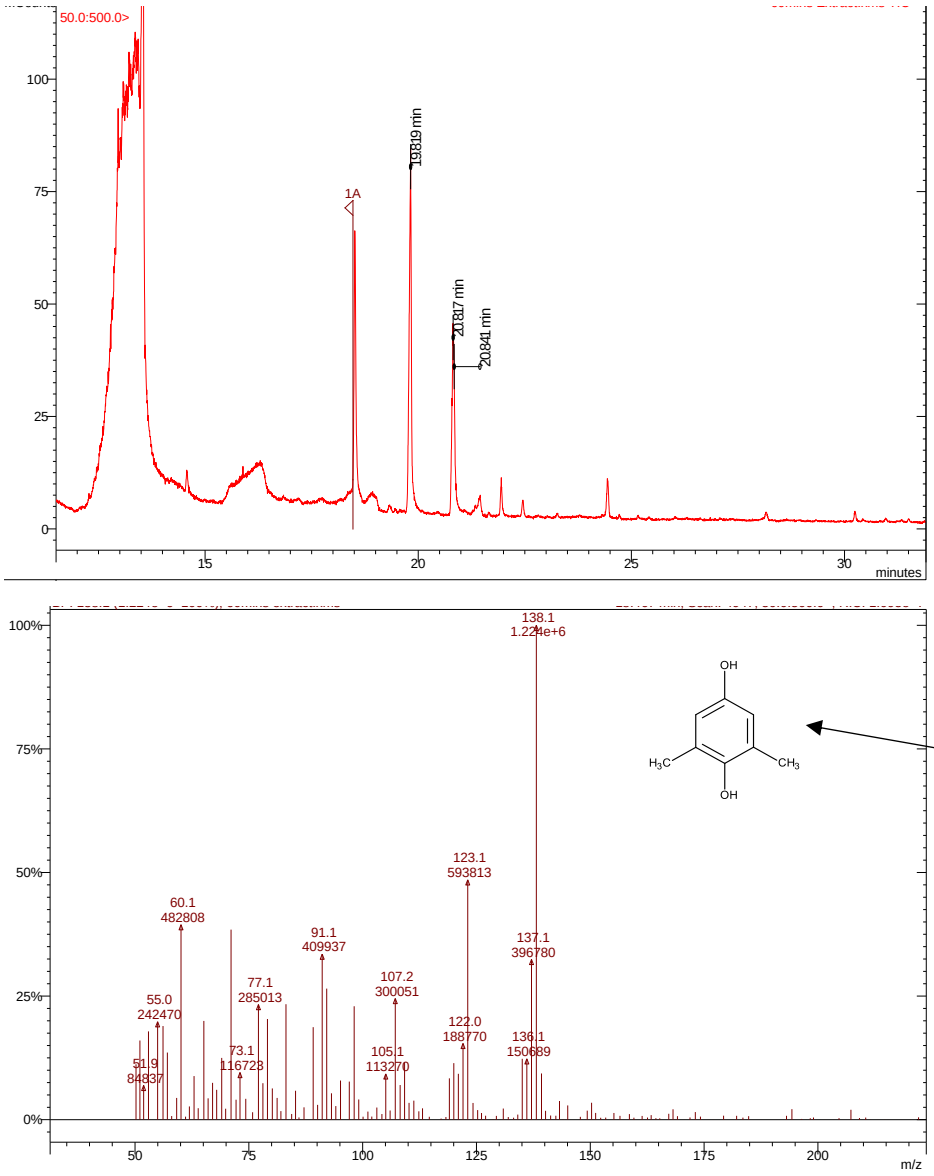

Likely a para-isomer based on retention time.

Figure 4.8: TIC and the mass spectrum of peak 2 on the chromatogram for the oxidation of DMP at 30 min reaction.

Peak 3

The fragmentation of the molecule at peak number 3 in Table 4.3 is shown in the mass spectrum and chromatogram in Figure 4.9 below. The molecular ion fragment at M = 138 is likely to be an isomer of peak 2 shown previously, suggesting more than one isomeric possibilities of this proposed intermediate for 3,5-DMP. The substitution of the OH group in the ortho, and para positions (previously shown in Figure 4.7) resulting in a

possible 3,5- dimethyl catechol, and 3,5-dimethyl hydroquinone is in agreement with Palacio et al., (2009) and Zazo et al., (2005) where they suggested a predominance of ortho and para hydroxylation while working with phenolic intermediates. This is because, alkylphenol molecular ions such as this, preferably dissociate by benzylic cleavage, which is the case for methylphenols where according to Gross (2004), $[M-H]^+$ are observed.

The fragmentation of peak 3 of MW 138 g/mol features an ion, which shows a relative abundance of 50% at 136 m/z (Figure 4.9). This fragment could have resulted from a sequential loss of two hydrogen ions to give a fragment at 137 m/z and then 136 m/z, likely to be a benzoquinone ion ($C_8H_8O_2^+$). A further loss of a $CH_3^\bullet$ (-15), from the molecular ion (M = 138) could result in the 123 m/z ion fragment, while the 107 m/z which is likely to be a hydroxy tropylium ion fragment, could result from 123 m/z by the loss of oxygen ion (-16). The 91 m/z (tropylium ion) could result from 107 m/z by the loss of oxygen radical (-16) while 77 m/z, a possible phenyl cation fragment ($C_6H_5^+$), is a possible product of a loss of $CH_2^\bullet$ (-14). Both 51 and 53 m/z fragments could result from the loss of C_2H_2 (-26) from 77 and 79 m/z respectively. This pattern has previously been identified with peak 1 fragmentation in Figure 4.7, it is a common fragmentation feature in benzylic alcohols (Silverstein et al., 2005).

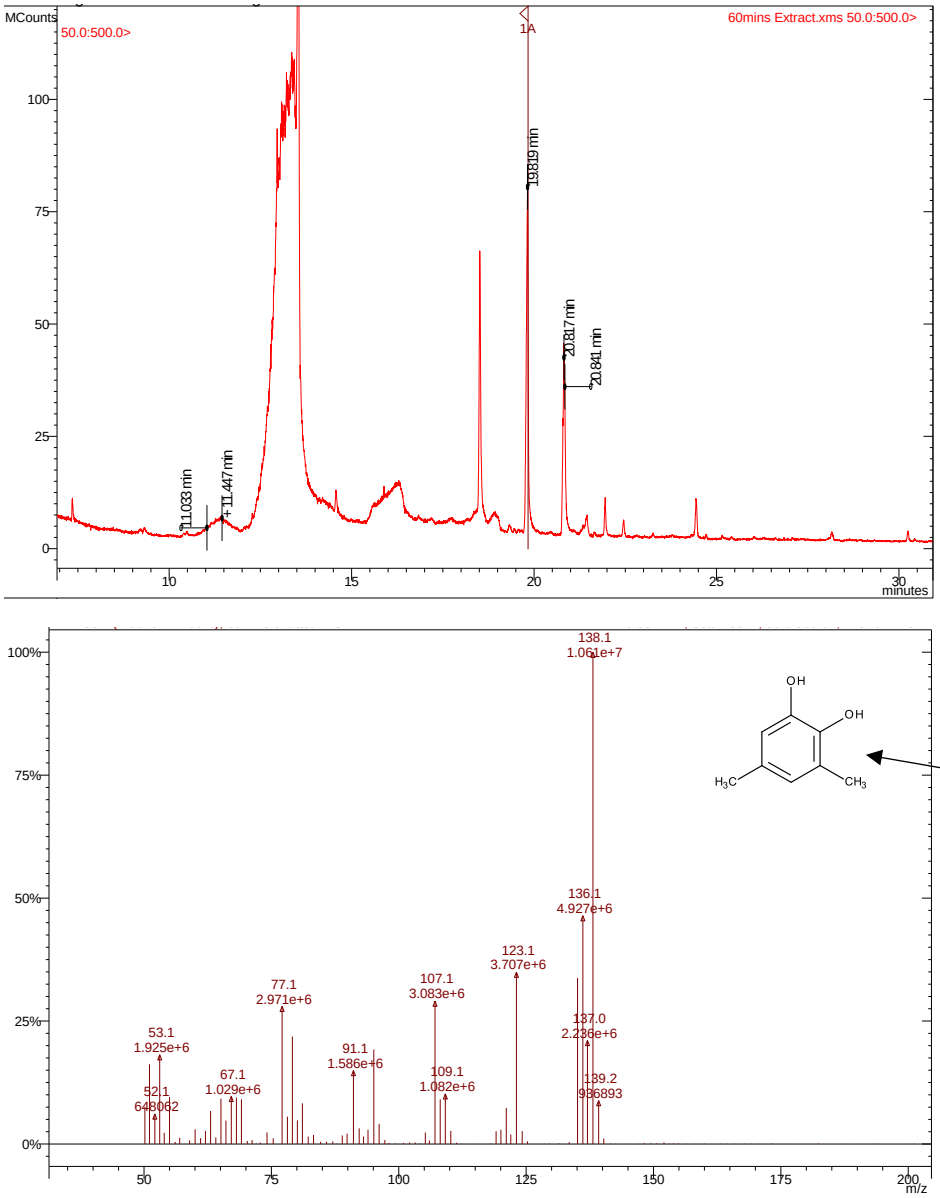

Likely an ortho -isomer based on retention time.

Figure 4.9: TIC and the mass spectrum of peak 3 in the chromatogram for the oxidation of DMP at 30 min reaction time.

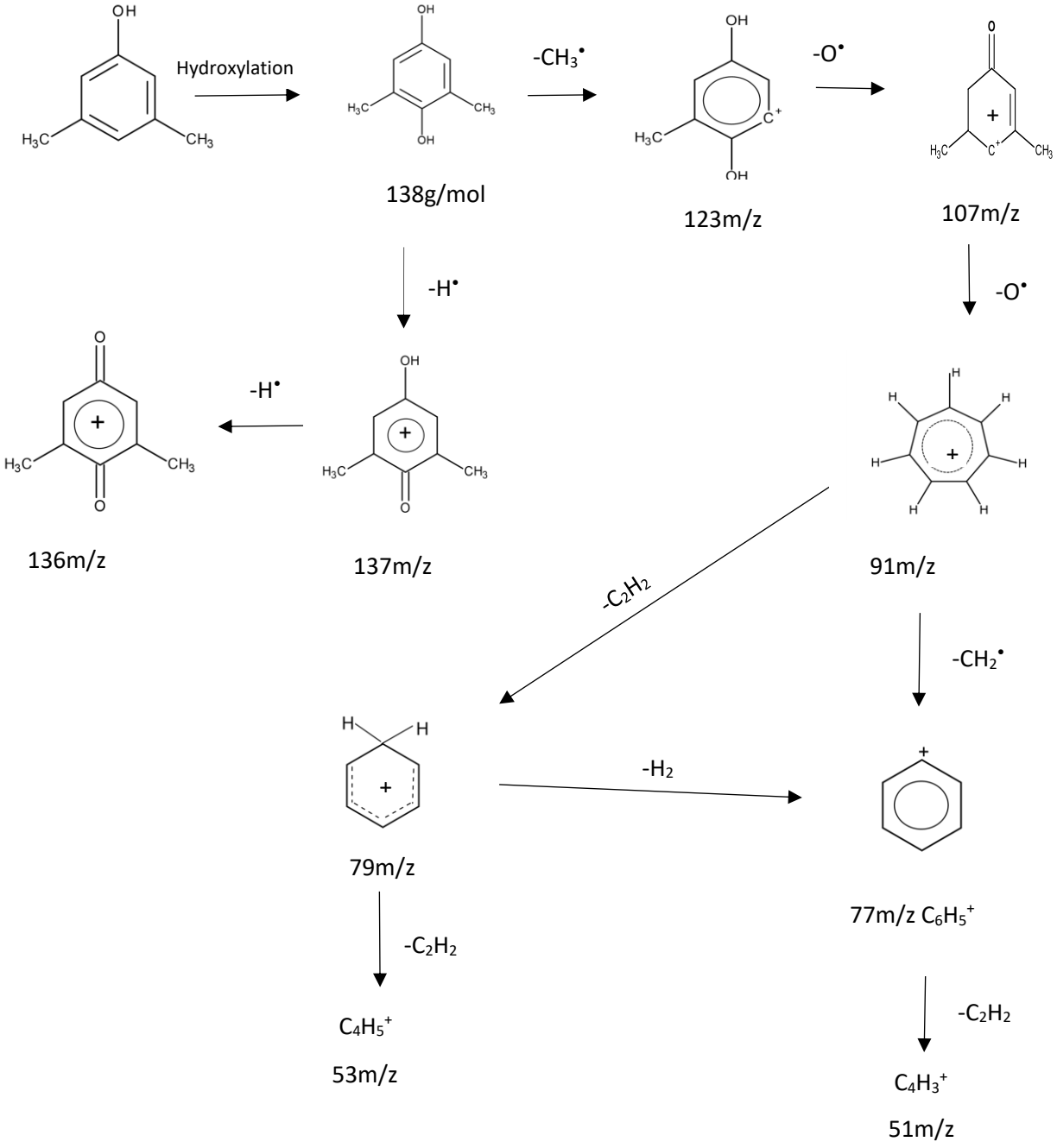

Figure 4.10: Proposed pathway for the formation of M= 138 mass (peak 3) tentative molecule from DMP and evolution of the fragments of this molecule previously shown in Table 4.3.

Peak number 4 is as shown in Table 4.3 while its chromatogram and mass spec is shown in Figure 4.11.

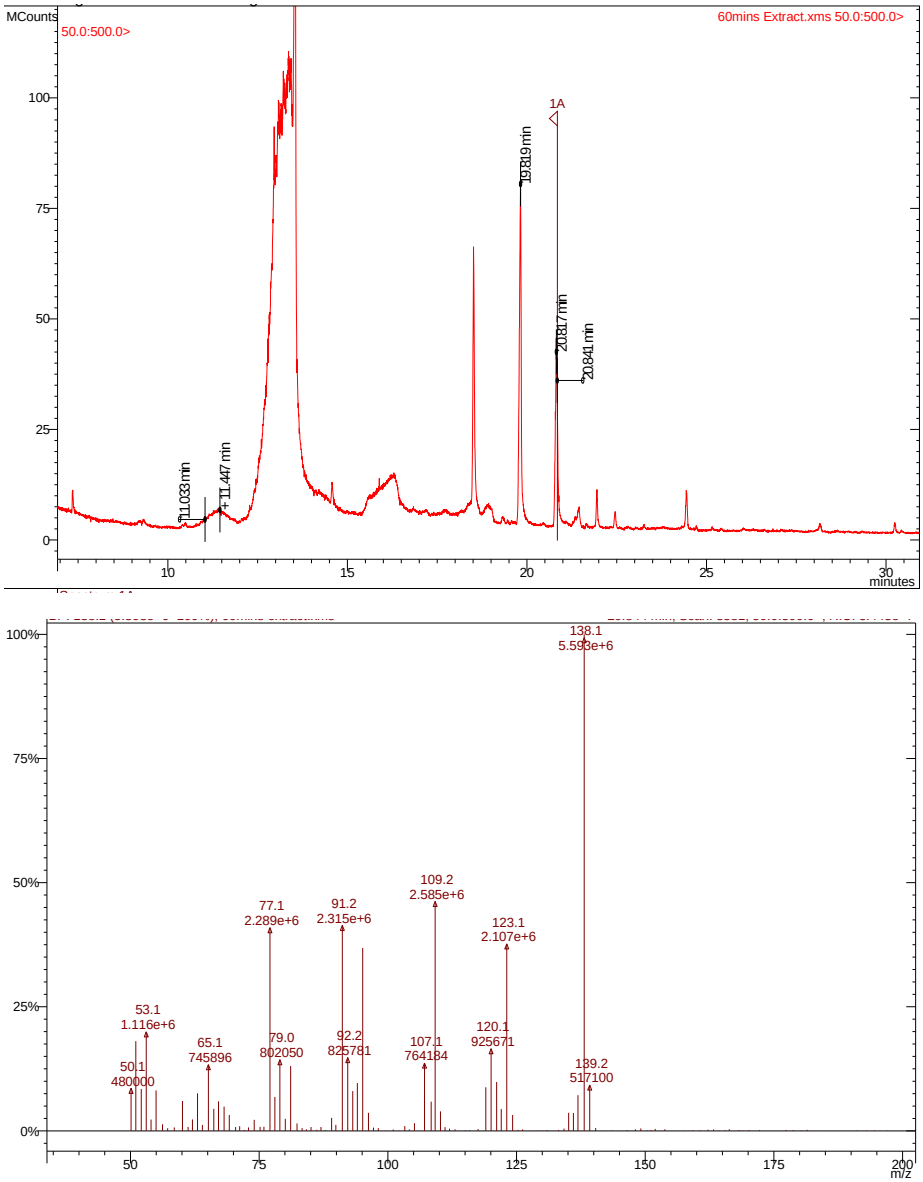

Figure 4.11: TIC and the mass spectrum of peak 4 in the chromatogram for the oxidation of DMP at 30 min reaction time

Peak 4

As earlier mentioned, it is a possible isomer of peaks 2 and 3. The fragmentation scheme shown in Figure 4.12 below evolved as follows: there was a loss of methyl ion (-15) to give 123m/z, and a possible loss of hydrogen ion to give the 137m/z ion. 109m/z could result from the loss of CO (-28) in Figure 4.12, while 91m/z fragment, suspected to be a tropylium ion could result from 109m/z through the loss of H_2O (-18). This is also the case for 120m/z, which is likely to have resulted from M 138 through the loss of H_2O (-18). 107m/z could result through the loss of H_2 (-2) from 109m/z. This is also the case for 77, and 51m/z which resulted from 79 and 53m/z respectively, by the loss of H_2 (-2). 78m/z fragment could result from 79m/z fragment by the loss of $H^{\bullet}$, while 53m/z fragment could result from 78m/z through the loss of C_2H_2 (-26).

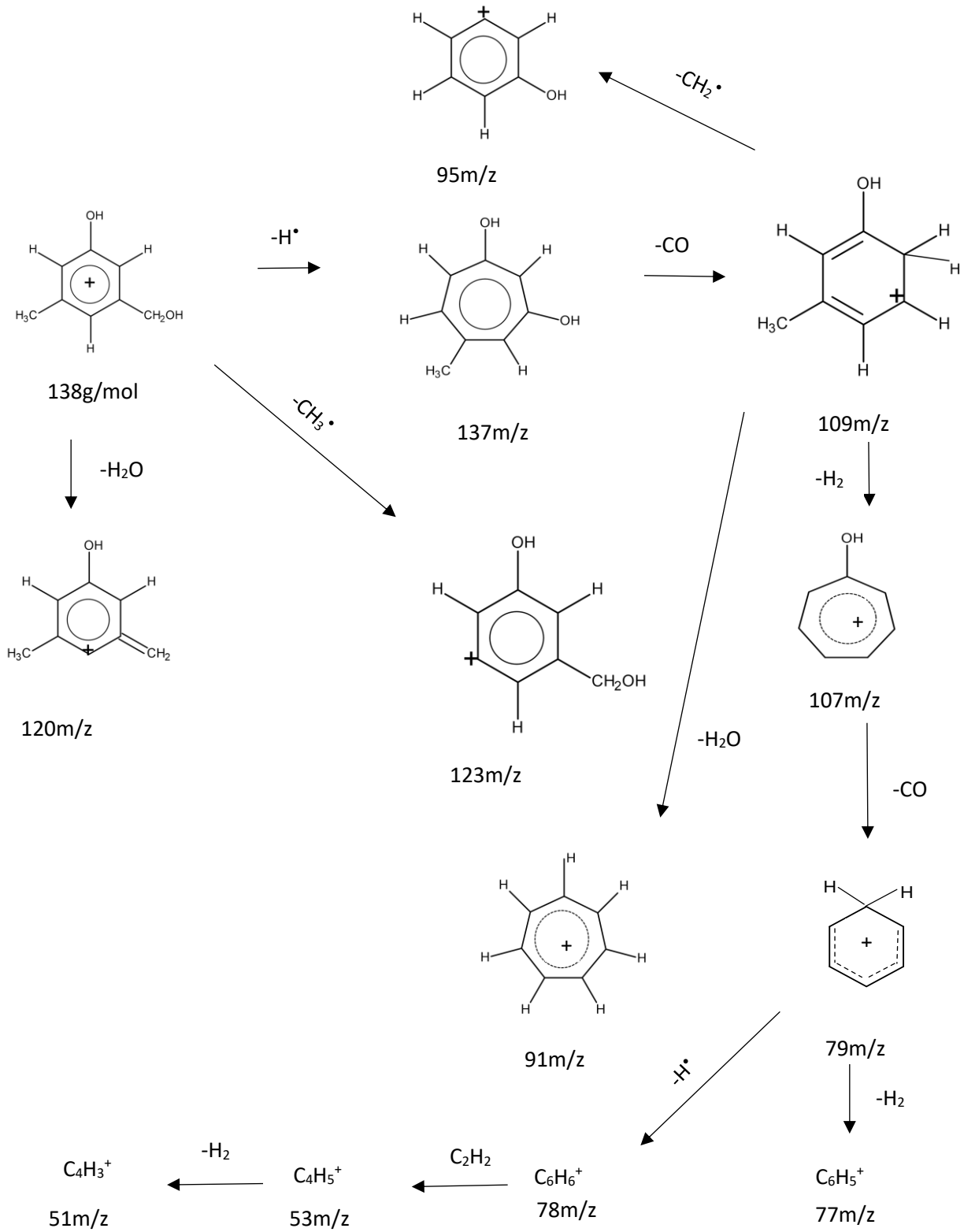

Figure 4.12: Proposed pathway for the formation of M= 138 (peak 4) tentative molecule from 3,5-DMP and evolution of the fragments of this molecule previously shown in Table 4.3.

Peak 5

The mass fragments identified from the mass spectrum of peak number 5 (Table 4.3) have been presented in the chromatogram and mass spectrum in Figure 4.13 below. The molecular ion of this peak, which had a mass of 166 g/mol, has three isotopic possibilities (Figure 4.24) and there could be more. This could have dissociated through a loss of COO (-44) to form 121 m/z ion fragment, which further dissociates through the loss of $H^{\bullet}$ to form the 121 m/z fragment. The M^{+} could also dissociate through the loss of CO (-28) to form a 138 m/z fragment. This could further dissociate sequentially through a three stage loss of $H^{\bullet}$, COH and $OH^{\bullet}$ to form 137 m/z, 109 m/z and 121 m/z respectively. The 65 m/z fragment could result from the loss of CO_2 from 109, while 92 m/z could result from the loss of CO from 120 m/z fragment. These are shown in Figure 4.14 below.

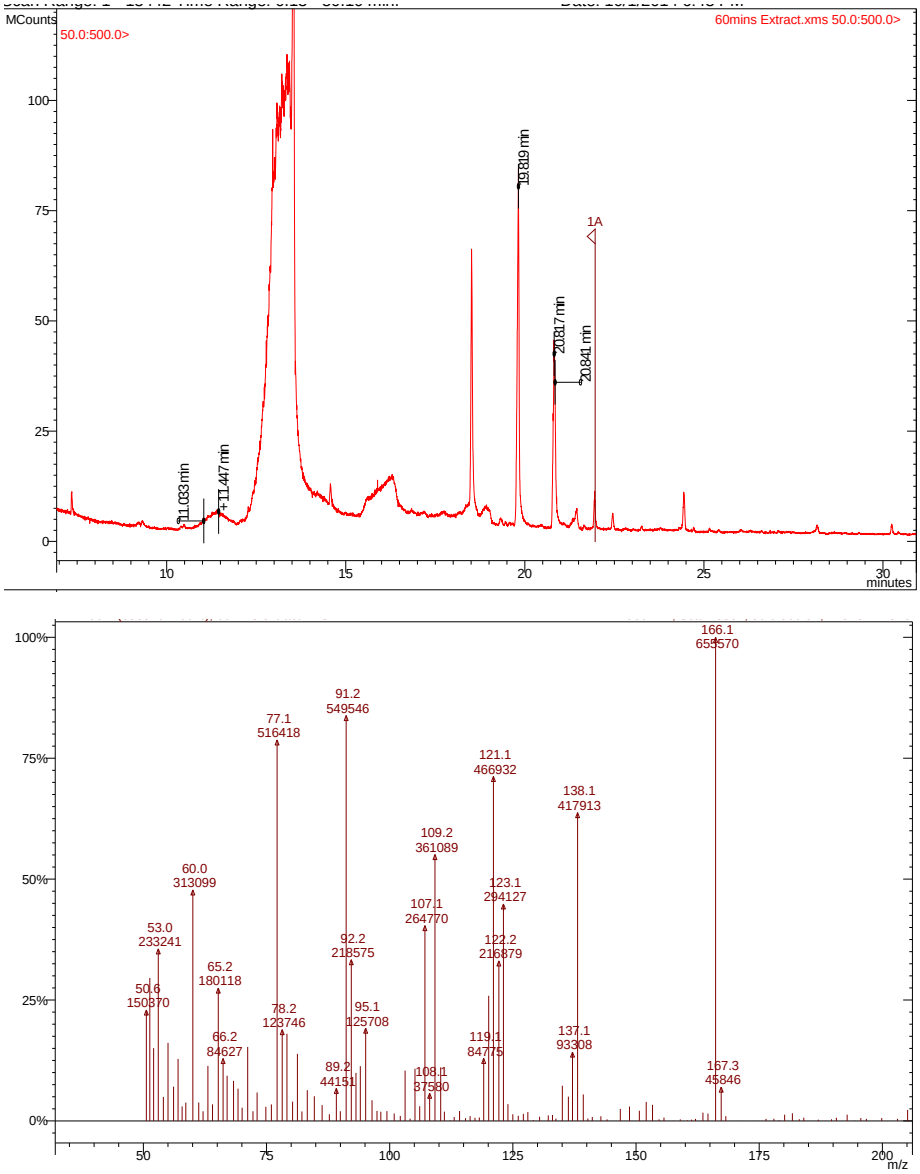

Figure 4.13: TIC and the mass spectrum of peak 5 in the chromatogram for the oxidation of DMP at 30 min reaction time.

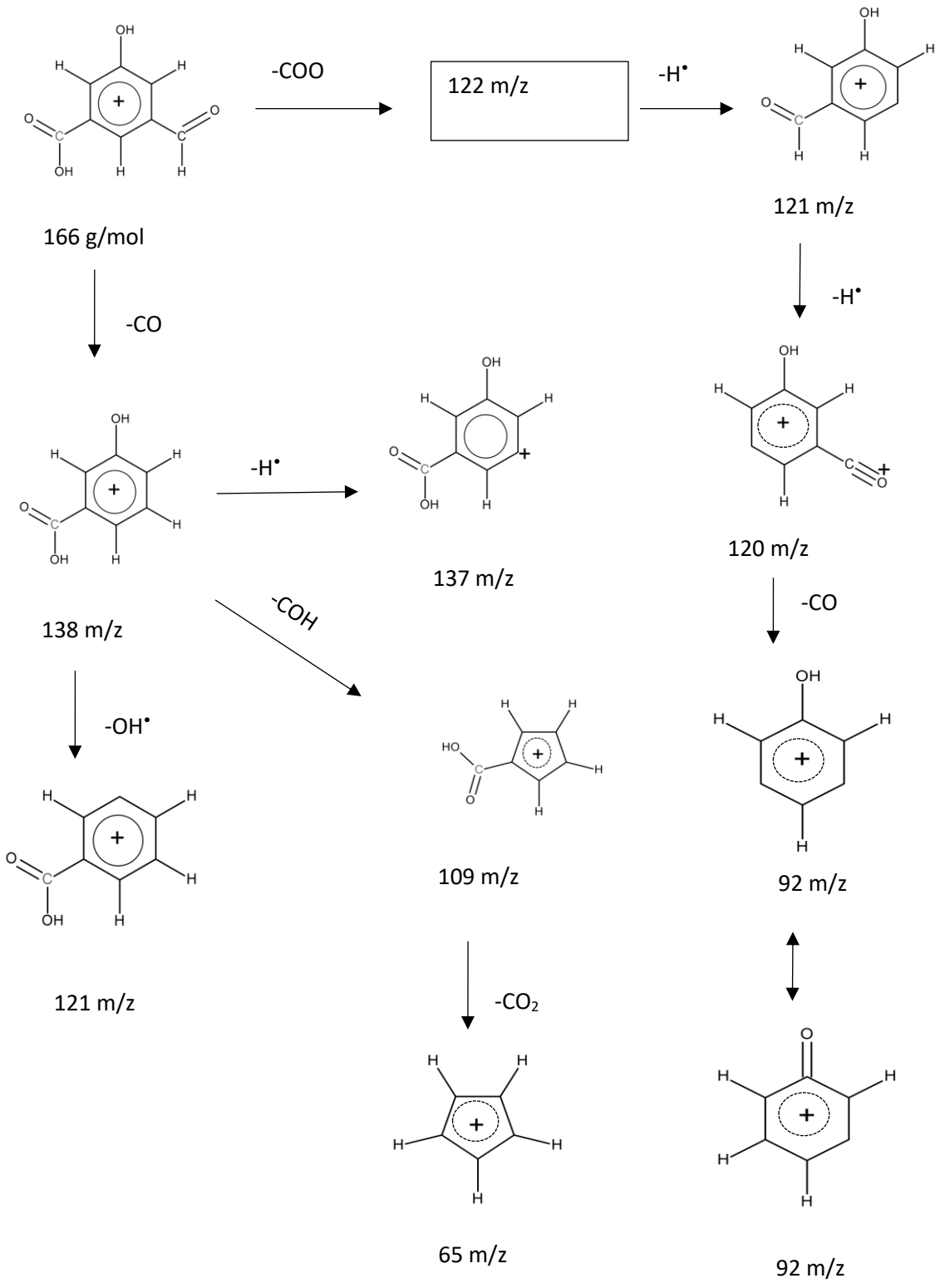

Figure 4.14: proposed pathway for the formation of 166 M^+ (peak 5) tentative molecule from 3,5-DMP and evolution of the fragments of this molecule previously shown in Table 4.3.

Peak 6

The fragmentation pattern of the molecule which also has four isotopic possibilities (Figure 4.24) expressed as peak number 6 fragmented as follows; a loss of CO (-28) is likely to have resulted in the 122 m/z fragment, while a loss of $H^{\bullet}$ could result in 121 m/z fragment. A further sequential loss of a methylene ion (-14) and C_4H_2 from 121 m/z mass fragment could result in 107 m/z and 71 m/z respectively. 149 m/z mass fragment (which is also prominent in the LCMS mass spectra in Figures 4.18 and 4.19) could result from the loss of $H^{\bullet}$ from the M^+ (150). 91 m/z mass fragment could result from 121 m/z through the loss of HCHO, while 57 m/z could result from 71 m/z through the loss of $CH_2^{\bullet}$. 53 m/z could result from 71 mass fragment by the loss of H_2O, while 56 m/z mass fragment could result from the 57 m/z through the loss of $H^{\bullet}$.

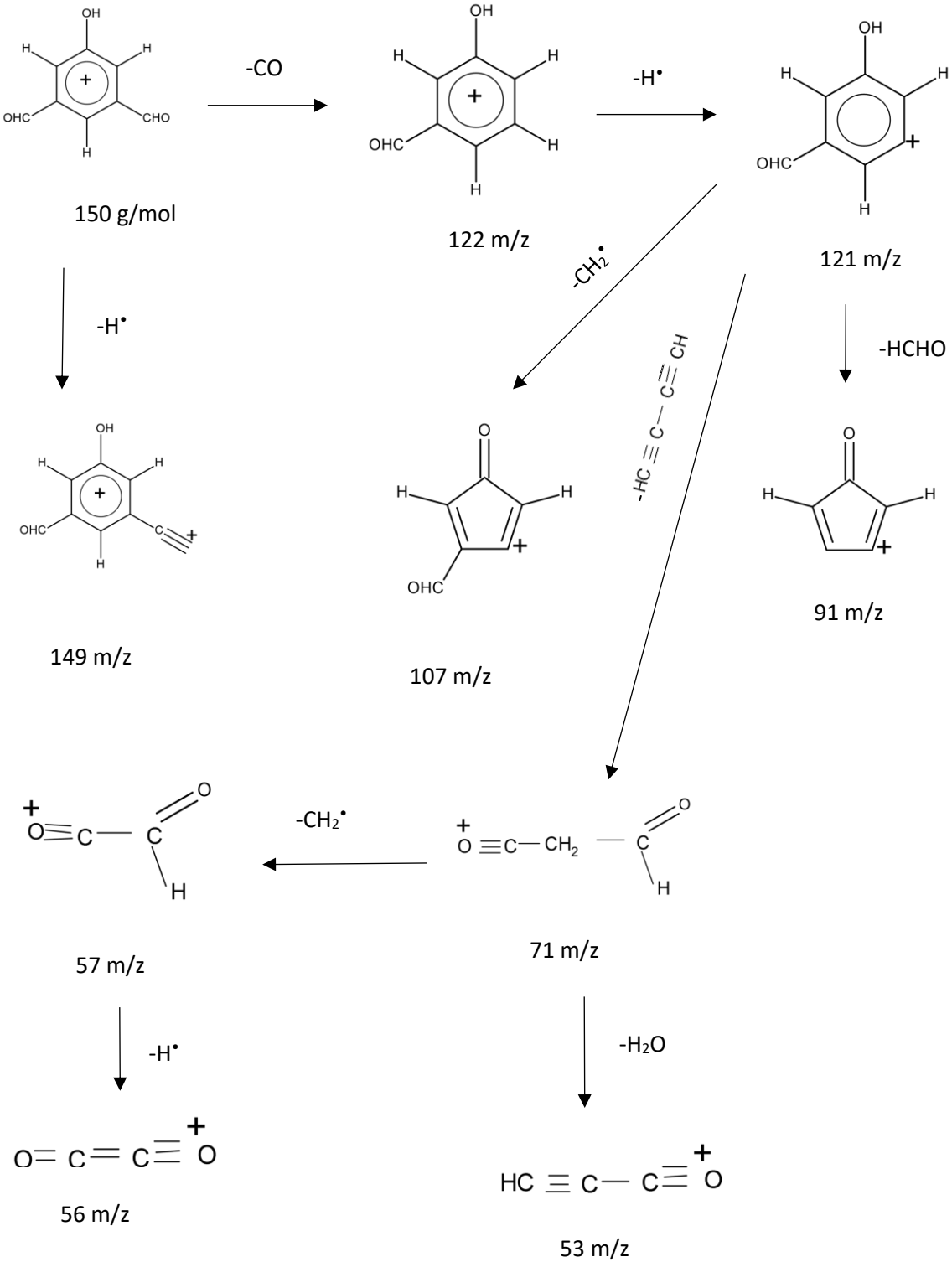

Figure 4.15: proposed pathway for the formation of 150 mass (peak 6) tentative molecule from 3,5-DMP and evolution of the fragments of this molecule previously shown in Table 4.3

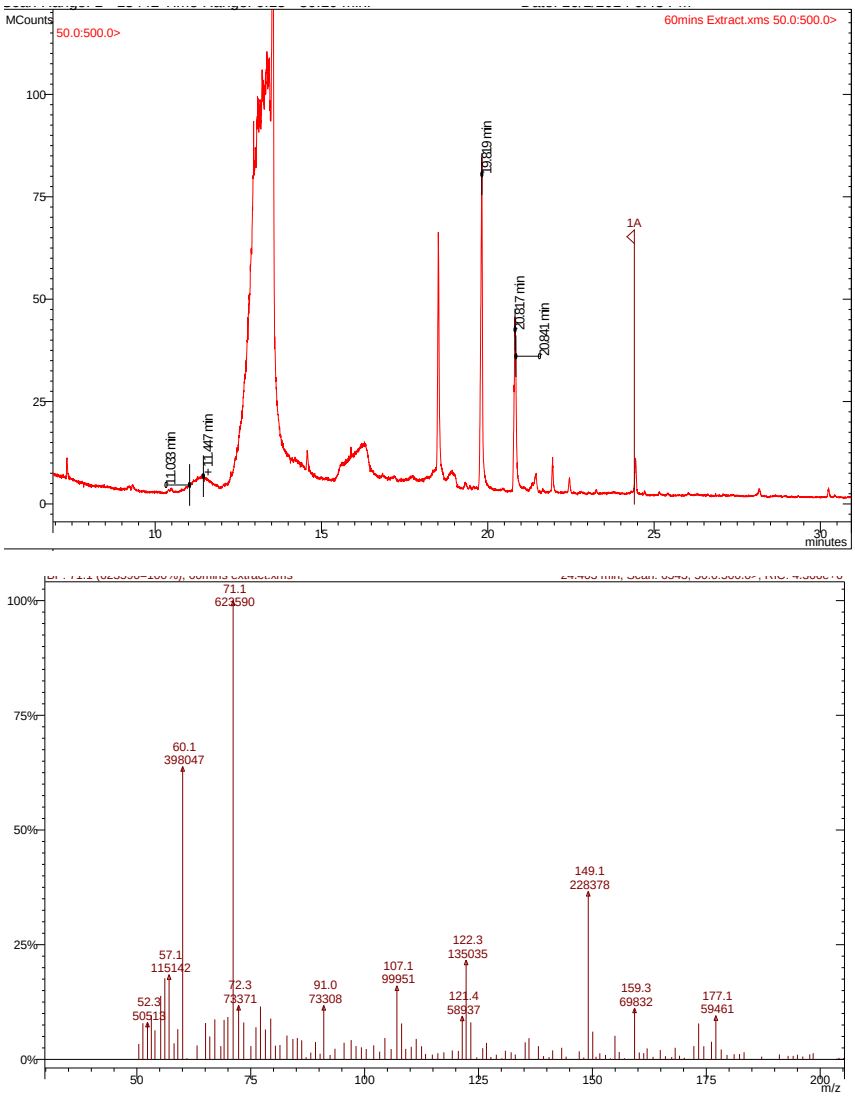

Figure 4.16: TIC and the mass spectrum of peak 6 in the chromatogram for the oxidation of DMP at 30 min reaction time.

4.5.1.3 LCMS Analysis Results

Based on the molecular ions identified from the total ion chromatograms from GCMS analysis, further attempts were made using LCMS to further verify the presence of these molecular ions/ compounds, owing to the complexity of the sample preparation step involved in the GCMS analysis. The results have been presented in Figure 4.17. The TIC shows two peaks in full scan mode at 4.5 min and 6.7 min retention times for a degradation intermediate and DMP respectively. Only one reaction intermediate peak was found in full scan mode for the LCMS analysis, suggesting ion suppression by competing analytes in the reaction matrix. Although the ionization method used in this study - atmospheric pressure electro spray ionization technique (API-ES), is suitable for medium polar to very polar compounds and medium to high molecular weight compounds, the analytes must however be ionic for this to work (Herderich et al., 1996; Shimadzu, 2016). This technique is mild, producing little or no fragmentation (Brewer and Henion, 1998).

This explains in part why the peaks recorded on the LCMS full scan chromatogram using APES ionization, are clearly fewer than those recorded on the GCMS Electron Impact ionization.

The mass spectrum of the intermediate peak is presented (Figure 4.18), while the significant characteristic ions are presented in Table 4.4.

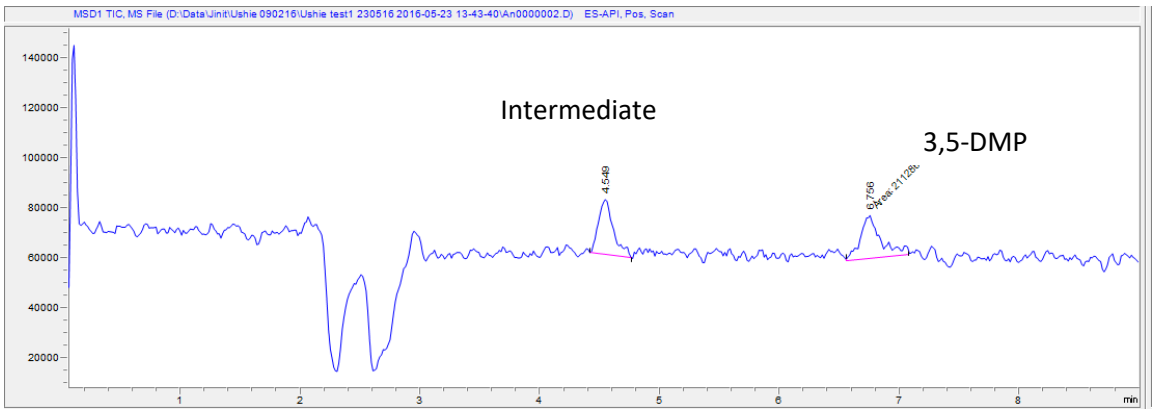

Figure 4.17: Full scan chromatogram for reaction sample of the heterogeneous catalysis of 3,5-DMP at 30 min reaction time (Positive scan).

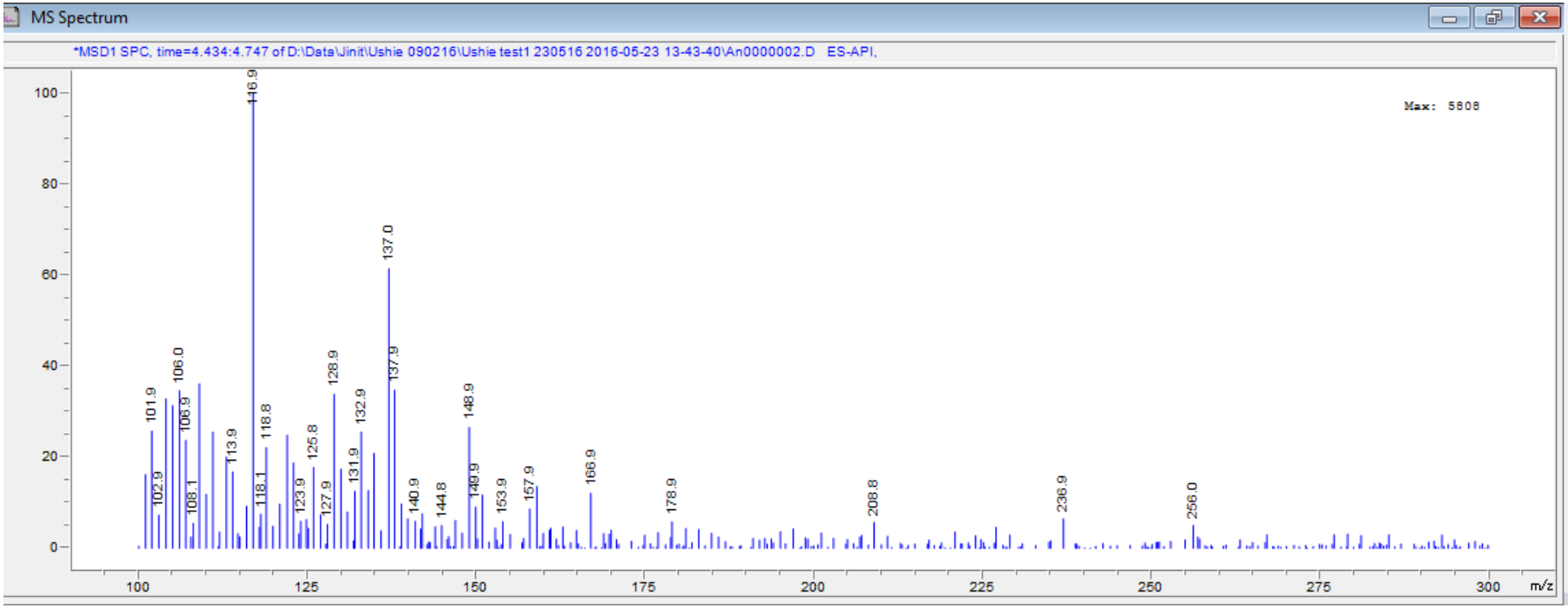

Figure 4.18: Mass spectrum 30 min reaction full scan at RT 4.555 (137.0 m/z) represents intermediate of DMP oxidation. Expected mass (137.2m/z).

The probable molecules that resulted from the mass fragmentation of the detected intermediate include; 123 m/z which is a positive ion fragment of DMP. In addition to this, there are 166 m/z and 149.9 m/z ion fragments, which are consistent with molecules tentatively identified in the GCMS mass spectrometry data presented in Figures 4.13 and 4.16 respectively, which gives credence to the presence of these compounds as reaction intermediates.

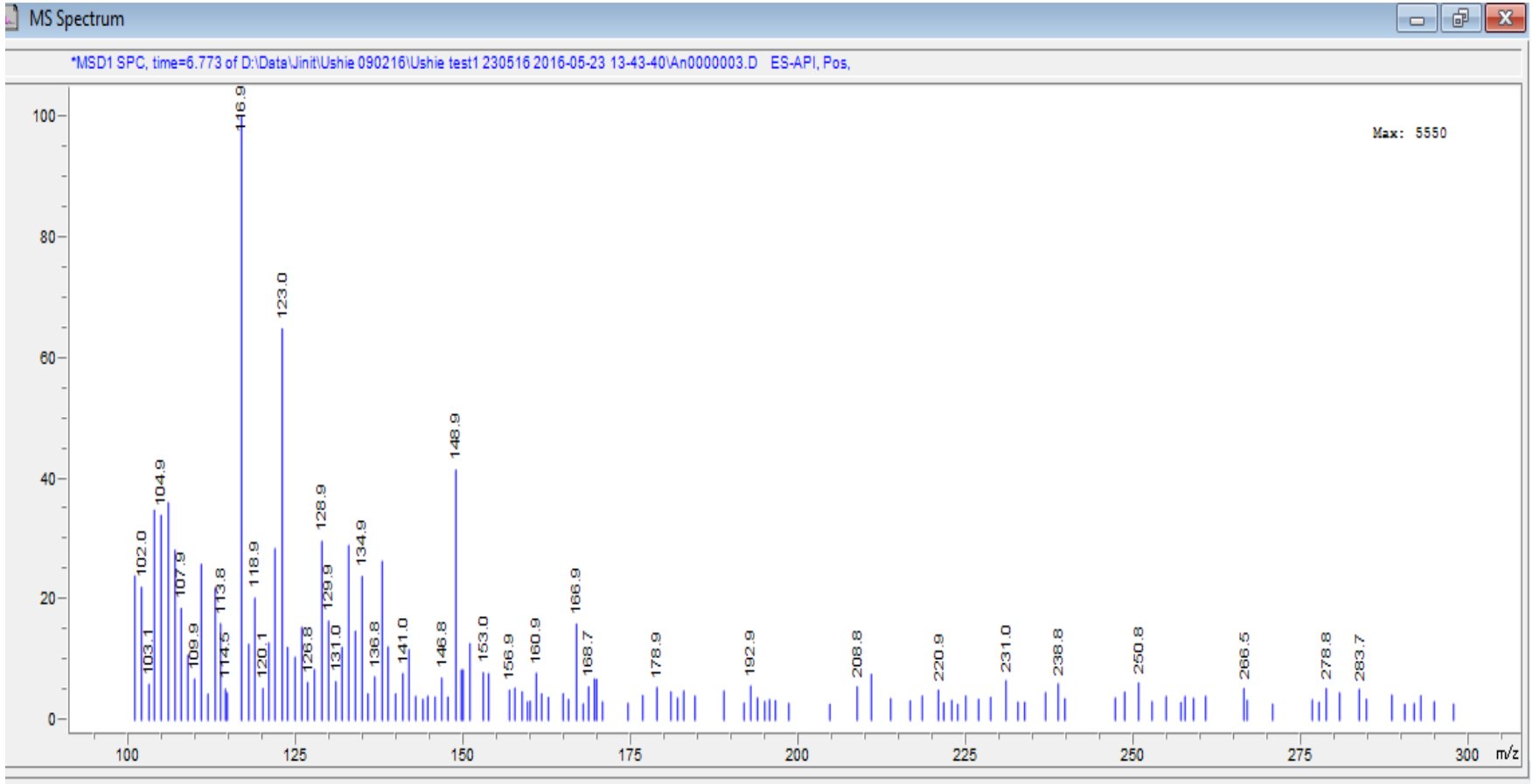

Figure 4.19: Mass spectrum 30 min reaction full scan mode at RT 6.77 (123 m/z) DMP Expected m/z of DMP 123.0 m/z

Table 4.4: Fragmentation patterns of GCMS analysis of possible intermediate compounds, including the parent ion showing retention times and molecular ions

Retention time (min)	Peak no	M(+)	Significant characteristic ions, m/z
4.5 (intermediate)	1	137	137 ,123, 116, 108
6.7 (DMP)	2	123	123, 120, 118.9, 116.9, 109.9, 107.9, 104.9, 102.

The ions detected on the mass spectrum data of DMP analyzed from the full scan TIC, also shows similar ions which have been previously determined in the fragmentation of molecules determined in the GCMS data analysis. The mass spectrum has been overlaid on the TIC of DMP in single ion monitoring mode (SIM) shows the M+1 (123) in positive mode for DMP (Figure 4.20).

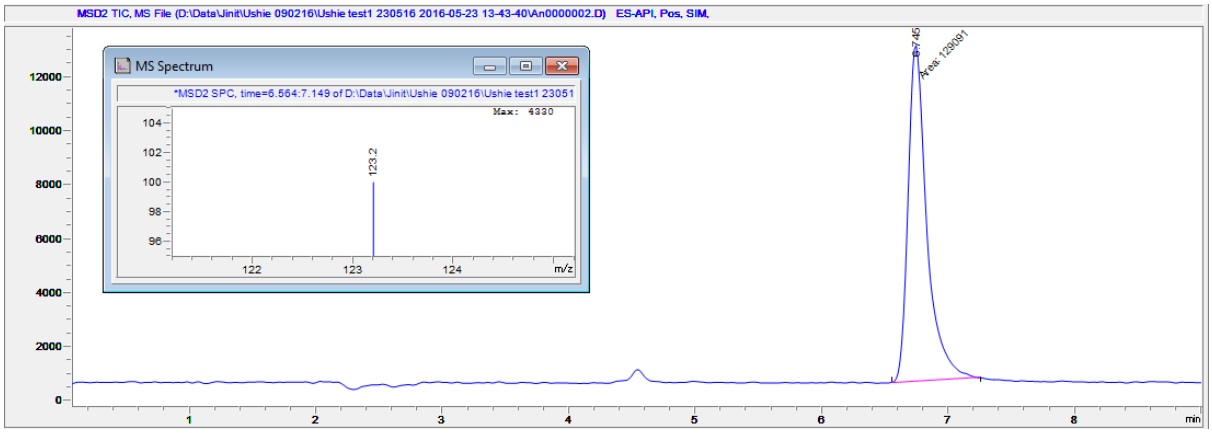

Figure 4.20: Mass spectrum overlaid on the TIC of DMP (123 m/z) in single ion monitoring mode (SIM).

4.5.1.4 Ion Chromatography Analysis Results and Discussions

Experimental analysis of the reaction for the presence of organic acid was done using the ion chromatogram (IC). Initial studies, involved carrying out control experiments in the absence of DMP and from the results, no organic acids were detected. The results of the experiments are as presented in Figure 4.24. Chi and Huddersman (2007) had reported an analytical technique for the rapid determination of low molecular weight organic acids using the Metrohm Modular MIC-2 advanced system, similar to the one used for this study and came up with retention times for 11 organic acids (Figure 4.21). This method has been repeated for this study, with a similar outcome.

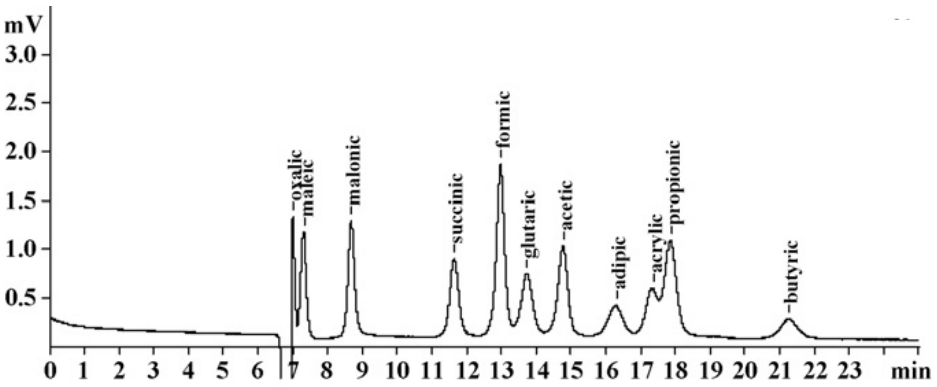

Figure 4.21: Chromatogram of a mixture of organic acids under mobile phase conditions; 0.38 mM H_2SO_4, flow rate of 0.5 mL/min, pressure 2.1 MPa, column temperature 30 ◦C (Reproduced from Chi and Huddersman, 2007).

Acetic acid and formic acid were suspected intermediates based on matching peak area retention times with those of Chi and Huddersman (2007). Confirmatory analysis was performed by injecting 10 ppm concentration of standards of the pure compounds (Figure 4.22).

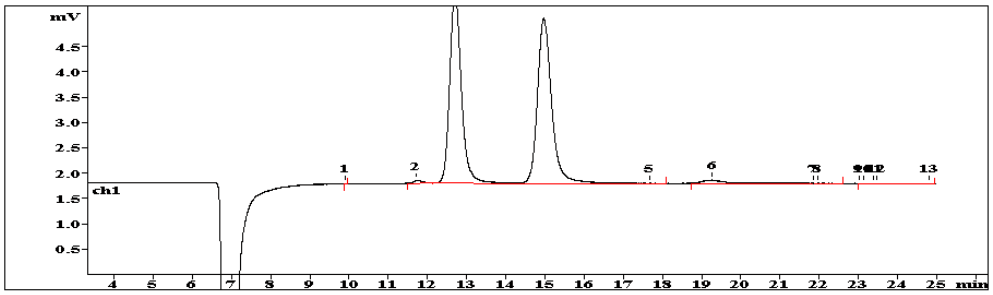

Quantitation method: Custom

No	Retention min	Height mV	Area mV*sec	Conc.	Name
1	9.89	0.01	0.007	0.007	
2	11.73	0.05	0.934	0.934	
3	12.70	3.72	77.571	77.571	
4	14.97	3.26	82.386	82.386	
5	17.67	0.00	0.046	0.046	
6	19.26	0.06	2.598	2.598	
7	21.86	0.01	0.104	0.104	
8	21.97	0.00	0.119	0.119	
9	23.02	0.00	0.005	0.005	
10	23.12	0.01	0.023	0.023	
11	23.39	0.01	0.006	0.006	
12	23.48	0.01	0.171	0.171	
13	24.80	0.01	0.025	0.025	
13	25.00	7.14	163.997	163.997	

Figure 4.22: Chromatogram of 10 ppm mixed standards of formic acid (retention time 12.70 peak 3) and acetic acid (retention time 14.97 peak 4).

These corresponded to the retention times reported by Chi and Huddersman, (2007) and also matched the retention times of the reaction intermediates detected using similar equipment as presented in Figure 4.23.

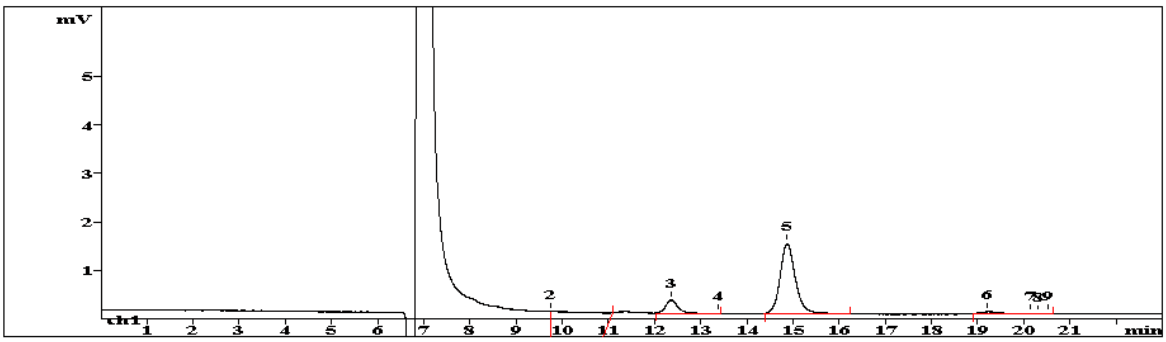

Quantitation method: Custom

No	Retention min	Height mV	Area mV*sec	Conc.	Name
1	6.95	82.36	2103.240	2103.240	
2	9.76	3.25	131.307	131.307	
3	12.36	0.27	5.115	5.115	
4	13.36	0.01	0.044	0.044	
5	14.87	1.44	33.354	33.354	
6	19.21	0.05	1.438	1.438	
7	20.14	0.01	0.056	0.056	
8	20.31	0.01	0.055	0.055	
9	20.51	0.01	0.067	0.067	
9	23.00	87.39	2274.674	2274.674	

Figure 4.23: Chromatogram of sample of the analysis of the heterogeneous catalysis of 25 mg/L 3,5-DMP in 400 ppm H_2O_2 at pH3, 25 °C 100 mL reaction volume and 5g catalyst at 120 min.

It was found that the peak area of Formic acid deminished over time when monitored from 90 min (where it peaked) to 120 min, whereas the peak area of acetic acid remained stable over this period, suggesting the recalcitrance of the latter to oxidation in a fenton-like system. This observation is in agreement with Zazo et al., (2005). They reported similar observations on the nature of acetic acids during phenol oxidation in a fenton system.

The proposed scheme for the catalytic degradation of 3,5-DMP in the presence of H_2O_2 using modified PAN catalyst is presented in Figure 4.24.

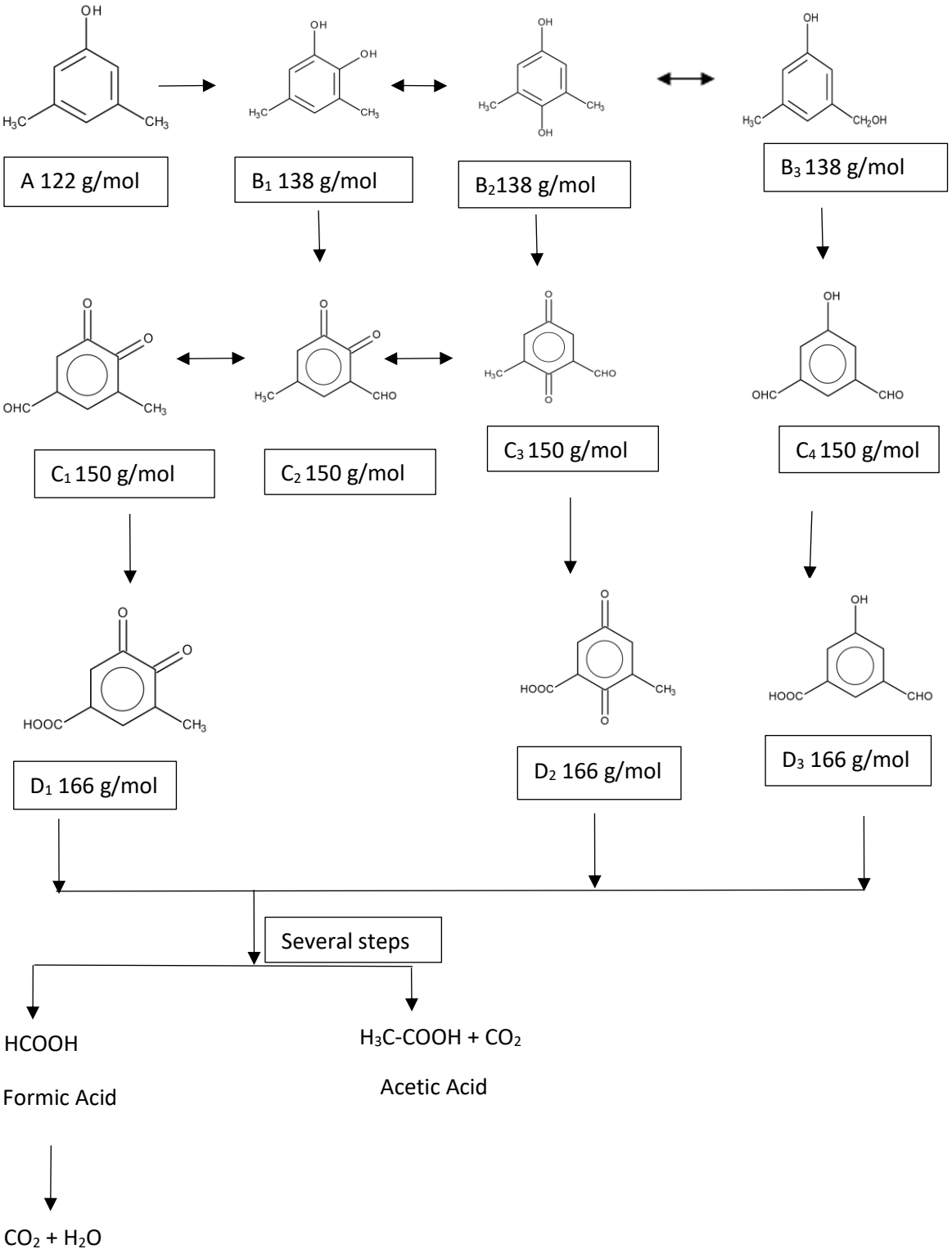

*B_1 to B_3, C_1 to C_4 and D_1 to D_3 are possible isomers (there could be more)

Figure 4.24: Proposed scheme for the catalytic degradation of DMP in the presence of H_2O_2 using modified PAN catalyst.

In Figure 4.31, molecule 'A' is DMP, which is the starting compound. The intermediate compounds that possibly resulted from the degradation of the DMP including their possible isomers include the following; 'B1' to 'B3' which are 3,5-dimethyl catechol (peak 2), 3,5-dimethyl hydroquinone (peak1), and 3-hydroxymethyl-5-methylphenol respectively (Figure 4.31). Peak 5 is likely to be one of the following four isomers codenamed 'C1' to 'C4'; 3-carbaldehyde-5-methyl-1,2-benzoquinone, 3-methyl-5-carbaldehyde-1,2-benzoquinone, 3-methyl-4-carbaldehyde p-benzoquinone or 3,5-dicarbaldehyde hydroxybenze respectively (Figure 4.31).

The sixth peak which has been codenamed 'D1' to 'D3' could be one of the following isomers; 3-methyl-4,5-benzoquinone carboxylic acid, p-benzoquinone-3-methyl-4-carboxylic acid and 3-carbaldehyde (hydroxybenzene) carboxylic acid respectively (Figure 4.31). This follows to the formation of organic acids and finally the formation of CO_2 and H_2O. This final step (CO_2 and H_2O) were not determined in this study. The possible isomers tentatively identified could be more.

4.6 Summary

Determination and identification of possible reaction intermediates has led to the identification of two organic acids (acetic and formic) and five compounds, including benzoquinones, hydroquinones and benzaldehydes, with some being isomers and which will require further investigation to distinguish.

The next chapter looks at the application of the optimised process in the treatment of simulated produced water, which in real life situations, usually contains DMP within the range of concentration used in chapter three.

5 Degradation of Simulated Produced Water Using a Novel Pan-Heterogeneous Catalyst in a Fenton-Like Reaction.

5.0 Introduction

An understanding of the chemistry of crude oil is essential in understanding the make-up of produced water. According to Yang, (2011) petroleum compounds are grouped into two groups namely Hydrocarbons (compounds containing essentially hydrogen and carbon) and heteroatom which in addition to containing hydrogen and carbon compounds, also contain nitrogen, oxygen and sulphur. Common petroleum products are derived from crude oil through a process called fractional distillation. This process separates the components of crude oil into hydrocarbon fractions that have a common number of carbon atoms and a corresponding boiling range (TUVNEL, 2016). This is shown in table 5.1.

Table 5.1: Common petroleum fractions and their boiling points (TUVNEL 2016)

Fraction	Carbon range	Boiling range (°C)
Petrol	C4-C12	25 – 200
Kerosene	C10-C15	150 – 300
Diesel	C12-C20	270 – 350
Lube Oil	C20-C40	350 - 500
Asphalt	C40+	> 500

The elemental composition of petroleum shows 83 -87% carbon, 11-16% hydrogen, 0-4% oxygen and 0-4% sulphur. Yang (2011) listed three groups of hydrocarbons;

- Saturated hydrocarbons, characterised by C-C single bonds, which are further subdivided into aliphatic and alicyclic hydrocarbons. Aliphatics are branched or straight-chained hydrocarbons with general molecular formula of C_nH_{2n+2}, Alicyclic on the other hand are saturated hydrocarbon compounds bearing one or more rings and having a general molecular formula of C_nH_{2n}. This group of

compounds are sometimes called cycloalkanes. In the industry, they are known as cycloparaffins or naphthenes.

- Unsaturated Hydrocarbons: These are not usually a component of crude oils, but may be introduced during cracking process (Yang, 2011). They are characterised by the C=C (double bonds or triple bonds) for alkenes or alkynes respectively.
- Aromatics hydrocarbons are typified by the cyclic or ringed benzene structures (Yang, 2011). They are a member of a rather complex group of unsaturated compounds composed primarily of carbon and hydrogen, however some may contain heteroatoms (OGP, 2002). This group of compounds have been further subdivided into the following by OGP (2002).
    i. Benzene, Toluene, Ethylbenzene and Xylene- all three isomers (BTEX). According to OGP, (2002), this group makes up the monocyclic aromatics.
    ii. Naphthalene, Phenanthrene and Dibenzothiophene (NPD). This group of compounds includes the C1 to C3 alkyl group and contains 2 to 3 cyclic rings.
    iii. Polycyclic Aromatic Hydrocarbons (PAH). As the name implies, this group has 3 to 6 ring structure. They are the 16 Environmental Protection Agency's priority pollutants; however, this excludes phenanthrene and naphthalene, which have been grouped under the NPD group (OGP, 2002).

5.1 Legal Framework

Industry policy formulation, which aids legislation and guidance for produced water management and or disposal, is based on a good understanding of the characteristics and composition of produced water (Veil et al., 2004). Over the years, the industry has been guided by operators' initiatives. More recently, however, regulations have been centred around reliance on best practicable technology (BPT) and best available technology (BAT) for accessing technologies for the treatment/management of produced water.

In the United States for instance, Subpart C of 40, Code of Federal Regulation (CFR) Part 435.13 under the Code of Federal Regulations, oil and gas extraction point source category, waste source, pollutant parameter, and BAT for effluent limitation are outlined. For produced water, the maximum discharge concentration for oil and grease for any given day is limited to 42 mg/L, while the average allowable discharge concentration over a thirty-day period (consecutively), is 29 mg/L. For free oil (macro emulsions of more than 20 µm in size and exhibiting a distinct phase difference from water and thermodynamically unstable) shown in Figure 5.1 and diesel oil, the Best Available Technology (BAT) effluent limitation is "no discharge" which effectively means zero effluent discharge (EPA 2016; GPO 2016). This means that, there should be no discharge of produced water known to contain free oil or diesel oil even if the best technology available technology has been applied.

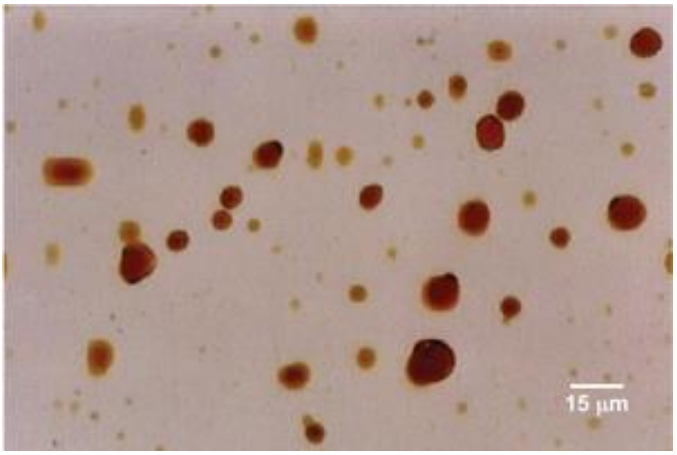

Figure 5.1: Photomicrograph of oil-in-water emulsion (Petrowiki, 2013)

In Nigeria, the key parameter that has been statutorily enforced in offshore locations has mostly been oil-in-water (OIW) or what is known in the United States as oil and grease (OG), and this is monitored on a daily basis. Oil has been defined by OSPAR Recommendation 2001/1 (as amended by Recommendation 2006/4), as the total hydrocarbons, determinable by the appropriate sum of analytical results obtained using prescribed reference methods for dispersed oil and aromatic hydrocarbons. It should also be pointed out that oil in water exists in three forms; dissolved, dispersed and free oil (Yang, 2011; Petrowiki, 2013). Other parameters monitored, in addition to the ones in Table 5.2 include electrical conductivity, and dissolved oxygen. These parameters are monitored weekly as are phenols, ammonium sulphide, ammonia, total phosphorus and metals (EGASPIN, 2000). Phenols, metals, ammonium sulphide etc. are monitored weekly in production tank farms (storage facilities where crude oil, associated formation water and gas from flow stations is pumped) and crude oil export terminals (where crude oil is dehydrated, badged and shipped for refining).

Table 5.2: Produced water discharge limits in Nigeria (Environmental Guidelines and Standards for the Petroleum Industry in Nigeria, EGASPIN, 2000).

Effluent Parameter	Inland area	Nearshore	Offshore
pH	6.5-8.5	6.5-8.5	No limit
Temperature ^{o}C	25	30	-
Oil/Grease content (mg/L)	10	20	40
Salinity (mg/L)	600	2,000	No limit
Turbidity (NTU)	<10	<15	-
Total dissolved solid (mg/L)	2,000	5,000	-
Total suspended solids (mg/L)	<30	<50	-
Chemical oxygen demand (mg/L)	10	125	-
Biochemical oxygen demand (mg/L)	10	125	-
Lead (ppm)	0.05	No limit	-
Iron (ppm)	1.0	No limit	-
Copper (ppm)	1.5	No limit	-
Chromium (ppm)	0.03	0.05	-
Zinc (ppm)	1.0	5	-
Sulphide (mg/L)	0.2	0.2	0.2
Sulphate (SO4-) mg/L	200	200	300
Mercury (ppm)	0.1	-	-

According to DECC (2011), offshore effluent discharges in the United Kingdom, is guided by the Offshore Petroleum Activities Oil Pollution Prevention and Control Regulations 2005 (OPPC) as amended 2011, which ensures discharges, especially oily ones, meet discharge regulations. The energy development unit, with precise sample and analytical methods, provides technical guidance on effluent discharges. The discharge of produced water into the sea in the United Kingdom is preconditioned on the following requirements;

- Analysis of the produced water for dispersed oil
- Analysis of hazardous and non-hazardous discharges for oil in water content

- Provision for and use of other analytical methods approved by DECC, such as the one used for this study
- Biannual analysis of produced water for the following;

1. Total Aliphatics.
2. Total Aromatics.
3. Total Hydrocarbons.
4. BTEX (Benzene, Toluene, Ethyl Benzene and Xylene).
5. NPD (Napthalene, Phenanthrene and Dibenzothiophene).
6. 16 EPA PAH's (excluding Naphthalene and Dibenzothiophene).
7. Organic Acids (Total Organic Acids, Formic, Acetic, Propionic, Butanoic, Pentanoic and Hexanoic Acids).
8. Phenols/alkylphenols C0-C3. (Specific details of these compounds have been discussed in chapter one section 1.5).
9. Metals (Arsenic, Cadmium, Chromium, Copper, Lead, Mercury, Nickel, Zinc)

The major guidance for permitted dispersed oil discharge within the United Kingdom continental shelf (UKCS) is based on OSPAR Recommendation 2001/1, which requires all oil installations to achieve a 30 mg/L oil in produced water discharged to sea. It is expected that the average monthly discharge must not exceed 30 mg/L and a maximum

concentration must not exceed 100 mg/L at any point, nor one tonne within any 12 h period.

In Australia, the statutory discharge quality for OIW is 30 mg/L, while China puts the discharge limit for OIW and COD at 10 mg/L and 100 mg/L respectively (Fakhru'l-Razi et al., 2009).

5.2 Justification of Study

According to the statistical review of world energy consumption by British Petroleum (BP) 2014, global energy consumption reached a new world record of 86.8million barrels per day in 2014 from 86.2 million barrels per day in 2013. With an average water/oil volume ratio for production wells averaging from 3:1 to 10:1 (Igunnu and Chen, 2012; Sumi 2005; Benko and Drewes, 2008), the volume of produced water generated daily constitutes waste of concern to the environment.

As mentioned earlier, the alkylated phenols which are among the most stable constituents of produced water, and which account for about 90% toxicity of produced water have until recently not been given the attention they deserve. Focus has always been on OIW concentration. There have been reports of endocrinal disruption effects in marine organisms attributed to these compounds in addition to birth defects to certain species of fishes, which has necessitated the routine monitoring of alkylphenols (C1-C5) in both the United Kingdom and the Norwegian sector of the North Sea (Thomas et al., 2009). The need to therefore undertake water treatment studies with potential to decontaminate produced water cannot be over emphasised.

5.3 Aims and Objectives

The aim of this chapter is to apply the optimised oxidation conditions developed for the decomposition of DMP in water to the degradation of synthetic produced water in both batch and continuous flow processes. The objectives of this study include;

- To establish from literature, the average composition of produced water,
- To identify analytical parameters used in the Industry for the monitoring produced of water discharge quality.
- To select or develop (if required) analytical methods and procedures for the analysis of oil-in-water which is an index parameter for produced water quality discharge criteria.
- To treat synthetic produced water in batch and continuous flow modes based on established optimum process parameters for the catalysis of DMP in water determined in chapters three and four.
- To monitor the catalytic process of produced water in batch and optimise if necessary to attain best conditions.
- To set up a rig for continuous flow treatment of synthetic produced water, and monitor loss of DMP, COD leached iron and OIW.

5.4 Experimental Methodology

5.4.1 Reagents/Chemicals and Materials

The materials used for this study are as shown in Table 5.3.

Table 5.3: Reagents/Chemicals and Materials used for this study.

Chemical/reagent	Linear formula/ Symbol	% Purity	Source
3,5-dimethyl phenol	$(CH_3)_2C_6H_3OH$	≥ 99	Sigma Aldrich
Hydrogen Peroxide	H_2O_2	30.0	Fisher Scientific
Hydrochloric acid	HCl	36.0	Fisher Scientific
Acetonitrile	CH_3CN	99.8	Fisher Scientific
Double distilled water	H_2O	-	DMU-Fistreem Cyclon: WSC044
n-Hexadecane	$CH_3(CH_2)_{14}CH_3$	99.0	Sigma Aldrich
Tridecane	$CH_3(CH_2)_{11}CH_3$	≥ 99	Sigma Aldrich
Acetic acid	CH_3CO_2H	99.7	Sigma Aldrich
Sodium hydrogen carbonate	$NaHCO_3$	99.0	Sigma Aldrich
Sodium Hydroxide	NaOH	98.0	Sigma Aldrich
Sodium Chloride	NaCl	99.0	Fisher Scientific
Benzene	C_6H_6	99.8	Sigma Aldrich
Toluene	$C_6H_5CH_3$	99.5	Sigma Aldrich
Ethylene Benzene	$C_6H_5C_2H_5$	99.5	Sigma Aldrich
Xylene	$C_6H_4(CH_3)_2$	99.5	Sigma Aldrich
2,6,10,14-tetramethylpentadecane (TMPD)	$(CH_3)_2CH(CH_2)_3CH(CH_3)$ $(CH_2)_3CH(CH_3)(CH_2)_3CH(CH_3)_2$	98.0	Sigma Aldrich
Tetrachloroethylene (TTCE)	$CCl_2=CCl_2$	≥ 99	Sigma Aldrich
Isooctane	$(CH_3)_2CHCH_2C(CH_3)_3$	≥99	Sigma Aldrich

Laboratory equipment and other materials used for the study include Radley carousel, flea, magnetic stirrer, rotating disc reactor, modified heterogeneous PAN catalyst, analytical balance, Marlow series 101U peristaltic pump, and P1000 Gilson pipette.

5.4.2 Analytical Equipment

Equipment used for this study included the following; Perkin Elmer HPLC series 200 fitted with a UV detector, PerkinElmer Flame atomic absorption spectrometer AAnalyst 200 model fitted with a touchscreen interphase, FTIR – Bruker Alpha model, and DR 3800 Hach Lange spectrophotometer.

5.4.3 Rotating Contacting Reactor

Figures 5.2 and 5.3 show the schematic of the reactor set-up and the photograph respectively of the rotating contacting reactor used for the continuous flow studies. It consists of a 900 mL cylindrical tank made of acrylic, fitted with 8 disks of 2.5 cm radius on a shaft which is connected to a motor, and rotates the disks, loaded in total with 180 g of modified PAN catalytic mesh. The shaft rotated at a low adjustable velocity of 8-10 rpm. The large shear forces of the rotating disks provide efficient mixing of the reaction system giving high mass transfer rates.

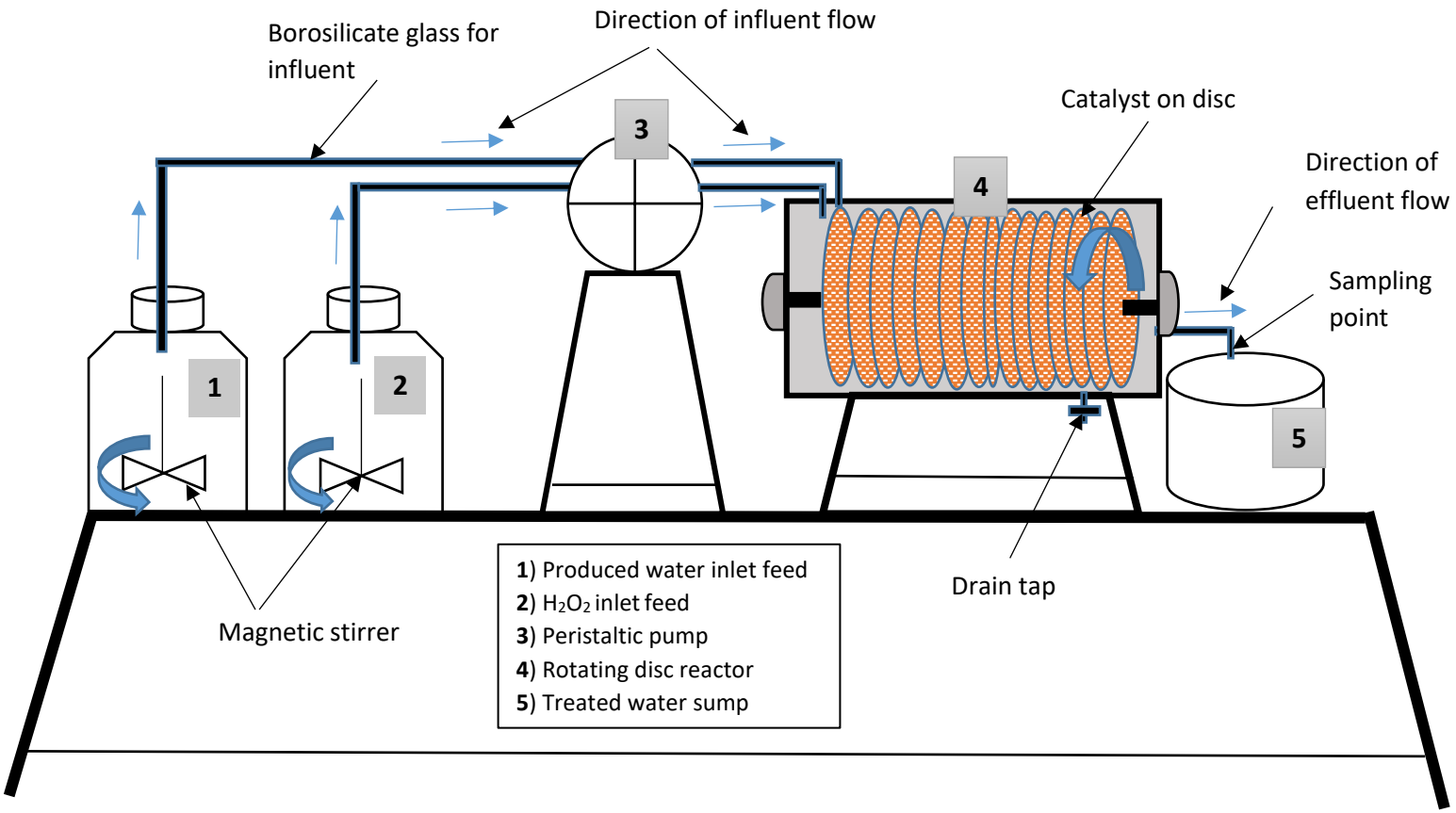

Figure 5.2: Schematic diagram of Rotating Contacting Reactor used for the continuous flow

Figure 5.3: Photograph of the reactor system and setup used for the continuous flow experiments

5.4.4 Methodology

A protocol developed for the preparation of synthetic produced water that is based on the composition described in Table 5.4 for batch experiments and Table 5.5 for continuous flow experiments. Parameters monitored in the reaction systems were namely; alkylphenol concentration (DMP), OIW and COD.

Table 5.4: Average composite concentrations of common organic and inorganic constituents in produced water from conventional oil and gas operations, from selected fields around the world. (Rice, 2000; Benko and Drewes, 2008; Igunnu and Chen, 2012). The third highlighted column shows the concentrations/values adopted in the batch study.

Compound/Unit	**Average range**	**Concentration adopted**	**Density of constituent (g cm^{-3})**	**Volumes/mass of constituent in 4 litres**
pH	4.3-10	2.9 - 3.2		
n-hexadecane mg/L	6.9-700	80	0.77	415 µL
Tridecane mg/L	6.9-700	80	0.76	423.2 µL
AlkylPhenols (3,5-DMP) mg/L	0.04-23	25		100 mg
Benzene mg/L	0.39-35	8.74	0.87	40.2 µL
Toluene mg/L	0.39-35	8.73	0.86	40.6 µL
Xylene mg/L	0.39-35	8.74	0.87	40.2 µL
Ethyl benzene mg/L	4.95	8.72	0.86	40.6 µL
		35		
Measured COD mg/L	48-1220	750 - 766		
HCO_3 mg/L	150-2000	200		1.1 g ($NaHCO_3$)
Chlorides mg/L	80-200000	1996		13.2 g (NaCl)
Acetic acid as Total Fatty Acids mg/L	2-4900	525	1.05	2 mL

Produced water samples were catalysed using a modified PAN fibrous catalyst previously described in chapter three and H_2O_2 as oxidant in duplicate in batch mode, where the loss of DMP, COD and OIW was monitored and reported. The reaction system was optimised with respect to H_2O_2 concentration and dosage. Subsequently, the optimised batch conditions were applied in continuous flow mode in a 900 mL rotating disc reactor described in section 5.4.3, where DMP, COD, and OIW were monitored for almost one month and reported.

Table 5.5: Average composite concentrations of common organic and inorganic constituents in produced water from conventional oil and gas operations, from selected fields around the world. (Rice and Nuccio, 2000; Benko and Drewes, 2008; Igunnu and Chen, 2012). The third highlighted column shows the concentrations/values adopted in the continuous flow study.

Compound/Unit	**Average range**	**Concentration adopted**	**Concentration in PW feed**	**Measured Concentration lifted into reactor**
pH	4.3-10	2.9 - 3.2	2.9 - 3.2	
n-hexadecane mg/L	6.9-700	40	96.25	2-27.9 as OIW
Tridecane mg/L	6.9-700	40	95	
AlkylPhenols (3,5-DMP) mg/L	0.04-23	25-30	25-30	24-29
Benzene mg/L	0.39-35	35	108.8	39 avg. as OIW
Toluene mg/L	0.39-35	35	107.5	
O-Xylene mg/L	0.39-35	35	108.8	
Ethyl benzene mg/L	4.95	35	107.5	
Measured COD mg/L	48-7220		~ 750	
HCO_3 mg/L	150-2000	200	200	1.1 g ($NaHCO_3$)
Chlorides mg/L	80-200000	1996	1996	13.2 g (NaCl)
Acetic acid as Total Fatty Acids mg/L	2-4900	525	525	2 mL

5.4.5 Instrumentation/ Analytical methods

5.4.5.1 Analysis of Oil- in- Water

Oil-in-water analysis was monitored using the Bruker Alpha FTIR in the transmission module. The sample holder was fitted with a 2''x 3'' square cuvette holder to enable the use of a 10 mm type 1 silica grade cuvette. The single wavenumber infrared method, also known as the DECC Infrared/Tetrachloroethylene method, was used for the

experiments conducted in batch mode. This has an absorbance peak at 2930 cm^{-1} that corresponds to the CH_3 stretch vibration, which theoretically quantifies the aliphatic constituents, and some of the aromatic hydrocarbon fractions such as ethylbenzene (Yang, 2011), owing to its relatively low solubility in water. On the other hand, a modified triple peak method, IP 426/98 was used for the analysis of oil-in-water for the continuous flow experiment to enable proper accounting for the aromatic fractions as well. This method has been described in more details in section 5.4.5.4. It should be noted that in continuous flow process, there is possible loss of volatile fraction due to a large exposed surface area in the reactor, the available headspace and continuous stirring of the feedstock (Libra, 1991). In addition to this, there is also the problem of sorption of the non-polar fraction of the PW constituents onto the connection tubing material (silicone hose).

This has therefore necessitated the preparation of a slightly different recipes for the produced water used for batch and continuous flow experiments. The concentrations of the volatile fraction has been increased as shown on Table 5.5 to make up for possible lost constituents.

5.4.5.2 Procedure for Oil-in-Water Analysis using FTIR/Tetrachloroethylene single wavenumber Method for Batch Experiments

Calibration standards for oil- in- water (OIW) for batch mode experiments were prepared using isooctane and n-hexadecane using the back extraction method (Yang, 2011). The calibration graph is presented in Figure 5.4. Alternatively, a dry (devoid of moisture) crude oil sample from a field under study is a preferred option for the

calibration standard. 200 mL produced water sample was completely transferred into a 500 mL separating funnel and was treated as per OSPAR reference method (Measurement of oil in water; FTIR/Tetrachloroehthylene method) for single wavenumber, which is a modified version of the ISO 9377-2 method as follows:

In this OSPAR method, 20 mL of the extraction solvent – tetrachlroethylene (TTCE), was added to the 200 mL sample (this is equivalent to 10% of extraction solvent). Following this, the pH of the 200 mL sample solution was adjusted to pH 2 by the drop-wise addition of a known volume of HCl (1:1 by volume HCl solution). The acid functions to dissolve any precipitates formed by the carbonates and any emulsions formed on the solvent/water boundary upon the addition of the TTCE.

This mixture was agitated vigorously for 2 min and then clamped to a retort stand and allowed to settle for another 15 min. The separated extract was collected over a glass funnel fitted with filter paper and a bed of 1g of silica gel activated by heating in a furnace at 500 ^{o}C for 4 h (Yang, 2011; DECC, 2011). The activated silica gel was applied to remove the polar organic compounds while an additional 1g of magnesium sulphate was added to the silica gel to remove moisture. The recovered extract (filtrate) was made-up with a known volume of TTCE to the original volume of the extraction solvent (20 mL) and analysed for OIW using FTIR. Samples were introduced into an FTIR fixed cell which had a spacer thickness of 5mm. The absorbance was measured at 2930 cm^{-1} and estimated as the peak area to the local baseline as demonstrated in Figure 5.4 below, designated as “B” on the OPUS 7.5 software available on the Alpha Bruker FTIR. The concentration of OIW was calculated from the line equation of the calibration graph

in Figure 5.5 given as (y=0.0009x + 0.0131). The concentration for the OIW measurement was determined from the equation;

$$\text{Corrected oil concentration (mg/l)} = \frac{\text{oil concentration (from calibration) x V (mL) x DF}}{\text{(Actual sample volume – vol. acid added)}}$$

Where, DF = dilution factor = (final volume of extract / initial volume of extract),

OIW = Final oil in water concentration (mg/L)

Oil concentration (mg/L) = concentration of oil from sample extract determined by applying the measured absorbance to calibration graph equation, and V (mL) is the volume of sample.

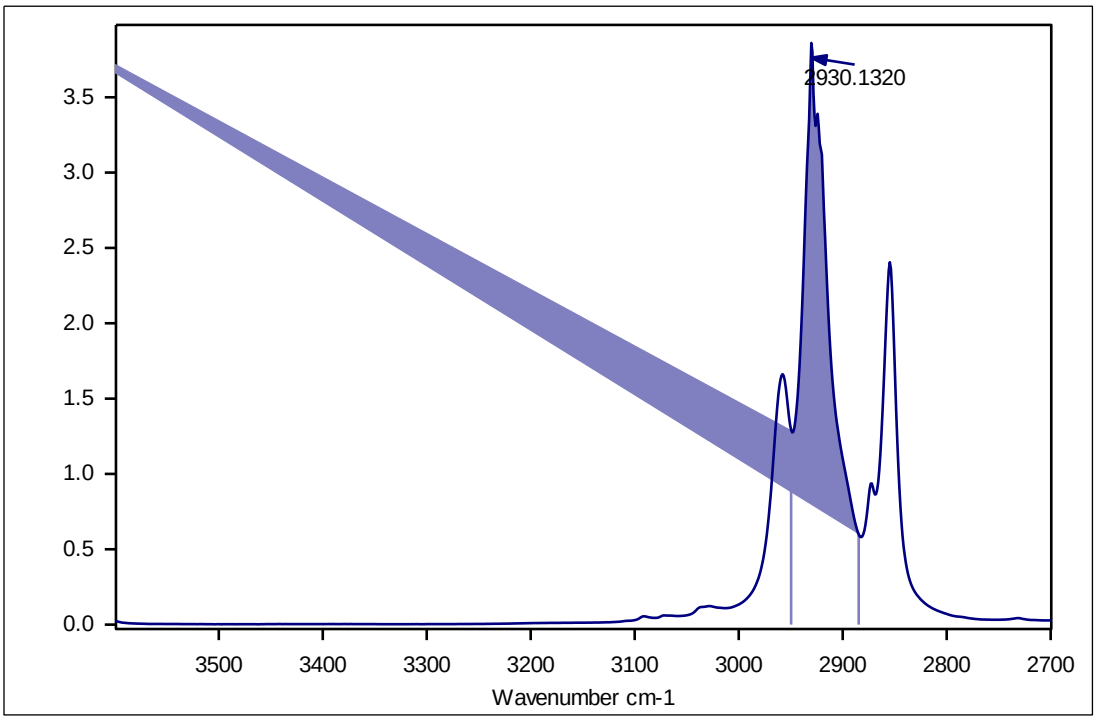

Figure 5.4: Illustration of how the absorbance at 2930 cm^{-1} was measured as peak area to the local baseline (designated as B in the Opus package)

5.4.5.3 OIL –in-Water Calibration for FTIR/Tetrachloroethylene single wavenumber Method used for Batch Experiments

Working standards spanning a range of 5 to 80 mg/L (5, 10, 20, 40 and 80 mg/L) were prepared by serial dilution of the reference oil stock (isooctane and n-hexadecane) for single wavenumber method. The reference oil stock was 1000mg/L of isooctane and n-hexadecane made up in TTCE (144.5 µL isooctane and 129.9 µL n-hexadecane in 100 mL TTCE). The average absorbances of respective working standards was used to plot the calibration curve presented in Figure 5.5.

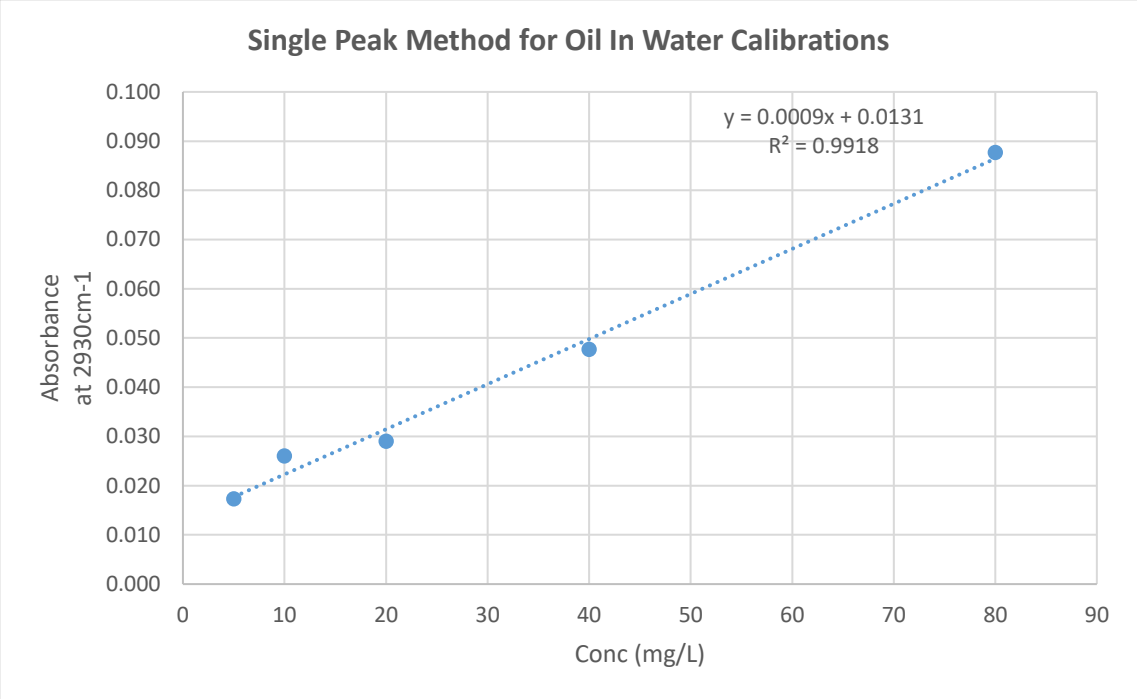

Figure 5.5: Calibration graph for oil in water analysis. Calibration standards used were isooctane and n-hexadecane of 5 to 80 mg/L mixed standard solution, made up in TTCE.

5.4.5.4 OIL –in-Water Calibration and Determination Using Triple Peak Method for Continuous Flow Processes

For continuous flow experiments however, the triple peak infrared method of oil in water analysis was used to determine the oil in water concentrations resulting from the aromatic hydrocarbons (BTEX) and aliphatic hydrocarbons (n-hexadecane and tridecane). In a triple peak or three-wavenumber infrared method, Infrared absorbance at three different wavenumbers is measured simultaneously instead of a single fixed wavenumber as with the single peak method. These wavenumbers are as follows; the stretch vibration of aromatics C–H at 3030 cm^{-1}, methylene HC–H at 2960 cm^{-1} and methyl H_2C–H at 2930 cm^{-1}.

Calibration was done using 50 ppm each of standards (Toluene, TMPD and n-Hexadecane) as per section 7.13 of modified IP426/98 method as described by Department of Energy and Climate Change (DECC 2011). Quantification was achieved using the following equations according to the modified IP426/98 method (DECC 2011; Yang 2011):

$$C = [X (A_{2930})] + [Y (A_{2960})] + [Z (A_{3030} – A_{2930} / F)] \quad \ldots (5.1)$$

Where C is the concentration of the hydrocarbons in the calibration standard;

A_{2930}, A_{2960} and A_{3030} are the absorbance determined by integrating peak height to the axis, designated as “J” in the OPUS software (Figure 5.6) at 2930 cm^{-1}, 2960 cm^{-1} and 3030 cm^{-1} while F is A_{2930}/A_{3030} for hexadecane standard respectively scanned between

2600 cm^{-1} and 3400 cm^{-1} for each extracted oil in water sample. And X, Y, and Z are weighted contributions of aliphatics (X and Y) and aromatics (Z) to OIW concentration.

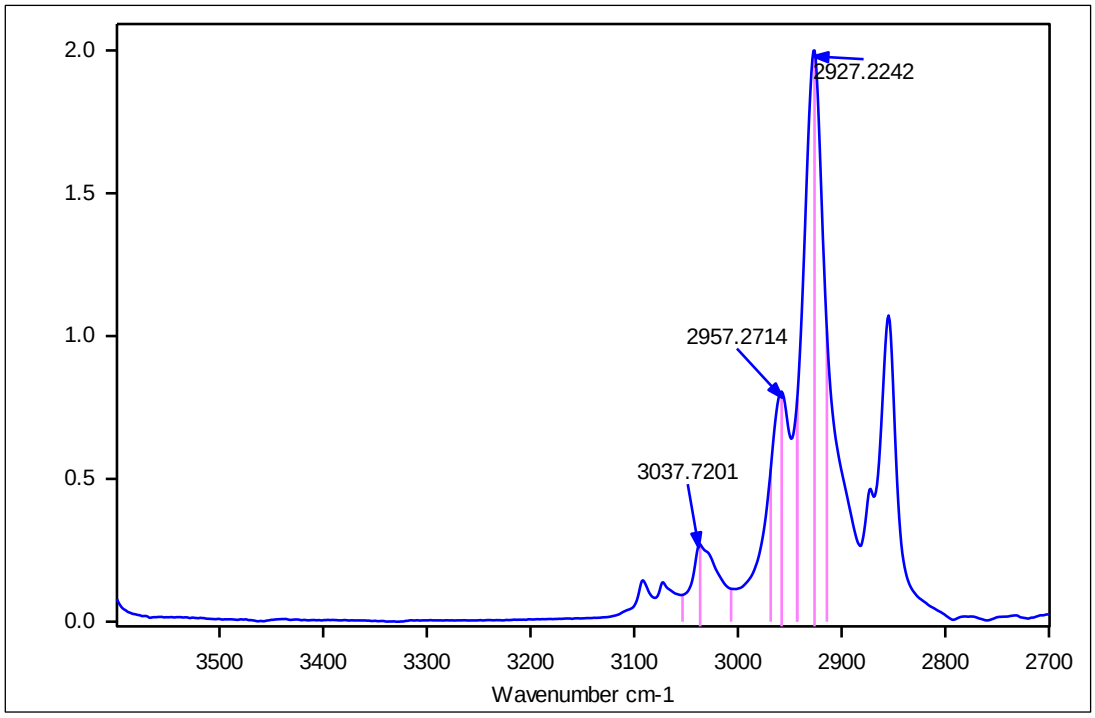

Figure 5.6: FTIR spectrum of an inlet sample showing an illustration of how the peak height to the axis (J) is integrated at 2930 cm^{-1}, 2960 cm^{-1} and 3030 cm^{-1} respectively, scanned between 2600 cm^{-1} and 3400 cm^{-1}

The FTIR absorbance spectra for each of the 50 ppm standards have been presented in Figure 5.7 to 5.9.

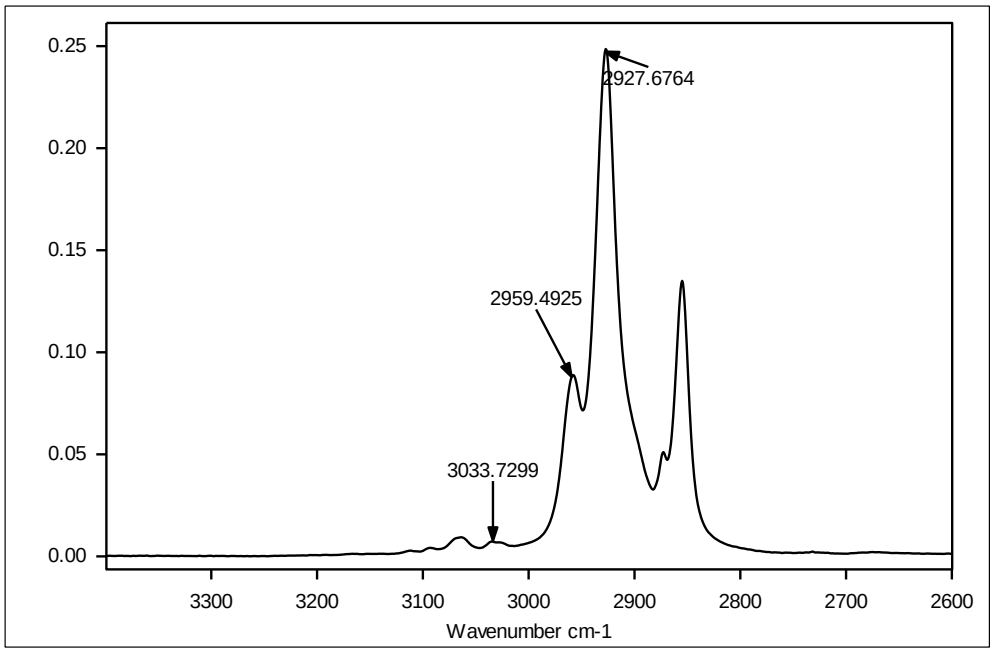

Figure 5.7: FTIR spectrum of n-hexadecane in TTCE at a 50 ppm concentration using the following instrument parameters; resolution 2 cm^{-1}, sample scan time 45 seconds, 20 sample and background scans with atmospheric compensation, saved data from 3600 cm^{-1} to 2700 cm^{-1}

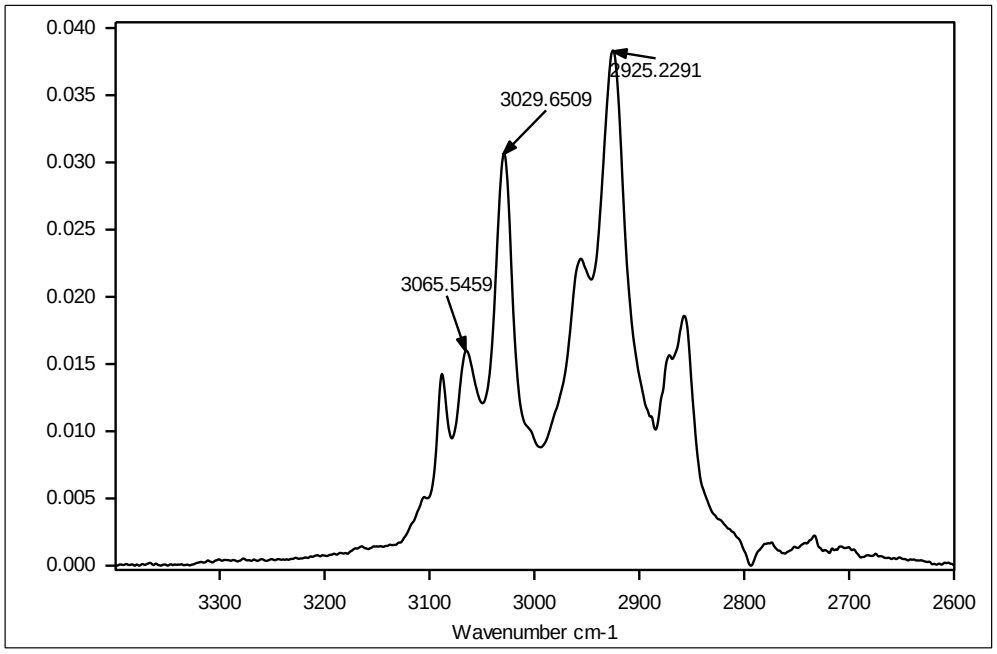

Figure 5.8: FTIR spectrum of Toluene in TTCE at a 50 ppm concentration using the following instrument parameters; resolution 2 cm^{-1}, sample scan time 45 seconds, 20 sample and background scans with atmospheric compensation, saved data from 3600 cm^{-1} to 2700 cm^{-1}.

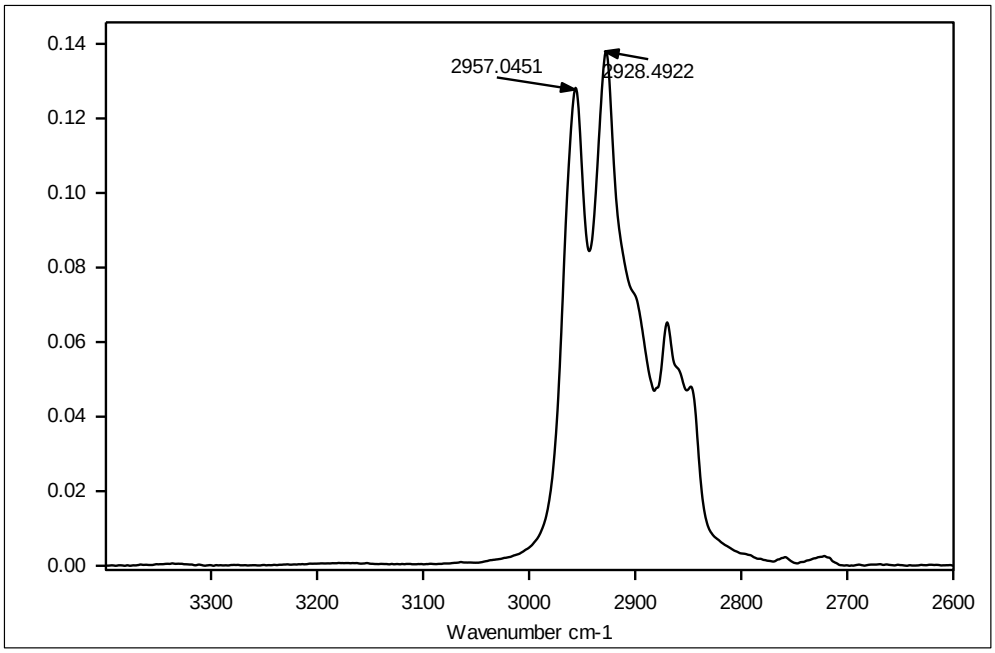

Figure 5.9: FTIR spectrum of TMPD in TTCE at a 50 ppm concentration using the following instrument parameters; resolution 2 cm^{-1}, sample scan time 45 seconds, 20 sample and background scans with atmospheric compensation, saved data from 3600 cm^{-1} to 2700 cm^{-1}.

For the hexadecane standard, the Z term is zero and for the TMPD standard, the Z term is assumed to be zero. Thus, the three simultaneous equations become:

$$C_{toluene} = [X (A_{2930, toluene})] + [Y (A_{2960, toluene})] + [Z (A_{3030, toluene} - A_{2930, toluene} / F)] \quad \ldots(5.2)$$

$$C_{TMPD} = [X (A_{2930, TMPD})] + [Y (A_{2960, TMPD})] \quad \ldots(5.3)$$

$$C_{hexadecane} = [X (A_{2930, hexadecane})] + [Y (A_{2960, hexadecane})] \quad \ldots(5.4)$$

Where $C_{toluene}$, C_{TMPD} and $C_{hexadecane}$ are the concentrations of the stock solutions. The values for X, Y and Z were simultaneously determined from the absorbance measurements on Table 5.6.

Table 5.6: Absorbance of OIW standards used for the triple peak method of OIW determinations

OIW Standard	Absorbance at 3030/cm	Absorbance at 2960/cm	Absorbance at 2930/cm
50ppm Hexadecane	0.007	0.089	0.247
50ppm Toluene	0.031	0.022	0.038
50ppm TMPD	No peak	0.131	0.141

The oil content of the sample, C_{Total}, in milligrams per litre, was therefore determined using equation 5.5:

$$C_{Total} = \{[X (A_{2930})] + [Y (A_{2960}] + [Z (A_{3030} – A_{2930} / F)]\} \frac{10vD}{VL} \quad \ldots (5.5)$$

Where X, Y and Z are factors determined simultaneously from equations 5.2, 5.3, and 5.4. *V* is the volume of produced water sample that was extracted, in millilitres; *D* is the dilution factor (if the sample is not diluted, D=1). *v* is the volume of TTCE in mL used to extract the produced water sample, in millilitres; and A is the absorbance at the specified wavenumbers; F is A_{2930}/A_{3030} for hexadecane standard; L is the cell path length in mm. The cuvette used for the triple peak method was a 10mm quartz-silica FTIR grade cuvette. This was used in the Alpha Bruker FTIR by using a 2”x3” cuvette holder adapter. To determine the aliphatic and aromatic fractions we have that:

$$C_{aliphatic} = \{ [X (A_{2930})] + [Y(A_{2960})]\} \frac{10vD}{VL} \quad \ldots (5.6)$$

$$C_{aromatic} = C_{total} - C_{aliphatic} \quad \ldots (5.7)$$

5.4.5.4.1 Determination of X, Y and Z values simultaneously

Using the absorbance, the values of X, Y, and Z in equation 5.5 were determined simultaneously using equations 5.2, 5.3, and 5.4 as follows:

$50 = [X(0.038)] + [Y(0.022)] + [Z(0.031 - 0.038/35.285)]$ …(5.8)

$50 = [X(0.141)] + [Y(0.131)]$ …(5.9)

$50 = [X(0.247] + [Y(0.089)]$ …(5.10)

$50 = 0.038X + 0.022Y + 0.030Z$ …(5.11)

$50 = 0.141X + 0.131Y$ …(5.12)

$50 = 0.247X + 0.089Y$ …(5.13)

From equation 5.12, X is given by:

$0.141X + 0.131Y = 50$ …(5.14)

$0.141X = 50 - 0.131Y$ … (5.15)

$X = \frac{50-0.131Y}{0.141}$ …(5.16)

Substituting X in equation 5.13 we have that:

$50 = 0.247\left(\frac{50-0.131Y}{0.141}\right) + 0.089Y$ … (5.17)

$50 = 1.752(50 - 0.131Y) + 0.089Y$ … (5.18)

$50 = 87.6 - 0.2295Y + 0.089Y$ … (5.19)

$50 = 87.6 - 0.1405Y$

$Y = 267.59$ …(5.20)

Substituting Y = 267.59 in equation 5.16, we have that:

$X = \frac{50-0.131(267.59)}{0.141}$ …(5.21)

$X = \frac{50-34.93}{0.141}$ … (5.22)

X = 106.86 … (5.23)

Substituting X and Y in equation 5.11, we have that:

50 = 0.038(106.86) + 0.022(267.59) + 0.030Z … (5.24)

50 = 4.061 + 5.865 + 0.030Z … (5.25)

$Z = \frac{40.072}{0.030}$ … (5.26)

Z = 1335.75 … (5.27)

5.4.5.5 Analysis of DMP and H_2O_2

The rate of loss of substrate (DMP) and hydrogen peroxide were monitored on a PerkinElmer series 200 LC Turbo model fitted with a UV detector. The procedure varies from the one previously described in chapter three. In this case, the UV detector wavelength was changed to 210 nm and column changed from phenomenex to Grace®. DMP was monitored at a detector wavelength of 210 nm and a pump flow rate of 1.5 mL/min. The isocratic mobile phase was acetonitrile and water 40:60 v/v. The stationary phase was a Grace® RP column with 4.6 ID, 5 microns internal packing material and a length of 250 mm. DMP had a retention time of 5.4 min while the H_2O_2 eluted at 2.2 min. The total run time was 8 min. The calibration graph is as shown on Figure 5.10.

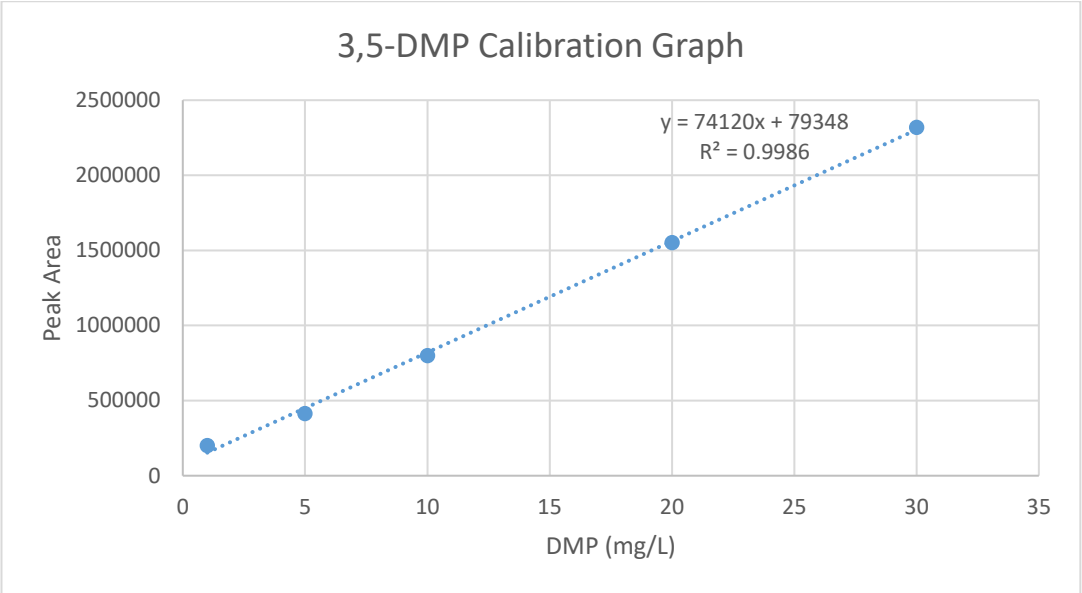

Figure 5.10: Calibration graph for 3,5-DMP

5.4.5.6 Analysis of Total Iron Leached into Reaction Solution and on the Catalyst

The impregnated iron on catalyst after acid digestion and leached iron in the reaction process was measured using a PerkinElmer flame atomic absorption spectrometer (AAS). The method and procedure has been described in detail in section 3.3.1.3, in chapter three.

5.4.5.7 Analysis of Chemical Oxygen Demand (COD)

The chemical oxygen demand COD, was monitored using spectrophotometry reference method –COD cuvette test ISO 15705, with cuvette vials of measuring range 0 - 1000mg/L and 100- 2000 mg/L for the synthetic produced water analysis. The detailed procedure has already been described in chapter three section 3.3.1.2.

Preliminary experiments designed to check possible interference of chloride ion on COD measurements involved COD test of acetic acid with high chloride solutions (500, 2000

and 4000mg/L NaCl as chloride). Acetic acid was chosen because of its high return on COD measurement (~ 98 to 100% return on COD).

COD analysis was also used for the determination of the stability of suspected volatile hydrocarbon compounds namely: BTEX and acetic acid.

5.5 Experimental Procedure for Batch Process

5.5.1 Control experiments

Preliminary experiments involved the setting up of four control experiments for possible loss of substrates through volatilization (due to headspace), sorption on catalyst and degradation by H_2O_2. The following duplicate samples of freshly prepared synthetic produced water (PW) were transferred into thermostated carousel reactor fitted with a magnetic stirrer and the pH was adjusted to 3.0;

1. 200 mL of 500 mg/L acetic acid in double distilled water at pH3, stirred for 240min
2. 200 mL PW only, stirred for 240 min
3. 200 mL PW with 10 g catalyst only, stirred for 240 min
4. 200 mL PW with 1000 mg/L H_2O_2 only

These have been presented in Table 5.7 below.

Table 5.7: control experiments for produced water degradation to monitor extent of volatility

Experiment N0.	Experimental Conditions	Reagents Added	Parameters determined
1	-500 mg/L acetic acid in 200 mL double distilled water -Stirred for 240 min	None	Initial and final COD
2	-200 mL of pure BTEX in double distilled water, stirred for 240 min	None	Initial and final COD and
3	-200 mL of mixed solution of n-hexadecane and tridecane, stirred for 240 min	H_2O_2	Initial and final COD and OIW (single peak method) for aliphatic hydrocarbon fractions
4	-200 mL PW, stirred for 240 min	1000 mg/L H_2O_2	Initial and final COD and OIW(single peak method) for aliphatics hydrocarbon fractions
5	-500 mg/L NaCl as chloride in 500 mg/L acetic acid solution	No reaction, determination of initial COD	COD
6	-2000 mg/L NaCl as chloride in 500 mg/L acetic acid solution	No reaction, determination of initial COD	COD
7	-4000 mg/L NaCl as chloride in 500 mg/L acetic acid solution	No reaction, determination of initial COD	COD

The results for all control experiments are presented in Tables 5.8, 5.9 and 5.10 in the results section.

5.5.2 Batch experiments

For the batch experiments, duplicate samples of produced water (PW) were again transferred into thermostated carousel reactor described previously at pH 3.0. The batch reaction was initiated by the addition of a modified PAN catalytic mesh and hydrogen peroxide as previously described in chapter three. This is as shown in Figure 5.11.

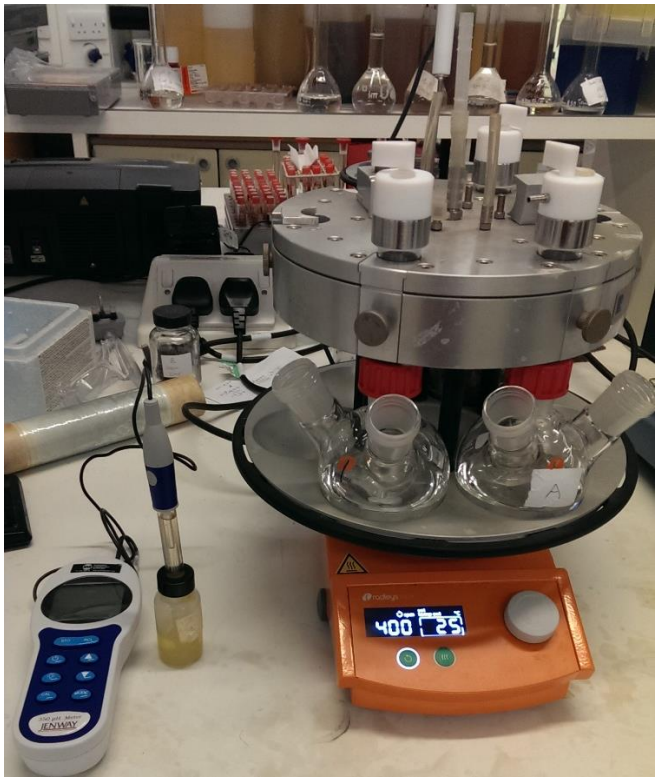

Figure 5.11: Batch process for the heterogeneous catalytic degradation of synthetic produced water using a modified PAN catalyst

The following parameters were monitored; COD, using DR 3800 Hach Lange spectrophotometer, after sample digestion on the Hach Lange LT200 digestion block. DMP was monitored on the HPLC and OIW was monitored using FTIR.

For Oil-in-water measurement, both residual concentration in the treated effluent and absorbed OIW concentrations (absorbed oils) were considered and accounted for. The oils absorbed on the catalyst were determined according to the modified method on Annex A, DECC IR Method for Determination of Oil on Sand/Scale/Solids. The determined concentration is presented as "desorbed OIW concentration".

5.5.3 Procedure for Desorption of Oils on Catalyst in Batch Experiments

The DECC IR method for determination of Oil on Sand/Scale/Solids (DECC 2011), was slightly modified with respect to volumes and adopted. The 10 g of catalyst used in the 200 mL batch reaction was removed from the reactor and 200 mL of the reaction solution was transferred into a clean dry 500 mL stoppered glass bottle and 50 mL of TTCE was added. This was shaken vigorously for two minutes, after which the catalyst was removed. The desorbed oil in TTCE (50 mL) was passed over a TTCE wetted filter paper stuffed with one gram of silica gel and $MgSO_4$ each and collected into 50mL volumetric flask. This was measured on the FTIR using FTIR/Tetrachloroethylene method for single wavenumber dispersed oil determination described in section 5.4.5.2 and calculated from the calibration graph in Figure 5.4. The actual concentration for the desorbed OIW measurement in mg/L was determined from the equation 5.28;

$$\text{Desorbed oil (mg/L)} = \frac{\text{oil concentration from calibration (mg/L)} \times \text{V (mL)}}{\text{Actual sample volume - volume of acid}} \quad \ldots (5.28)$$

Desorbed oil (mg/L) = Corrected oil concentration

Oil concentration (mg/L) = concentration of oil from sample extract determined by applying the measured absorbance on the FTIR to the calibration equation, and V (mL) is the volume of sample.

5.6 Experimental Procedure for Continuous Flow Treatment System

Continuous flow experiments create a better opportunity to study in more detail certain catalyst properties and process parameters that in the end gives a better understanding for upscaling wastewater treatment processes. The advantages of having a catalyst on an immobilised support in continuous flow reactor systems is given by Chaplin (2014). This advantage is due to the loss of catalyst material in slurry reactor systems as some catalyst exits with the effluent which results in less contact time for catalyst and substrate in reacting systems as well as contaminating the treated effluent.

Chaplin (2014) classified continuous flow reactors into three main groups. These are; Continuous Stirred Tank Reactor (CSTR) which has complete and rapid mixing properties, the Packed Bed Reactor (PBR) which has no mixing and flows are typically plug flows and the Fluidised Bed Reactor (FBR) which is between the previous two, with little or no mixing.

The continuous flow treatment system is usually a scale-up of laboratory scale reactor designs and experiments. The laboratory reactions afford the opportunity for optimization towards pilot scale treatments where process parameters such as diffusivity, mixing, heat flow (conduction, convection, thermal radiation, or phase-change transfer) etc, can be optimised to overcome mass transfer limitations which is a potent problem in heterogeneous catalytic systems.

5.6.1 Materials

In addition to the materials used for the batch reaction process, the materials used for the continuous flow study were: 5 mm borosilicate glass tubes, Marlow series 101U peristaltic pumps, fume hood, Masterflex platinum cured silicon tubing, and 900 mL rotating disc reactor.

5.6.2 Procedure

The continuous flow experiments were carried out in a fume hood, using the rotating disc reactor shown in Figures 5.2 and 5.3. The produced water was fed through 5mm OD borosilicate glass tubing to avoid loss of oils through sorption where possible. Where unavoidable, especially around the peristaltic pumps, 4.8 mm OD silicon tubing was used. Two feed glass bottles, one containing H_2O_2 and the other synthetic produced water, were fed into the reactor where the 180g of washed and normalised catalyst to pH3 was affixed to 8 discs, which were rotated by a motor. The pH of both the produced water and H_2O_2 was adjusted to pH3.

Produced water was made to double the required strength (with respect to the concentration of constituents) and was diluted by H_2O_2, to the required strength, which was pumped at an equal flowrate using the same pump and tubing of the same diameter. These (PW and H_2O_2) were pumped into the 900 mL reactor via a peristaltic pump (Figures 5.2 and 5.3) at a combined flow rate of 3.75 mL/min, to achieve a retention time of 240 min with an average theoretical inlet H_2O_2 concentration of 1000 mg/L in the reactor. The H_2O_2 was the optimised value from batch processes. Mixing was achieved by the shear rotation of the catalyst discs and the reaction was at room

temperature. The experiments were carried out in the spring, with average room temperature at about 23±2 ^{0}C. As already mentioned, OIW for continuous flow experiments was determined using the triple peak method while oil on catalyst was desorbed and measured using the same method (triple peak).

5.6.3 Procedure for Desorption of Oil from Catalyst after Continuous Flow Experiments

Due to environmental and health concerns, the use of large volumes of TTCE for desorption of residual oils on the catalyst in continuous flow catalysis (because of the large amount of catalyst involved) was not considered. At the end of the continuous flow experiment, attempts were made to use a non-petroleum based surfactant for the desorption oils from the catalyst.

Small aliquots of Fairy^{TM} – 5 mL in 4000 mL of double distilled water (Proctor and Gamble 2015) at 40 ^{o}C (Gitipour et al., 2014; Perfumo et al., 2007) were made up as a stock solution. 500 mL of the surfactant/water solution was transferred into the empty reactor with the used catalyst still in place. The wheels (with catalyst on) were rotated slightly faster than during normal experimental runs (15 rpm) with the reactor lid on for 10 min, and the oils were collected into the surfactant/water solution through a process described as psuedosolubility by surfactant addition (Gitipour et al., 2014; Stroud et al., 2007; Perfumo et al., 2007).

The contents were emptied into a 1 L stoppered glass sample bottle. This desorbed sample was extracted using 50 mL of TTCE, however, there was poor separation between the surfactants and the oils. It was therefore not possible to extract the oils

from the surfactant, but the experiment led to the insight that surfactant solution could effectively desorb the oils from wheels, and could be applied as a regeneration step for catalyst desorption.

The process of desorption was repeated with only water (500 mL) at 40 ^{o}C, followed by extraction using TTCE, which was then treated with 2 g each of silica gel and $MgSO_4$ followed by FTIR analysis according to the procedure described in 5.4.5.4. Extraction and analysis was repeated two more times until no oil was found in the extract. The measured OIW concentrations from the three procedures were summed up to get the total desorbed oil concentration in the continuous flow process i.e aromatic and aliphatic oils. Oil recovery using this procedure was 78%.

5.7 Results and Discussions for Batch Mode Experiments

5.7.1 Results for control experiments

Results for control experiments are presented in Tables 5.8, 5.9 and 5.10. Experiments 1 to 4 (Table 5.7) were designed, to evaluate the stability of the volatile organic components of the produced water, in the reaction system such as BTEX, aliphatics (tridecane and n-hexadecane) and acetic acid in the absence of a catalysed Fenton-like oxidation. Experiments 5 to 7 (Table 5.7) were intended to examine the interference, if any, the extent and the onset of chloride ion interference in COD reading with respect to the concentration of chloride.

5.7.1.1 Stability of acetic acid in the absence of any treatment

Results from COD experiments of pure acetic acid solution stirred for 240 min at pH three without any treatment showed that the acetic acid component of the PW lost only 1.7% COD, which means it was stable throughout the three hours of no treatment. The initial COD and final COD were 545 and 536 mg/L respectively as shown in Table 5.7 below (the theoretical COD (ThOD) for 500 mg/L acetic acid is 560 mg/L). COD was used as assessment parameter for its stability because the return on COD as seen in this study for acetic acid is almost 100% of the ThOD. This has been discussed in more details in section 5.7.2 below.

5.7.1.2 Stability of BTEX in the absence of any treatment

Pure solution of BTEX in concentrations similar to the ones in the produced water was made up in double distilled water and stirred for 240 min without any treatment and the initial and final COD was also determined.

The results show that 32.5% of BTEX was lost within 240min of stirring and this is likely due to volatility. The initial measured BTEX COD was 85.5 mg/L (ThOD of the solution was 110.1 Table 5.8) which is 77.6% return on COD. The final COD of the reaction after stirring for 240minutes was 58mg/L.

5.7.1.3 Stability of aliphatic hydrocarbon compounds in the absence of any treatment

Results from similar experiments (as for BTEX) conducted for the aliphatic hydrocarbon component of produced water (represented by hexadecane and tridecane) showed an initial COD of 163 mg/L (ThOD of solution was 555.9 mg/L Table 5.8), which is a poor

COD recovery 29.32 mg/L. The final COD of tridecane and hexadecane reaction after 240 minutes of stirring was 46 mg/L, indicating a loss of recoverable COD of 71% (based on measured initial COD) for aliphatic constituents after 240 min.

The measured COD values of aliphatic hydrocarbons (highlighted in green) in Table 5.8 below do not appear realistic owing to their low return on COD (Table 5.8). Aliphatics are heavier molecules than BTEX, with a vapour pressure of < 0.01 kPa at 20 ^{o}C, while benzene for instance has a vapour pressure of 12.7 kPa at 25 °C (volatility increased with increased vapour pressure). It is therefore practicable to use COD as a parameter to measure the loss of acetic acid which has between 95 to 100% return on COD and BTEX compounds which have an average of 77% return on COD (for all four compounds). However, this may not be accurate for measuring aliphatics that have a very low return on COD of less than 5% in some cases.

Baker et al., (1999) explained that the oxidation of most organic compounds is assumed, rather vaguely to be up to about 95-100% of the theoretical value. In practical terms however, this value ranges from as low as < 3 to 100%, depending on the group of organic compounds. According to them, acetic acids return the most accurate COD (when compared with ThOD) giving coefficients of up to 1 (100%), while hydrophobic aliphatic hydrocarbons such as hexadecane has coefficients of 0.03 (3%). Benzene on the other hand has 65%, Toluene 40%, ethylbenzene 75%, O-xylene 72% and phenols which falls under the group referred to as well-correlated aromatics, with a mean COD/ThOD of 0.98 (98%). This means that the most correlated class of compounds with respect to COD/ThOD is the saturated organic acids (Baker et al., 1999).

Table 5.8: Stability of suspected volatile PW constituents based on initial and final COD after 4 h

Compound	ThOD in Reaction	Initial COD	Final COD	% loss
Acetic acid	560.0	545.0	536.0	1.7
BTEX	110.1	85.5	58.0	32.5
Aliphatics	555.9	163.0	46.0	71.0

In addition to COD measurements, the single peak method of OIW was further used to evaluate the stability of aliphatics and the results are presented in Table 5.9 below. The single peak/wavelength method was used for quantification as with all batch processes in this study (CH_2-H methyl vibration, mainly the aliphatic components at 2930 cm^{-1}), based on the calibration graph for OIW analysis in Figure 5.5.

Table 5.9: Absorbance and concentrations showing aliphatic hydrocarbon concentrations

Wave number (cm^{-1})	Initial Absorbance of PW at zero min	Conc. of aliphatics at zero min (mg/L)	Measured absorbance after 4 h: PW and H_2O_2 only	Conc. of aliphatics after 4 h with H_2O_2 (mg/L)	Measured absorbance after 4 h: PW without treatment	Conc. of aliphatics after 4 h of no treatment (mg/L)
2930	0.153	155.44	0.118	118.00	0.123	122.11

The results in Table 5.9 suggests that the aliphatic hydrocarbon (AHC) compounds were relatively stable in the absence of Fenton-like oxidation for 240 min. The initial measured AHC concentration was 155.44 mg/L (Table 5.9), while the final concentration after 4 h in the presence of only H_2O_2 was 118 mg/L, which indicates a 24% loss of AHC due to the combined effect of H_2O_2 and volatilization.

The results for the untreated reaction solution exposed to only stirring for 4 hours recorded 21.44% reduction in the concentration of AHC at the end of 4 h (Table 5.9). There was a probable loss of 2.56% AHC due to the effect of H_2O_2 as seen in the difference of 4.11 mg/L AHC lost in the presence of H_2O_2 compared to when there was no H_2O_2 in the system; however, this loss is within the margin of error. The overall result suggests that the AHC compounds were relatively stable.

5.7.1.4 Interference of chloride ion in COD measurement

Results of the investigation of chloride interference in COD measurement has been presented in Table 5.10. It showed that chloride had no influence in the COD measurement within the range of the chloride ion concentration used in this work (1996 mg/L). Chloride ion however showed a contribution of about 18.89% to COD at 4000mg/L chloride concentration.

Table 5.10: Effect of high chloride concentration on COD measurement

Concentration of Acetic acid (mg/L)	Measured COD of Acetic acid (mg/L)	Concentration Cl^- (mg/L)	Total COD after Cl^- addition (mg/L)	% Change in COD
500	545	500	540	0
500	545	2000	536	*1.65 ↓
500	545	4000	648	18.89 ↑

* Within the margin of error

The results suggest that the onset of chloride ion interference in COD is when the concentration of chloride is > 2000 mg/L. It was therefore safe to carryout accurate COD

measurements in the prevailing concentrations of chloride used for these experiments, which was 1996 mg/L.

Chloride interferes with COD measurement owing to the oxidation of chloride ions according to equation 5.29 and $HgSO_4$ is often used to overcome this effect (Vyrides and Stuckey 2009):

$$Cr_2O_7^{2-} + 6Cl^- + 14H^+ \rightarrow 3Cl_2 + 2Cr^{3+} + 7H_2O \quad \ldots (5.29)$$

5.7.2 Effect of 400mg/L H_2O_2 on the Degradation of PW

The catalytic degradation of synthetic produced water was carried out with conditions previously optimised for the degradation of DMP, which represents the alkyl-phenolic components of PW, mainly responsible for its toxicity. Set parameters were; 10 g of Fe^{3+} PAN catalyst, 400ppm H_2O_2, 25 ^oC temperature, pH3 and a 200 mL reaction volume. The constituents of the simulated produced water in this reaction are as shown in Table 5.5, designated as 'adopted concentrations'.

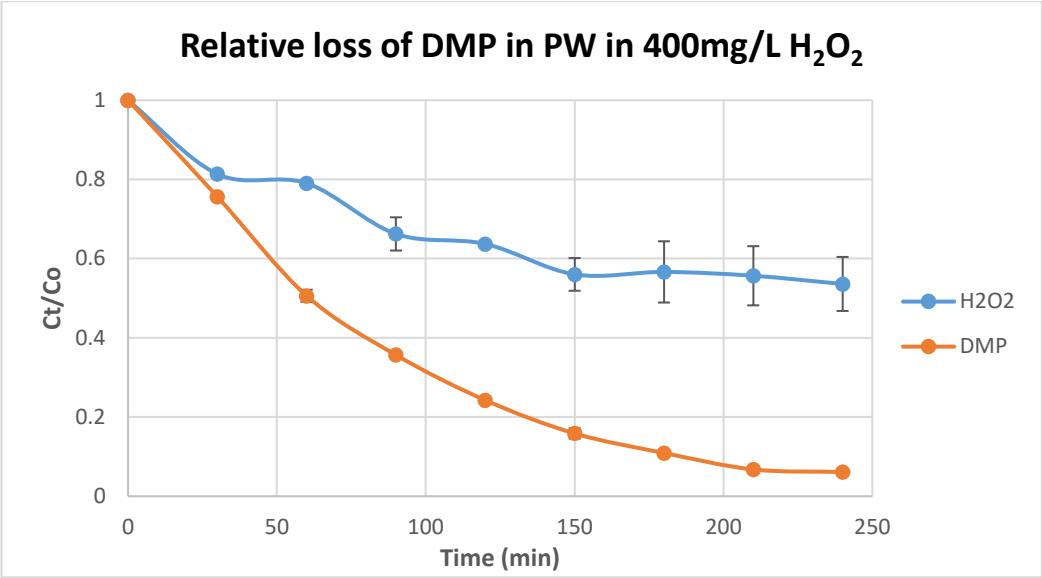

Figure 5.12: Decomposition of simulated produced water, showing loss of DMP and H_2O_2. Initial H_2O_2 concentration 400mg/L, Initial DMP concentration 25mg/L, 200mL reaction volume, 10g catalyst while reaction time 240 minutes at pH3 and 25±1°C.

The results of this experiment are as shown in Figure 5.12 and 5.13. DMP showed a constant degradation with time throughout the reaction in the presence of other PW constituents. About 94% DMP removal was recorded after 4 hours, while H_2O_2 recorded 47% loss, which corresponds to 188 mg/L of H_2O_2 in absolute terms. There was gradual loss of H_2O_2 evident in the gentle slope in Figure 5.12, which suggests that the loss of DMP was enabled by the decomposition of H_2O_2, which released OH radical for the oxidation process.

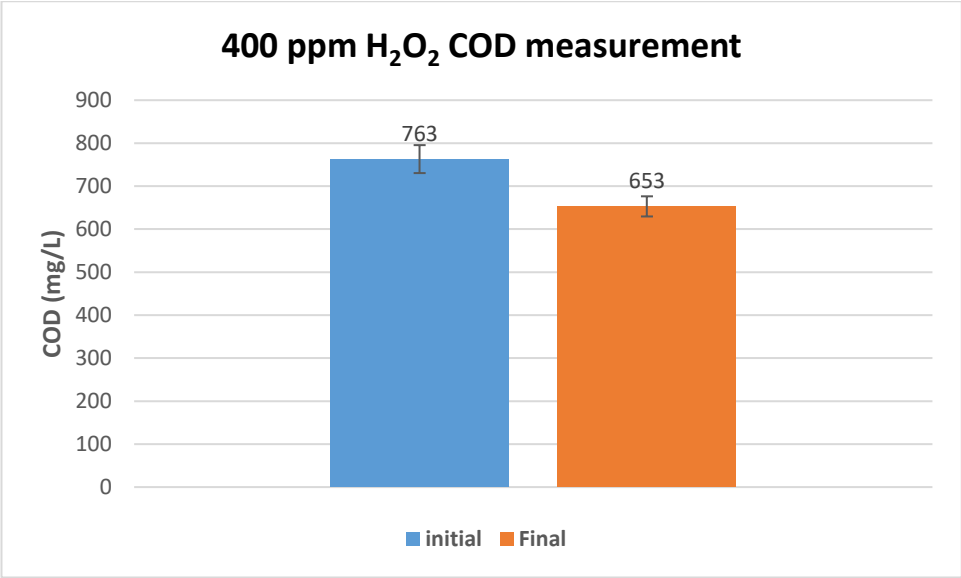

Figure 5.13: Initial and Final COD of produced water, Initial H_2O_2 concentration 400 ppm, Initial DMP concentration 25 mg/L, 200 mL reaction volume, 10 g catalyst while reaction time 4 h at pH3 and 25±1 ^oC

The initial and final COD for this reaction were 763 mg/L and 653 mg/L respectively after 120 min, which represents only about 14.42% reduction in COD. The total theoretical COD (ThOD) of 25 mg/L DMP (65.5mg/L) accounts for 5% of total theoretical COD of 1291.5 mg/L (Table 5.11). Therefore, 94% DMP removal means 61.57 mg/L COD resulting from DMP was clearly removed by 400 mg/L H_2O_2 after 2 h. The remaining 48.48 mg/L COD (judging from the difference between the initial and final COD of the reaction) was likely due to the loss of BTEX and the aliphatic hydrocarbon compounds.

The reason for the slow loss of COD could be due to the limiting of H_2O_2 on one hand and refractory compounds present in the system such as acetic acid. The concentration of acetic acid in the reaction system was 525 mg/L, which corresponds to a ThOD 560 mg/L of recalcitrant COD determined as shown:

$CH_3COOH + 2O_2 \rightarrow 2CO_2 + 2H_2O$ … (5.30)

525 mg/L CH_3COOH = 8.75 mM/L (RMM of CH_3COOH is 60)

1 mole of CH_3COOH requires 2 moles of O_2 for complete mineralization (from equation 5.30),

∴ mg/L of O_2 for mineralization of 8.75Mm/L CH_3COOH = 2 X 8.75 X 32 mg/L = 560 mg/L COD.

Other compounds that contributed to COD in the catalytic degradation of synthetic produced water and their corresponding ThOD contribution are presented in Table 5.11.

Table 5.11: ThOD values from possible COD contributing compounds in the synthetic produced water used for batch reactions

Compound	**RMM (g/mol)**	**Conc. (mg/L)**	**Conc. (mmol/L)**	**Moles of O_2 required for mineralization of 1 mole of compound**	**COD(mg/L)**
3,5-DMP	122	25	0.205	10.0	65.5
Benzene	78	35	0.112	7.5	26.9
Toluene	92		0.095	9.0	27.4
Ethyl xylene	106		0.083	10.5	27.9
Xylene	106		0.083	10.5	27.9
n-Hexadecane	226	80	0.354	24.5	277.5
Tridecane	184	80	0.435	20.0	278.4
Acetic acid	60	500	8.333	2.0	560
				Total theoretical COD	**1291.5**

The COD for the continuous flow experiments was also determined in a similar fashion, based on concentrations of constituents show in section 5.4.4, Table 5.5. Initial COD was sampled and measured before introducing the catalyst into the reaction system.

The difference between the initial measured COD and initial ThOD was 318.5 mg/L. The reason for this has already been discussed in section 5.7.1.3. In addition to the extremely poor return on COD for aliphatic hydrocarbons (~ 3%), there are several other factors, including loss of some constituents due to volatilization as shown by control experiments in Table 5.8.

According to Jenkins et al., (1973), straight chain organic acids are unlikely to be completely oxidized in the COD test even in the presence of a catalyst (usually silver sulphate) in addition, volatile organic compounds can only be oxidized if they are in solution (Eaton et al., 1995). Besides this, Wolff (1975) believes that the exothermic reaction which takes place between the strong acid and the volatile organic compound can displace them from the test solution (made up of potassium dichromate, concentrated sulphuric acid and a catalyst- silver sulphate). It is therefore almost impossible to have COD/ ThOD = 1 in the present system due to the presence of these class of compounds. Parker (1999), indicated that the effects are stronger in solutions with ThOD of less than 50mg/L. Hence, it is still possible to have a sense of the strength of the effluent solution using COD.

5.7.3 Effect of 1000ppm H_2O_2 on the Degradation of PW

Figure 5.14 shows the effect of increasing H_2O_2 dosing from 400 to 1000mg/L for 4 hours of produced water catalysis in batch mode on the loss of DMP and H_2O_2, while 5.15 shows the effect on COD. There was similar rates and percentage of loss of DMP as for 400mg/L initial H_2O_2 concentration, while the total loss of H_2O_2 in 4 h was 23.7%, which translates to about 237 mg/L total H_2O_2 in four hours. i.e. about 37 mg/L more loss of H_2O_2 when more H_2O_2 was used, which suggests that H_2O_2 could be limiting at 400 mg/L with respect to COD removal.

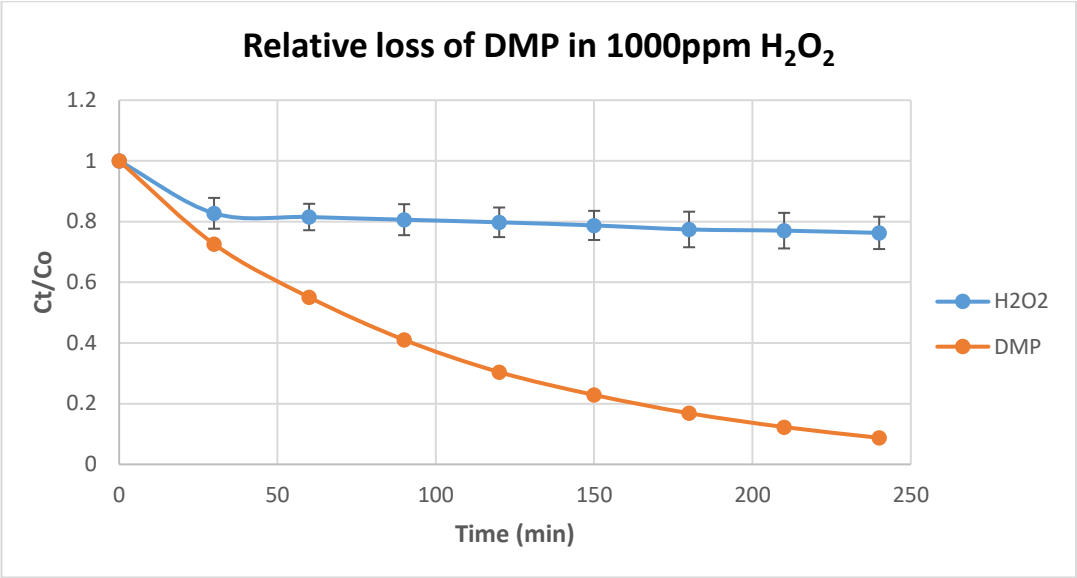

Figure 5.14: loss of DMP and H_2O_2 and COD. Initial H_2O_2 concentration of 1000 ppm, 25 mg/L DMP 200 mL reaction volume, 10 g catalyst at pH3, at 25 °C, for 4 h. Other constituents are as shown in Table 5.5.

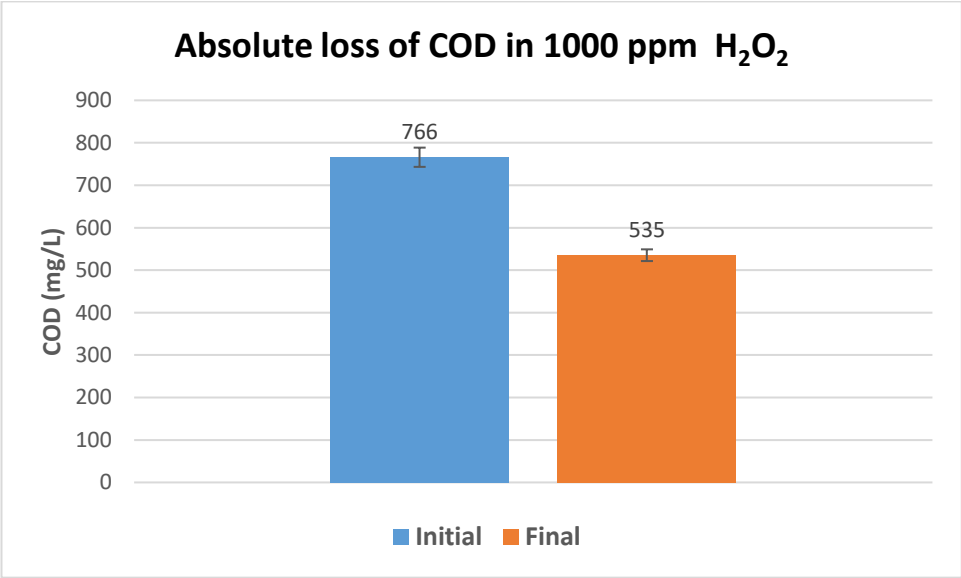

Figure 5.15: loss of COD in the experiments reported in Figure 5.14. Initial H_2O_2 concentration of 1000mg/L, 25 mg/L 3,5-DMP 200 mL reaction volume, 10 g catalyst at pH3, at 25 °C, for 4 h. Other constituents are as shown in Table 5.5.

There was 30.1% loss of COD and > 90% loss of DMP as shown in Figures 5.15 and 5.14 respectively. Figure 5.14 also shows a H_2O_2 loss of 20% which corresponds to 200 mg/L H_2O_2 (slightly more than the loss recorded when 400 mg/L H_2O_2 was used), which suggests that H_2O_2 was limiting with respect to COD reduction in the previous system. This assessment is supported by the increased loss of COD with increase in H_2O_2 to 1000 ppm, leading to more than 30% loss of COD, compared to 14.48% loss reported for 400 ppm H_2O_2 (Figure 5.13). This observation is corroborated by Collivignarelli et al., (2017). They reported an enhanced COD removal from 60% to 70% with increase in H_2O_2/COD_o ratio from 1/4 to 1/2 in a UV- enhanced homogeneous Fenton catalysis of wastewater from pharmaceutical and surfactants manufacturing process. A further 3/4 increase in H_2O_2/COD_o ratio had no influence in their process.

The increase in the loss of COD with increase in H_2O_2 observed in the present study is likely due to increased diffusion/contact between H_2O_2 and the catalyst, leading to increased breakdown of H_2O_2, which results in more OH radical for substrates degradation. According to USP Technologies, (2016), the extra peroxide helps to push the oxidation process further down the oxidation chain as a result of the build-up recalcitrant intermediates.

5.7.4 5.7.3 Effect of 2000 ppm H_2O_2 on the Degradation of PW

A further increase in the concentration H_2O_2 from 1000 ppm to 2000 ppm (which was about the stoichiometric requirement for the complete oxidation of produced water), yielded further loss of the COD and DMP as shown in Figure 5.17 and 5.16. Based on the

initial COD value of 752 mg/L, the H_2O_2 requirement for the complete mineralization in this reaction was calculated as follows;

$$2H_2O_2 \rightarrow 2H_2O + O_2 \quad \ldots (5.31)$$

From equation 5.31, two moles of H_2O_2 are required for each mole of O_2. Therefore, the amount of O_2 (moles) required for the measured COD is given as:

moles of O_2 required = $\frac{COD\ (mg/L)}{Molar\ mass\ of\ O_2\ (g/mol)} \frac{766}{32} = 23.94$

This indicates that the complete mineralization of synthetic produced water with measurable COD of about 766 mg/L, requires 23.94 moles of O_2

From equation 5.31, 2 moles of H_2O_2 are required for each mole of O_2. Hence;

Concentration of H_2O_2 = 2 * 23.94 * 34 = 1627.92 mg/L H_2O_2

This suggests that a further increase in H_2O_2 beyond 1000 ppm was theoretically required for complete mineralization of this PW. However, it is obvious from Tables 5.8 and 5.11 that the measured COD is not a true representation of the actual COD, due to poor return on COD for aliphatic compound (about 5% of ThOD) and the volatile aromatic fraction. As a result, an increase to 2000 ppm H_2O_2 was made. The results of this experiment has been presented in Figure 5.16.

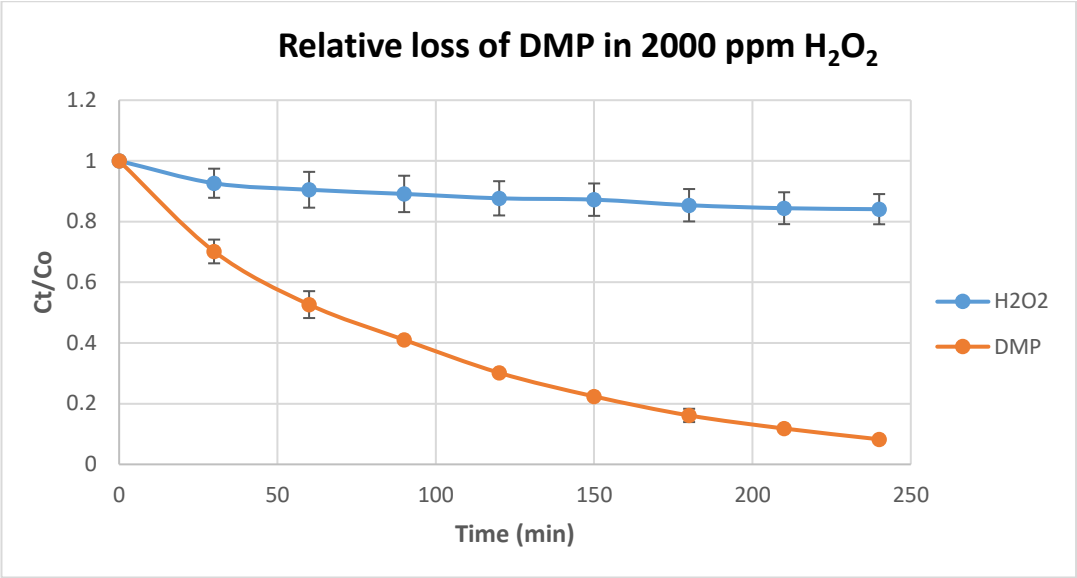

Figure 5.16: Decomposition of synthetic produced water showing loss of DMP and H_2O_2. Initial H_2O_2 concentration of 2000 ppm, DMP 25 mg/L, 10 g of catalyst, pH3, 200 mL reaction volume and reaction 4 h reaction time.

There was 15.9% loss of H_2O_2 (318 mg/L in absolute terms) after 4 h of reaction i.e. 81mg/L more degradation of H_2O_2 than when 1000 mg/L H_2O_2 was used, as shown in Figure 5.14. There was a total COD removal of 267 mg/L, which is about 35.5% removal in 4 h. This further increase in H_2O_2 resulted in about 5% more reduction on COD (compared to 1000 ppm H_2O_2) which is not a significant additional effect on COD reduction.

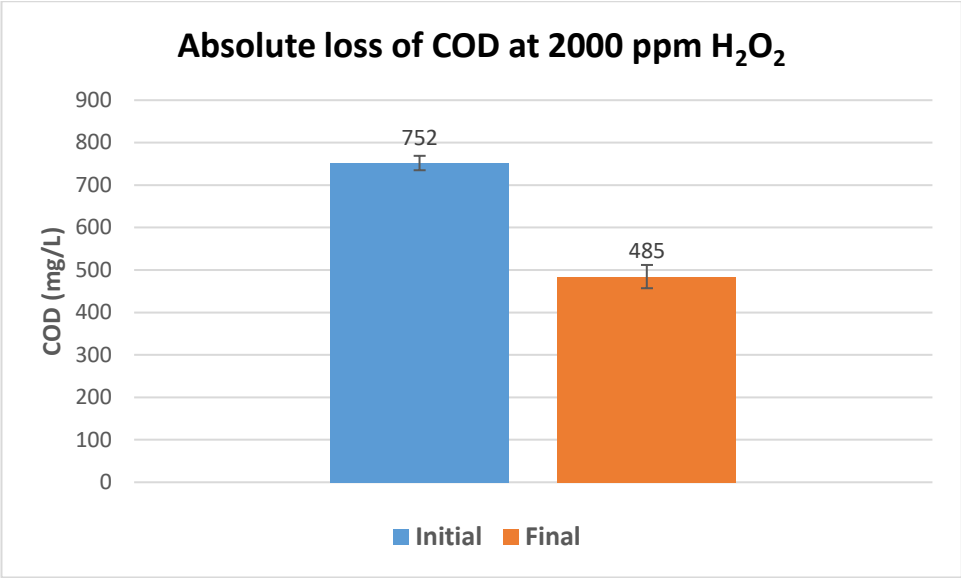

Figure 5.17: loss of COD in the experiments reported in Figure 5.16. Initial H_2O_2 concentration of 2000 mg/L, 25 mg/L DMP, 200 mL reaction volume, 10 g catalyst at pH3, at 25 °C, for 4 h. Other constituents are as shown in Table 5.5.

The loss of DMP was similar in all three systems (400, 1000 and 2000 ppm H_2O_2), averaging about 94% loss after 4 h. This has to do with diffusivity of H_2O_2 in the reaction system and the availability of catalyst active sites. However, excess H_2O_2 can possibly result in radical scavenging of $^{\bullet}OH$ by H_2O_2 according to equation 5.30.

The concentration of both DMP and oils (Figure 5.18A and 5.18B) were found to have also reduced with reduction in the COD. Bar charts have been used to represent the initial and final concentration of COD, OIW and DMP in Figures 5.18A and 5.18B respectively.

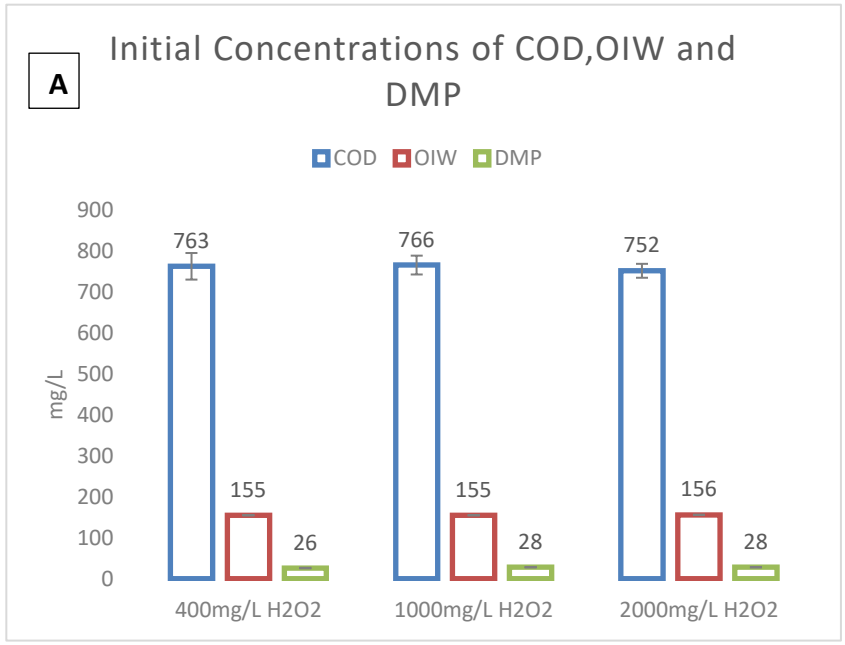

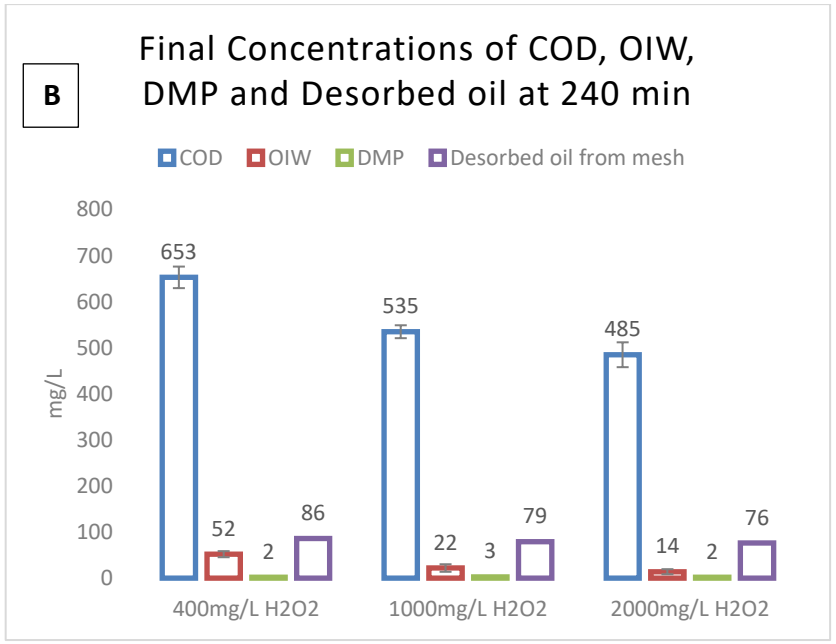

Figure 5.18A: Initial concentrations of COD, OIW and DMP in simulated PW sample, while **5.18B** shows the concentrations of COD, OIW, DMP and Desorbed oil from the mesh after reaction. Experimental condition: 400, 1000 and 2000 ppm H_2O_2, 10 g catalyst, pH3, temp 25 ^oC±1, reactions duration t= 240 min.

The loss of OIW showed slight variation between 1000 and 2000 ppm H_2O_2. For 400 mg/L H_2O_2 OIW concentration decreased from 155 mg/L to 52 mg/L however, this was mostly due to sorption on the mesh. It decreased from 155 mg/L to 22 mg/L in solution when the initial concentration of H_2O_2 was 1000 ppm and to 14 mg/L in solution when the initial concentration of H_2O_2 was 2000 ppm. In both these cases, about half the initial concentration of OIW was removed due to sorption on the mesh. Thus increasing H_2O_2 concentration from 400 to 2000 ppm significantly reduced OIW concentration in solution phase.

5.7.5 Effects of competing Inorganic Anions (Bicarbonates and Chlorides ions)

Produced water with and without chlorides was catalysed. The results of the experiments are presented in Figure 5.19. The results indicate that chlorides had a greater influence on the loss of DMP in the reaction compared to bicarbonates, which could have been due to the differences in their respective concentrations (chloride had higher concentration) in the solution in addition to their respective rate constants in reactions with $^{\bullet}OH$ shown in equations 5.32 and 5.33.

These side reactions fall under the category of competing non-productive reactions (Siegrist et al., 2011). Collectively and independently, both ions slowed down the rate of loss of DMP in the reaction as shown in Figure 5.19 below. The reduction of DMP by 50% took about 30 minutes in the absence of bicarbonates and chloride ions, while 50% reduction in the presence of bicarbonates and chloride ions took 90 min. The reaction of $^{\bullet}OH$ with aqueous bicarbonate species results in the formation of a bicarbonate

radical according to equation 5.32, which is thought to have much lower reactivity and tendency to degrade the substrate than $^{\bullet}OH$.

Chloride ion on the other hand, is found to have much more severe effects on hydrogen peroxide systems, especially those catalysed by iron III catalyst (De Laat et al,. 2004 in Siegrist et al., 2011). This is thought to occur by scavenging reactions (Yu and Baker 2003 in Siegrist et al., 2011) leading to less reactive radicals (equations 5.33 to 5.35) and the complexation of catalyst mineral sites. Under certain reaction conditions (low pH and high chloride concentration - > 1000mg/L), the formation of dichloride radical is possible through a series of propagation reactions. This radical has very high reaction rates with other chloride species, which can form chlorine gas, leading to possible halogenation of organic substrates, (Pignatello, 1992; Laat et al., 2004) that may be recalcitrant. Yuan et al., (2011) also reported that chloride ion showed greater scavenging effect than bicarbonate ions.

$HCO_3^- + {}^{\bullet}OH \rightarrow HCO^{\bullet}_3 + OH^-$ $k = 8.5x10^6\ M^{-1}\ S^{-1}$ … (5.32)

$^{\bullet}OH + Cl^- \leftrightarrow ClOH^{\bullet\ -}$ $k = 4.3x10^9\ M^{-1}\ S^{-1}$ … (5.33)

$ClOH^{\bullet\ -} + H^+ \leftrightarrow Cl^{\bullet} + H_2O$ $k = 3.2x10^{10}\ M^{-1}\ S^{-1}$ … (5.34)

$Cl^{\bullet} + Cl^- \leftrightarrow Cl_2^{\bullet\ -}$ $k = 7.8x10^9\ M^{-1}\ S^{-1}$ … (5.35)

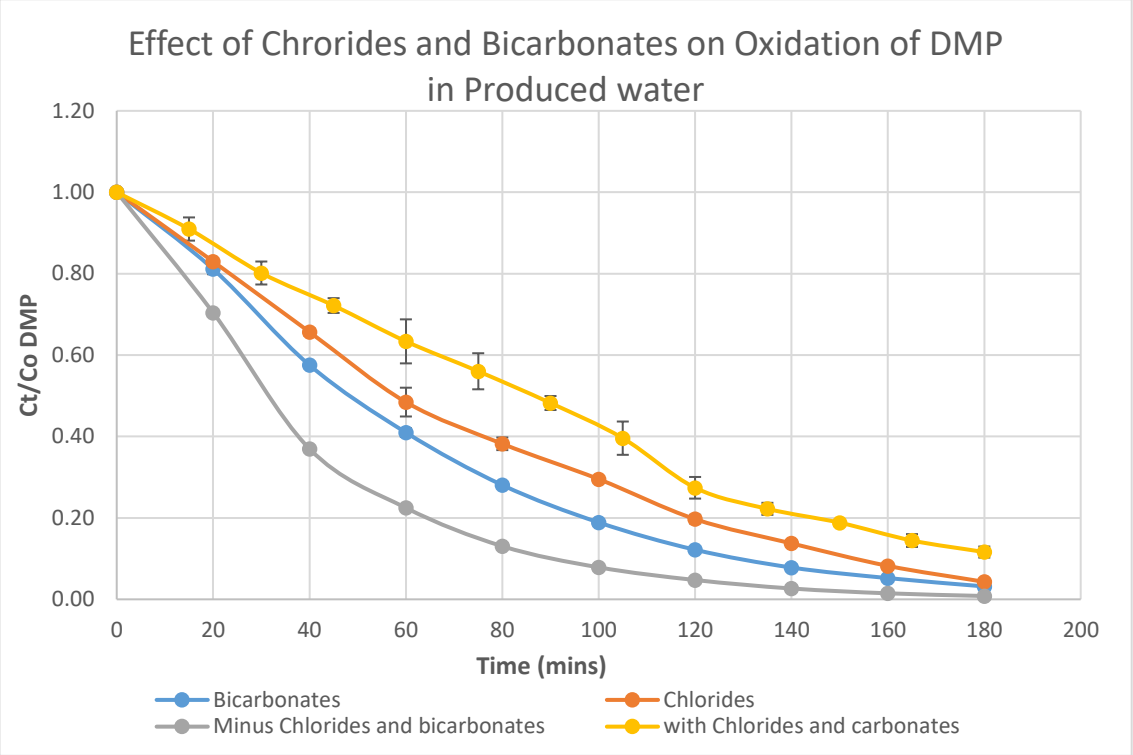

Figure 5.19: Effect of chlorides and bicarbonate ions on the loss of DMP in PW, in batch reaction. 10 g catalyst, 25 mg/L DMP, pH3, 1996 mg/L NaCl as chloride, 200 mg/L $NaHCO_3$ as bicarbonate, 200 mL reaction volume 25±1 ^oC.

5.8 Results and discussion for continuous flow experiments

The results and discussions for the continuous flow experiment studies is presented below. The mesh to liquor ratio for the continuous flow experiments was 1: 5 (180 g : 900 mL), that is, 180 g of catalyst in 900 mL of reaction volume.

5.8.1 Material Balance in Rotating Disc Reactor

This presents a wide range of possible issues or problems to be articulated and solved, and methodically accounts for every material or mass of compounds that has passed through the treatment system.

To compute the material balance of the reacting system, oxidizable aromatics and aliphatics were the focus. In assessing the total organics entering the reaction, only the measurable components determined at the point of entry into the reactor were considered owing to loss of compounds through sorption on the tubing walls, and the loss of volatile components due to stirring of the effluent feed (Libra 1991). This was factored into the makeup of the mock produced water and has been explained previously in section 5.4.5.1 and presented in Table 5.5.

Structural formulae of aliphatic hydrocarbon compounds and BTEX and DMP are shown in Figures 5.20 to 5.26, for tridecane, n-hexadecane, benzene, toluene, ethyl benzene and xylene and DMP respectively

Figure 5.20: Chemical formula of tridecane

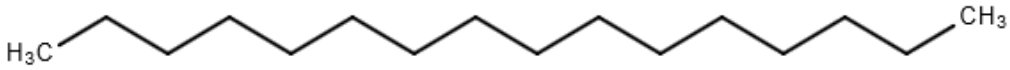

Figure 5.21: Chemical formula of n-hexadecane

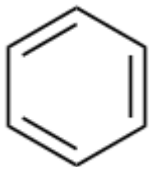

Figure 5.22: Benzene

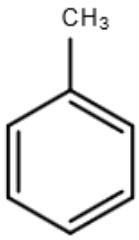

Figure 5.23: Toluene

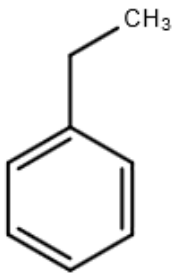

Figure 5.24: Ethyl Benzene

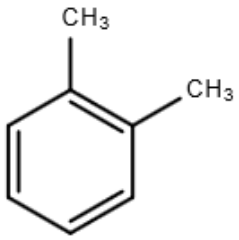

Figure 5.25: 0rtho Xylene

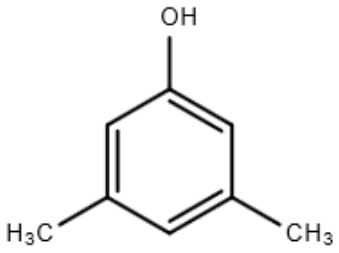

Figure 5.26: 3,5-DMP

a) To calculate the mass of DMP passed through the reactor for example;

Total initial [DMP] of 2 5 mg/L flowed @ 3.73 mL/min, for 42480 min.

Hence 42480 min @ 3.73 = 42480*3.73 = 158450.4 mL, = 158.45 L

Therefore, total mass of DMP fed into reactor over 42480 min = 25mg *158.45 = 3961.25 mg of DMP.

b) To calculate the mass of aliphatic hydrocarbons (tridecane and hexadecane) passed through treatment system, weighted average concentration was used because the concentrations delivered into the reaction system varied between 0.5 and 27 mg/L due mainly to their hydrophobicity i.e. sorption on walls of tubing and poor solubility in water.

Weighted average (W.A), given as:

$$\mathrm{W.A} = \frac{(\text{Measured conc} * \text{Duration (hours)}) + (\text{measured conc} * \text{Duration (hours)}) + \cdots}{\text{sum of hours}} \quad .. \qquad (5.36)$$

Total days of treatment process was 29 days and 12 h

Using Microsoft excel 2016 for computation we have that:

$$\text{W.A} = \frac{([aliphatic\ at\ t1]*t1(hrs)+[aliphatic\ at\ t2]*t2(hrs)\ldots..}{(t1+t2)\ldots..} \quad (5.37)$$

Where t1 and t2 are the times samples were taken and measured (in hours)

∴ W.A concentration of aliphatics received by reactor = 4492.82/708 = 6.35 mg/L

c) The procedure was repeated for the calculation of BTEX concentration. Results are as presented in Table 5.12.

d) To calculate the % remove, the amount desorbed of respective compounds from wheels (Table 5.12) was subtracted from the sum of the respective measured residual compounds after treatment and applied as follows:

$$\%\ removed\ = \frac{total\ amount\ of\ substrate\ received\ in\ reactor\ -\ residual\ after\ treatment}{total\ amount\ of\ substrate\ received\ by\ reactor} \times 100$$

Where Residual after Treatment is:

= measured residual after treatment + amount desorbed from catalyst after treatment

Table 5.12: Total oxidizable materials received by treatment system during experiment

Compounds	**Avg. Conc. (mg/L)**	**Flow rate (mL/min)**	**Duration (mins)**	**Total Volume (mL)**	**Total mass (mg)**	**% Removed**
DMP	25.00	3.73	42,480	158450.4	3961.3	99.04
Aliphatics	6.35	3.73	42,480	158450.4	1006.2	95.28
BTEX	36.77	3.73	42,480	158450.4	5826.2	94.77
Total Oxidizable Organics Received in Treatment System					**10793.7**	

5.8.2 Procedure for Desorption Organic Substrates after Treatment Using Warm Water at 40 ^{o}C

The first step involved determination of the percentage recovery of the process, by desorbing known concentrations of the hydrocarbon compounds in Table 5.12 above using warm water. This was done for DMP (measured as DMP concentration using HPLC) and then for aliphatics and BTEX (both measured together as OIW). To desorb aliphatics from wheels, 900 mL of warm water was transferred into the reactor and the wheels were rotated for 10 min. The water was then collected into a 1 L glass sample bottle. This procedure was repeated three times and on each occasion, the effluent was collected in 1 L sample bottle. Each 1 L bottle of effluent was then extracted as per section 5.4.5.2 and the extract analysed as per procedure in section 5.4.5.4 using the triple peak OIW analytical method. The results for aliphatic constituents is presented in Table 5.13 below.

Table 5.13: Desorbed organics from wheels using warm water at 40 ^{o}C

Compound	Conc A (mg/L)	Conc B (mg/L)	Conc C (mg/L)	Total (mg)
Aliphatics	7.2	4.0	1.4	12.6
DMP	4.5	1.8	ND	6.3
BTEX	73	38	ND	111.0

*ND= Not detected

Percentage recovery for oxidizable organic compounds:

The percentage recovery for all oxidizable organic compounds in produced water was examined. For aliphatics, 50 mg/L mixed standard of n-hexadecane and tridecane and 10 g of catalyst was used.

$$\%\, recovery = \frac{amount\ of\ aliphatics\ (mg/L)\ extracted\ and\ measured}{amount\ in\ mg/L\ of\ aliphatic\ in\ solution} \times 100$$

$$= \frac{19}{50} \times 100 = 38\%$$

The percentage recovery for DMP and BTEX was calculated using the same method above to be 89 and 72% respectively.

The use of surfactants for the desorption was successful for the removal of the oils from the catalyst; however the extraction of the oils from the surfactants was not successful. The oils were well mixed with the surfactants and separation was not possible as shown on Figure 5.27.

Figure 5.27: The use of Surfactant for desorption of oil from catalyst.

5.8.3 Procedure for the Determination of Total Mass of Materials left after Treatment

The total mass of materials left after treatment were determined at the end of the experiments i.e 29.5 days according to section 5.6.3. In addition to aliphatics and aromatic hydrocarbons, DMP was also determined from the desorbed oil in water solution before extraction of aromatics and BTEX from catalyst mesh. The results are presented in Table 5.14 below.

Table 5.14: Total recovered oxidizable materials on catalyst after experiment

Compound	Desorbed from catalyst (mg)	Amount desorbed
DMP	6.3	7.07
Aliphatics	12.6	33.16
BTEX	111.0	154.16
Total oxidizable materials left as residue on catalyst after treatment	**124.05**	**194.36**

The percentage removed is subjective due to loss through volatilization and the desorption procedure for aliphatics using warm water. The percentage recovery of aliphatics desorption using warm water (at 40 ^{o}C) was 38%.

5.8.4 Catalyst Activity

The activity of a catalyst is a measure of the speed of the various reactions happening in the presence of the catalyst (Hagen, 2006). Different parameters are often used to assess the activity of catalysts. These include; the kinetic data analysis (reaction rates), the Turnover Number (TON), Space Velocity, Space Time Yield (STY), Turnover Frequency (TOF), temperature of reactions, etc. The data obtained from material balance determination, is useful in appraisal of catalyst activity.

The use of turnover number (TON) as a parameter for measuring the activity of a catalyst for homogeneous systems is well established and straightforward. In that case, the catalyst molecules are well defined and present in solution. This approach for heterogeneous catalysis has been hugely criticised owing to the difficulty associated with determining activity on a non-uniform structure (Hagen, 2006). The catalytic activity in heterogeneous systems is generally thought to depend on the area of the surface, however, the dispersion of the reactive surface on the catalyst is probably uneven. Measurements of active sites per unit mass or volume of heterogeneous catalysts are possible but not very dependable. The use of temperature has also been used for catalyst activity measurement, where the best catalyst is the one which gives the best conversion rate at the lowest temperature (Hagen, 2006). This has however been criticised as well because different reactions and by extension catalysts have different optimum conditions for conversion of substrates. The turnover number (TON), more correctly called turnover frequency or rate has been successfully used for assessing the activity of heterogeneous catalysts in the synthesis of ammonia on iron (Boudart, 1985).

5.8.4.1 Turnover Frequency

Turnover frequency (TOF) is a quantitative measure of the number of molecules converted in a given reaction, per unit time per catalytic reactive site under specific reaction conditions (Boudart, 1985; Hagen, 2006). TOF serves to compare catalyst performance, to assess structural sensitivity, etc. To determine catalytic activity for the catalyst used for this study, all constituents converted in this study were put into consideration by introducing the chemical oxygen demand (COD) parameter in TOF analysis. This accounts for all converted constituents including oxidation intermediates, which are often, ignored in catalyst activity determinations using TOF.

COD is equivalent to the moles of oxygen converted to form products. Thus, the total COD input to the reactor is the whole area of the curve (Figure 5.28) for a plot of inlet COD versus volume (litres), while the moles of oxygen used, which is equal to the COD removed is the area under the COD dynamic curve, (Figure 5.29) in a plot of residual COD versus volume (litres). The shaded areas in both curves in Figures 5.28 and 5.29 represent the total input COD fed into reactor and the COD removed (converted) respectively were determined using the trapezium rule (the sum total of the trapezoids) in Microsoft Excel Spreadsheet, given by;

$$\mathrm{A} = \frac{1}{2}(a + b)h \qquad \ldots (5.38)$$

Where A is area of the individual trapezoids, *a* and *b* are the parallel sides (concentration of COD in mg/L), and *h* height (volume in liters). Using Microsoft Excel, we have 8924.79 mg/L as the total area below the curve (the shaded area in Figure 5.28), which is equal to the COD input into the reactor during the continuous flow reaction.

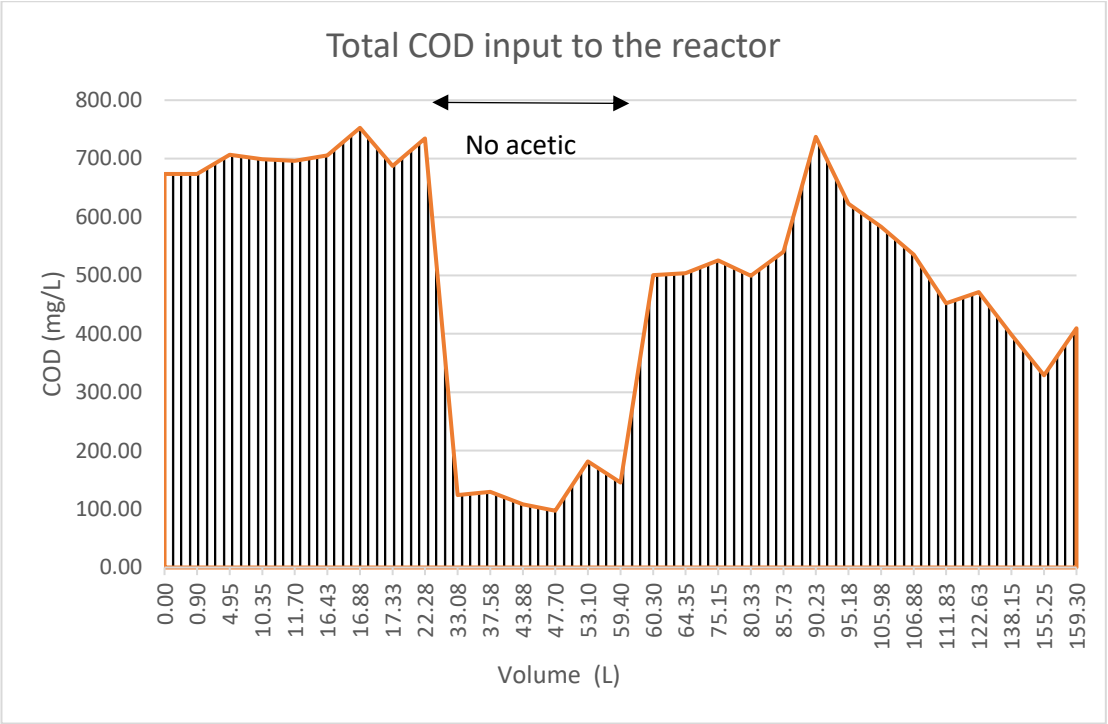

Figure 5.28: Total area of the curve representing the total COD fed into the reaction system during the whole treatment process.

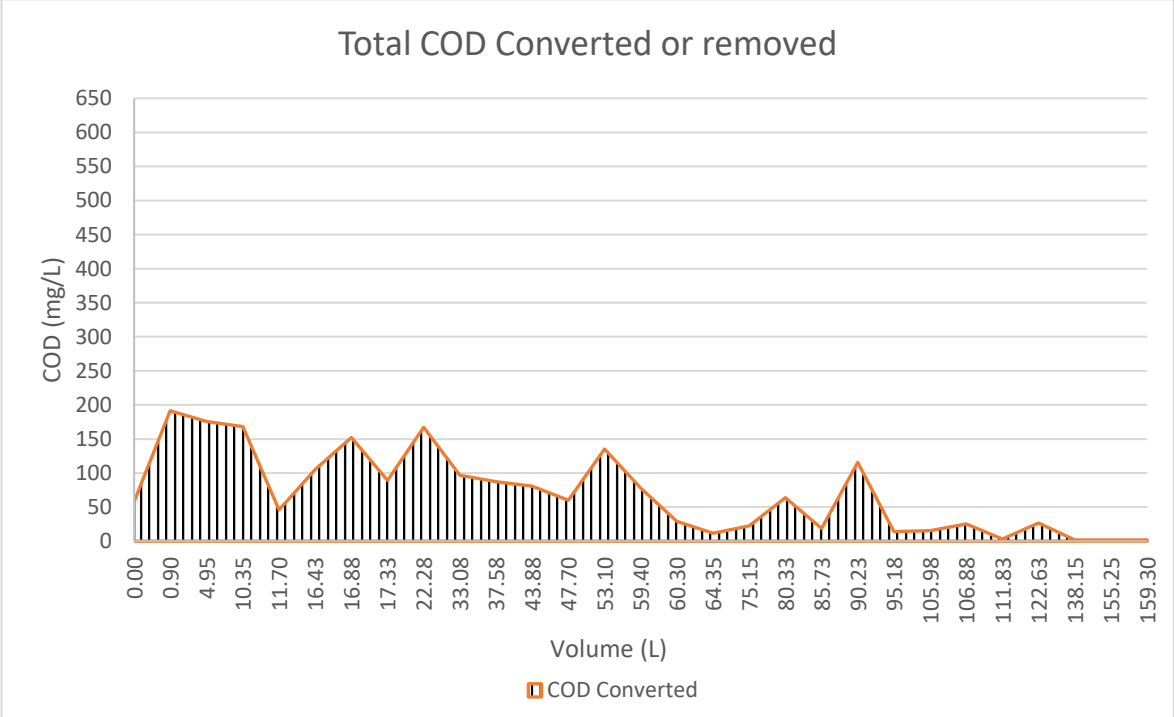

Figure 5.29: Area below the dynamic curve for COD conversion in produced water continuous flow experiments. Catalyst load 180 g, reactor volume 900 mL, H_2O_2 1000 ppm, pH3 at room temperature

COD converted is equivalent to total O_2 used up, which equal to area below the curve in Figure 5.29.

To get the area above the curve, we subtract the area below the curve from the total area of the curve representing the COD fed into reactor during the period.

Therefore:

Area of the whole curve i.e. total COD fed into reactor (Figure 5.28) was 72274.08 mg

Area below the curve i.e. COD converted (Figure 5.29) was 8924.79 mg

∴ Unconverted COD = Total area – Area below the curve

= (72274.08 - 8924.79) =63349.29 mg

∴ From 8924.79 mg O_2 used (in moles) from total effluent volume of 159.45 L;

Moles of O_2 $= Conc\ (gL^{-1}) * Volume(L)/MW(gmol^{-1})$

i.e, moles of O_2 = 8924.79 X 159.45/32 = 44345.05 mM = 44.34 mol.

$$\text{TOF} = \frac{moles\ of\ substrate\ catalysed}{Moles\ of\ Fe\ per\ gram\ catalyst \times mass\ \ of\ catalyst \times time} = \frac{1}{t} = \ t^{-1} \qquad \ldots (5.39)$$

The calculated TOF was 0.00079 hr^{-1} from equation (5.39). This has been presented on Table 5.15.

Table 5.15: Dynamic study data used for the determination of Turnover Frequency

Moles of O_2 Converted (M)	[Fe] Per gram of PAN catalyst (mMol)	Total volume of Solution (L)	Mass of Catalyst (g)	Duration (hrs)	TOF (hr^{-1})
44.34	0.435	159.45	180	708	$7.9X10^{-4}$

Industry values for TOF usually range between 0.01 to 100 s^{-1} (Hagen, 2006) , suggesting that the value of $7.9X10^{-4}$ hr^{-1} is low when compared to industrial scale catalytic processes. However, considering that this is COD conversion, which describes the extent towards mineralization, not just degradation of initial substrate, it includes the contribution of 525 mg/L of acetic acid (AA) which is recalcitrant to COD reduction (Bradford et al., 2003; Coste et al., 2003) and which contributes more than half the total COD in the system. If the COD of acetic acid is taken out then the COD conversion would be a lot better and TOF would improve. The absolute COD removal for the continuous flow experiment for the catalysis of synthetic produced water is as shown in Figure 5.30.

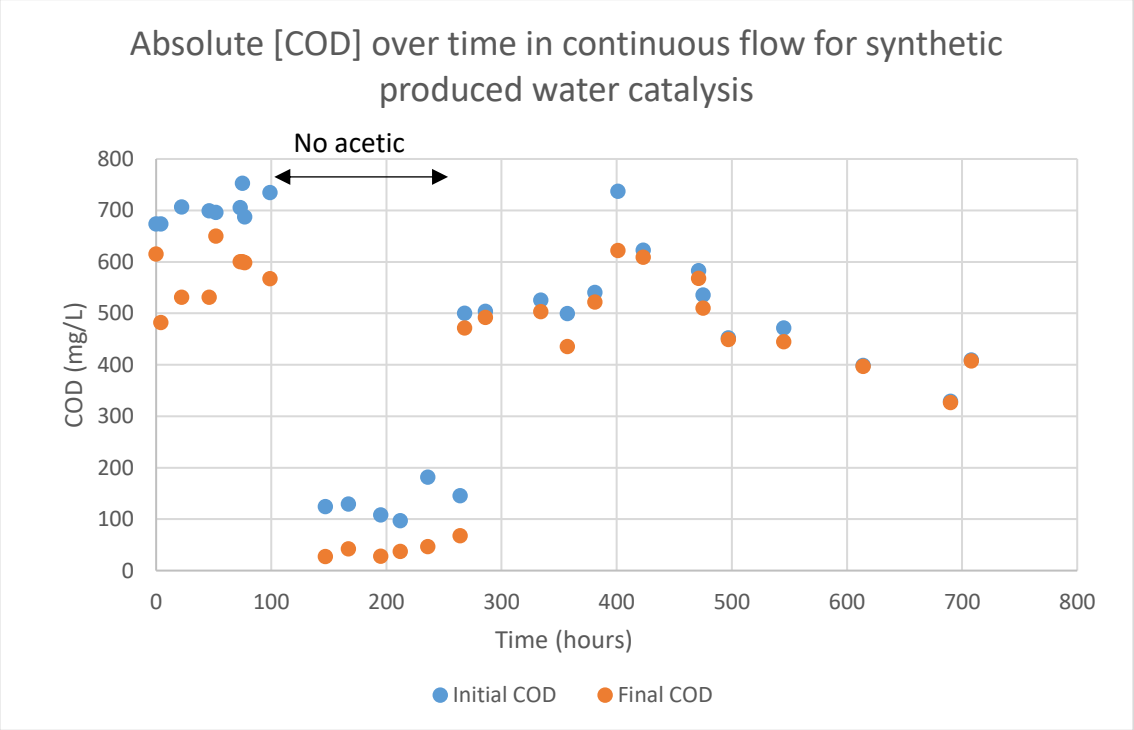

Figure 5.30: Variation of COD in PW water over time in continuous flow reaction system. Flow rate 3.75 mL/min, Co [DMP] = 25 mg/L, Co H_2O_2 = 1000 ppm, Average COD_0 = 655 mg/L (without acetic acid), catalyst load 180 g, pH3, 900 mL reaction volume, retention time of 240 min, at 25±3 °C.

When acetic acid is present in reaction system, COD range from 326 to 752 mg/L, but with a weighted average of 655 mg/L, whereas in the absence of acetic acid, COD was between 97 and 236 mg/L. There was an average loss of 65% COD in the absence of acetic acid, as acetic acid contributes a ThOD of about 560 mg/L in this PW solution, this suggests that it was the acetic acid that was largely responsible for the slow loss of COD. Its recalcitrance and resistance to oxidation is thought to be due to the difficulty to oxidize the methyl group in the α-position (Figure 5.31) to a carboxylate group (Centi et al., 2000). It was observed that the produced water solution became weaker when left to stir over long periods, and this is obvious after 500 minutes of reaction (Figure 5.30). This observed solution weakness (diminished COD) is likely due to loss of volatile hydrocarbon components into head space as the solution was left to stir over long periods.

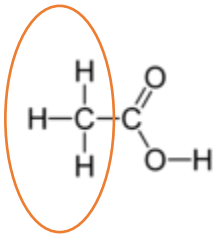

Figure 5.31: Structural formula of acetic acid showing methyl group circled in orange

Organic acids are generally thought to constitute part of what has been termed refractory COD (Bradford et al., 2003; Coste et al., 2003). Figure 5.32 below shows the oxidability scale of some organic compounds under wet air chemical oxidation which is considered a severe reaction treatment with harsh conditions. This is an indication of the recalcitrance of acetic acid in particular. Confirming this, Centi et al., (2000), carried

out a Fenton-like oxidation of acetic, formic and propionic acid under the same conditions and concentrations and found that while only 22% of acetic acid was removed after 4 h, about 60% of formic acid was removed over the same time, and 80% removal of propionic acid respectively. In that study, they were able to correlate leached iron with the reaction temperature, as increased temperature, resulted in increased in leached iron.

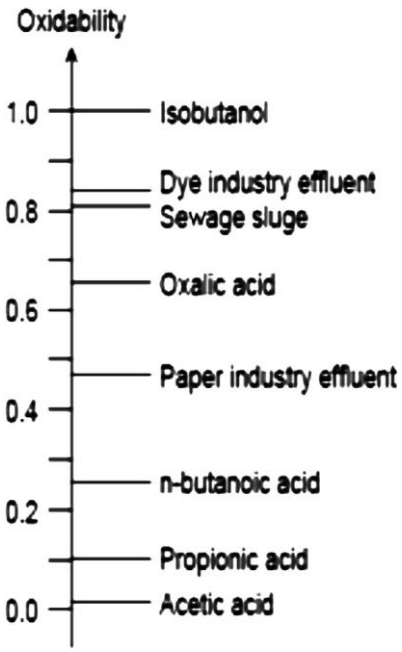

Figure 5.32: Oxidability scale of some organic compounds under wet air chemical oxidation where 0.0 is considered unoxidizable and 1, very oxidizable (Debellefontaine et al., 1996)

Cihanoglu et al., (2015), did previous work on the application of heterogeneous Fenton catalysis for the degradation of acetic acid. They used Fenton–like oxidation over iron containing ZMS-5 zeolite at pH4. The Fe^{2+} used for the study was prevented from further oxidation, by reacting it with HCl in the presence of inert nitrogen. They worked with relatively small concentrations of 10, 25, 75 to 100 and 125 mg/L acetic acid, and

temperatures of about 30 to 60 ^{o}C, (303 K to 333 K). They recorded the highest COD loss of 73.2% at the lowest initial acetic acid concentration of 10 mg/L and 60 ^{o}C, after 2 hours, while the lowest COD loss of 34.9% was achieved at 100 mg/L concentration acetic acid using 60 ^{o}C after 2 h. They concluded that COD reduction decreased with increase in concentration of acetic acid and increased with increase in temperature of reaction.

In the present study, a longer retention time and increased concentration of H_2O_2 has proven successful for more efficient COD removal. Under similar reaction conditions, but with 4-fold increase in the mesh to liquor ratio in the batch mode, the COD removal in batch mode was better than in the continuous flow mode. The mesh to liquor ratio in the batch experiments was 1: 20 (10 g : 200 mL), while the continuous flow was 1:5 (180 g : 900 mL) Separation of refractory compounds such as mineral acids is a useful pre-treatment step in some treatment processes (Gulyas, 1997).

The COD removal became poorer with time especially after 600 h in Figure 5.30 and this ties with the tailing of the reduction in DMP after 600 h (Figure 5.33 below), suggesting a reduction in catalyst activity after 600 h.

In terms of statutory discharge limits, although the contributors to COD are monitored biannually in UK, the COD itself is not a direct regulatory requirement (DECC 2011). In China, COD for produced water discharge limit is 100 mg/L (Fakhru'l-Razi et al., 2009), while in Nigeria, the inland and nearshore discharge limits are 10 and 125 mg/L respectively, however there is no regulation or guidance for offshore COD discharge limit (EGASPIN 2000).

5.8.5 Catalytic conversion of DMP in PW in Continuous Flow Treatment System

The loss of DMP in PW was independent of the presence of other constituents of the PW solution as presented in Figure 5.33. There was > 98% conversion of DMP in PW during the first week of the treatment process. Overall, there was an average of about 90% DMP removal and a total of 3961.3 mg of DMP was removed from a total volume of 158.45 L after 708 h.

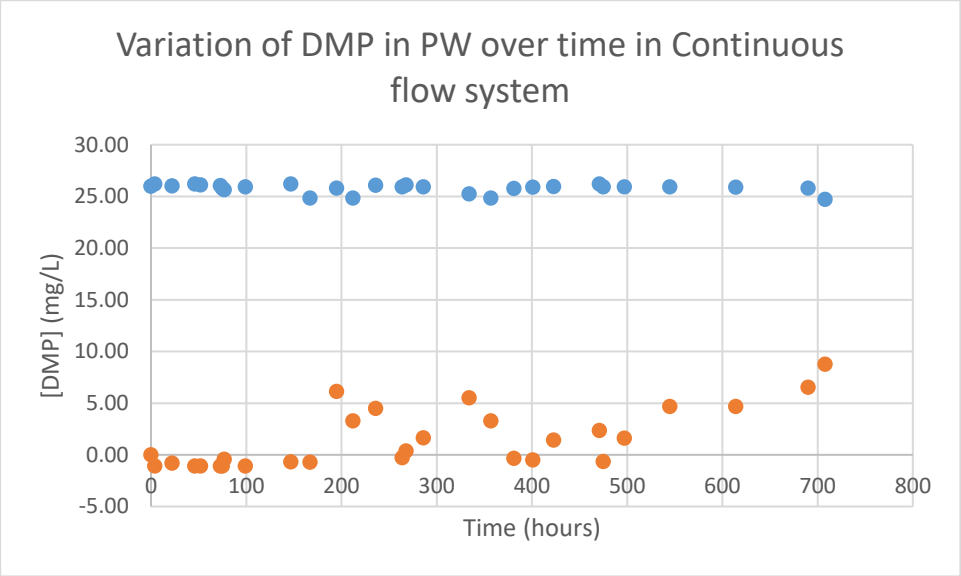

Figure 5.33: Variation of DMP in PW water over time in continuous flow reaction system. Flow rate 3.75 mL/min, Co DMP = 25 mg/L, Co H_2O_2 = 1000 ppm, catalyst load 180 g, pH3, 900 mL reaction volume, retention time of 240 min, at 25±2 °C

5.8.6 Catalytic Removal of OIW in PW in Continuous Flow Treatment System

The results of the variation of OIW concentration with time in the continuous flow process in the degradation of produced water is as shown in Figure 5.34a. There was a slight improvement in the removal of OIW in the absence of acetic acid, which also suggest a possible competition by recalcitrant organic acids in the oxidation of the oils.

The OIW inlet concentration was highly variable over time as seen in Figure 5.34a and this is likely due to the dispersive nature of most of the PW constituents. This is especially so for the aliphatic fraction. They are very insoluble in water and this results in non-uniform lifting of these constituents by the pump, in addition to some being adsorbed on the walls of the tubing material.

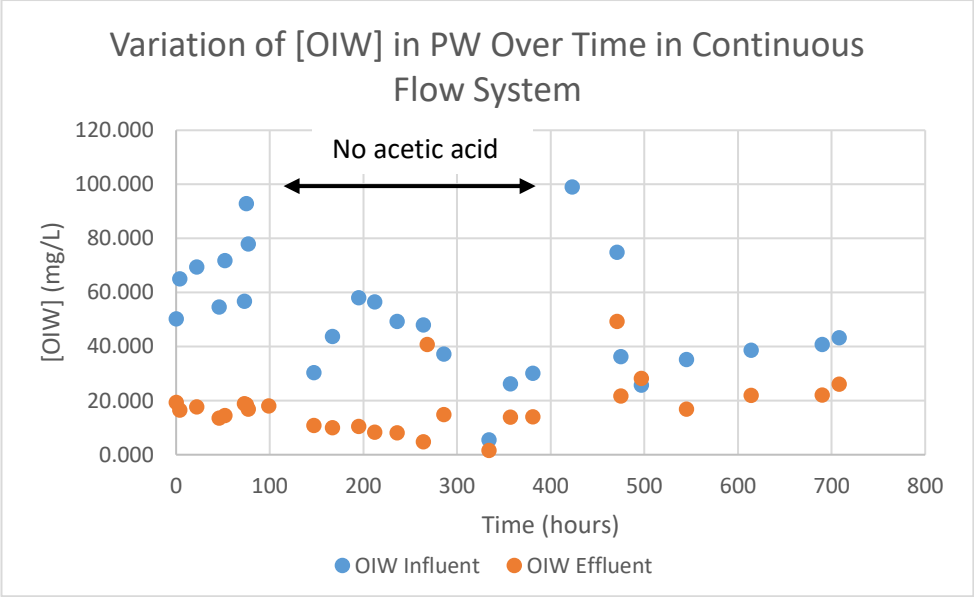

Figure 5.34a: Variation of OIW in PW water over time in continuous flow reaction system. Flow rate 3.75 mL/min, Co DMP 25 mg/L, Co H_2O_2 = 1000 ppm, catalyst load 180 g, pH3, 900 mL reaction volume, retention time of 240 min, at 25±2 ^{o}C.

Overall, compared to statutory discharge limits of 30 mg/L for OIW (EPA 2016; GPO 2016; EGASPIN 2000), the results were within acceptable discharge band, except for two out- layers at 270 and 480 h. There was more than 50% average removal of OIW in continuous flow mode. There was a drop in the removal rate after 250 h of treatment. This is not likely to be due to saturation of the catalyst discs from adsorbed oils, as

evident from the desorbed oils after the treatment process (using warm water), as saturation of the catalyst discs by absorbed oils happens within the first few hours. This was observed in the preliminary sorption studies presented in Figure 5.34b below, which shows maximum sorption within 30 min. The presence of high concentrations of acetic acid on the surface of the catalyst is capable of catalyst poisoning or choking and could be responsible for this drop in oil removal.

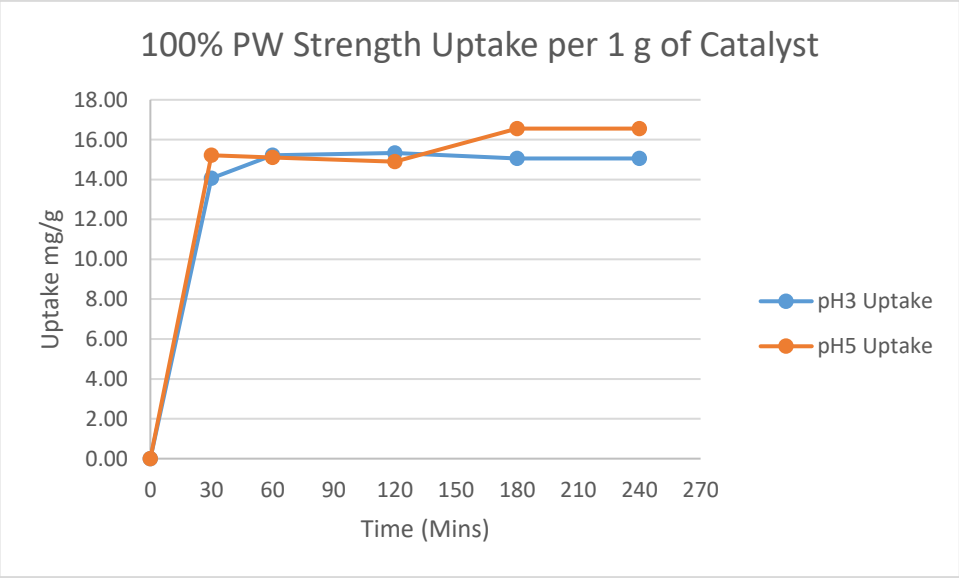

Figure 5.34b: Adsorption of produced water using 1 g of catalyst at pH3 and 5, in the absence of H_2O_2

5.8.7 Leached Iron from Catalyst

To investigate the possible cause of reduction in catalyst activity, evident from the tailing of COD reduction and the apparent decrease in the extent of removal of DMP, the amount of iron leached from the catalyst in the continuous flow studies was investigated. The results have been presented in Figure 5.35.

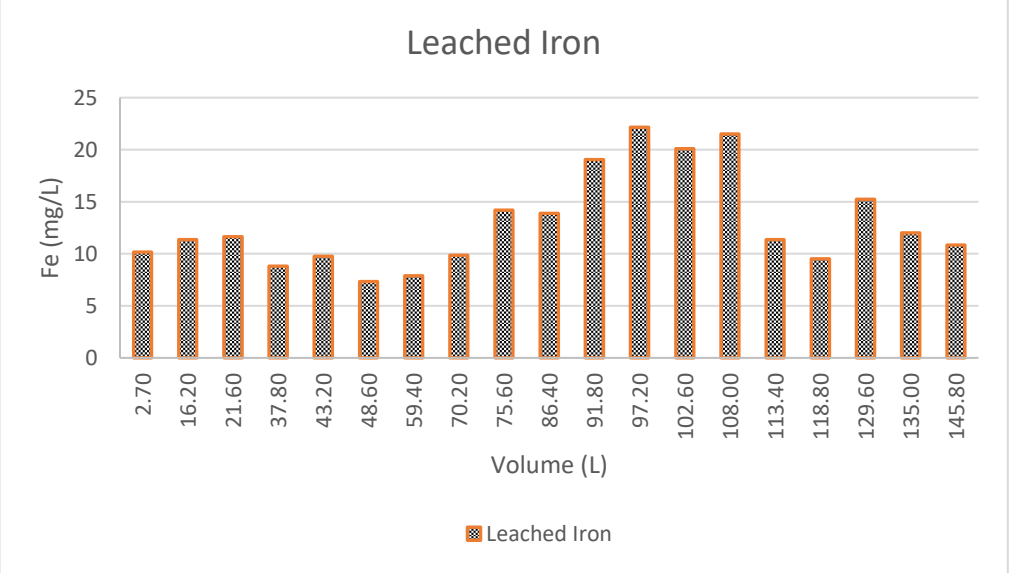

Figure 5.35: Average daily concentration of leached iron in produced water continuous flow experiments. Catalyst load 180 g, reactor volume 900 mL, H_2O_2 1000 ppm, pH3 at room temperature and 240 min retention time.

The maximum amount of iron leached in any one day was 22.15 mg/L, which was almost half way through the whole continuous flow treatment. A minimum leached Fe concentration of 4.3 mg/L was recorded at the end of the treatment process when catalyst was considered going towards deactivation.

The total leached iron from the catalyst, equal to the area under the dynamic curve (Figure 5.36), was 1868.33 mg (Table 5.16). It was determined by applying the trapezium rule; the sum of the areas of the trapezoids according to equation (5.38) using Microsoft

Excel 2013, using a plot of absolute concentrations versus volume in Liters. The results are presented in Table 5.16.

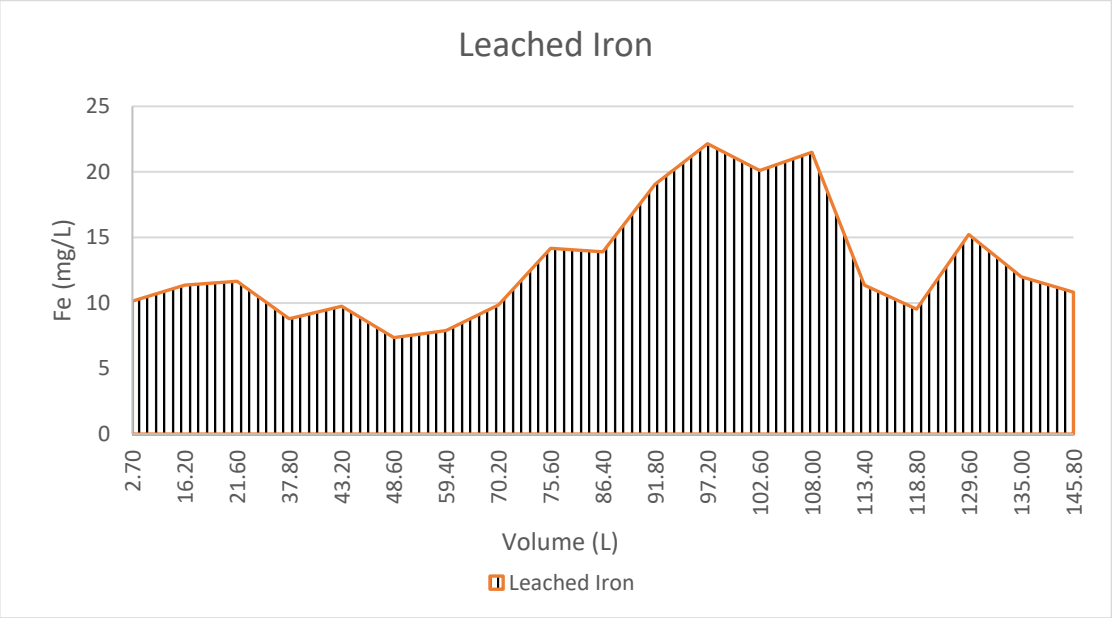

Figure 5.36: Iron leached during continuous flow experiments in the catalysis of produced water. Catalyst load 180 g, reactor volume 900 mL, H_2O_2 1000 ppm, pH3, at room temperature, flow rate of 3.75 mL/min.

The results show that, almost half of the Fe on the catalyst (42.72%) had leached from the catalyst in almost 30 days. Therefore, the reduced catalytic activity could have been due to the loss of Fe through leaching. According to Hagen, (2006), due to competing reactions, catalysts undergo chemical changes, resulting to slower activity, which leads to “catalyst deactivation”.

Table 5.16: Parameters used for amount of Fe leached from catalyst

Total amount of catalyst on discs (g)	Fe per gram of PAN catalyst (mMol/g)	Total Iron on catalyst in reactor (mg)	Total Fe leached from catalyst (mg)	Fe left on catalyst after experiment (mg)	Fe loss (%)
180	0.435	4373.06	1868.33	2504.73	42.72

Catalyst deactivation has been described as the loss of selectivity and/or catalytic activity over time, where activity is the reaction rate at time *t,* compared to reaction rate at time t_0 (Argyle and Bartholomew, 2015; Denny and Twigg, 1980; Bartholomew, 1984). As evident from the results of iron leachate in relation to catalytic activity with respect to the rate of loss of COD, DMP and OIW, there is an indication of loss of catalytic activity with respect to COD and DMP, however, the rate of loss of OIW remained steady. Although sorption of OIW cannot be ruled out, loss of activity may not be due to loss of iron from the catalyst. In many processes, deactivation is inevitable and there are several possibilities and processes that can lead to heterogeneous catalyst deactivation (Argyle and Bartholomew, 2015; Hughes, 1984). Although not all of them apply in this case. These include;

a. Poisoning by contaminants in feed
b. Conversion of active catalytic constituents into non-reactive complexes
c. Thermal deactivation due to high reaction temperatures leading to collapse of support (which does not apply in this case)
d. Leaching and or transport from catalyst surface

e. Abrasion or crushing (not applicable in this case)

These have been summarized by Argyle and Bartholomew, (2015) in Table 5.17 below.

Table 5.17: Mechanisms of catalyst deactivation. Reproduced from Argyle and Bartholomew (2015)

Mechanism	Type	Description
Poisoning	Chemical	Strong chemisorption of species on catalytic sites which block sites for catalytic reactions
Fouling	Mechanical	Physical deposition of species from fluid phase onto the catalytic surface and in catalyst pores.
Thermal degradation sintering (NA)	Thermal Thermal/chemica	Thermally induced loss of catalytic surface area, support area, and active phase-support
Vapour formation (NA)	Chemical	Reaction of gas with catalyst phase to produce volatile compound
Vapour–solid and solid–solid reactions	Chemical	Reaction of vapour, support, or promoter with catalytic phase to produce inactive phase
Abrasion/crushing (NA)	Mechanical	Loss of catalytic material due to abrasion; loss of internal surface area due to mechanical-induced crushing of the catalyst particle

*NA means not applicable

A combination of these causes or factors are possible for deactivation to occur, it is however not very clear which factor(s) is/are responsible for the loss of catalytic activity in the present case. Reactivation or regeneration from poisoning or fouling has been successfully done by treating this catalysis with a moderate dose of oxidant, in the region of 5 to 10 g/L H_2O_2 (Asuelimen, 2015). However, poisoned catalysts are difficult and most times impossible to regenerate. Argyle and Bartholomew, (2015) recommended the following interventions for loss of catalytic surface sites due to poisoning (not all apply in this case):

(1) Purify feed and/or use guard bed to adsorb poison

(2) Employ additives that selectively adsorb poison

(3) Choose reaction conditions that lower adsorption strength of poison to the catalyst sites

(4) Optimize pore structure and choose mass transfer regimes that minimize adsorption of poison on active sites and

(5) Apply coating that serves as diffusion barrier to poison.

It is likely that leached iron (42.72%) could have caused deactivation or loss of catalyst activity, in addition to the potential conversion/modification of active catalytic constituents into non-reactive complexes. It is not known whether all sites on the catalyst surface are active or accessible. In addition to this, chelation with oxidation products such as oxalic acid to active site will also result in catalyst poisoning.

5.9 Summary

The treatment of produced water is essential for the sustainability of the ecosystem in both onshore and offshore environments. Several treatment technologies are currently being used in the treatment of produced water; however, coupled technologies have shown better promise in confronting this challenge.

In batch studies, increase in H_2O_2 concentration has not shown a corresponding increase in DMP removal and there has not been a commensurate removal of COD (about 5% more removal for 100% increase in H_2O_2). This is likely to be due to high loading of acetic acid in produced water. Acetic acid is refractory and difficult to decompose under moderate Fenton conditions. The OIW showed quite remarkable results, with an overall average degradation of over 52% and 48% removal by sorption in batch mode as H_2O_2 concentration was increased to 2000 ppm and over 50% in continuous flow mode after 4 h reaction. Further study is required to fully unravel the precise cause of catalyst deactivation.

The next chapter looks at coupling the normal Fenton-like process to a UV/Microwave assisted process, to evaluate how the assisted system compares to the unassisted Fenton-like process, in terms of extent and duration of treatment.

6 UV/Microwave/Fenton Oxidation of 3,5-DMP in Simulated Produced Water using a Novel PAN Heterogeneous Catalyst.

6.1 Introduction

This chapter looks at the application of UV/microwave assisted Fenton-like oxidation, using a novel modified polyacrylonitrile catalyst (PAN) in wastewater treatment as a coupled technology. The aim is to improve reaction rates in catalysed Fenton-like processes as well as effect degradation of compounds considered recalcitrant to traditional Fenton processes.

6.2 Photochemical Reactions

The history of photochemical reactions dates back to the early 1800s, with early studies pioneered by a German physicist, Theodore Grotthus (Kornblum, 2010). In 1817, he found that, for a light radiation to cause a chemical change, the light must be absorbed. During his study of the reaction between moist hydrogen and chlorine gas, American chemist John William Draper in 1841, found that after a certain inhibition period, the intensity of light absorbed is proportional to the rate of reaction, which culminated in the first law of photochemistry known as the Grotthuss Draper law (Kornblum, 2010). It has been reported that Draper's studies may have been done in 1801, and those may have constituted the first recognised photochemical reaction.

Further development of quantitative aspects of photochemistry continued a century later and were championed by Max Plank and Albert Einstein with studies of quantum theory (Kornblum, 2010).

The quantum theory according to Planck, who is regarded as the founder of the quantum theory, states that only a fixed quanta or quantities of light energy can be

absorbed by a molecule or an atom and this energy which he called E, is proportional to the frequency, f of the light. He gave the energy of a single quantum of light as;

$$E = hf \quad \ldots (6.1)$$

Where h is a proportionality constant called "Planck's constant" (Kornblum, 2010). Einstein did further development of this quantum theory and his conclusions led to the second law of photochemistry.

The germicidal effect of sunlight was however first observed by Downes and Blunt, (1877) according to them, "we find that the contents of a tube, which remain perfectly clear so long as they are freely exposed to the sun's rays, swarm with *Bctoteria* after being deprived of the access of light". In 1906 however, the large-scale application of UV radiation for drinking water disinfection was advanced (Masschelein, 2002).

Fenton reactions are sustained by the oxidation-reduction interplay between Fe^{2+} and Fe^{3+} which is aimed at initiating a reaction between Fe^{2+} and H_2O_2 leading to the formation of a hydroxyl radical responsible for the degradation of organic compounds (Pignatello and Huang, 1993). The oxidation of Fe^{2+} to Fe^{3+} is known to be more favoured in the Fenton reaction process and thus much faster than the reduction of Fe^{3+}. Thus, the combination of UV and Fenton process at a radiation wavelength of between 180 and 400nm leading to the photo-reduction of Fe^{3+} to Fe^{2+} will produce additional OH radical from water for the reaction system (Pignatello and Huang, 1993). The Fe^{2+} formed can further react with H_2O_2 in the system to produce more OH radical provided there is H_2O_2 present in the system (Pignatello and Huang, 1993; Wadley and Waite,

2004). This redox cycle is expected to speed up the reaction rate with the formation of hydroxyl radicals according to equation (6.2);

$$Fe^{3+} + H_2O + h\nu \rightarrow HO^{\bullet} + Fe^{2+} + H^{+}. \quad \ldots (6.2)$$

Sun and Pignatello, (1993) have also attributed this increased reaction rate to the decomposition of the photo-active $Fe(OH)^{2+}$, an iron species which forms between pH 2 and 4 in most homogeneous catalytic systems when iron (lll) salts are dissolved in water and which is the dominant monomeric species in this pH range see equation 6.3. This generation of a reactive OH radical from H_2O has the potential to realise huge cost savings on oxidation reagents as given by equation 6.3 (Machulek Jr. et al., 2012).

$$Fe^{3+}(OH)^{2+} + h\nu \rightarrow Fe^{2+} + HO^{\bullet} \quad \ldots (6.3)$$

Burkhard, (2013), listed what he termed “essential criteria” for photo induced reactions to occur. According to him, these conditions are; firstly, the molecules in the reaction must absorb light. Secondly, the irradiation from the light source must be such that, it is proportional to the difference in energy between the ground state and the excited state of the molecule. According to him, when light is absorbed by a molecule, a change in the electronic configuration of the atom results. According to the *Frank Condon principle* however, the nucleus of heavy atoms do not experience any change when light is absorbed. In the same vein, the electron spin does not change, and spin inversion is highly unlikely during excitation resulting from light absorption. Burkhard, (2013) also listed the significant things about photochemical reactions to include the following;

a. Reactions that are naturally endothermic in ground state can proceed because excited states are energy rich.

b. Because anti-bonding orbitals are occupied in excited state, there is greater possibility for reactions, which naturally may not happen due to electronic reasons, to proceed in the ground state. Thus, excitation of molecules upon absorption of radiation can initiate reactions, which are otherwise impossible in ground state.

c. Photochemical reactions have an advantage over thermal reactions; firstly, while thermal reactions usually only have singlet states, their photochemical counterparts include both singlet and triplet states. Secondly, photochemical reactions may lead to the formation of oxidation intermediates, which are not accessible in thermal reactions (Burkhard, 2013).

6.3 Microwave assisted reactions

The use of microwave energy (MW) as an alternative to conventional heating, to minimize environmental impacts in chemical reactions transformation, by the reduction in the amounts of reagents used and reaction times is well documented (Abramovitch, 1991; Caddick ,1995). This involves irradiating reaction mixtures with microwave energy at a frequency of 2.45 GHz. Higher speed of heating is achieved from the interaction of matter with electromagnetic waves at this frequency and wavelength, which can lead to the alteration of ion migration and the rotation of ions dipoles, known as dipolar polarization without interfering with the structure of the molecules. This is achieved through effective temperature distribution, volumetric heating and selective heating of

more polar molecules (Saillard et al., 1995; Kingston and Haswell, 1997; Remya and Lin, 2012).

The reason for the so-called microwave effect is still a subject of speculation, however several hypothesis have proposed a dielectric and conductance mechanism (Kingston and Haswell, 1997). The main heating mechanisms of MW radiation are dipolar polarization, conduction, and interfacial polarization. Majority of heating in solvent systems is caused by intermolecular inertia, which results from dipolar polarization. What happens is, when the dipole is subjected to a high frequency alternating electric field of the MW, usually around (300 MHz to 300 GHz), this leads to the rotation (reversing) of the dipole, which is not fast enough to adequately follow the rate of change of direction of the electric field. This results in a time delay, and causes a substantial amount of energy to be spent, that converts into heat (Hidaka et al., 2007).

In this study, microwave assisted heterogeneous catalytic oxidation and UV-microwave assisted catalytic oxidation have been investigated with a view to combining their individual advantage in a cost effective manner, with environmental considerations.

6.4 AIMS

The aims of this chapter are to:

a. Determine the effect of process parameters and establish optimum conditions for the reaction.
b. Conduct batch and continuous flow UV and UV/MW assisted Fenton-like reactions on simulated produced water and compare same with the unassisted Fenton reaction.

6.4.1 Fundamentals of Photochemistry.

The use of light energy or radiation to cause a chemical reaction upon direct absorption is known as photolysis. The use of a catalyst in the process to increase the rate of reaction is known as photocatalysis (Goswami et al., 2000; Abhang et al., 2011). Photocatlytic oxidation however involves the addition of an oxidant e.g., H_2O_2, to enhance the process of pollutant breakdown (Guus et al., 2007). Photochemistry on the other hand, deals with the chemistry involved as a result of the impact of energy in the form of photons on materials. The principle of photochemistry is hinged on the first law of Photochemistry otherwise known as Grotthus-Draper's law, which states that light or radiation must be absorbed for a photochemical reaction to occur and this has been explained previously. This has been expressed as;

$$M + light \longrightarrow M^* \quad \text{.... (6.4)}$$

Where M* represents a molecule after being irradiated and is now in an excited state. Transmittance measures the amount of light or radiation a sample has absorbed from the total radiation entering the sample. This is given as;

$$T = \frac{I_0}{I} \quad \text{.... (6.5)}$$

Where I_o and I represents the radiation intensity before striking the sample and after striking the sample respectively. Accordingly, if no light is absorbed then $I=I_o$.

Beer's law also explains the relationship between the absorbance of radiation or light and the concentration of a sample or solution. That is;

$$A = \log (I_o/I) \quad \text{... (6.6)}$$

Where A is absorbance. It follows from equation (6.5) that,

$$A = \log (1/T) = -\log T \quad \ldots (6.7)$$

If we assume (according to Beer-Lambert's law) that absorbance A is proportional to both concentration c and path length of the light l, then;

$$A \alpha \ell c \quad \ldots (6.8)$$

this proportionality can be converted into an equality by including a proportionality constant;

$$A = \varepsilon c \ell \quad \ldots (6.9)$$

Where ε is a proportionality constant called molar extinction coefficient, which gives an indication of the extent of absorption of light in a medium.

Photoactive compounds absorb light in proportion to their concentration; hence, once an accurate value of ε is established for a known compound, the concentration can be calculated from its absorbance (Pace et al., 1995). Care must however be taken to account for possible interferences from other absorbing species in solution.

6.4.2 Photochemical Oxidative Decomposition in water treatment

The application of photolysis in combination with Fenton catalysis is an example of an advanced oxidation process (AOP). Other OAPs using UV radiation include, UV/H_2O_2, O_3/UV, UV/H_2O_2/O_3, UV/TiO_2, etc. (Ibhadon and Fritzpatrick, 2013). The key reactions are illustrated in Table 6.3.1. The focus of this study is UV/MW/Fenton and UV-Fenton, otherwise called photo-Fenton which according to Pignatello et al., (2006), holds more

promise for practical industrial applications due to the ease of application and less chemical requirements and hence, reduced impact on the environment.

Table 6.1: Advanced Oxidation Processes key Reactions and Wavelengths (Burkhard, 2013)

AOP	Key Reactions	Wavelength
UV/H_2O_2	$H_2O_2 + hv \rightarrow 2OH^{\bullet}$	$\lambda < 300$ nm
UV/O_3	$O_3 + hv \rightarrow O_2 + O(^1D)$ (singlet) $O(^1D) + H_2O \rightarrow 2OH^{\bullet}$	$\lambda < 310$ nm
UV/H_2O_2/O3	$O_3 + H_2O_2 + hv \rightarrow O_2 + OH^{\bullet} + OOH^{\bullet}$	$\lambda < 310$ nm
Photo-Fenton	$H_2O_2 + Fe^{2+} \rightarrow Fe^{3+} + OH^{\bullet} + OH^-$ $Fe^{3+} + H_2O_2 + hv \rightarrow Fe^{2+} + H^+ + OOH^{\bullet}$	$\lambda < 580$ nm
UV/TiO_2	$TiO_2 + hv \rightarrow TiO_2 (e^- + h^+)$ $TiO_2(h^+) + OH^-_{ad} \rightarrow TiO_2 + OH^{\bullet}_{ad}$	$\lambda < 390$ nm

6.4.3 Types of Photocatalytic reactors

The system of classification of reactor types is vast and sometimes very convoluted. This is because; several categorizations of reactors are based on industry of application. Some of the factors that have been used in classifying reactors include the following:

- Mode of attachment of catalyst
- Lamp configuration with respect to aqueous solution
- Pattern of UV lamp orientation
- Reactor wall configuration
- Reactor size

- Mode of operation

Accordingly, with respect to mode of attachment of catalyst, two main types of reactor configurations used for photocatalytic processes have been described, namely; *Slurry* (Mills et al., 1993; Herrmann, 1999; Almquist, 2003) and *immobilized reactors* (Herrmann, 1999; Chan and Lynch, 2003; Ray and Beenackers, 1998). The Slurry reactor shows greater catalytic efficiency in terms of reaction rates improvement in comparison to the immobilized support reactors (Pueh, 2010; Yatmaz et al., 2000). However, there are advantages in the latter; for example, there is a post-treatment requirement, which involves the separation of particles, or sludge from the liquid phase, which adds to the overall cost which makes the immobilized reactor preferred for water treatment (Balasubramanian et al., 2004).

In terms of the lamp configuration with respect to aqueous solution, reactors have also been further classified into three groups namely; *immersion types, external types* and *distributive type reactors* (Ray, 1999). The immersion type reactors as the name implies have their lamps immersed in the treatment solution within the reactor. For these types of reactors, emitted radiation may have to travel through lamps protective jacket, then through the reaction solution where radiation may be lost to absorption (by solution substrates) and deflection (caused by turbidity) before reaching the catalyst. For the external type reactors, the lamps are outside the reactor tank, however the emitted radiation can also be affected by turbidity of the solution and/or absorption and deflection depending on the how the catalyst is deployed. The distributive type reactors

on the other hand have the radiation dispersed from the source using reflectors or optical fibres (Ray, 1999) and has similar challenges as the former.

With respect to the pattern of UV lamp orientation/configuration, two fundamentals types of chemical reactors are known; annular reactors and cylindrical reactors (Akehata and Shirai, 1972). Annular reactors are irradiated from a cylindrical light source inside an annulus, while the cylindrical reactors have irradiation source positioned radially around the reactor to provide uniform irradiation. Other reactor types include flat or tubular wall reactors which are based on the reactor wall configuration (Ibhadon and Fritzpatrick, 2013). Monolith and micro reactors have also been used to describe reactors based on size and composition (Gerven et al., 2007).

With respect to mode of operation, two types of reactors have been described by Yatmaz, (1993), namely; falling film reactors and spinning or rotating disk reactors. These reactors have been designed to overcome the mass transfer challenges in photocatalytic reactors. There are instances where a combination of these reactor names are used to suitably describe a specific reactor. In all cases, therefore the challenge in the design of a photochemical reactor for heterogeneous systems is largely on the uniform distribution of irradiance on the catalyst surface (Gerven et al., 2007).

6.4.4 Reactor design

Design considerations seek to overcome the existing challenges and shortcomings, which hinder the efficiency of photocatalytic reactor systems. The design considerations that have been summarized by Yue, (1985) in Yatmaz, (1993), Gerven et al., (2007),

Ibhadon and Fritzpatrick, (2013), Masschelein, (2002), Meulemans, (1986) and Cabaj et al., (2000) are as follows:

- Heat Exchange – Design considerations should anticipate effective heat transfer mechanisms. The heat generated by the radiation source (lamps) in addition to heat energy resulting from reaction system. Designs should incorporate the possible need for heat removal or addition.
- Mixing and flow characteristics – The rate-limiting step in most systems especially heterogeneous catalytic reactors is the mass transfer limitations. Effective mixing is even more important in multiphase reactor systems. The reactor geometry should support proper mixing to make for good contact between the photon, the substrate and the catalyst.
- Reactor material – The material used for construction of a photocatalytic reactor is an important design factor for several reasons; corrosivity, resistance to reactive oxidants, cost, thermal properties of material, etc. The most important criteria is the radiation/light transmission properties of the material. Commercially available glass types include Pyrex glass, optical glass, etc. block wavelengths below 300 nm down to 120 nm, and quartz is usually the best material of good quality. However, this fused quartz is a high-end material with significant cost implications.
- Energy consumption- The cost efficiency of any treatment system forms one of the most important factors usually considered before deployment. For most UV systems, the major cost component lies in its energy consumption and cost of H_2O_2 (if required). Higher energy corresponds to higher irradiance and it is crucial

to meet the energy band-gap requirement, for the compounds undergoing excitation; however, this must be balanced in terms of cost efficiency. The type of UV lamps (in terms of energy consumption) used for this purpose can make a huge difference resulting in huge savings.

- Location of Lamps- Lamps can either be embedded in the reaction solution or placed externally. Embedded lamps would prove more efficient provided the turbidity of the medium is low. Precipitation of deposits (slime) on lamps embedded within the reaction volume can significantly reduce treatment efficiency. Precipitates of mineral salts of Ca and Mg account for between 30 and 80% of deposits on lamp surfaces (Masschelein, 2002). In waters which have undergone primary treatment by flocculation, Fe and Al may well account for 20 to 30% slime deposits (depending on solution pH). This can however be managed by effective pre-treatment such as flocculation and coagulation, pH adjustment and filtration to clarify the medium.

Lamps positioned externally to the reaction solution will not suffer deterioration from slime deposition; however, the further the lamps are from the reaction tank, the lower the flux intensity, and the less able to penetrate through the solution. This can however be overcome by the use of shallow bed reactors, which have shallow depth of penetration.

Others important features include composition and optical absorbance of non-target compounds or materials in the water and geometry, relationship between the optical absorption band of the catalyst and that of the target compound/medium, film thickness on thin film reactors, etc.

6.5 Ultraviolet (UV) Radiations and Their Sources

Electromagnetic spectrum, (Figure 6.1) describes the distribution of electromagnetic wave according to energy with respect to wavelength and frequency (NASA, 2007). It consists of about seven differently classified radiations, spanning wavelengths of a few pico meters to over one meter (Figure 6.1). Photochemical processes are predominantly within the visible and the ultraviolet regions, but because the photochemical effects of UV radiation varies substantially at different wavelengths for different compounds, the UV spectrum has been further subdivided into three regions UVA (400-320 nm), UVB (320-290 nm) and UVC (290-200 nm) (Diffey, 2002). Photochemical activity is thought to be most effective in the range of 250-400 nm, which corresponds to the ultraviolet (UV A-C) region of the spectrum and is the most commonly used in photochemical degradation processes (Braslavsky et al., 2011). It is also sometimes referred to as the disinfection range because it is wavelength range used for disinfection (usually 254 nm but between 200 and 300 nm). With the exception of carboxylic acids and alkanes, most organic compounds have their maximum optical absorbance within this region as shown in Table 6.1.

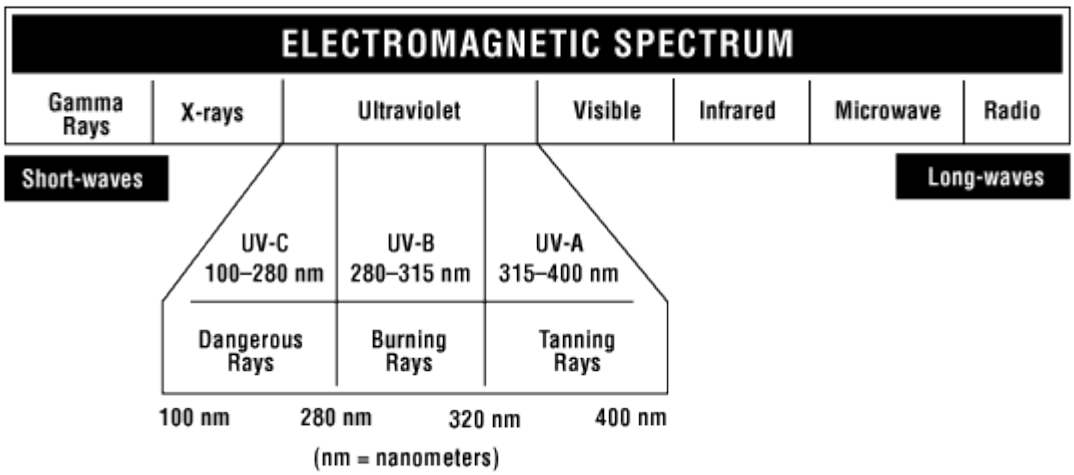

Figure 6.1: Electromagnetic spectrum (not to scale). Source: (CCOHS, 2016)

Most aromatic compounds, including DMP used in this study absorb through 254 nm (Figure 6.2). The UVC region where the aromatic compounds absorb is a narrow region of the spectrum, and some materials and compounds do not absorb in this region. Carboxylic acids, which form the bulk of the recalcitrant component of Produced water, absorb at the UVC region, around 210 and 230 nm (and not 254 nm from monochromatic low energy lamps) as shown in Table 6.2 (Burkhard, 2013; Kalisvaart, 2000). Thus, the use of low-pressure monochromatic lamps for UV oxidation although effective when targeting specific compounds, it is often not effective for a complex mixture of wastewater with varied spectral properties. This has been discussed in more details under lamp properties and types (Section 6.5.1.1 to 6.5.1.3).

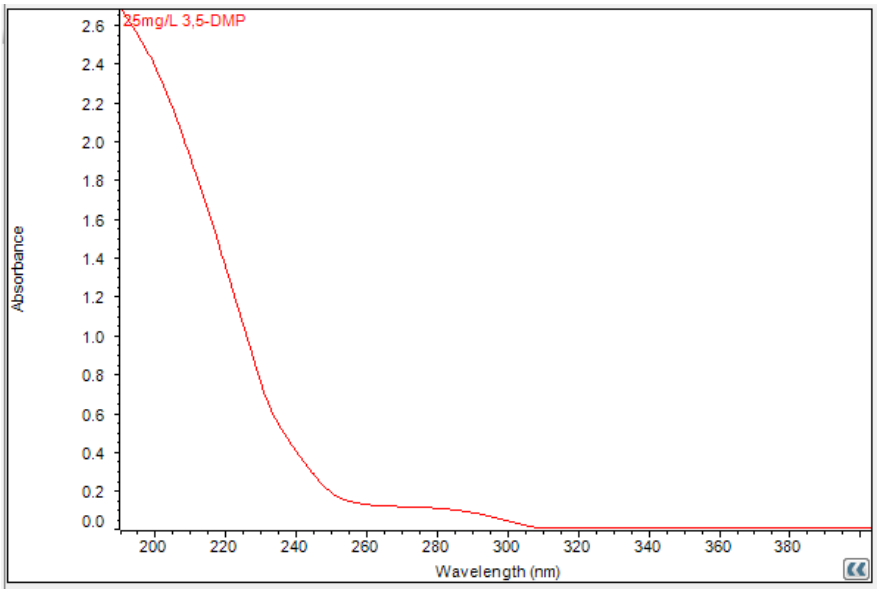

Figure 6.2: Absorbance spectrum of 25 mg/L DMP in water.

Table 6.2: Regions of absorption of UV light for selected classes of organic compounds (Burkhard 2013, Kalisvaart, 2000)

S/no	Organic compound	Absorption wavelength range (nm)
1	Simple alkanes	190-200
2	Acyclic diene	220-250
3	Cyclic diene	250-270
4	Styrene	270-300
5	Saturated ketones	270-280
6	α, β-Unsaturated ketones	310-330
7	Aromatic ketones/ aldehyde	280-300
8	Aromatic compounds	250-280
9	Carboxylic acids	210-230

Because aromatic compounds can be excited by UVC, there is a dual impact efficiency of substrate electronic excitation (excited states are energy rich) by direct photolytic action and an increase in hydroxyl radical production given by equation 6.10;

$$H_2O_2 + hv \rightarrow 2HO^{\bullet} \quad \text{.... (6.10)}$$

The solar system only accounts for 7 to 9% of UV radiation at sea level. Thus, most of the UV radiation used for UV enhanced reactions is artificially generated. Commercial generation is commonly done by two main methods; incandescence and fluorescence (Diffey, 2002). The former involves heating a body to an incandescent temperature at which point it glows, an example is Solar UV or tungsten element, while the latter involves passing electric current through a gas, which becomes excited and fluoresces.

The principle behind generation of radiation or emission of light is by activation of electrons to a higher orbital state or higher energy level of an element. When such an activated specie returns to a lower energy level, it is accompanied by light emission and the wavelength obtained is dependent on the energy difference between the activated or excited state and the returned state (Masschelein, 2002). This is as shown in Figure 6.3.

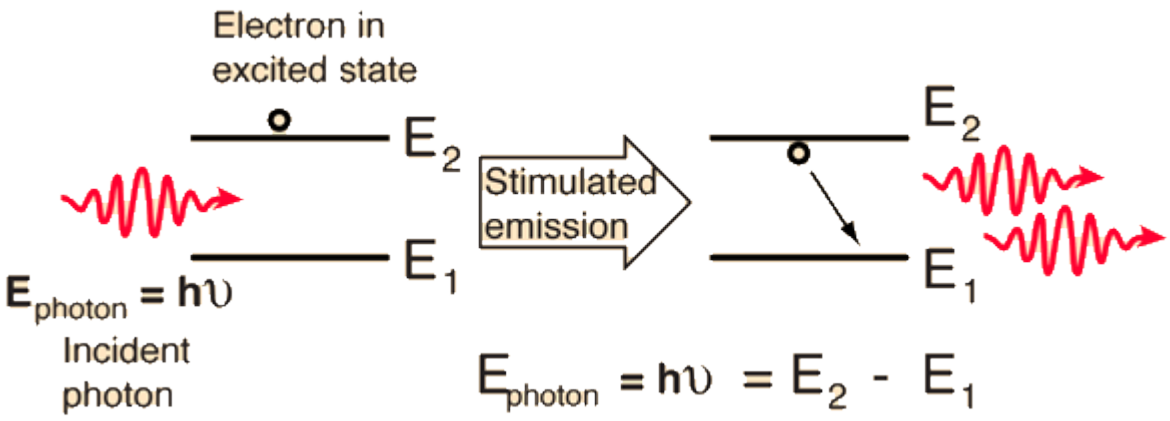

Figure 6.3: Emission of radiation by matter. Source (Nave R., 2015)

The principle of incandescent UV radiation, which involves the thermal activation of matter, is based on the Black Body (opaque and non-reflective) radiation theory – That the total radiant energy (quantified by Stefan-Boltzmann law) depends on the temperature of the matter (Masschelein, 2002). All normal matter is able to absorb electromagnetic radiation to some degree, a black body which is in thermodynamic equilibrium on the other hand absorbs all electromagnetic radiation at all wavelengths and is able emit radiation of a characteristic frequency distribution which corresponds to its temperature (Kuhn,, 1978). Black body radiation as a means of commercial generation of UV does not enjoy a huge commercial application compared to fluorescence (Masschelein, 2002).

Artificial UV sources are commonly produced by fluorescence using mercury emission lamps. An example of this is the vaporised mercury emissions which is also known as lamp or burner technologies. It is the dominant means for commercial production of UV radiation. This is because, mercury is the most volatile metal and as a result, activation of mercury at the temperatures amenable to the structures of the lamps is easy

(Masschelein, 2002). Mercury based lamps are differentiated based on the operating pressure temperature and emissions spectrum and based on this, we have two main types; low pressure and medium pressure lamps (Schalk et al., 2005).

6.5.1.1 Low Pressure (LP) Lamps

Low pressure mercury lamps operate at a pressure of about 10^2 to 10^3 Pa, which is equivalent to 1 to 10 mbar (Masschelein, 2002). They have a narrow spectral radiation mainly at 254 and 185 nm (Schalk et al., 2005). The 254 nm radiation is suited for disinfection, while the 185 nm obtained from LP lamps is suited for AOPs such as UV/O_3 or UV/H_2O_2 and water, where direct photolysis of O_3, H_2O_2, or water is required to liberate $^{\bullet}O$ and $^{\bullet}OH$ (Schalk et al., 2005). The preferred envelop material for LP lamps is fused silica because of low wall temperature, However soft glass, made from sodium/barium has also been in use, which does not transmit at 185 nm (Schalk et al., 2005). Optimised LP lamps called fused quartz amalgams also exist, which have longer life, better transmittance and higher operating temperatures.

6.5.1.2 Medium Pressure (MP) Lamps

These lamps operate at pressures of about 1 to 3 bar. These lamps operate, based on plasma emission at high internal temperatures of between 500 to 950 ^{o}C as shown in Table 6.3 (Masschelein, 2002). They have higher electrical output than LP lamps, which gives them a higher vapour pressure, with a corresponding continuous spectrum. They are polychromatic (broad spectral capabilities) however; their high surface temperature is a major setback owing to poor compatibility with heat sensitive materials (Schalk et al., 2005). A comparison of the LP and MP lamps is as shown in Table 6.3 below.

Table 6.3: Comparison of Low Pressure and Medium Pressure Lamps (Schalk et al., 2005)

Characteristic	**LP Amalgam**	**MP**
UV spectrum	185, 254 nm	polychromatic
Hg vapour pressure (bar)	1 x 10-5	1 – 6
Surface Temperature (°C)	90 – 120	500 – 950
Electrical Power (W)	40 – 500	400 – 60,000
Specific Elect. Power (W/cm)	1 – 3	50 – 250
Specific UVC flux* (W/cm)	<1	<35
UVC efficiency (%)	35	5 – 15
Lifetime (h)	<16,000	<5,000

** per unit arc length*

6.6 EXPERIMENTAL METHODOLOGY

6.6.1 Reagents/Chemicals and Materials

Table 6.4: Reagents and chemicals used for this study.

Chemical/reagent	Linear formula/ Symbol	% Purity	Source
3,5-dimethyl phenol	$(CH_3)_2C_6H_3OH$	≥ 99	Sigma Aldrich
Hydrogen Peroxide	H_2O_2	30.0	Fisher Scientific
Hydrochloric acid	HCl		Fisher Scientific
Acetonitrile	CH_3CN	99.8	Fisher Scientific
Double distilled water	H_2O	-	DMU-Fistreem Cyclon: WSC044
n-hexadecane	$CH_3(CH_2)_{14}CH_3$	99.0	Sigma Aldrich
Tridecane	$CH_3(CH_2)_{11}CH_3$	≥ 99	Sigma Aldrich
Acetic acid	CH_3CO_2H	99.7	Sigma Aldrich
Sodium hydrogen carbonate	$NaHCO_3$	99.0	Sigma Aldrich
Sodium Chloride	NaCl	99.0	Fisher Scientific
Benzene	C_6H_6	99.8	Sigma Aldrich
Toluene	$C_6H_5CH_3$	99.5	Sigma Aldrich
Ethyl Benzene	$C_6H_5C_2H_5$	99.5	Sigma Aldrich
Xylene	$C_6H_4(CH_3)_2$	99.5	Sigma Aldrich
2,6,10,14-tetramethylpentadecane (TMPD)	$(CH_3)_2CH(CH_2)_3CH(CH_3)(CH_2)_3CH(CH_3)(CH_2)_3CH(CH_3)_2$	98	Sigma Aldrich
Tetrachloroethylene	$CCl_2=CCl_2$	≥ 99	Sigma Aldrich

Other material used for the study include the following; modified catalytic mesh, 300 mL capacity jacketed dish reactor vessel with an exposed surface area of 103.87 cm^2 (reactor diameter was 11.5 cm). An Isotemp refrigerated-heating circulator model 4100 R20F, with controls from -20°C to 100 °C was used to regulate the temperature of the reactor. 8W T5 GR3 WEMLITE germicidal ultraviolet irradiation lamps, magnetic stirrer, mini height adjustable work platform (jack), P1000 Gilson pipette, KERN ALJ 220-4

balance, Watson Marlow series 101U peristaltic pump. A photocatalytic reactor, described in Section 6.6.3, Figures 6.4 and 6.5, housed in a cabinet, measuring 80 cm x 50 cm x 50 cm (HxWxD) made from steel plates was used for batch reactions. A UV/microwave assisted reactor incorporating a rotating disc reactor described in Section 6.6.4, figures plate 6.6a to 6.6c, was used for continuous flow reaction.

6.6.2 Equipment

The following analytical equipment were used for the study; Perkin Elmer HPLC series 200 fitted with a UV detector, PerkinElmer Flame atomic absorption spectrometer AAnalyst 200 model fitted with a touchscreen interphase, Alpha FTIR spectrometer DR 3800 Hach Lange spectrophotometer. ILT 1400A Radiometer, fitted with SEL240 and SEL220 – solar blind vacuum photodiode detector.

6.6.3 Description of Photocatalytic Dish Reactor

The photolysis unit used for the batch study consisted of up to 4 x 8 W GT Wemlite germicidal ultraviolet irradiation bulbs, emitting at wavelengths of 253.7 nm fitted to a plate above the reaction solution. The reaction vessel was a jacketed dish type reactor of 300 mL capacity, mounted on a magnetic stirrer. The stirring was achieved by the use of a stirring bar, which was rotated at 400 rpm. The magnetic stirrer was mounted on a mini height-adjustable work platform to enable vertical variation/adjustment of distance of reaction solution from the irradiation source as shown in Figures 6.4 and 6.5.

The reaction temperature was regulated by the use of a refrigerated-heating circulator, with controls from -20 ^{o}C to 100 ^{o}C, while the reaction was monitored by sampling using a peristaltic pump to withdraw a sample when needed, to avoid frequent opening and

closing of the UV cabinet door. The reactor was housed in a cabinet, which had a built in automatic UV cut-off when the door opens. The dish reactor and the cabinet were black coated to diminish reflection, refraction and deflection of irradiation.

Figure 6.4: Photograph of the UV- reactor system used for the study

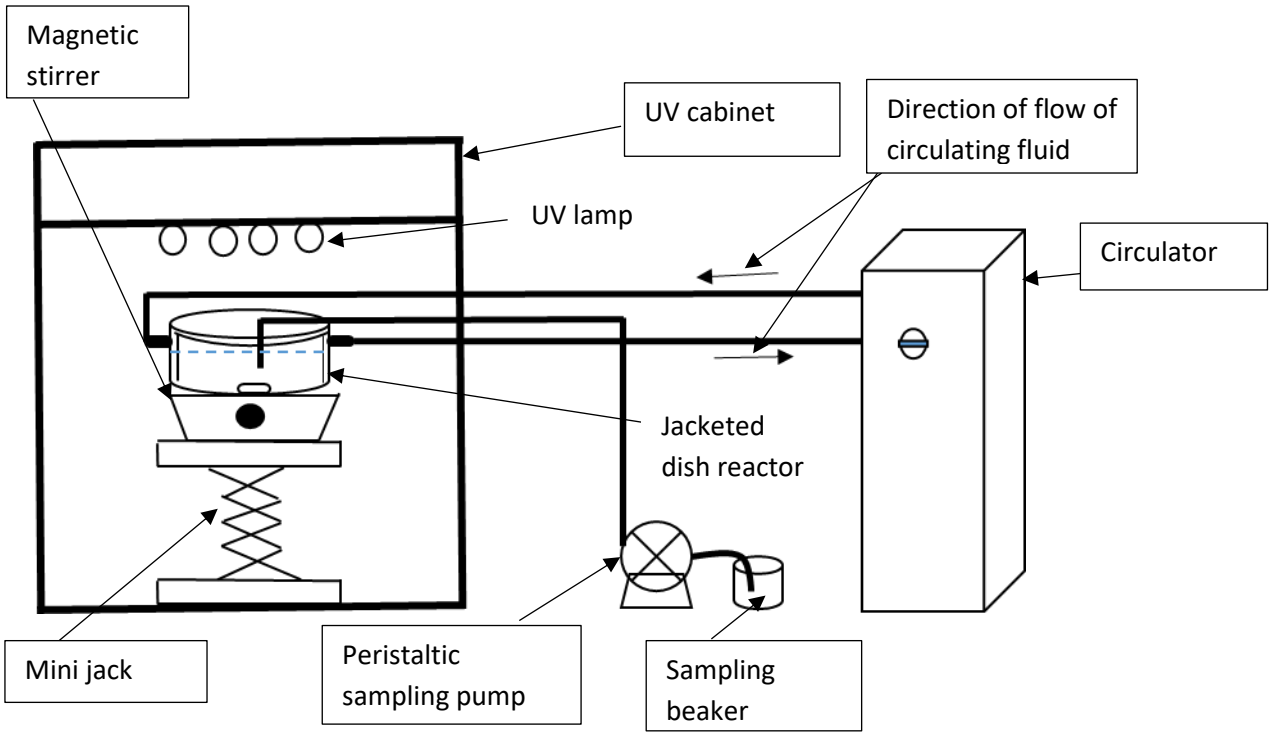

Figure 6.5: Schematic drawing of experimental setup of the UV- reactor system

6.6.4 Description of UV/Microwave Reactor

The UV/Microwave reactor consisted of a steel casing measuring about one meter cubed, which housed a Mars 6 programmable microwave oven of 0-1.8 kW microwave power, irradiating at a frequency of 2.45 GHz. The door of the microwave oven had the plastic sheet removed and was fitted with 8 x 8 W UV lamps with an average irradiation output of 700 mW measured at 5 cm from reaction surface. The average irradiance measured at the surface of the reaction was only 500 µW. The irradiance was low because the lamps were distant from the position of the reactor relative to the lamps. In addition, the reactor material was not transparent to UV. Within the cavity of the microwave is fitted the 950 mL volume, cylindrical rotating disk reactor with discs and

tank made of acrylics, while gears and support were made of Teflon, HDPE respectively. A motor rotates 8 discs of 2 cm radius, loaded with 180 g of the modified catalyst, slotted on a shaft, rotating at a low velocity of 8-10 rpm. The large shear forces of the rotating disks provides efficient mixing of the reaction system giving high mass transfer rates. The reactor is as shown in Figures 6.6a to 6.6c.

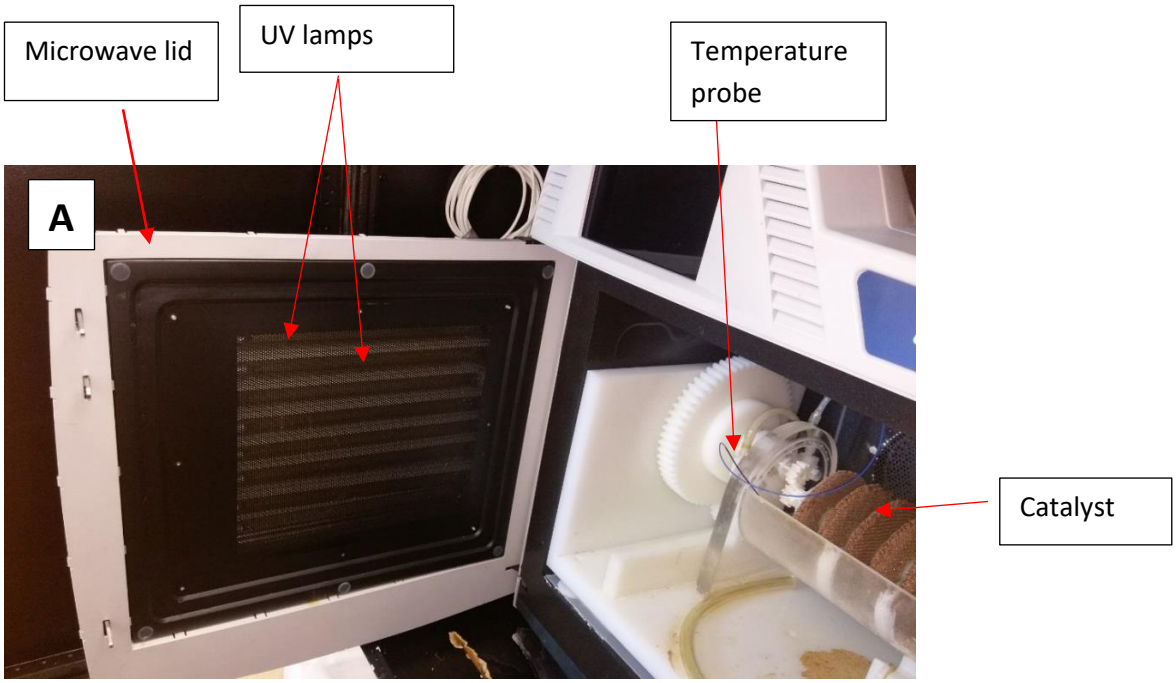

Figure 6.6a: Photograph of UV/Microwave reactor B showing the UV lamps

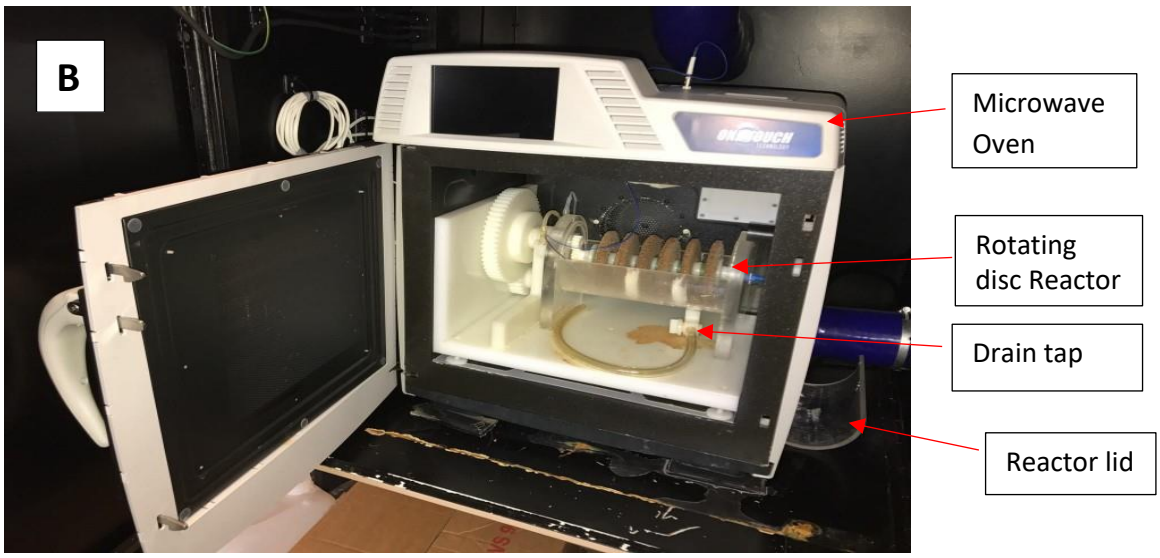

Figure 6.6b: Photograph of UV/Microwave reactor B showing the rotating disc reactor

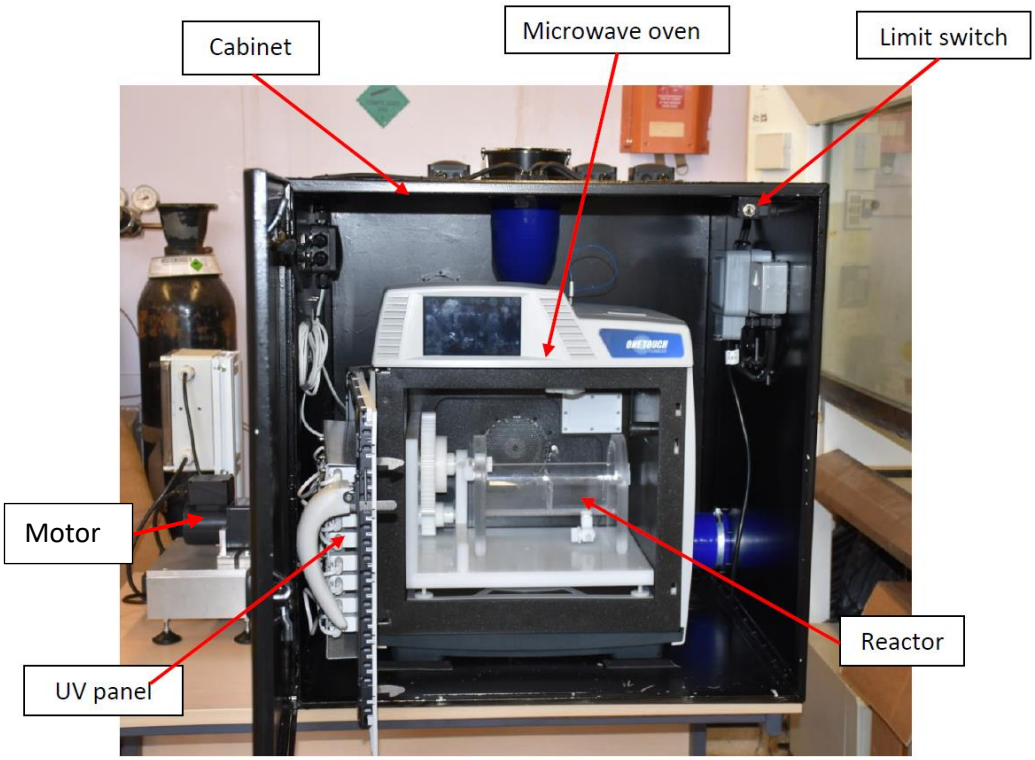

Figure 6.6c: Photograph of UV/Microwave reactor B showing the UV panel and motor

6.6.5 Experimental Setup

The UV photocatalytic experiments were conducted first in batch on DMP in water and subsequently synthetic produced water, using the dish reactor described in Figure 6.4 and 6.5. The control experiments included the following; DMP alone using process time of 4 h, UV radiation alone in the presence of DMP, and UV + hydrogen peroxide in the presence of DMP. These were followed by the photocatalytic experiments (uv+peroxide+catalyst and DMP). Similar set of experiments were carried out on synthetic produced water in the same order mentioned above also in dish reactor. Finally, continuous flow experiments were then carried out on synthetic produced water using the continuous flow reactor, (Figure 6.6a to 6.6c) which in addition to the experiments in dish reactor above, included microwave assistance i.e. (UV+peroxide+Catalyst + microwave + PW).

6.6.6 Experimental conditions

Batch UV-Fenton experiments in dish reactor for the oxidation the model compound, DMP and synthetic produced water, were conducted using the following conditions; Reaction volume was 200 mL, stirred at 400 rpm, with 10 g catalyst, 400 and 1000 ppm H_2O_2 for 25 mg/L DMP and produced water respectively. The reaction temperature was 26 ^{0}C ± 1, at pH3. The UV irradiance was 2.66 mW/cm^2 on the exposed reaction surface area of 103.87 cm^2, which was 5 cm from the UV source with a total power of 24 W.

The continuous flow reaction in continuous flow reactor was carried out in phases, and consisted of the following reaction systems; UV-Fenton- microwave, UV-Fenton, microwave-Fenton, Fenton alone, and control experiment (no treatment) on synthetic

produced water in the presence of H_2O_2. The conditions for this reaction were as follows; Reactor volume was 950 mL, with the eight discs set to rotate at 8-10 rpm. The catalyst load was 180 g, H_2O_2 concentration in reaction was 1000 mg/L, however the peroxide feedstock was 4000 mg/L, on a flow rate of 0.8 mL/min (pump setting to achieve this flow was 06). The synthetic produced water, which was prepared as described previously in chapter five, was delivered into the reactor at a flow rate of 2.4 mL/min, (pump setting of 16), using a platinum-cured silicone tubing with ID of 1.6 mm, OD of 4.8 mm and wall thickness of 1.6 mm. This resulted in a flow ratio of 4:1 synthetic produced water: H_2O_2, giving a H_2O_2 reaction concentration of 1000 ppm after mixing. Total flow rate for peroxide and synthetic produced water was 3.2 mL/min, giving a residence time of 4 h and 55 min (Reaction volume 950 mL, Flow rate 3.2 mL/min)

6.6.7 Substrates preparation

Solutions of DMP and synthetic produced water were prepared as per protocols described previously in chapter three section 3.4.1 for DMP, and chapter 5 section 5.4.4 for produced water respectively.

6.6.8 Experimental Procedure

The batch mode experiments were carried out in reactor A that has been previously described. UV lamps in the reactor were turned on for thirty minutes to warm up and stabilize at constant UV irradiance. Thereupon, the pH adjusted solution of DMP was transferred into the jacketed reactor vessel which was connected to a circulator pre-set to the required temperature. The reaction system was initially optimised by investigating three photochemical reactor parameters, namely; Influence of distance of

reaction solution from the irradiation source, the influence of irradiation time on the reaction solution and the influence of radiation intensity. The following processes were performed:

- UV radiation in the presence of substrate alone
- UV radiation in the presence of hydrogen peroxide and substrate
- UV radiation in the presence of catalyst, H_2O_2, substrate

The magnetic stirrer was set to 400 rpm and the sample for the initial zero reading was taken. The UV experiments were initiated by shutting the reactor door (which automatically activated the UV radiation source). Sampling was achieved with the use of a peristaltic pump for the analysis of DMP and hydrogen peroxide. For the produced water system, the reaction solution after 240 min was analysed for oil-in- water while the catalyst was processed further for oil in sediment according to DECC IR method for determination of Oil on Sand/Scale/Solids (DECC, 2011), described previously in chapter five, section 5.5.1. The result from this process was recorded as desorbed concentration.

For the continuous flow experiments in Reactor B, the reaction solution was fed into the reactor from two tanks, one containing H_2O_2, and produced water at flow rates already stated in section 6.6.6. The rate of loss of the model compound (DMP), COD and oil-in-water were monitored while total iron was monitored for both the continuous flow and batch processes. The following continuous flow processes were carried out on the synthetic produced water:

- Substrate in the absence of any treatment scheme
- UV radiation in the presence of substrate alone

- UV radiation in the presence of hydrogen peroxide and substrate and catalyst
- UV radiation in the presence of catalyst, H_2O_2, substrate and Microwave radiation (power set to 600 W, delivering 35 ^oC constant temperature).

6.6.9 Instrumentation/Analytical methods

6.6.9.1 Analysis of DMP and H_2O_2

For the batch process, the rate of loss of substrate (DMP) and hydrogen peroxide were monitored on a PerkinElmer series 200 LC Turbo model fitted with a UV detector. The procedure and method have previously been described in chapter five section 5.4.5.5.

6.6.9.2 Analysis of total iron

The dissolved iron concentration for the reaction process was monitored using a PerkinElmer flame atomic absorption spectrometer (AAS) AAnalyst 200 model, and this has previously been described in chapter three section 3.3.1.3.

6.6.9.3 Analysis of Chemical Oxygen Demand (COD)

The chemical oxygen demand COD, was monitored using spectrophotometry reference method –COD cuvette test ISO 15705. This has previously been described in details in chapter three, and chapter five section 5.4.5.7.

6.6.9.4 Analysis of Oil-in-water

Oil-in-water analysis was monitored using the Bruker Alpha FTIR in the transmittance/absorbance module. This procedure has previously been described in details in chapter five section 5.4.5.1.

6.7 Results and Discussions

6.7.1 Effect of Radiometric Irradiance on Oxidation of DMP

Radiometric irradiance has been defined as the measurement of the density of light striking a surface with units in mW/cm^2. Preliminary studies investigated The effect of irradiance intensity was evaluated by varying two factors, namely; total lamp power (number of lamps) and the distance of the reacting solution from the irradiance source (lamps), which formed part of the preliminary studies.

The influence of reactor distance from radiation source on the irradiance was investigated for 8, 16 and 24 W. The reactor dish, which sat on a height-adjustable mini jack inside the UV cabinet, was varied in a vertical fashion between 5 cm and 18 cm. The sensor was placed within a black cardboard, cut to the shape and dimension of the dish reactor and placed on the adjustable mini jack (Figure 6.7). The measured and calculated irradiances are as shown in Table 6.5.

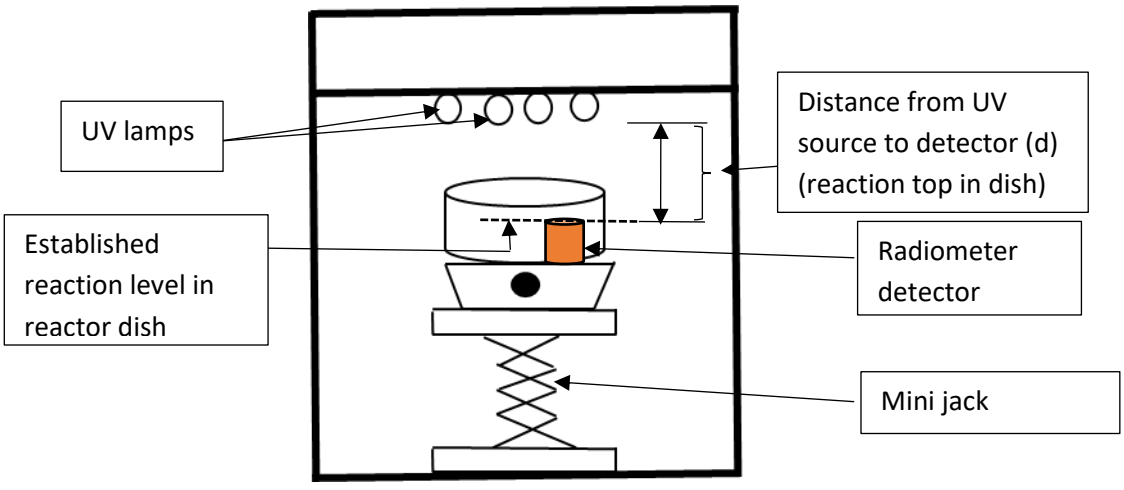

Figure 6.7: Investigation of the effect of irradiance by varying the distance

Table 6.5: Measured irradiance at different detector distances from UV source

Distance from lamps	8 Watt lamp Measured Irradiance (mW/cm^2)	16 Watt lamp measured Irradiance (mW/cm^2)	24 Watt lamp measured Irradiance (mW/cm^2)
5 cm	1.31	2.55	3.28
8 cm	1.07	1.69	2.79
10 cm	0.75	1.49	2.45
13 cm	0.53	1.19	1.72
15 cm	0.45	0.91	1.49
18 cm	0.37	0.66	1.10

The Irradiance Intensities for 16 W source ranged from 2.55 to 0.66 mW/cm^2 while 24 W lamps recorded between 3.28 to 1.10 wW/cm^2 at 5 cm and 18 cm respectively as shown on Table 6.5. As the detector was moved away from the source, inside the UV cabinet, irradiance reduced as shown in Figure 6.9. This observation followed the inverse square law (equation 6.11):

$$\text{Intensity} = \frac{1}{d^2} \qquad \ldots(6.11)$$

Where d is the distance of the radiation/light detector from source.

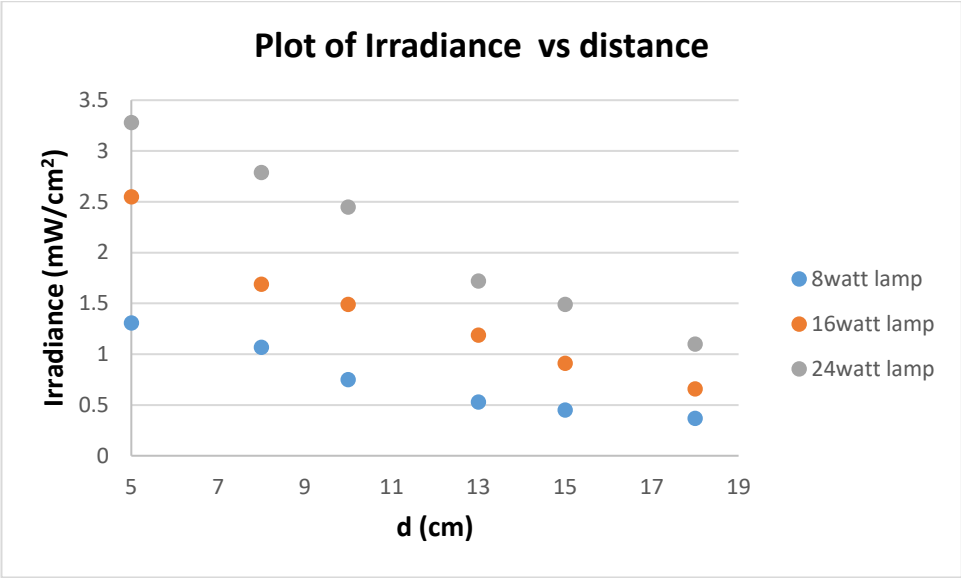

Figure 6.8: Variation of irradiance at different distances from the irradiance source at different lamp power

This means, the flux density will drop off as the measurement plane gets farther from a point light source (International light technologies, 2007). However, the law was not strictly obeyed mathematically and the reason for this is not very clear.

However, Borg, (2009) explained that the precondition for the inverse square law to be obeyed is that the source of radiation or light must be a point source as shown in Figure 6.8, unlike the radiation source in the UV cabinet used for this study. Other instances where the inverse square law is not obeyed include possible absorption and reflection of irradiated light.

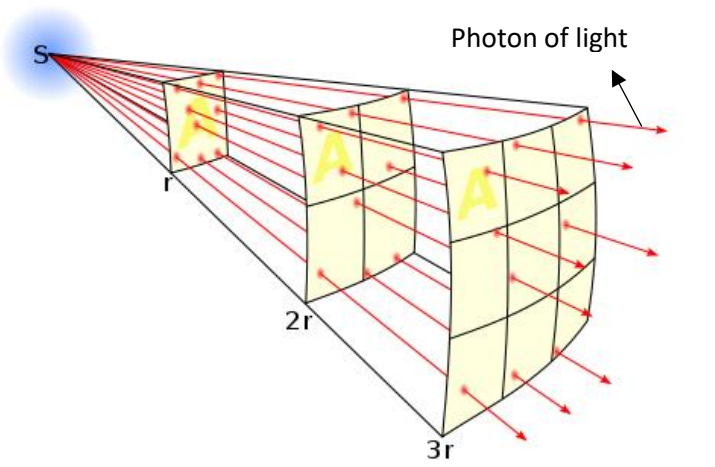

Figure 6.9: Point source Light illustrating inverse square law. (Source: Borb, 2008)

Catalytic degradation of DMP using the optimised conditions from normal Fenton catalysis over a range of irradiances is shown in Figure 6.10.

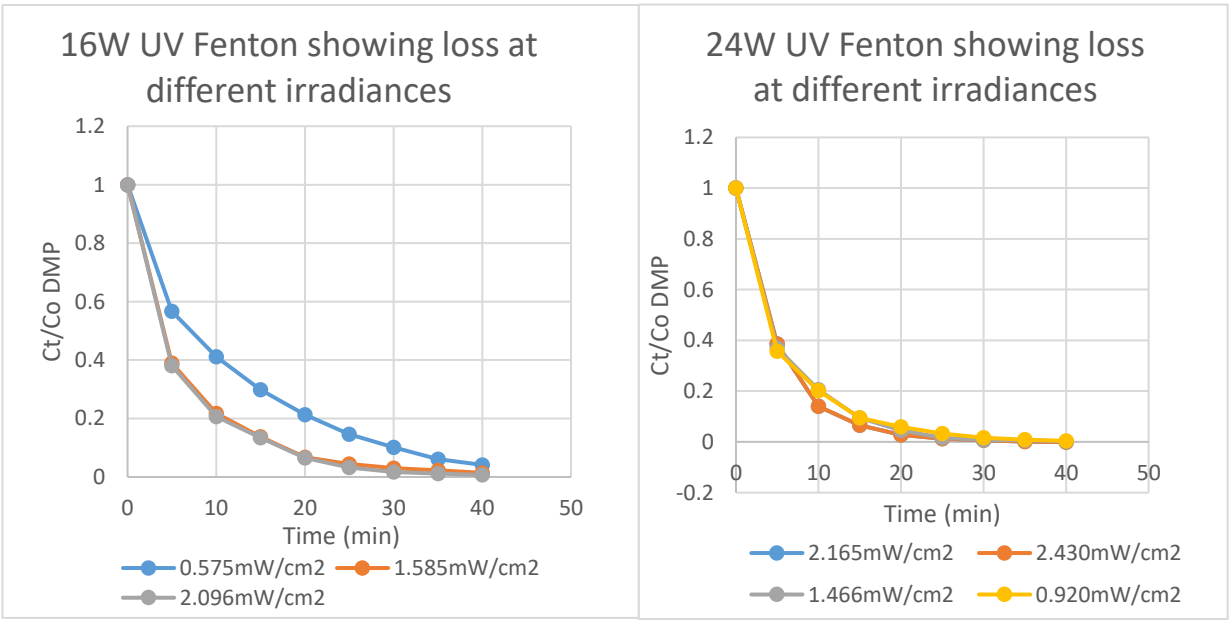

Figure 6.10: Loss of DMP with respect to irradiance in UV- Fenton catalysis using 25 mg/L DMP, 400 ppm H_2O_2, 10 g catalyst, 200 mL reaction solution, pH3 at 25±2 ^{0}C for 16 and 24 W lamp outputs.

From the graphs of 16 and 24 W lamp radiant power, there is no significant difference in the rate of loss of DMP with respect to irradiance intensity after 0.920 mW/cm^2. This could be due to a rate limiting effect such as the experimental setup at this range of irradiance for this reaction. The irradiance intervals used for the comparison, which is a function of the variable distance available in the UV cabinet was small. Thus, large irradiance intervals were not achievable. This may also be because the energy requirement for the excitation of DMP and the photolysis of water/H_2O_2 was easily attained at 0.9m W/cm^2 and further increase was not required (based on quantum theory). However, the effect on the excess irradiance on the oxidation products was not investigated.

6.7.2 Effect of Photolysis on H_2O_2, H_2O and Catalyst on the oxidation of DMP.

The effect of photolysis on H_2O_2, H_2O and the catalyst in the oxidation of DMP was evaluated using a series of controls. 400 mg/L H_2O_2 concentration of was used where relevant (this was shown to be optimum concentration see chapter three, section 3.5.2). The results are as shown in Figure 6.10.

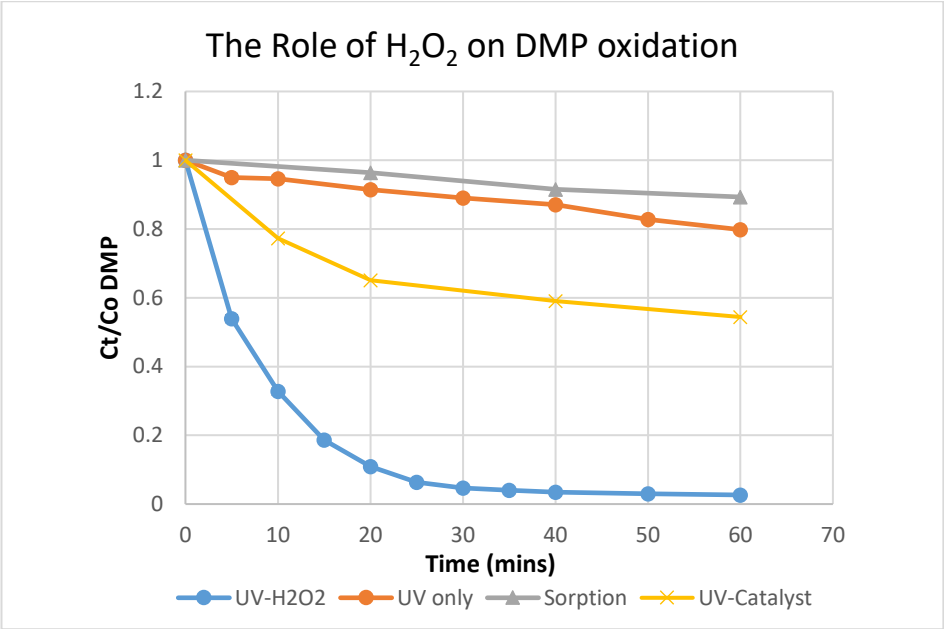

Figure 6.11: shows a comparison between UV-H_2O_2, UV Only, Sorption, and Catalyst exposed to UV Only in 200 mL volume, 10 g catalyst (where required), 25 mg/L DMP, 400 PPM H_2O_2 (where required) pH3, T =25 ^oC±1, 2.26 mW/cm^2 irradiance, and t= 60 min.

From Figure 6.11, there is almost complete loss of DMP in 60 minutes for UV/ H_2O_2, while UV alone resulted in a 20% loss of DMP in 60 min, which is faster than catalyst-H_2O_2 system which of 2 h reaction time (chapter three). However, a well optimised reaction system using the catalyst is likely to result in reasonable reduction in the amount of H_2O_2 used in the reaction, which is the single most expensive component of the reaction. There was also 10% loss due to sorption of DMP by the catalyst. The reaction of UV radiation in aqueous solution releases reactive free radical species in a slow process known as photo dissociation of water (Cervera and Esplugas, 1983), usually at a wavelength of about 185 nm (Schalk et al., 2005) as shown in equation (6.8).

$$H_2O + hv \rightarrow H^{\bullet} + OH^{\bullet} \quad \ldots (6.12)$$

The interaction of ultraviolet radiation with water molecules, dissociates it into hydrogen and hydroxyl radicals (equation 6.12) at the favourable wavelength of 185 nm vacuum UV (VUV).

The UV peroxide oxidation process achieved over 95% loss of DMP in 60 min. This arises from two main processes, enhancing the rate of loss of DMP. These are the absorption of UV radiation resulting to the excitation of the substrate which can lead to chemical transformations such as; intramolecular rearrangement, isomerization H atom abstraction, dimerization, electron transfer, etc. or a physical transformation such as; vibrational loss of energy (heat transfer), energy loss by light emission, etc. (Burkhard, 2013). The second process involves the photolysis of H_2O_2 and H_2O, to form reactive free radical species for the oxidation of the substrate according to equations 6.10 and 6.12 respectively. The reaction for equation 6.10 has a quantum yield of 1 at 253.7 nm (Guus et al., 2007; Cataldo, 2014). The simultaneous occurrence of H_2O_2 photolysis couples with H_2O photolysis results in the formative of more reactive free radical species which are thought to have been responsible for the faster rate of loss of DMP as shown on 6.7.2.

The degradation curve for UV alone can be seen to be better than the sorption curve as shown on Figure 6.10. This because DMP being an aromatic molecule absorbs in the UVC range (see Figure 6.5b). According to Phillips, (1983) and Stefan, (2004), the absorption of UV radiation by these aromatic compounds in the UVC range can result in their photolysis, leading to their degradation.

Machulek et al., (2012), showed that, the reaction of Fe^{3+} with UV radiation in an aqueous medium can result in the reduction of Fe^{3+} to Fe^{2+} in addition to forming OH radical according to equation (6.2) and this has been corroborated by Pignatello and Huang, (1993). The wavelength of this photo-reduction according to pignatello and Huang, (1993) is between 180 and 400 nm.

In their study of the photochemistry of $Fe(OH)^{2+}$, Pozdnyakov et al., (2000) showed that $Fe(OH)^{2+}$, if present in a catalyst can undergo photochemical reaction to produce Fe(II) and the hydroxyl radical, as shown in equation 6.3 and again in equation 6.13 (which will be elaborated in the next section). This could explain why there is a better rate of loss during irradiation of the catalyst as shown in Figure 6.10. However, there is also a very good chance that the increased rate of reaction is as a result of the combination of UV photolysis and sorption (an additive effect). Although it is not exactly clear what form or species the Fe is held in the catalyst, but ferric iron has a maximum absorption band at 240 nm, while $FeOH^{2+}$ has a maximum absorption at 300 nm (Turner and Miles 1957) which agrees with the absorption band for this switch, documented by pignatello and Huang, (1993). It is therefore possible to have minor absorption (depending on the form/species of Fe) which can result in a faster redox cycle from ferric to ferrous specie (equation 6.2), leading to the 40% loss of DMP in Figure 6.10. However, as there is only 40% loss of DMP, it highlights the importance of H_2O_2 to provide a good source of $^{\bullet}OH$. This was not helped by light scattering and/or attenuation of light density as a result of decreased irradiation penetration arising from the presence of the catalyst (Belattar et al., 2012).

6.7.3 Photocatalytic degradation of DMP and Cost benefit with respect to H_2O_2 Dose

H_2O_2 constitutes the most expensive non-reusable cost element in Fenton catalysis, in addition to the problem of residual H_2O_2 concentrations that may require removal as a post-treatment measure more so if a biological polishing stage is being considered. As a result of this, any positive step to cut cost while reducing environmental impact is sought in this work.

As shown in Figure 6.12, there was an increase in the rate of loss of DMP resulting in about 99.4% removal in 30 min when UV was coupled to the catalytic Fenton reaction using the same H_2O_2 concentration (400 ppm). There was however 93% loss of DMP within the same time when the H_2O_2 concentration was reduced to 100 ppm, (Figure 6.12) and this showed similar rate of loss of DMP as UV/H_2O_2 using 400 ppm H_2O_2 which had a loss of about 95.4% DMP also in 30 min (Figure 6.11).

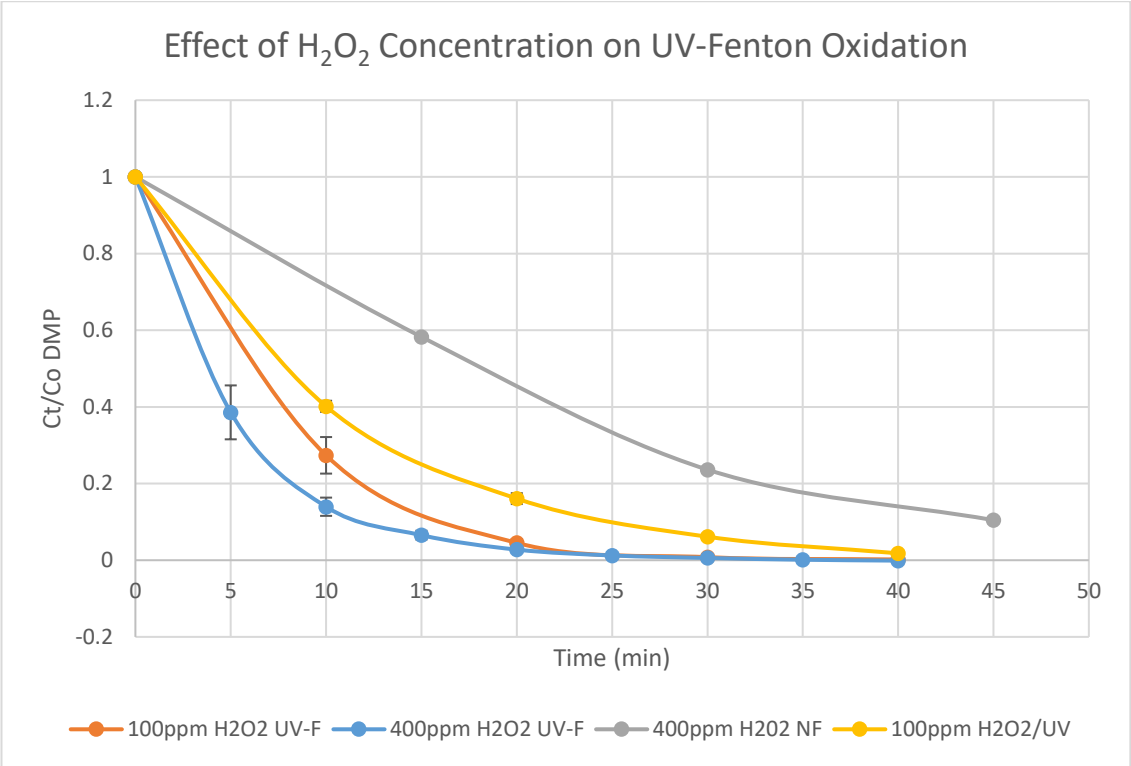

Figure 6.12: Oxidation of DMP using Normal Fenton(NF) at 400 ppm H_2O_2, UV assisted Fenton (UV-F) at 400 ppm H_2O_2, UV assisted Fenton (UV-F) with 100 ppm and UV with 100 ppm H_2O_2 concentration 25 mg/L, pH3, 200 mL reaction volume, 10 g catalyst, T= 25°C, t= 40 min and 2.66 mW/cm^2 irradiance.

Pozdnyakov et al., (2000), showed that the photolysis of $Fe(OH)^{2+}$ produced Fe(II) and the hydroxyl radical according to the equation (6.13) below:

$$Fe(OH)^{2+} + h\nu \longrightarrow Fe^{2+} + HO^{\bullet} \quad \ldots(6.13)$$

This suggests that, UV irradiation in the Fenton reaction, in addition to the formation of Fe(II) species, also regenerates OH radical, which is the vital reactive species in the Fenton reaction, responsible for the oxidation of organic matter. As a result of this double effect, the photo-Fenton process progresses faster than the conventional Fenton process, in addition to requiring less H_2O_2. The catalyst also provides active surface-area for sorption, followed by catalytic oxidation.

The role of Fe^{3+} species in UV-Fenton processes cannot be over emphasised. As shown in previous chapter, the optimum pH range for Fenton or photo Fenton oxidation is pH3. This has been attributed mainly to the speciation of Fe^{3+}. According to Machulek et al., (2012), Fe^{3+} ie ($[Fe^{III}(H_2O)_6]^{3+}$) which absorbs weakly above 300 nm is the dominant species of iron at pH2, while at considerably less acidic pH, the dominant specie is $Fe(OH)_3$. This species is thought to form colloidal iron hydroxide, which precipitates hydrated iron oxides on standing for long periods. Martyanov et al., (1997), noted that at pH3, the dominant Fe^{3+} species present in aqueous solution is $Fe(OH)^{2+,}$ which absorbs throughout much of the ultraviolet region of the electromagnetic spectrum. In their study of the photochemistry of $Fe(OH)^{2+}$, Pozdnyakov et al., (2000), showed that $Fe(OH)^{2+}$ can undergo an effective photoreaction to produce Fe(II) and the hydroxyl radical as shown in equation (6.13) above, given the right wavelength of UV radiation which according to Pignatello and Huang, (1993), is between 180 and 400 nm. It is possible that a similar species of Fe exists on the catalyst.

Accordingly, the UV irradiation of the Fenton reaction not only regenerates Fe(II) which reacts with H_2O_2 to generate $^{\bullet}OH$ (a critical part of Fenton reaction process), but it generates further additional $^{\bullet}OH$. As a result of these simultaneous effects, there is considerable reduction in the dose requirement of H_2O_2 in the reaction system.

6.7.4 Comparison of unassisted Fenton, UV Photolysis of DMP, UV-Peroxide and UV-Fenton

Unassisted Fenton, UV-Fenton, sorption, UV/H_2O_2 and photolysis of DMP solution were compared at optimum reaction conditions. The results are as shown on Figure 6.14.

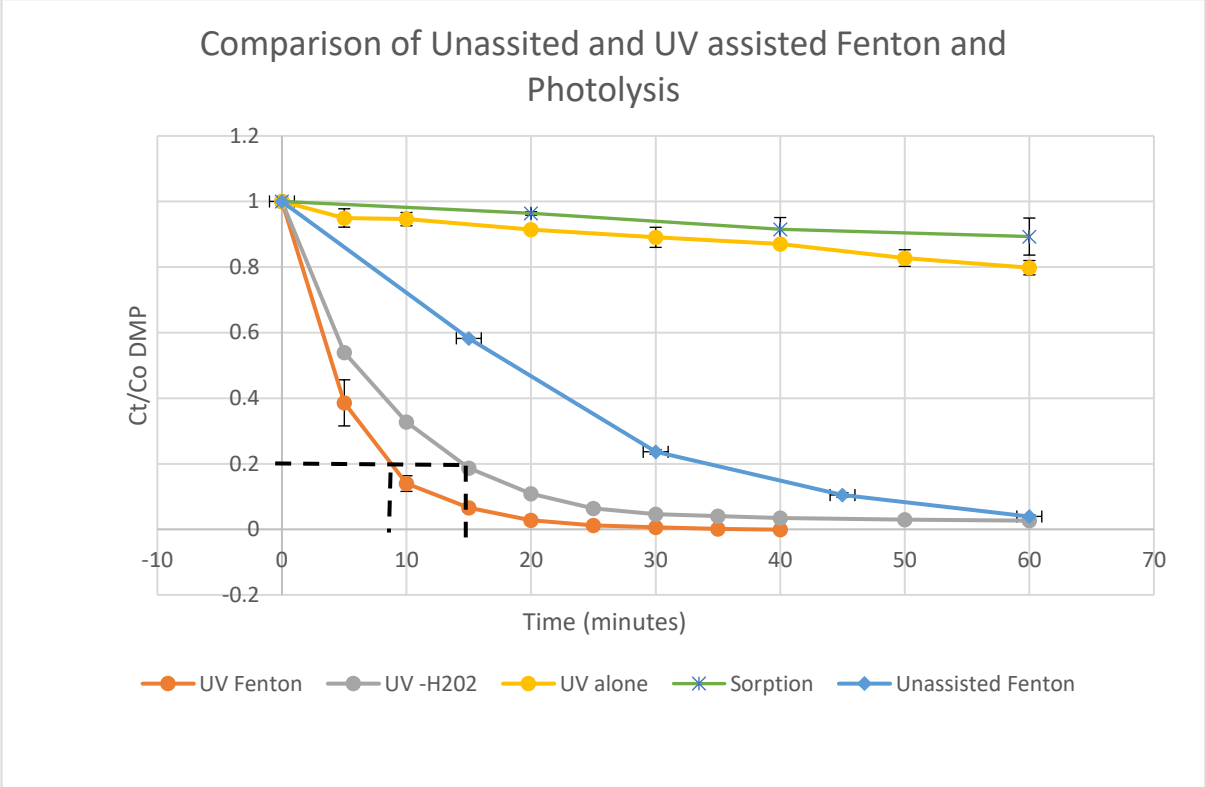

Figure 6.13: Results of unassisted Fenton, UV-Fenton, H_2O_2/UV, UV alone and sorption in respect to the rate of loss of DMP. Conditions: 25 mg/L DMP, pH3, 400 ppm H_2O_2 where required, 10 g catalyst where required, 200 mL pure DMP solution at 25 $^oC\pm$ 2 and irradiance of 2.43 mW/cm^2.

As expected, the results showed an advantage for the coupled process (UV-Fenton), which terminated after 30 min. UV/Fenton attained 80% removal of DMP in 8 min while UV/H_2O_2 in comparison did not attain complete removal of DMP even after 60 minutes, but did achieve 80% removal in 15 min as marked in dotted lines in Figure 6.13. The reason for this has already been explained as possibly due to the simultaneous but independent oxidation resulting from both UV photolysis and Fenton catalysis. The advantage is that, this coupled system has capacity to progress at the same rate even at lower concentrations of H_2O_2. This has been proven as shown in Figure 6.11 using a fourfold lower concentration of 100 ppm H_2O_2.

The reaction of unassisted Fenton after 40 min at the stated conditions showed 80% DMP removal while UV/H_2O_2 and sorption resulted in about 20% and 15% removal of DMP respectively.

6.7.5 Flow of Photons absorbed by 3,5-DMP, H_2O_2

As mentioned previously, the first law of photochemistry demands that a compound must absorb a photon of radiation in order for photolysis to occur. It is therefore imperative to determine if the species in the reaction solution actually absorbs radiation and to what extent. This information helps the design of the treatment processes and forms the basis for treatability studies.

To describe the photon flow absorbed by the constituents of the UV-Fenton reaction and possible photolysis. This process is guided by two main laws of photochemistry: The First law of photochemistry otherwise called the Grotthus-Draper, which has been described in section 6.2.1, and Stark-Einstein law: "*Number of activated molecules = number of quanta of radiation absorbed".*

In their study of chemical actinometry, Calvert and Pitts, (1967), Rodriguez, (2003), and Willett and Hites, (2000) held that, the rate of loss of an actinometric compound (Act) is the product of the incident light intensity (I_0), the quantum yield (ϕ) and the fraction of light absorbed by the compound (*f*);

$$-\frac{d[Act]}{dt} = I_0 \phi f \qquad \ldots (6.14)$$

Where ϕ the quantum yield, is the ratio of the number of molecules decomposed to the number of photons absorbed. ϕ and f are dimensionless, the units of I_0 is

Einstein L^{-1} S^{-1}, Where Einstein is defined as Avogadro's number or a mole of photons. The fraction of light absorbed (*f*) is given by;

$$f = \frac{I_0 - I}{I_0} = 1 - \frac{I}{I_0} \quad \text{... (6.15)}$$

Where I is light intensity after passing through sample. The ratio of the incident to transmitted light in equation (6.15), can be derived from the Beer-lambert law as follows;

$$A = -\log_{10}\left(\frac{I}{I_0}\right) = \varepsilon cL \quad \text{... (6.16)}$$

Where A is absorbance of sample, Ɛ is molar absorptivity in L mol^{-1} cm^{-1} and L is path length of light, C is the concentration in Mole L^{-1} and not all photons are absorbed by sample. Combining (6.15 and 6.16) we have;

$$f = 1 - 10^{-\varepsilon cL} \quad \text{... (6.17)}$$

The probability of survival or transmission T of a photon after a path length L is given as;

$$T = \exp(-\mu_a L) \quad \text{... (6.18)}$$

Where μ_a = the absorption coefficient (cm^{-1}). This is simply the cross sectional area per unit volume of medium. It describes a medium containing many chromophores at a concentration described as a volume density p_a (cm^3) (Jacques and Prahl 1998)

Equation 6.18 hold true for survival of photon irrespective of whether path followed by photon is straight or irregular due to multiple scattering (Jacques and Prahl 1998).

But $\mu_a = \varepsilon.c \ln(10)$, ... (6.19)

Where μ_a with units (cm^{-1}) are inverse for length, such that $\mu_a L$ is dimensionless and L (cm) is photon's path length travelled through the medium. The fraction of photon absorbed by sample, *f* is a ratio of the absorbed photon flux W_{abs} to the incident photon flux W_e, which equals 1-T (equation 6.15). That is;

$\frac{Wabs}{We}$ = 1 - T, and T= $\exp(-\mu_a L)$, therefore. Bearing in mind that not all photons are absorbed.

$$\frac{Wabs}{We} = 1 - \exp(-\mu_a L) \quad \text{.... (6.20)}$$

Where W_{abs} = The absorbed photon flux (μEinstein m^{-2} s^{-1})

W_e = The photon flow entering the reactor (μEinstein m^{-2} s^{-1})

L = Photon's path travelled in medium (cm) same the thickness of water column in the reactor.

μ_a = The absorption coefficient (cm^{-1}). This is simply the cross sectional area per unit volume of medium. It describes a medium containing many chromophores at a concentration described as a volume density p_a (cm^3) (Jacques and Prahl 1998).

To calculate the photons absorbed by the absorbing species in the reaction, the measured irradiance (mW/cm^2) which was obtained using a radiometer had to be converted to photon flux (μEinstein m^{-2} s^{-1}). The photon flux, also called quantum flux is defined as the number of photons in µmol per second and unit area on a surface. This has been calculated below.

6.7.6 Radiometric Calculations

6.7.6.1 Conversion of measured Irradiance to Photon flux

According to Stark-Einstein's law, "each molecule of absorbing substance, absorbs one photon of radiation in the process". Therefore:

A molecule acquires energy by absorbing a photon: $A + hf \rightarrow A^*$

Where A* is the excited state of A, and hf is energy absorbed.

Thus, energy of a photon is $E_p = hf$ … (6.21)

But $f = C/\lambda$, $\therefore Ep = h.(\frac{C}{\lambda})$ …(6.22)

Where planks constant h= 6.63 x 10^{-34} (Js), speed of light C = 2.998 x 10^{8} (m/s), frequency, f has units (1/s), and wavelength λ, (m).

Number of photons N_p is given by;

$N_p = E/E_p$ … (6.23)

Where E is the measure irradiance in (W/m^2) and Ep is the energy of the photon (equation 6.17)

$$N_p = \frac{E*\lambda*10^{-9}}{h*c} \quad \text{… (6.24)}$$

$= E.\lambda .10^{-9}\,(m)/h.C\,(Jm^{-1})$

$= E.\lambda.5.03 \times 10^{15}\,(J^{-1})$

(The irradiance E used for this study was 2.66mW/cm^2 (2.66 x 10^{-3} W/cm^2) and λ of radiation was 253.7 nm).

∴ N_p = 2.66 x 10^{-3} *253.7* 5.03 x 10^{15}

= 3.394 x 10^{13} m^{-2} s^{-1}

6.7.6.2 Determination of Photon Flux entering the reaction (W_e)

The photon flux or Quantum flux was determined as follows;

$E_{QF} = N_P/N_A$, … (6.25)

Where N_A is Avogadro's number (6.022 x 10^{23} mol-^{1}) and N_p is number of photons (equation 6.20).

∴ E_{QF} = 3.394 x 10^{13} m^{-2} s^{-1} / 6.022 x 10^{23} mol^{-1}

Total photon flux entering reaction E_{QF} = *We* =0.56 x 10^{-10} mol m^{-2} s^{-1}

Einstein = mole of photons

µEinstein m^{-2} s^{-1} = µmoles m^{-2} s^{-1}

∴ E_{QF} = 0.56 X 10^{-4} µEinstein m^{-2} s^{-1}

To estimate the photons absorbed by the various species of reactants, the following considerations and assumptions were made;

- In view of the operating wavelength of radiation, which was monochromatic at 253.7 nm, the main absorbing species in the reaction was 3,5-DMP which absorbs from 305 to about 180 nm (Figure 6.2) and H_2O_2. Hydrogen peroxide is thought to absorb throughout the UVC region (see Figure 6.15) and increases in absorbance as you move towards smaller wavelength in the UVC band from 300nm (Beers and Sizer 1951; USP Technologies 2016). Holts et al., (1948) also noted that hydrogen peroxide absorb from visible region and increases towards the UV region right up to about 200 nm.

- The Fe^{3+} catalyst is expected to perform a dual function; absorb radiation if the wavelength is suitable and hence undergo a faster reduction to Fe^{2+}, or attenuate the photon flux by decreasing penetration and increasing scattering (Belatter et al., 2012). Photocatalysts are generally thought to possess high reactivity using wavelengths of light in the region of 380 nm < λ < 500 nm (Ibhadon and Fitzpatrick 2013). Fe^{3+}, which is the reactive constituent of the present catalyst, is thought to absorb weakly at > 300 nm (Machulek et. al., 2012). Stuglik and Zagorski (1980) reported an absorption maxima (λ_{max}) of 300 nm for $Fe(OH)^{2+}_{(aq)}$, which is the photoactive Fe specie, it is not clear if $Fe(OH)^{2+}$ is present in the catalyst.

- This is likely to be a reaction system of conventional Fenton and UV photolysis of H_2O_2 and H_2O happening simultaneously, but independently, rather than a photocatalysis, initiated through the known Fe^{3+} reduction to Fe^{2+}, facilitated by UV radiation.

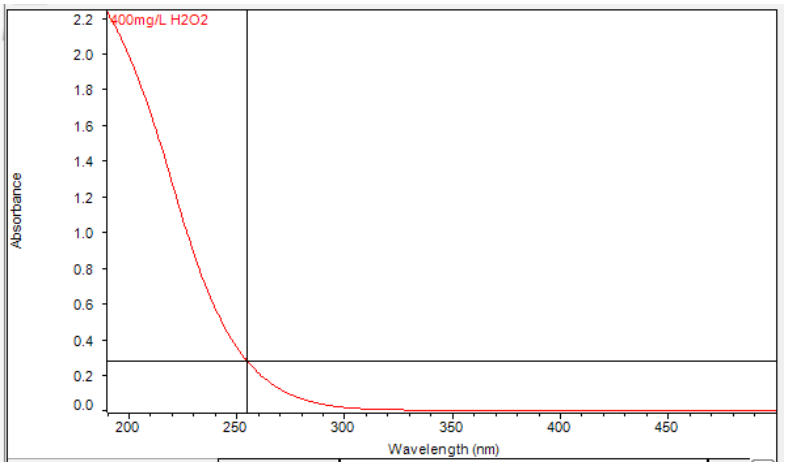

Figure 6.14: Absorbance spectrum of 400 ppm H_2O_2 in water.

6.7.6.3 Determination of photon flux absorbed by DMP and H_2O_2

To determine photon flux absorbed by 25 mg/L DMP we apply equation (6.20);

$$\frac{Wabs}{We} = 1 - \exp(-\mu_a \mathrm{L})$$

Where W_{abs} is absorbed photon flux, W_e is photon flux entering the reactor, μ_a is absorption coefficient and L is path length of the radiation in the reacting solution. To find the absorption coefficient μ_a, we have that:

$\mu_a = Ɛ.c \ln(10)$, (from equation. 6.19)

But to find the extinction coefficient Ɛ, we have that;

$A_\lambda = ƐcL$ (from equation 6.16,)

Where c is the molar concentration and L is 1 cm cell path and $A\lambda$ is the measured absorbance 0.142 at 253.7 nm for this reaction. The molar concentration of 25 mg/L DMP was calculated as 2.04×10^{-4} mol/L

Hence, 0.142 = Ɛ * 2.04 x 10^{-4} * 1

Ɛ = 696.08 cm^{-1} mol^{-1} L

∴, to find the absorption coefficient μ_a, from equation (6.19) we have that:

μ_a=Ɛc ln(10)

μ_a = 696.08 * 2.04 x 10^{-4} *ln(10)

μ_a = 0.33 cm^{-1}

To find the absorbed photon flux W_{abs} from equation (6.20) where *We* (E_{QF}) which is total photon flux entering the reaction has been calculated as 0.56 x 10^{-4} μEinstein m^{-2} s^{-1} we have that:

$$\frac{Wabs}{We} = 1 - \exp(-\mu_a L)$$

W_{abs} = 0.56 x 10^{-4} (1- exp (-0.33))

=0.1574 x 10^{-4} μEinstein m^{-2} s^{-1}

To find the absorption coefficient μ_a for H_2O_2 at 253.7 nm given by:

μ_a=Ɛ.c. ln(10), but extinction coefficient at 253.7nm is given by A_λ = ƐCL, hence Ɛ= A_λ/cL, where measured absorbance of H_2O_2 at 253.7 nm was 0.253 and molar concentration of 400 ppm H_2O_2 used in this reaction is 400/34 = 11.765 mmole/L.

Hence,

Ɛ= A_λ/cL

Ɛ = 0.253/0.01176

21.5 cm^{-1} $mole^{-1}$ L

Hence, to calculate the absorption coefficient μ_a, we have that:

$\mu_a = \text{Ɛ.c.L. ln(10)}$

$\mu_a = 21.5 * 0.01176 * 1 * 2.3$

$= 0.58\ cm^{-1}$

∴, to find the amount of photon flux absorbed by H_2O_2 in reaction system:

$$\frac{Wabs}{We} = 1 - \exp(-\mu_a L)$$

$W_{abs} = 0.56 \times 10^{-4} (1 - \exp(-0.58))$

$= 0.2465 \times 10^{-4}\ \mu Einstein\ m^{-2}\ s^{-1}$

Table 6.6: Photon flow entering the reactor and photon flow absorbed

Compounds	**ε ($cm^{-1}M^{-1}$)**	**μ_a (cm^{-1})**	**W_e (μEinstein $m^{-2}\ s^{-1}$)**	**1-exp(-μ_aL)**	**W_{abs} (μEinstein $m^{-2}\ s^{-1}$)**
3,5-DMP	696.08	0.33	0.56×10^{-4}	0.28	0.1585×10^{-4}
H_2O_2	21.50	0.58	0.56×10^{-4}	0.44	0.2482×10^{-4}

The molar extinction coefficient (ε) of DMP at 254 nm is not available in literature, Belattar et al., (2012) calculated this to be 1550 $cm^{-1}\ M^{-1}$ at 272 nm, while values of ε for H_2O_2 at 254 nm in literature are between 19.6 to 27.06 $cm^{-1}\ M^{-1}$ (Giri et al., 2011; Lay 1989). This slight variation in the determined values of ε is as a result of the variation in the degree of purity and standardization methods of commercial H_2O_2. The photon flow absorbed by DMP and H_2O_2 in Table 6.10 corresponds to the absorbed energy at initial

time when DMP and H_2O_2 concentrations were at maximum. It is obvious from the results that at 253.7 nm, only a little over a quarter of the photon flow was absorbed by DMP and this explains why photolysis of the compound resulted in only slight degree of degradation. H_2O_2 on the other hand absorbed almost half of the photon flow entering the reactor, which resulted in a higher degree of photolysis, leading to the release of reactive intermediates, the OH radicals. This is evident in the greater loss of DMP when both UV + H_2O_2 are present, as a result of increased OH radical formation as shown in Figure 6.14.

6.8 Effect of Coupling UV radiation to Heterogeneous Fenton Catalytic Oxidation of Synthetic Produced Water

This section focuses on the effect 0f UV assisted Fenton on produced water (Figure 6.12 A and B). 'A' shows the initial concentrations while 'B' shows the final concentrations of assessed parameters namely COD, DMP and OIW after UV exposure using 1000 ppm H_2O_2, which was then compared to similar experiments using 400, 1000 and 2000 ppm H_2O_2 in unassisted Fenton oxidation.

Figure 6.15 shows COD reduction of 110 mg/L from 763 mg/L using 400 ppm H_2O_2 initial concentration, which constitutes 14.4% COD loss. The loss of DMP for the same concentration of H_2O_2 was 92% while OIW recorded a total removal of 66.4%, with a desorbed OIW concentration of 86 mg/L recovered from the catalyst after reaction. Real net oxidation of OIW was therefore only 17 mg/L (10.96%).

The sluggishness of the overall oxidation process using 400 ppm of H_2O_2 suggested that H_2O_2 was limiting in the reaction system, as this batch-optimised value (400 ppm) for

DMP degradation was less that the stoichiometric peroxide demand for the PW reaction system. From equation 5.31, $2H_2O_2 = 2H_2O + O_2$. Therefore, the amount of O_2 (moles) required for the measured COD is given as:

Moles of O_2 required = $\frac{COD\ (mg/L)}{Molar\ mass\ of\ O2\ (g/mol)} \frac{766}{32} = 23.9$

This indicates that the complete mineralization of synthetic produced water with measured sample COD = 766 mg/L, requires 25 moles of O_2

From equation 5.31, 2 moles of H_2O_2 follows that;

$2H_2O_2$ (mg/L) = 2 * O_2(moles) * 34 * 23.9 = 1625.2

Hence COD of 766 mg/L (determined from produced water sample), requires 1625.2 mg/L H_2O_2.

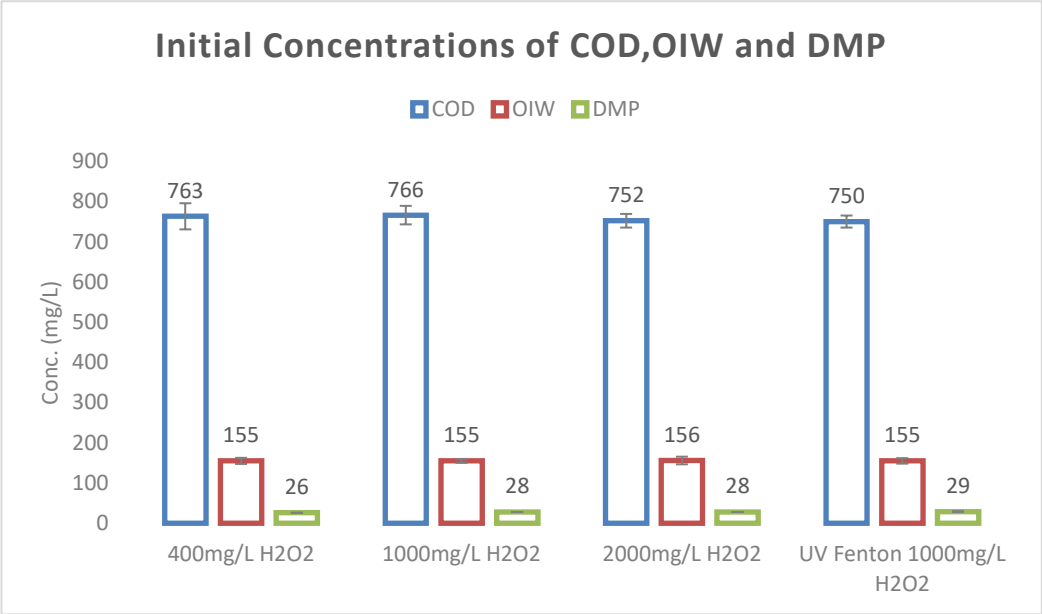

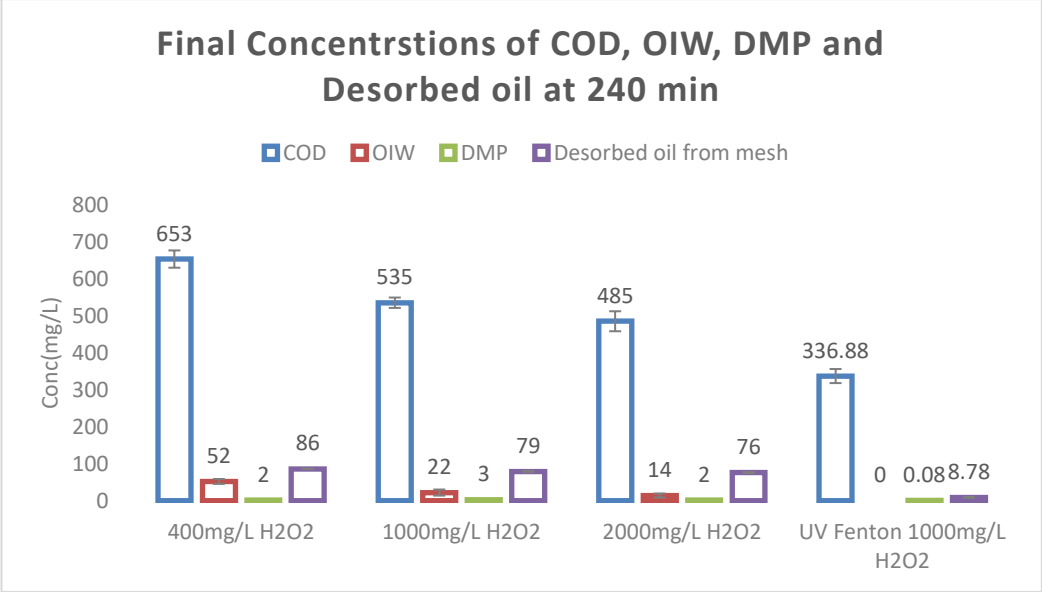

Figure 6.15: Effect of H_2O_2 concentration on the loss of COD, OIW and DMP in synthetic produced water. Initial DMP 26-29 mg/L, Initial OIW conc 155 – 156 mg/L, initial COD 750 – 766 mg/L, pH3, H_20_2 400 -2000 ppm, reaction vol 200 mL, catalyst 10 g, T = 25±1 ^oC, t = 240 and irradiance 2.66 mW/cm^2.

For the produced water degradation reaction, using 1000 ppm H_2O_2 in unassisted Fenton catalysis, there was 30.16% COD removal, 89.29% DMP loss and 85.81% OIW removal with a recovery of 79.0 mg/L oil recovered from the catalyst by desorption. Although limited COD removal was achieved, DMP removal was very good. This is

because, the H_2O_2 concentration of 1000 mg/L did not appear to be limiting in the system given that the chemical oxygen demand was measured as about 750 – 766 mg/L. The results in terms of concentrations are as shown in Tables 6.6 to 6.10. The reaction system using 2000 ppm H_2O_2 did not show significant difference from that using 1000 ppm, which suggest that the H_2O_2 was in excess.

Table 6.7: Percentage removal of COD, DMP and OIW at 400 ppm H_2O_2

	400 ppm H_2O_2				
	Initial Conc.	**Final Conc.**	**Total Removal**	**% Removal**	**Desorbed Amount**
COD (mg/L)	763	653	110	14.4	N.A
DMP (mg/L)	26	2	24	92.3	N.A
OIW (mg/l)	155	52	103	66.4	86

Table 6.8: Percentage removal of COD, DMP and OIW at 1000 ppm H_2O_2

	1000 ppm H_2O_2				
	Initial Conc.	**Final Conc.**	**Total Removal**	**% Loss**	**Desorbed Amount**
COD (mg/L)	766	535	231	30.16	N.A
DMP (mg/L)	28	3	25	89.29	N.A
OIW (mg/l)	155	22	133	85.81	79

Table 6.9: Percentage removal of COD, DMP and OIW at 2000 ppm H_2O_2

	2000 ppm H_2O_2				
	Initial Conc.	**Final Conc.**	**Total Removal**	**% Loss**	**Desorbed Amount**
COD (mg/L)	752	485	267	35.5	N.A
DMP (mg/L)	28	2	26	92.85	N.A
OIW (mg/l)	156	14	142	91.03	76

Table 6.10: Percentage removal of COD, DMP and OIW at 1000 ppm H_2O_2 + UV-Fenton (2.66 mW)

	UV-FENTON 1000 ppm H_2O_2				
	Initial Conc.	**Final Conc.**	**Total Removal**	**% Loss**	**Desorbed Amount**
COD (mg/L)	750	336.88	383.12	51.08	N.A
DMP (mg/L)	29	0.08	28.92	99.72	N.A
OIW (mg/l)	155	0	155	100	8.78

Table 6.9 shows the Fentons's reaction of synthetic produced water using 1000 ppm H_2O_2 assisted by 2.66 mW UV radiation in batch mode. There was a significant increase in the extent of treatment notable in the more extensive reduction and OIW removal in comparison to the non-coupled systems catalysed at various concentrations of H_2O_2. This is as a result of the simultaneous photolysis of both the organics in the reaction and increased hydroxyl radical formation due to photolysis of H_2O_2 and $Fe(OH)^{2+}$ as noted in section 6.7.3.

6.9 Results for Continuous flow experiments

These experiments were set up as previously described in section 6.6.4. Figures 6.15 to 6.20 shows the variation of DMP, COD and Oil in water (OIW) using 180 g or 120 g catalyst as the case may be, over the experiment duration stated in the graph legend, using fresh catalyst on each phase of reaction. The removal percentage have also been summarised in Tables 6.11 to 6.13 in terms of catalyst load and percentage degradation. All reactions unless otherwise stated were carried out under room temperature. In the control experiment (A) the reaction solution was passed through the system without catalyst and without any treatment initiated in the reaction system for 20 h.

The next phase was exposure to UV only, labelled control (B) in Figure 6.16a for 26 h. This was followed by exposure of reaction solution to microwave (MW) and H_2O_2 alone in the presence of the catalyst. The reaction was then exposed to the catalyst, H_2O_2 and UV radiation and finally the experiment was carried out in the presence of UV, microwave, H_2O_2 and catalyst, changing the catalyst to fresh catalyst after each phase of experiment. The results have been presented in Figures 6.16 to 6.21.

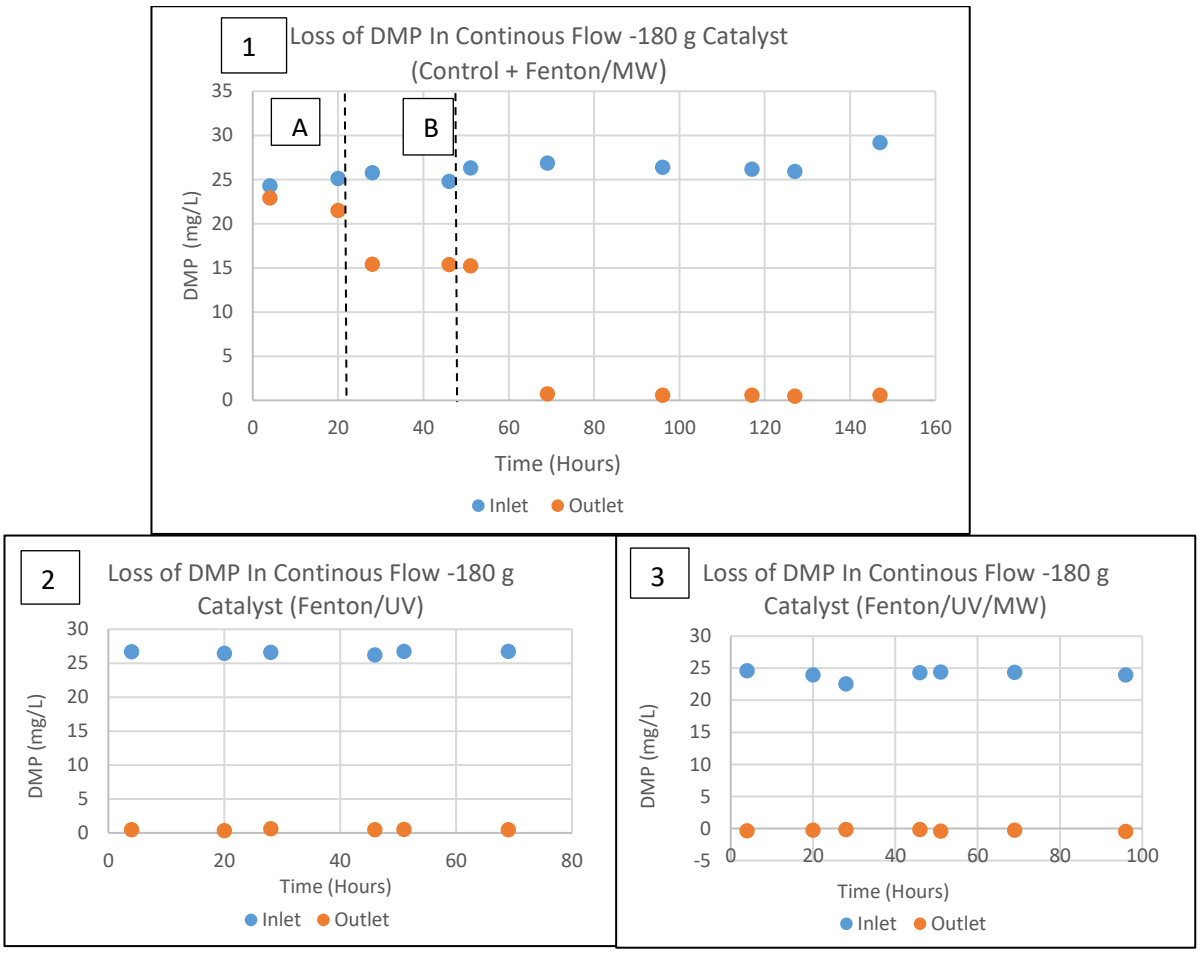

Figure 6.16: Loss of DMP in synthetic produced water. Reaction times: Control experiment A (empty wheels only) 20 h, control experiment B (UV only) 26 h, Fenton/MW 96 h, Fenton/UV 70 h, Fenton/UV/MW 95 h in continuous flow reaction using a rotating disc reactor, with a modified PAN heterogeneous catalyst and 1000 mg/L H_2O_2, 180 g catalyst pH3, residence time of 4 h 55 min, avg. irradiance of 500 µW, 600 W MW power, at 35 °C, non-MW assisted at room temperature (~ 18 -23 °C).

For 180 g catalyst load (Figure 6.16a) the control experiment B (UV only) showed 40% maximum loss of DMP, while control experiment A (empty wheels) showed only 11.5% loss of DMP, which although is consistent with sorption of DMP in batch work, shown previously in chapter three, may be due to poor mixing due to the absence of a catalyst on the discs. There was no remarkable advantage of UV assisted Fenton over UV/MW assisted Fenton. This is likely due to the reactor design. The angle of incidence of the UV irradiance on the reaction was less than 50 degrees resulting in very low irradiance

impinging on the reaction surface. Measured irradiance on the reaction surface averaged only about 500 μW/cm^2. The reaction of UV/MW assisted Fenton reaction recorded slightly better degradation of DMP under the given conditions as shown in Figure 6.15 (2). This suggests that, a higher irradiance intensity would have resulted in a faster reaction according to Stark-Einstein law: "Number of activated molecules = number of quanta of radiation absorbed".

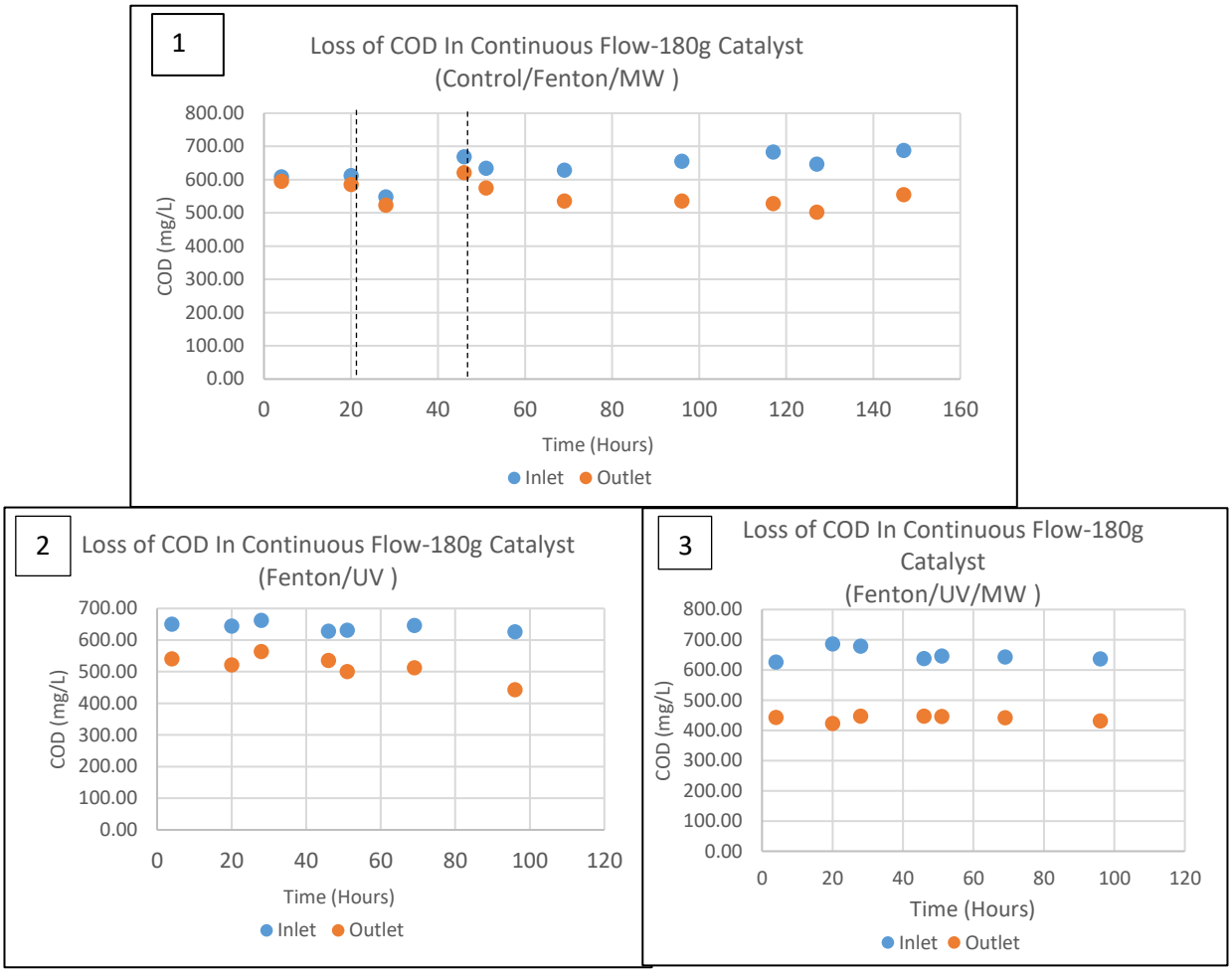

Figure 6.17: Loss of COD in synthetic produced water. Reaction times: Control experiment A (empty wheels only) 20 h, control experiment B (UV only) 26 h, Fenton/MW 96 h, Fenton/UV 70 h, Fenton/UV/MW 95 h in continuous flow reaction using a rotating disc reactor, with a modified PAN heterogeneous catalyst and 1000 ppm H_2O_2, 180 g catalyst pH3, residence time of 4 h 55 min, avg. irradiance of 500 µW, 600 W MW power, at 35 °C, non-MW assisted at room temperature (~ 18 -23 °C).

For COD (Figure 6.17), the effect of dielectric heating using microwave radiation on the Fenton process was similar to effect of UV on the Fenton-like process. UV assisted Fenton is thought to have more positive influence on reaction rates than microwave assisted Fenton process (Gromboni et al., 2007), however in this case where UV/Fenton is not as expected, it is likely due to the low irradiance due to the experimental set-up. There is a slight enhancement in using UV/MW/Fenton.

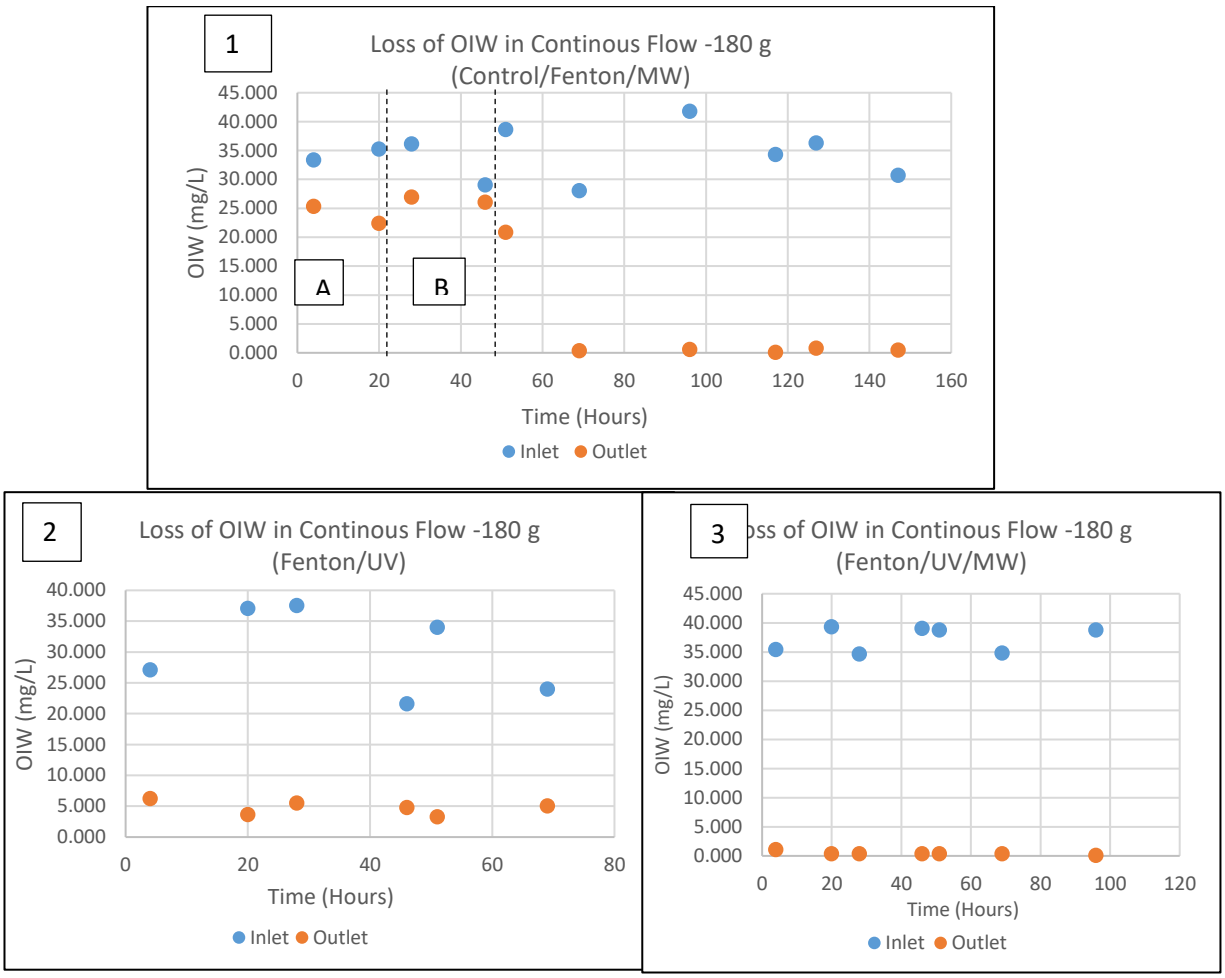

Figure 6.18: Loss of OIW in synthetic produced water. Reaction times: Control experiment A (empty wheels only) 20 h, control experiment B (UV only) 26 h, Fenton/MW 96 h, Fenton/UV 70 h, Fenton/UV/MW 95 h in continuous flow reaction using a rotating disc reactor, with a modified PAN heterogeneous catalyst and 1000 ppm H_2O_2, 180 g catalyst pH3, residence time of 4 h 55 min, avg. irradiance of 500 µW, 600 W MW power, at 35 °C, non-MW assisted at room temperature (~ 18 -23 °C).

The OIW degradation using 180 g of catalyst was better with MW /Fenton Figure 6.18(1) than with UV/Fenton 6.18(2), however in both cases the outlet was below regulatory limits for both inland and offshore discharge limits. A combination of UV/MW/Fenton process did not show a clear difference from the MW/Fenton, indicating that the irradiance intensity was low as already suggested. This also suggested that the system

required optimization. Accordingly, the catalyst load was reduced from 180 g to 120 g, to evaluate the efficiency of the system at lower catalyst load.

The results in Figures 6.17 to 6.20 were obtained from 120 g catalyst load for loss of DMP, COD and OIW and followed a similar trend as 180 g loaded discs. Whilst there was a slight reduction in the % of loss of DMP and COD, however, the overall final results for the 120 g catalyst were efficient. OIW does not seem to have been affected by the reduction in catalyst load, where as DMP and COD are with slightly less removal. This is perharps because OIW dominates the system and goes onto the wheels, preventing DMP and COD from interacting with the reagents in the system. This may have been exacerbated with reduced number of wheels. Coupling UV and MW to the Fenton reaction can also results in costs savings from the amount of catalyst used in the reaction.

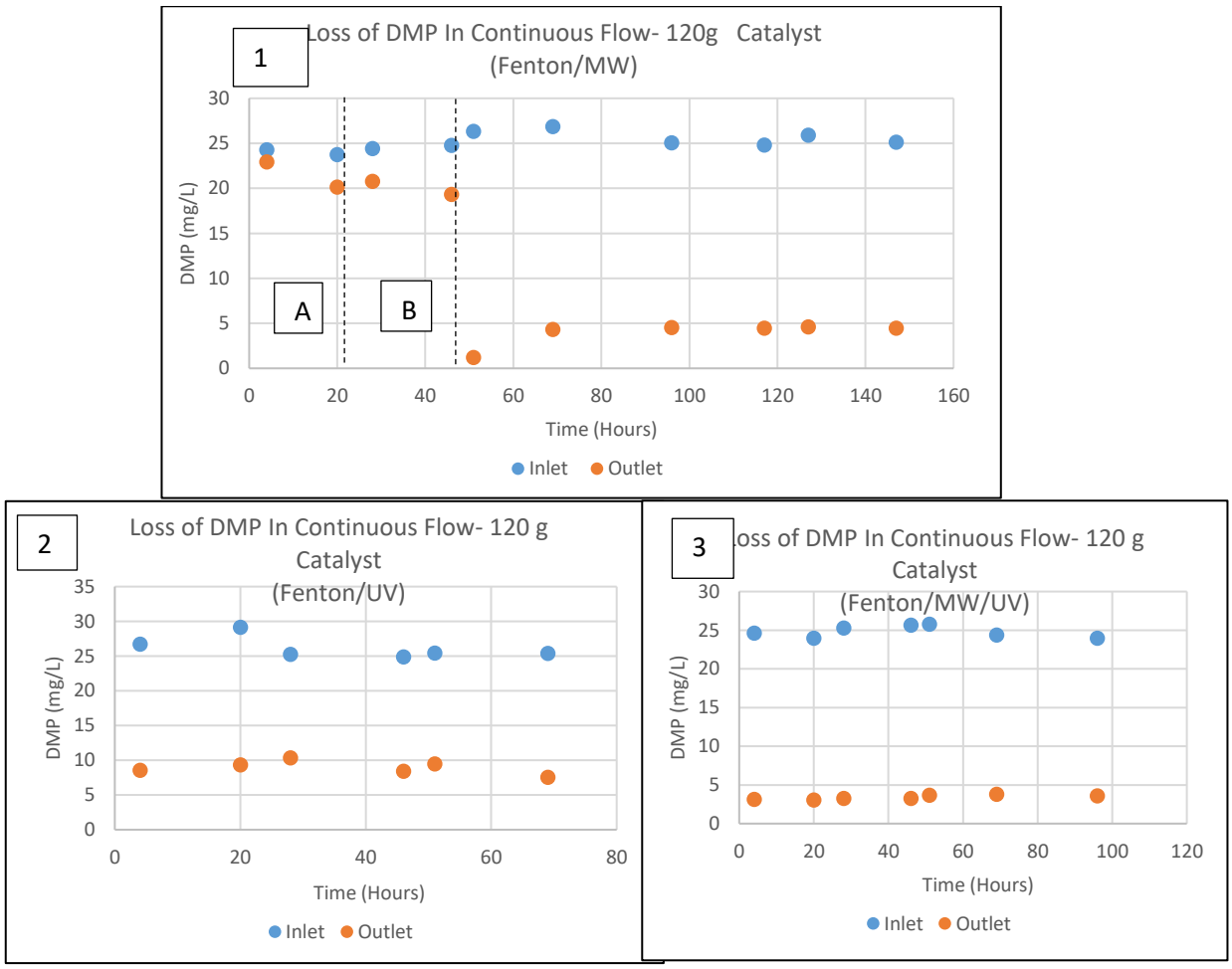

Figure 6.19: Loss of DMP in synthetic produced water. Reaction times: Control experiment A (empty wheels only) 20 h, control experiment B (UV only) 26 h, Fenton/MW 96 h, Fenton/UV 70 h, Fenton/UV/MW 95 h in continuous flow reaction using a rotating disc reactor, with a modified PAN heterogeneous catalyst and 1000 ppm H_2O_2, 120 g catalyst pH3, residence time of 4 h 55 min, avg. irradiance of 500 µW, 600 W MW power, at 35 °C, non-MW assisted at room temperature (~ 18 -23 °C).

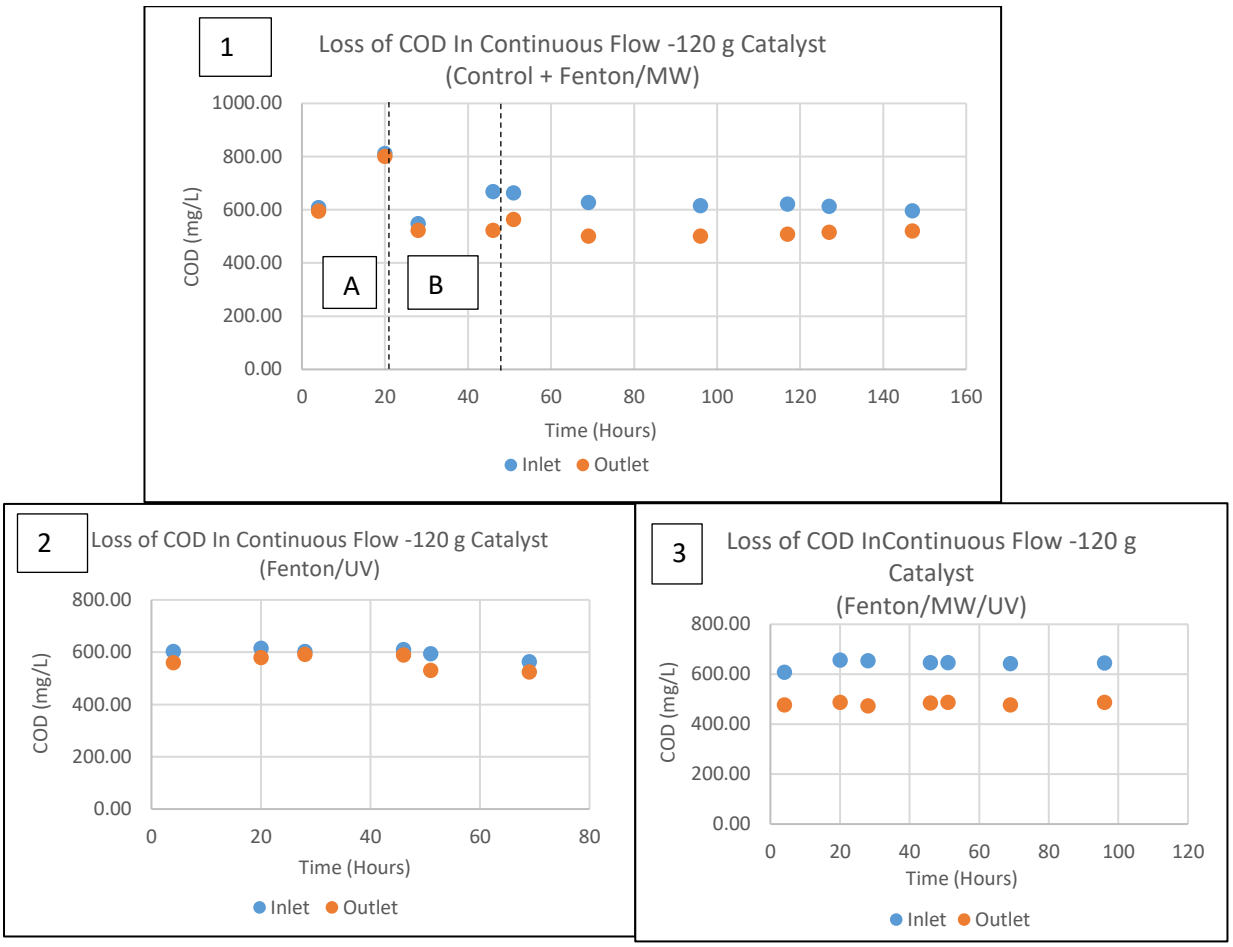

Figure 6.20: Loss of COD in synthetic produced water. Reaction times: Control experiment A (empty wheels only) 20 h, control experiment B (UV only) 26 h, Fenton/MW 96 h, Fenton/UV 70 h, Fenton/UV/MW 95 h in continuous flow reaction using a rotating disc reactor, with a modified PAN heterogeneous catalyst and 1000 ppm H_2O_2, 120 g catalyst pH3, residence time of 4 h 55 min, avg. irradiance of 500 µW, 600 W MW power, at 35 °C, non-MW assisted at room temperature (~ 18 -23 °C).

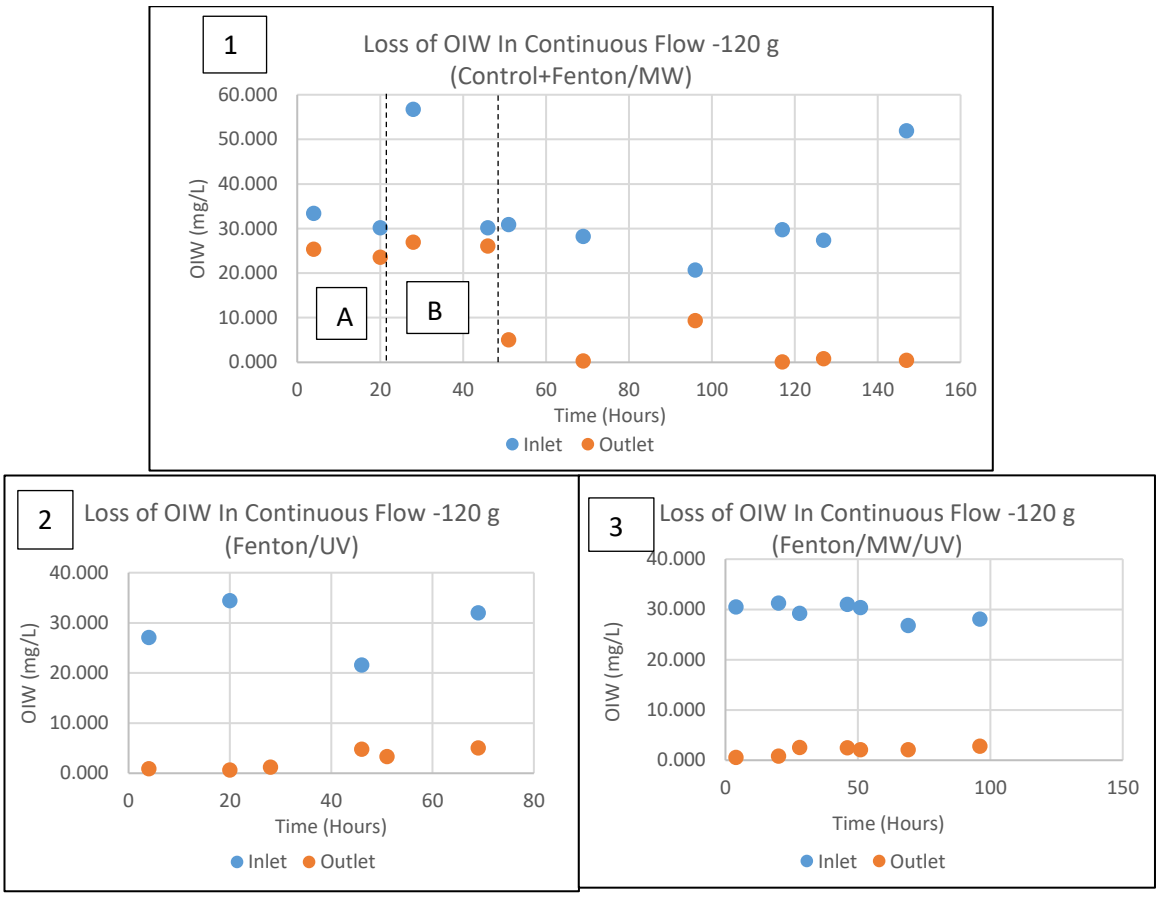

Figure 6.21: Loss of OIW in synthetic produced water. Reaction times: Control experiment A (empty wheels only) 20 h, control experiment B (UV only) 26 h, Fenton/MW 96 h, Fenton/UV 70 h, Fenton/UV/MW 95hrs in continuous flow reaction using a rotating disc reactor, with a modified PAN heterogeneous catalyst and 1000 ppm H_2O_2, 120 g catalyst pH3, residence time of 4 h 55 min, avg. irradiance of 500 µW, 600 W MW power, at 35 °C, non-MW assisted at room temperature (~ 18 -23 °C).

Table 6.11: DMP (mg/L) Reduction

		Treatment system				
	No treatment	**UV alone**	**Catalysis***	**MW/Catalysis**	**UV/Catalysis**	**UV/MW/Catalysis**
	A	**B**		**C**	**D**	**E**
180 g catalyst	5-15%	40%	>99%	>99%	>99%	>99%
120g catalyst	5-15%	(40%)		84%	60%	88%

***over duration of treatment of 150 h

Table 6.11 shows the percentage loss of DMP in 180 g catalyst and 120 g of catalyst load. For UV system, the loss was 40% for both 180 and 120 g of catalyst, however this increased to over 99% when this was coupled to either of normal Fenton, microwave Fenton or both for 180 g catalyst, this was not the case for 120 g catalyst load. UV/Catalysis especially showed the least loss %, of 60, due to the poor irradiance transmitted into the reactor as previously mentioned.

Table 6.12: OIW (mg/L) Reduction

		Treatment system				
	No treatment	**UV alone**	**Catalysis***	**MW/Catalysis**	**UV/Catalysis**	**UV/MW/Catalysis**
	A	**B**		**C**	**D**	**E**
180 g catalyst	22-37%	10-45%	60-85% (av~66%)	>99%	84%	>99%
120 g catalyst	13-20%	13-83%		>92%	85%	>91%

***over duration of treatment of 150 h

The loss of OIW however was not so sensitive to the reduction in the catalyst load down to 120 g, compared to DMP, although a difference of about 7 to 8% was recorded for MW and UV/MW/Catalysis. UV/catalysis showed no difference in loss with reduction in

catalyst load. This is could be because the oils dominate the sorption process, and because they stick on the wheels, they are more exposed to the UV radiation which is perpendicular to the wheels, and hence better exposed to UV effect.

Table 6.13: COD (mg/L) Reduction

		Treatment system				
	No treatment	**UV alone**	**Catalysis***	**MW/Catalysis**	**UV/Catalysis**	**UV/MW/Catalysis**
	A	**B**		**C**	**D**	**E**
180 g catalyst	4%	5-7%	9-28% (av~16%)	15%	15%	31%
120 g catalyst	2%	3-15%		14%	5%	25%

*over duration of treatment of 150 h

UV however played a prominent role in the scheme of things with respect to COD. There was 5% loss COD when catalyst load was reduced to 120 g, which made it the most significant loss in terms of COD change response to catalyst load. MW had an insignificant 1% change in loss as the catalyst was reduced, while UV/MW/catalysis recorded 4% change in loss due to reduction in catalyst load. Over all, the MW and UV contributed equally to the coupled system ~15% each, making a total COD loss of 31%, while in the 120 g system, the MW contributed 9% more than the UV, giving total COD loss of 25% in 120 g catalyst. This observation could be due to increased sorption of even hard COD (mainly acetic acid) due to increased catalyst load.

6.10 Summary

There is limited literature on the use of UV- Heterogeneous Fenton oxidation for the treatment of produced water. However, the application holds great promise for the simultaneous removal of alkylated phenols as well as oils (aliphatic and aromatic fractions) in oil mining produced water.

The coupling of UV radiation to conventional Fenton considerably reduces the amount of H_2O_2 used by four folds, while still reducing the reaction time by another four folds. This is a huge cost savings in terms of H_2O_2, and reactor footprint, which is the single most cost intensive element in Fenton processes.

Coupling MW to UV/Fentons is shown to improve the removal of COD and OIW in continuous flow. The coupled technology appear to be a simultaneous advanced oxidation process of UV-photolysis and conventional Fenton- like process happening independent of each, rather than photocatalysis of the PAN heterogeneous mesh as previously thought. On the possible contribution to the redox activity (from Fe^{3+} to Fe^{2+}), there is little evidence since $Fe(OH)^{2+}$, absorbs above 300 nm (if indeed this is present in the mesh during reaction). A polychromatic UV source, with wavelengths extending to the UVA region is recommended for further studies.

The final chapter is the conclusion and recommendation for further work and other perspectives on the application of UV/MW/Fenton assisted catalysis of produced water.

7 Conclusion and Perspectives

7.1 Conclusion

This work has shown that the menace resulting from oil and gas mining activity is a potent one and can lead to grave environmental and health consequences if not properly managed through appropriate legislation and the deployment of suitable treatment techniques/methods.

It has also demonstrated that the application of Fenton-like catalysis using a modified PAN heterogeneous catalyst has been effective for the oxidation of alkylphenol in water as well as in simulated produced water whilst still simultaneously degrading other dissolved organic compounds in the process such as oil-in-water. The influence of inorganic anions on the oxidation process, namely; Cl^- and HCO_3^- (which are known radical scavengers) have been investigated and based on their concentrations used in the present work, 90% removal of both DMP and OIW was still feasible.

Oxidation intermediates arising from this process, which are also susceptible to the oxidation process (except acetic acids), have been tentatively identified. These include two organic acids (acetic and formic) and five hydrocarbon compounds, some of which are benzoquinones, hydroquinones and benzaldehydes.

The use of one factor at a time (OFAT) approach for process parameters optimization showed that pH was the most important process parameter under the defined experimental conditions. The parameters considered in the decomposition of 25 mg/L DMP were; catalyst concentration, initial H_2O_2 concentration and pH of reaction solution for the heterogeneous oxidation process. In addition to this, this work also demonstrated that the treatment system is driven by a heterogeneous process, which

is evident as only 12% loss of DMP was achieved by the use of homogeneous the equivalence of the concentration of leached iron from the catalyst.

The degradation of DMP in the small continuous flow vertical reactor which had a mesh to liquor ratio of 1: 15, and a total volume flow of about 24.2 L over about one month duration resulted in the decomposition of 282.08 mg of DMP using about 12.5 g of catalyst in 200 mL reactor volume. This resulted in 0.8588 yield degree with only 13.16% loss of iron in the catalyst after about one month of treatment, which demonstrates the durability of the catalyst system with respect to the DMP as substrate. The 900 mL rotating contacting flow reactor used for the degradation of produced water was catalyst-heavy with a mesh to liquor ratio of 1:5, which is about 3 times the catalyst load of the 200 mL vertical flow reactor in relative terms and hence, the total iron loss in the 900 mL reactor was far more (42.72%) than in the vertical reactor. The total mass of oxidizable organic compounds which made up the produced water (DMP, hexadecane, tridecane and BTEX) decomposed in this reactor was 10.79 kg compared to just 282.08 mg and this does not include acetic acids, which although present, was recalcitrant to the oxidation process as demonstrated by COD results. It is possible that some of the compounds present in the PW soup had chelating properties. Also the total volume of produced water treated in 29.5 days was about 154 L compared to just 24 L of DMP treated by the smaller reactor. This explains why the percentage loss of iron in the big reactor was 3.2 folds more than obtained in the smaller reactor. In addition to this, the catalyst used in both reactors were of different production batches, suggesting that this may not be a fair comparison.

Most treatment methods for produced water currently in use are able to remove the oils (both aromatic and aliphatic), however, most dissolved organic components that partition into the water phase, some of which are the main toxicants in the produced water, such as alkylphenols, (which are known endocrine disruptors), remain untreated. This study has demonstrated that the application of a novel modified PAN heterogeneous catalyst in H_2O_2 system is capable of simultaneous removal of about 90% DMP (about 3961 mg) and about 50% OIW using 180 g catalyst and a constant initial H_2O_2 concentration of 1000 ppm in the 900 mL continuous flow treatment of produced water. The average COD removal for this system in the presence of acetic acid was about 10% but more than 50% in the absence of acetic acid. It has been established that the most recalcitrant component to Fenton-like oxidation in produced water is acetic acid. This is difficult to oxidize in the moderate Fenton reaction conditions such as used in this study.

There is limited literature on the use of UV- Heterogeneous Fenton oxidation for the treatment of produced water. This work has demonstrated that coupling UV radiation and conventional Fenton processes greatly enhances the simultaneous removal of alkylated phenols and oils (aliphatic and aromatic fractions) in oil mining simulated produced water. COD removal was increased from 10 to 15%, DMP removal was increased from about 90 to > 99% and OIW removal was increased from about 50 to 84% using about 4 h retention time. The UV/Fenton coupled technology is most probably a simultaneous advanced oxidation process of UV-photolysis and conventional Fenton- like process occurring separately, and resulting in an additive enhancement, rather than photocatalysis involving an unknown iron species on the PAN

heterogeneous mesh as previously thought. On the possible contribution to the photocatalytic redox activity (from Fe^{3+} to Fe^{2+}), there is little evidence since $Fe(OH)^{2+}$ though to be the photoactive species in the homogeneous system, absorbs above 300 nm and only UVC lamps with wavelength of 254 nm were used in this work.

Enhancing the conventional Fenton treatment system with microwave radiation showed similar effects as enhancement with UV. Enhancing the conventional Fenton system with both UV and MW together resulted in 31% COD removal, > 99% DMP removal and > 99% OIW removal. In addition to this, the batch process involving UV/Fenton demonstrated a fourfold reduction in the amount of H_2O_2 requirement, thus saving cost on H_2O_2 (which is the single most expensive component in Fenton catalysis).

7.2 Recommendations and Further work

The following recommendations and suggestions for further research into the simultaneous oxidation of alkylphenols and other dissolved organics in produced water are offered:

- With respect to oxidation intermediates tentatively identified in this study, namely: 3,5-dimethyl catechol (peak 2), 3,5-dimethyl hydroquinone (peak1), and 3-hydroxymethyl-5-methylphenol (B1 to B3 in Figure 4.31) are all possible isomers of 138 M^+ peaks, while 3-carbaldehyde-5-methyl-1,2-benzoquinone, 3-methyl-5-carbaldehyde-1,2-benzoquinone, 3-methyl-4-carbaldehyde p-benzoquinone or 3,5-dicarbaldehyde hydroxybenze also possible isomers of peak M^+ 150. In addition, 3-methyl-4,5-benzoquinone carboxylic acid, p-benzoquinone-3-methyl-4-carboxylic acid and 3-carbaldehyde (hydroxybenzene) carboxylic acid are all possible isomers of 166 M^+ peak. These compounds are not presently commercially available. It is therefore recommended that these compounds be synthesized to enable confirmatory tests using LC/GC MS-MS. The MS-MS fragmentation pattern for the various isomers will differ, allowing identification of the molecular ions and hence the isomer.
- There are indications from continuous flow studies that catalytic activity was starting to tail after one month of treatment. The precise cause of catalyst deactivation was suspected to be one or more of the following: loss of iron through leaching, possible blockage of catalyst active sites, and poisoning

resulting from possible complexation of reactive iron species, to form non-reactive species by substrate decomposition products. Further investigations to fully unravel the precise cause(s) of deactivation, so as to develop an in situ reactivation mechanism is recommended.

- The hypothesis that the UV radiation used in the UV/Fenton catalysis in this study only assisted the coupled system by the photolysis H_2O_2, H_2O and absorbing organic species but not through recycling of Fe^{3+} to Fe^{2+} requires further testing to be proven. This can be done by extending the wavelength of the lamps used to cover UVA region (combining both UVC and UVA lamps) thus, giving a polychromatic UV source, with is recommended to test this hypothesis. Further to this, the specie of iron present on the catalyst during reaction can be determined by the use of Electron Spin Resonance (ESR). This is expected to clarify if the photoactive iron species $(FeOH)^{2+}$ is present or not during the reaction process.
- Studies have shown that harsh reaction conditions (mainly high temperatures) such as those obtained in wet air oxidation has the capacity to degrade acetic acid, however such raised temperatures (over 100 ^oC) are likely to denature the catalyst. It is therefore recommended that: temperature profiling be undertaken to achieve the optimum temperature for acetic acid degradation. This should be supported by the extension of the UV range down to 210 nm (the region where acetic acid absorbs) to enable effective decomposition of acetic acids which appear to be the most recalcitrant constituents of produced water, although highly unstable due to biodegradation.

References

Aaron O. G., Benito S. R., De Lasa H., (2008). Enhanced Mineralization of Phenol and other Hydroxylated Compounds in a Photocatalytic Process Assisted with Ferric Ions. *Chemical Engineering Science*. Pp 520-557.

Abhang M., Kumar D. and Taralkar S., (2011). Design of Photocatalytic Reactor for Degradation of Phenol in Wastewater. *International Journal of Chemical Engineering and Applications, Vol. 2, No. 5* Pp 337-340.

Abramovitch R. A., (1991). Applications of Microwave Energy in Organic Chemistry. A Review, *Organic Preparations and Procedures International*, Vol. 23, No. 6, 1991, pp. 683-711.

Ahmadun F.R., Pendashteh A., Abdullah L. C., Biak D. R., Madaeni S. S., Abidin Z. Z., (2009). Review of Technologies for Oil and Gas Produced Water Treatment. *Journal of Hazardous Materials.* Pp 530-551.

Akehata, T. and Shirai, T., (1972). Effect of light-source characteristics on the performance of circular annular photochemical reactor. *Journal of Chemical Engineering of Japan*, *5*(4), pp.385-391.

Akira F., Rao T. and Tryk D., (2000). Titanium Dioxide Photocatalysis. *J. Photochem. Photobiol*. (1), 1–21.

Al-Degs Y., Khraisheh M. and Ahmad M., (2000). Effect of Carbon Surface Chemistry on the Removal of Reactive Dyes from Textile Effluent. *Water Research* Vol.34 Pp. 932-934.

Almquist C. B., Sahle-Demessie E., Enriquez J., Biswas P., (2003). The Photocatalytic Oxidation of Low Concentration MTBE on Titanium Dioxide from Groundwater in a Falling Film Reactor. *Environmental Progress*, 22 (1), 14-23.

API (1990). Monographs on Refinery Environmental Control -Management of Water Discharges (Design and Operation of Oil-Water Separators). Publication 421, First Edition.

API (2000). Overview of Exploration and Production Waste Volumes and Waste Management Practices in the United States. Accessed online from: http://www.api.org/~/media/files/ehs/environmental_performance/icf-waste-survey-of-eandp-wastes-2000.pdf?la=en. [Accessed on 17th January 2017].

Arnold, K.E. Stewart, M., (2008). Surface production operations-Design of Oil Handling Systems and Facilities, vol. 1, third ed., Gulf Publishing Co, Houston, Texas.

Arthur J.D. Langhus B.G. and Patel C., (2005). Technical Summary of Oil and Gas Produced Water Treatment Technologies, http://www.rrc.state.tx.us/commissioners/williams/environment/produced water trtmnt Tech.pdf.

Asim K. Dutta K., and Bhattacharjee S., (2005). Degradation of Phenol and Chlorinated Phenols Using Fenton's Reagent. *Wiley InterScience*. 25 (1), Pp 66.

Aygun A., Yilmaz T., Nas B. and Berktay A., (2012). Effect of Temperature on Fenton Oxidation of Young Landfill Leachate: Kinetic Assessment and Sludge Properties. *Global nest journal* Vol. 14, (4) Pp. 490.

Babuponnusami A. and Muthukumar K., (2012). Advanced Oxidation of Phenol: A Comparison Between Fenton, Sono-electro-Fenton and Photo-electro-Fenton processes. *Chemical Engineering Journal* 183. Elsevier Pp6.

Baedecker, M. J., Cozzarelli I. M., Eganhouse R. P., Siegel D. I., and Bennett P. C., (1993). Crude oil in a shallow sand and gravel aquifer-III. Biogeochemical reactions and mass balance modeling in anoxic groundwater. *Applied Geochemistry*, 8:569-586.

Balasubramanian G., Dionysiou D. D., Suidan M. T., Baudin I., Laine J. M., (2004). Evaluating the Activities of Immobilized TiO2 Powder Films for the Photocatalytic Degradation of Organic Contaminants in Water. *Applied Catalysis B: Environmental*, 47(2), 73-84.

Barros F., Barros A., Silva M., and Nascimento R., (2013). Use of Microwave-Assisted Oxidation for Removal of the Pesticide Chlorpyrifos from Aqueous Media. *International Journal of Civil & Environmental Engineering* Vol: 13 No: 06.

Bartholomew, C.H., (1984). Catalyst Deactivation. *Chem. Eng.*, *91*, 96–112.

Bautista, P., Mohedano, A. F., Gilarranz, M. A., Casas, J. A., & Rodriguez, J. J., (2007). Application of Fenton oxidation to cosmetic wastewaters treatment. *Journal of Hazardous Materials, 143*(1-2), 128-134.

Baychoke M., (2007). A Typical Gravimetric API Separator. Available online from: https://en.wikipedia.org/wiki/API_oil%E2%80%93water_separator#/media/File:API_Separator.png. [Accessed on 17th January 2017].

Beers R. and Jr. and Sizer W., (1951). A Spectrophotometric Method for Measuring the Breakdown of Hydrogen Peroxide by Catalase. *J. Biol. Chem. 1952, 195:133-140.*

Bekins B. A., Cozzarelli I. M., and Godsy E. M., (2001). Progression of natural attenuation processes at a crude oil spill site: II. controls on spatial distribution of microbial populations. *Journal of Contaminant Hydrology.* 53: 387-406.

Belatter S., Mameri Y., Seraghni N., Debbache N., and Sehili (2013). Catalytic degradation of 3,5-Dimethylphenol with Geothite and Hydrogen Peroxide. *Journal of Environmental Engineering and Technology*. Vol. 1, No. 3.

Bele M., Kodre A., Arcon I., Grdadolnik J., Pejovnic S and Besenhard J., (1998). Adsorption of Cetyltrimethylammoniumbromide on Carbon Black from Aqueous Solution, Carbon. 36;1207-1212.

Beltran, F. J., Ovejero, G., and Rivas, J., (1995). Oxidation of Polynuclear Aromatic Hydrocarbons in Water. 1. Ozonation. *Ind. Eng. Chem. Res.* 35, 891–898.

Benko, K.L. and Drewes, J.E., (2008). Produced water in the Western United States: geographical distribution, occurrence, and composition. *Environmental Engineering Science*, *25*(2), pp.239-246.

Binet M., Stauber J., and Winton T., (2011). The Effect of Storage Conditions on Produced Water Chemistry and Toxicity. Available online from: http://link.springer.com/chapter/10.1007%2F978-1-4614-0046-2_7#page-1 [Accessed on 06th May 2017].

Bird, R.B., Stewart, W.E. & Lightfoot, E.N. (2002). *Transport Phenomena* (2nd Edition), Pp 679-689, John Wiley & Son, New York.

Bishop D. F., Stern G., Fleischman M., and Marshall L. S., (1968). Hydrogen Peroxide Catalytic Oxidation of Refractory Organics in Municipal Waste Waters. *Ind. & Eng. Chem., Processs Design & Development* Vol. 7, Pp 113.

Boitsov S., Meier S., Klungsoyr J., Svardal A., (2004). Gas Chromatography-Mass Spectrometry Analysis of Alkylphenols in Produced Water From Offshore Installations as Pentaflourobenzoate Derivatives. *Journal of Chromatography* A, 1059 Pp 131.

Borb (2008). Inverse Square Law. Available online from: http://www.scantips.com/lights/flashbasics.html#1. [Accessed on 15th January 2017]

Borg X. B., (2009). The Inverse Cube Law For Dipoles. The General Science Journal. Accessed online from: http://blazelabs.com/inversecubelaw.pdf. [Accessed on 7th October 2016).

Boudart, M., (1995). Turnover Rates in Heterogeneous Catalysis, *Chem. Rev.*, 95 (3), pp 661–666.

Boysen J. E., Harju J. A., B. Shaw B., Hayes T., (1997). Field Demonstration of the Freeze-Thaw/Evaporation Process for the Treatment of Produced Waters in the San Juan Basin of New Mexico. *Society of Petroleum Engineers. SPE/EPA Exploration and Production Environmental Conference*, Dallas, Texas.

Boysen, J. E., Harju, J. A., B. Shaw, M. Fosdick, A. Grisanti & Sorensen, J. A., (1999). The Current Status of Commercial Deployment of the Freeze Thaw Evaporation Treatment of Produced Water. *SPE/EPA 1999 Exploration and Production Environmental Conference.* Austin, TX.

Bradford M., McDonald C., & Helmig, Ed. (2003). Refractory Cod in Wastewater Proceedings of the Water Environment Federation, WEFTEC: Session 41 through Session 50. *Water Environment Federation* pp. 54-71(18).

Bradley B.W., (1990). Produced Water Treatment Technology Assessment. Prepared for the American Petroleum Institute-Offshore effluent guidelines steering committee, Washington,DC.

Bravo M. N, Silva S., Coelho A. V., Boas L. V., and Bronze M. R., (2006). Analysis of Phenolic Compounds in Muscatel Wines Produced in Portugal. *Anal Chim. Acta* 563: 84-92 (2006).

Brewer E., and Henion J., (1998). Atmospheric Pressure Ionization LC/MS/MS Techniques for Drug. *Journal of Pharmaceutical Sciences*. Vol. 87, No. 4, Pp 396.

Burkhard, K., (2013). Organic Photochemistry. Available from: http://www-oc.chemie.uni-regensburg.de/OCP/ch/chb/oc5/Photochemie-08.pdf [Accessed online on 15th March 2015].

Burin M. V., Arcari S. G., Costa L. F, and Bordignon-Luiz M., (2011). Determination of Some Phenolic Compounds in Red Wine by RP-HPLC: Method Development and Validation. *Journal of Chromatographic Science*, Vol. 49 Pp 647.

Burns, K.A. and Codi, S., (1999). Non-Volatile Hydrocarbon Chemistry Studies Around a Production Platform on Australia's Northwest Shelf. *Estuar. Cstl. Shelf Sci*. 49:853-876.

Caddick S., (1995). Microwave Assisted Organic Reactions, *Tetrahedron*, Vol. 51, No. 38, 1995, pp. 10403-10432

Calvert, J.G. and Pitts, J.N., (1967). Chemical actinometer for the determination of ultraviolet light intensities. *Photo chemistry, Wiley and Sons: New York*, p.780.

Canadian Centre for Occupational Health (CCOHS 2016). Ultraviolet Radiation. Available from:

https://www.ccohs.ca/oshanswers/phys_agents/ultravioletradiation.html. [Accessed online on 10th May 2017].

Cataldo F., (2014). Hydrogen Peroxide Photolysis with Different UV Light Sources Including a New UV-Led Light Source. *New front. Chem*. Vol. 23, No 2, pp. 99-110.

Catrinescu C., Arsene D., Teodosiu C., (2011). Catalytic Wet Hydrogen Peroxide Oxidation of *Para*-chlorophenol Over Al/Fe Pillared Clays (AlFePILCs) Prepared From Different Host Clays. *Applied Catalysis B: Environmental.* Vol. 101, (3–4), Pages 451–460.

Centi, G., Perathoner, S., Torre, T., Verduna, M.G., (2000). Catalytic wet oxidation with H_2O_2 of carboxylic acids on homogeneous and heterogeneous Fenton-type catalysts. *Catalysis Today* 55 61-69.

Cervera, S. and Esplugas, S., (1983). Obtaining Hydrogen by Photolysis of Water. *Energía* , 9: 103-107.

Chamarro, E., Marco, A., Esplugas, S., (2001). Use of Fenton Reagent to Improve Organic Chemical Biodegradability. *Water Research*, Vol. 35, No. 4, pp. 1047–1051.

Chan M. S. M. and Lynch R. J., (2003). Photocatalytic Degradation of Aqueous Methyl-Tertbutyl- Ether (MTBE) in a Supported-Catalyst Reactor. *Environmental Chemistry Letters*, 1 (3), 157-160.

Chaplin Martin (2014). Continuous Flow Reactors. Enzyme Technology. Cambridge University Press. Available from: http://www1.lsbu.ac.uk/water/enztech/continuous.html [Accessed 18th November 2016].

Chi, G. T., Churchley, J., & Huddersman, K. D., (2013). Pilot-Scale Removal of Trace Steroid Hormones and Pharmaceuticals and Personal Care Products from Municipal Wastewater Using a Heterogeneous Fenton's Catalytic Process. *International Journal of Chemical Engineering*, *2013*, 1–10.

Chi, G. T., & Huddersman, K. D., (2011). Maleic Acid Oxidation Using a Heterogeneous Modified Polyacrylonitrile (PAN) Fibrous Catalyst. *Journal of Advanced Oxidation Technologies*, *14*(2), pp. 235-243.

Chi G. T. and Huddersman, K. D., (2007). Novel Ion Chromatography Technique for the Rapid Identification and Quantification of Saturated and Unsaturated Low Molecular Weight Organic Acids Formed During the Fenton Oxidation of Organic pollutants. *Journal of Chromatography* A, Vol. 1139 Pp 95–103.

Cihanoğlu, A., Gündüz, G. and Dükkancı, M., (2015). Degradation of Acetic Acid by Heterogeneous Fenton-Like Oxidation Over Iron-Containing ZSM-5 Zeolites. *Applied Catalysis B: Environmental*, *165*, pp.687-699.

Coste, M., Batbedat, C., Feliers, C., Olejnik, D., Cigana, J., Cervantes P., (2003). Refractory Cod Removal in The Chemical Industry: Technico-Economic Comparison Of Advanced Oxidation Processes. *Water Environment Federation,* Vol. 12, pp. 25-36.

Dean J. A., (1992). Lange's Hand Book of Chemistry, 14th Edition. McGraw-Hill, Inc., New York.

De Laat J. and Gallard H., (1999). Catalytic Decomposition of Hydrogen Peroxide by FE(III) in Homogeneous Aqueous Solution: Mechanism and Kinetic Modelling. *Environ. Sci. Technol*, Vol. 33, Pp2726-2732.

Denny, P.J.; Twigg, M.V., (1980). Factors Determining the Life of Industrial Heterogeneous Catalysts. In *Catalyst Deactivation (Studies in Surface Science and Catalysis)*; Delmon, B., Froment, G.F., Eds.; Elsevier: Amsterdam, The Netherlands, 1980; Volume 6; pp. 577–599.

Department of Energy and Climate change (2011). Methodology for the Sampling and Analysis of Produced Water and Other Hydrocarbon Discharges. Available from: https://www.google.co.uk/url?sa=t&rct=j&q=&esrc=s&frm=1&source=web&cd=1&ved=0CCYQFjAA&url=https%3A%2F%2Fwww.gov.uk%2Fgovernment%2Fuploads%2Fsystem%2Fuploads%2Fattachment_data%2Ffile%2F286015%2FMethodology_for_the_Sampling_and_Analysis_of_Produced_Water.docx&ei=5CpTVbfiN8S2Ua_EgdgG&usg=AFQj

CNFIsdx5Hd1ACj9BnVzfqJglTQgpag&bvm=bv.93112503,d.d24 [Accessed 12th May 2015].

Downes A. and Blunt T. P., (1877). Researches on the Effect of Light on Bacteria and Other Organisms. *Proc. R. Soc*. *Lond*. 26. 488-500.

Ekins P., Vanner R., and Firebrace J., (2005). Management of Produced Water On Offshore Oil Installations: A Comparative Assessment Using Flow Analysis; Final Report. *Working Paper, PSI, London Institute.* Available from: http://www.psi.org.uk/docs/2005/UKOOA/ProducedWater-Workingpaper.pdf. [Accessed on 18th January 2017].

Emami, F., Tehrani-Bagha, A. R., Gharanjig, K., & Menger, F. M., (2010). Kinetic Study of the Factors Controlling Fenton-Promoted Destruction of a Non-Biodegradable Dye. *Desalination, 257*(1-3), 124-128.

E&P (Exploration & Production) (1994). North Sea Produced Water: Fate and Effects in the Marine Environment, The E&P Forum May 1994, Report No. 2.62/204.

Eisenberg, G., (1943). Colorimetric Determination of Hydrogen Peroxide. *Industrial & Engineering Chemistry Analytical Edition*, *15*(5), pp.327-328.

Eisenhauer, H. R., (1968). The Ozonization of Phenolic Wastes *J. Water Pollute Control Fed*. V. 40 Pp. 18897-1889.

ESCO International (2014). Industrial Advanced Oxidation Pilot System for Produced Water Treatment. Accessed online from: http://www.escouk.com/industrial-advanced-oxidation-pilot-system-for-produced-water-treatment/ [Accessed 7th February 2017].

Evonik Industries (2016). Hydrogen Peroxide Stability and Decomposition. Available from:http://h2o2.evonik.com/product/h2o2/en/about-hydrogen-peroxide/basic-information/stability-and-decomposition/pages/default.aspx [Accessed on 03/06/16].

Fakhru'l-Razi A, Pendashteh A, Abdullah L. C., (2009). Review of technologies for oil and gas produced water treatment. *J Hazard Mater*; 170:530-551.

Faksness L. G., Grini P. G., and Daling P. S., (2004). Partitioning of Semi-Soluble Organic Compounds Between the Water Phase and Oil Droplets in Produced Water. *Marine Pollution Bulletin* 48 (7-8), 731-742.

Farzadkia M., Dehghani M., Moafian M., (2014). The Effects of Fenton Process on the Removal of Petroleum Hydrocarbons from Oily Sludge in Shiraz Oil Refinery, Iran. *Journal of Environmental Health Science & Engineering*, No. 12 Vol. 31 Pp 2-7.

Fenton H.J.H., (1894). Oxidation of Tartaric Acid in Presence of Iron. *Journal of the Chemical Society, Transactions*. 65, 899-910.

Fogler, H. S., (2006). External Diffusion Effects on Heterogeneous Reactions, In: *Elements of Chemical Reaction Engineering*, N.R. Amundson (Ed), pp. 757-801, Prentice-Hall Inc., New Jersey.

Forni, L., (1999). Mass Transfer in Catalytic Reactions. Catalysis Today, Vol.52, No.2-3, (September 1999), pp. 147-152, ISSN: 0920-5861.

Forster, C., (2003). Wastewater Treatment and Technology. London: Thomas Telford.

Frankiewicz F. and Walsh J., (2017). The Savvy Separator: Physical Processes Behind Oil Droplet Coalescence During Water Treatment. *Minerals Technology Inc*. Vol 01. Available online from: https://spe.org/en/print-article/?art=3009 [Accessed on 12/08/17].

Frost T.K., Johnsen S., Utvik T.I.R., (1998). Produced water discharges to the North Sea, Fate and Effects in the water column; OLF (Oljeindustriens Landsforening) December 1998, Available online from : http://www.olf.no/static/en/rapporter/producedwater. [Accessed on 15/04/15].

Future Market Insights (2014). Produced Water Treatment Systems Market: Global Industry Analysis and Opportunity Assessment 2014 – 2020. Available online from: https://www.futuremarketinsights.com/reports/produced-water-treatment-market [Accessed on 3/05/15].

Gary L. L. and Winefordner J. D., (1983). Limit of Detection a Closer Look at the IUPAC Definition. *Analytical Chemistry* vol. 55 No 7 Pp712.

General Electric Power and Technology (1997). Open Recirculating Cooling Systems. *Water Process Technologies.*

Gerven T., Mulc G., Moulijn J., Stankiewicz A., (2007). A Review of Intensification of Photocatalytic Processes. *Chemical Engineering and Processing* 46 781–789.

Gitipour S., Hedayati M., and Madadian E., (2014). Soil Washing for Reduction of Aromatic and Aliphatic Contaminants in Soil. *Clean- Soil Air Water*. Vol 43 (10). Accessed online from: http://onlinelibrary.wiley.com/doi/10.1002/clen.201100609/abstract [Accessed 12th October 2016].

Glaze W.H., Kang J.W., and Chapin D. H., (1987). The Chemistry of Water Treatment Processes Involving Ozone, Hydrogen Peroxide, and Ultraviolet Radiation. *Ozone Science and Engineering*. Vol. 9 Pp. 335-352.

Glimmerman, E.D., (2006). Assessment of the Available Technologies for Slop and Bilge Water Treatment and Monitoring Offshore. *Master's Thesis, Chalmers University of Technology,Goteborg,Sweden.*

Goetzberger, A., Knobloch, J. and Voss, B., (1998). *Crystalline silicon solar cells* (pp. 79-85). Chichester: Wiley.

Gogate P. R. and Pandit A. B. (2004). A Review of Imperative Technologies for Wastewater Treatment: Oxidation Technologies at Ambient Conditions. *Adv. Environ. Res.,* 8(3-4), 501- 551.

Goldberger M. and Watson K., (1964). Collision Theory. John Wiley and sons Inc. New York 11501.

Goswami D. Y., Kreith F. and Kreider J. F., (2000). Principles of Solar Engineering. Second edn: Taylor & Francis Group.

Gozzo, F., (2001). Radical and Non-Radical Chemistry of Fenton-like Systems in the Presence of Organic Substrates. *Journal of Molecular Catalysis A: Chem*. 171, 1-22.

(GPO) (2016). Available from: http://www.ecfr.gov/cgi-bin/text-idx?SID=e2ca4bf1da4551cca5b692e33b20126b&mc=true&node=se40.32.435_113&rgn=div8 [Accessed on 29th October 2016].

Giri, R.R., Ozaki, H., Takayanagi, Y., Taniguchi, S. and Takanami, R., (2011). Efficacy of ultraviolet radiation and hydrogen peroxide oxidation to eliminate large number of pharmaceutical compounds in mixed solution. *International Journal of Environmental Science & Technology*, *8*(1), pp.19-30.

Grini, P.G., Hjelsvold, M., Johnsen, S., (2002). Choosing produced water treatment technologies based on environmental impact reduction. SPE Paper SPE 74002. *Presented at the 2002 HSE Conference.*

Gromboni C. F., Kamogawa M. Y., Ferreira A. G., N´obrega J. A., Nogueira A. R., (2007). Microwave-assisted photo-Fenton decomposition of chlorfenvinphos and cypermethrin in residual water. *Journal of Photochemistry and Photobiology A: Chemistry* Vol. 185 Pp. 32–37.

Gulkaya, İ., Surucu, G. A., & Dilek, F. B., (2006). Importance of H_2O_2/Fe^{2+} ratio in Fenton's Treatment of a Carpet Dyeing Wastewater. *Journal of Hazardous Materials, 136*(3), 763-769 Conference in Kuala Lumpur, Malaysia, 20–22 March 2002.

Gulsen H. and Turan M., (2004). Treatment of Sanitary Landfill Leachate Using a Combined Anaerobic Fluidized Bed Reactor and Fenton's Oxidation. *Environ Eng Sci*. Vol. 21, 627-636.

Gulyas H., (1997). Processes for the Removal of Recalcitrant Organics From Industrial Wastewaters. Water Science and Technology. Vol. 36(2-3) Pp 9-16

Gumus D., Akbal F., (2016). Comparison of Fenton and electro-Fenton processes for oxidation of phenol. *Process Safety and Environmental Protection*.

Guus F. IJpelaar, Danny J. H., Harmsen and Minne H., (2007). UV disinfection and UV/H_2O_2 Oxidation: By-Product Formation and Control. Techneau, D2.4.1.1.

Hagen, J., (2006). Industrial catalysis. A practical approach. *JOURNAL FUR PRAKTISCHE CHEMIE*, *342*(1), pp.111-111.

Hall S., Tang R., Baeyens J., and Dewil R., (2009). Removing Polycyclic Aromatic Hydrocarbons from Water by Adsorption on silica gel *Polycyclic Aromatic Compounds*, 29: 168–172.

Han Z. B., Dong Y. C., and Dong S. M., (2011). Copper Iron Bimetal Modified Pan Fiber Complexes as Novel Heterogeneous Fenton Catalysts for Degradation of Organic Dye Under Visible Light Irradiation. *Journal of Hazardous Materials*, 189(1-2): 241--248.

Hathway T. L., (2009). Titanium Dioxide Photocatalysis: Studies of the Degradation of Organic Molecules and Characterization of Photocatalysts Using Mechanistic Organic Chemistry. A dissertation submitted to the graduate faculty in partial fulfilment of the requirements for the degree of doctor of philosophy, Iowa State University. Available from: http://lib.dr.iastate.edu/etd [Accessed 6th February 2017].

Hayes T. and Arthur D., (2004). Overview of emerging produced water treatment technologies. *Proceedings - 11th Annual International Petroleum Environmental Conference,* Albuquerque, USA.

Henderson S.B., Grigson, S.W., Johnson P. and Roddie B.D., (1999). Potential Impact of Production Chemicals on Toxicity of Produced Water Discharges in North Sea Oil Platforms. *Marine Pollution Bulletin* 38(12): 1141-1151.

Herderich M., Richling E., Roscher R., Schneider C., Schwab W., Humpf H., Schreier P., (1997). Application of Atmospheric Pressure Ionization HPLC-MS-MS for the Analysis of Natural Products. *Chromatographia* Vol.45.

Hermosilla D., Cortijo M. and Huang C. P., (2009). Optimizing the Treatment of Landfill Leachate by Conventional Fenton and Photo-Fenton Processes. *Science of the total Environment*. Elsevier Pp3479.

Herrmann Jean-Marie (1999). Heterogeneous photocatalysis: Fundamentals and Applications to the Removal of Various Types of Aqueous Pollutants. *Catalysis Today 53 (1)*. 115-129.

Herrmann J. M., Guillard C., Arguello M., Aguera A., Tejedor A., Piedra L., and Fernandez Alba A., (1999). Photocatalytic Degradation of Pesticide Pirimiphos-Methyl. Determination of the Reaction Pathway and Identification of Intermediate Products by Various Analytical Methods. *Catal. Today*, 54 (2-3), 353-367.

Hidaka, H., Saitou, A., Honjou, H., Hosoda, K., Moriya, M., Serpone, N., (2007). Microwave Assisted Dechlorination of Polychlorobenzenes by Hypophosphite Anions in Aqueous Alkaline Media in the Presence of Pd-loaded Active Carbon, J. Hazard. Mater. 148 (2007) 22–28.

Holt R., McLane C., and Oldenberg O., (1948). Ultraviolet Absorption Spectrum of Hydrogen Peroxide. *The Journal of Chemical Physics* Vol. 16. No 3.

Homem, V., Alves, A., & Santos, L., (2010). Amoxicillin Degradation at ppb Levels by Fenton's Oxidation Using Design of Experiments. *Science of the Total Environment, 408*(24), 6272-6280.

Hughes, R., (1984). Deactivation of Catalysts; Academic Press, London, UK.

Ibhadon A. and Fitzpatrick P., (2013). Heterogeneous Photocatalysis: Recent Advances and Applications. *Catalysts 3*, 189-218.

Ibragimov V. A., (2011). Catalysis. *Thermopedia.* Vol.10, 1615.

Igunnu E. T., and Chen G. Z., (2012). Produced Water Treatment Technologies. International *Journal of Low-Carbon Technologies* Vol. 0 Pp. 3.

International Chemicals Safety Cards (2017). 3,5-Dimethylphenol. Available from: http://www.ilo.org/dyn/icsc/showcard.display?p_card_id=1356. [Accessed online 24th May 2017].

Isehunwa s., and Onovae s., 2011. Evaluation of Produced Water Discharge In The Niger-Delta. *Journal of Engineering and Applied Sciences* Vol 6, No 8.

Ishtchenko V. V., Huddersman K. D., Vitkovskaya R. F., (2003). Production of a Modified PAN. Fibrous Catalyst and its Optimisation towards the Decomposition of Hydrogen Peroxide. *Applied Catalysis A*, 242(1): 123-137.

Ishtchenko V. V., Huddersman K. D., Vitkovskaya R. F., (2002). Investigation of the Mechanical and Physicochemical Properties of a Modified PAN Fibrous Catalyst," *Appl. Catal. A: General 6378*, 1-10.

IUPAC, (1999). Terminology, Relative Photonic Efficiencies and Quantum Yields in Heterogeneous Photocatalysis. Part i: Suggested Protocol. *Pure Appl. Chem*. 71, 303–320.

Jacques S. and Prahl S., (1998). Definition and Units of Absorption Coefficient μ_a [cm^{-1}]. *Biomedical Optics* ECE532.

Jiang C., Pang S., Ouyang F., Ma J. and Jiang J., (2010). A new Insight into Fenton and Fenton-like Processes for Water Treatment. *Journal of Hazardous materials*. Elsevier 174 Pp813-817.

Johnsen S., Frost T.K., Hjelsvold M. and Utvik T., (2000). The Environmental Impact Factor – A Proposed Tool for Produced Water Impact Reduction, Management and Regulation. SPE paper (61178). *Proceedings of 2000 HSE Conference*, Stavanger, Norway.

Johnsen S., Smith A., Brendehaug, J., Riksheim, H., Gjøse, A. L., (1994). Identification of Sources of Acute Toxicity in Produced Water". Paper SPE 27138 presented at the 1993 SPE Conference in Djakarta.

Johnsen, S., Røe Utvik T.I., Garland E., De Vals B., and Campbell J., (2004). Environmental Fate and Effects of Contaminants in Produced Water. SPE 86708. Paper Presented at the Seventh SPE International Conference on Health, Safety, and Environment in Oil and Gas Exploration and Production. Society of Petroleum Engineers, Richardson, TX. Pp 9.

Joshi R., Adhikari S., Patro B., Chattopadhyay S., and Mukherjee T., (2001). Free Radical Scavenging Behaviour of Folic Acid: Evidence for Possible Antioxidant Activity. *Free Radical Biology and Medicine* Elsevier vol. 30 (12) Pp.1390.

Kalisvaart B. F., (2000). Photoelectrical Effects of Berson Multiwave Lamps to Prevent Microbial Recovery. *Benson UV Techniek, Nuenen, the Neithrlands.*

Kanel S. R., Neppolian B., Heechul C. and Yang J., (2003). Heterogeneous Catalytic Oxidation of Phenanthrene by Hydrogen Peroxide in Soil Slurry: Kinetic Mechanism and Implication. *Soil and Sediment Contamination* 12 (1) Pp. 101-117.

Kavita V. and Palanivelu K., (2005). Destruction of Cresols by Fenton Oxidation Process. *Water Research*. Elsevier 39 Pp 3065.

Kaya Y., Gonder Z., Vergili I. and Barlas H., (2008). Removal of Cetyltimethylammonium Bromide and Sodium dodecylether Sulfate by Granular Activated Carbon. *Journal of Scientific and Industrial Research* V. 67, Pp250.

Khamaruddin p., Bustam M. and Omar A., (2011). Using Fenton's Reagents for the Degradation of Diisopropanolamine: Effect of Temperature and Ph. *International Conference on Environment and Industrial Innovation.* IPCBEE vol.12 Pp 12-16.

Khan, A. J. and Watts, R. J., (1994). Mineral-Catalysed Peroxide of Tricholoroethylene. *Water, Air and Soil pollut*. 88, 247–260.

Kingston, H.M., and Hasswell S. J., (1997). Microwave –Enhanced Chemistry: Fundamentals, *Sample Preparation and Applications*. American Chemical Society. Washington, DC.

Klaewkla, R., Arend, M., Hoelderich W. F., (2011). A Review of Mass Transfer Controlling The Reaction Rate in Heterogeneous Catalytic Systems. Chapter 29 in *Mass Transfer - Advanced Aspects*, Nakajima, H. (Ed.).

Klaus Christmann, (2010). Modern Methods in Heterogeneous Catalysis Research Institut für Chemie und Biochemie, Freie Universität Berlin Lecture Series /2011

Knapp D. R., (1979). Hand Book of Analytical Derivatization Reactions. *John Wiley and Sons.* New York.

Knudsen B., Hjelsvold M., Frost T., Grini P., Willumsen C., Torvik H., (2004). Meeting The Zero Discharge Challenge For Produced Water, In: Proceeding Of The Seventh SPE International Conference On Health, Safety, And Environment In Oil And Gas Exploration And Production, Calgary, Alberta, Canada, 29–31.

Kornblum, Z., C. (2010). Photochemistry. *Encyclopaedia Americana*. Available from: https://edelsteincenter.files.wordpress.com/2010/07/photochemistry.pdf. [Accessed February 28th 2015].

Krause, P.R., (1995). Spatial and Temporal Variability in Receiving Water Toxicity near an Oil Effluent Discharge Site. *Archives of Environmental Contamination and Toxicology*. 29:523-529.

Kupiec T., (2004). Quality Control Analytical Methods: High Performance Liquid Chromatography. *International Journal of Pharmaceutical Compounding.* Vol. 8 No. 3 Pp 223.

Laine D. F., and Cheng I. F., (2007). The Destruction of Organic Pollutants Under Mild Reaction Conditions: A review. *Microchem. J.,* 85(2), 183-193.

Larter S. and Bennett B., (2011). A Review of the Systematics of Alkyl Phenol Occurrence in Conventional and Heavy oil Petroleum Systems. *SCPG CSEG CWLS Convention.*

LAY, Y. S., (1989). Oxidation of 1,2-dibromo-3-chloropropane in Ground Water Using Advanced Oxidation Processes. Ph.D. Thesis, University of California at Los Angeles.

Lee H. S., (2000). HPLC analysis of phenolic compounds. L.M.L. Nollet. *Food analysis by HPLC*, 2nd ed., Marcel Dekler Inc., New York, NY.

Legrini, O., Oliveros, E. and Braun, A. M., (1993). Photochemical Processes for Water Treatment, Chemical Reviews, v. 93, p. 671-698.

Lejin Xu and Jianlong W., (2013). Degradation of 4-Chloro-3,5-Mimethylphenol by Heterogeneous Fenton-Like Reaction Using Nanoscale Zero-Valent Iron Catalyst. *Environ Eng Sci.* 30 (6) Pp294.

Li, B., Dong, Y., & Ding, Z., (2013). Heterogeneous Fenton Degradation of Azo Dyes Catalysed by Modified Polyacrylonitrile Fiber Fe Complexes: QSPR (Quantitative Structure Property Relationship) Study. *Journal of Environmental Sciences*, *25*(7), 1469–1476.

Liang C., Wang Z-S., and Mohanty N., (2006). Influence of Carbonates and chlorides on Persulfate Oxidation of Trichloroethylene at 20 ^{o}C. *Science of The Total Environment* 370 (2-3) 271-7.

Liao C-H., Kang S., and Wu F., (2001). Hydroxyl Radical Scavenging Role of Chlorides and Bicarbonate ions in the H2O2/UV process. *Chemosphere* Vol.44. 1193-1200.

Libra J. A., (1991). Volatilization of Organic Compounds in an Aerated Stirred Tank Reactor. *A dissertation submitted in partial satisfaction of the requirements for the degree Doctor of Philosophy in Civil Engineering University of California, Los Angeles.*

Licha T. and Sauter M., (2002). Use of Short Chained Alkylphenols (SCAP) in Analysis of Transport Behaviour of Oil Contaminated Groundwater. *Agricultural Sciences*, 7(2):29-30.

Logsdon G. S., (1987). Treatment Plant Evaluation for Particulate Contaminant Removal. *Presented at Preconference Seminar, Pacific Northwest Section, American Water Works Association, Bellevue, Washington.*

Lorenc J., Lambeth G. and Scheffer W., (2001). Alkylphenols. John Wiley & Sons, Inc.

Loubna Nouri, Ilhem Ghodbane, Oualid Hamdaoui and Mahdi Chiha, (2007). Batch sorption dynamics and equilibrium for the removal of cadmium ions from aqueous phase using wheat bran *Journal of Hazardous Materials* 149. Pp. 119.

Lu, M.C., Chen, J.N., Chang, C.P., (1999). Oxidation of Dichlorvos with Hydrogen Peroxide Using Ferrous Ion as Catalyst. *Journal of Hazardous Materials*, Vol. B65, pp. 277–288.

Lurascu B., Siminicianu I., Vione D., Vicente M. and Gil A., (2009). Phenol Degradation in Water Through Heterogeneous Photo-Fenton Processes Catalysed by Fe-treated Laponite. Water Research. Vol. 43, no. 5, Pp 1313-1322.

Ma y., Bing Chen, Baiyu Zhang, Jisi Zheng, Bo Liu and He Zhang (2014). Fenton Oxidation Process for Remediation of Produced Water Containing Polycyclic Aromatic Hydrocarbons (PAHs). *CSCE 2014 13th International Environmental Specialty Conference - 13e Conférence internationale spécialisée sur l'environnement de la SCGC.*

Machulek Jr. A., Quina F., Gozzi F., Silva V., Friedrich L., and Moraes J., (2012). Fundamental Mechanistic Studies of the Photo-Fenton Reaction for the Degradation of Organic Pollutants, Organic Pollutants Ten Years After the Stockholm Convention - Environmental and Analytical Update, (Ed.), ISBN: 978-953-307-917-2, InTech, Available from: http://www.intechopen.com/books/organic-pollutants-ten-years-after-the-stockholm-convention-environmentaland-analytical-update/fundamental-mechanistic-studies-of-the-photo-fenton-reaction-for-the-degradation-oforganic-pollutan.

Martyanov, I.N.; Savinov, E.N. and Parmon, V.N., (1997). A comparative Study of Efficiency of Photooxidation of Organic Contaminants in Water Solutions in Various Photochemical and Photocatalytic Systems: Phenol Photoxidation Promoted by Hydrogen Peroxide in a Flow Reactor. *Journal of Photochemistry and Photobiology A: Chemistry,* Vol. 107, No. 1-3, pp. 227-231.

Masschelein W. J., (2002). Ultraviolet Light in Water and Wastewater Sanitation. Lewis Publishers London.

Mastouri R., Iran A., Nadim F., Kargari N., and Qazvin T., (2010). A Time To Review The Produced Water Treatment Technologies, A Time To Look Forward for New Management Policies. Accessed online from: http://ipec.utulsa.edu/Conf2010/Powerpoint%20presentations%20and%20papers%20received/Mastouri.pdf [Accessed on 23rd January 2017].

Mehmet A. Oturan and Jean-Jacques Aaron (2014). Advanced Oxidation Processes in Water/Wastewater Treatment: Principles and Applications. A Review, Critical Reviews in Environmental Science and Technology. Accessed online from: http://dx.doi.org/10.1080/10643389.2013.829765 [Accessed on 4th February 2017).

Merino-Solís M., Villegas E., José de Anda, and López-López A., (2015). The Effect of the Hydraulic Retention Time on the Performance of an Ecological Wastewater Treatment System: An Anaerobic Filter with a Constructed Wetland. *Water*. Vol. 7, 1149-1163.

Michael, M., (2000). *Principles of Chemistry*; W. W. Norton & Company.

Milman, B. L., (2005). Identification of Chemical Compounds. *Trends Analyt. Chem.* V. *24,* Pp493–508.

Milman B. L., (2011). Techniques and Methods of Identification. Accessed online from: http://www.springer.com/978-3-642-15360-0. [Accessed on 6th January 2017].

Mills A., Davies R. H., Worsley D., (1993). Water Purification by Semiconductor Photocatalysis. *Chemical Society Reviews*, 22 (6), 417-425.

Mohammadi K. M., (2013). Microwave-Assisted Oxidation of Organic Compounds with Cetyltrimethylammonium Chlorochromate. *Open Journal of Synthesis Theory and Applications*, Vol. 2, Pp87-90.

Moldoveanu S., Kiser M., (2007). Gas Chromatography/Mass Spectrometry Versus Liquid Chromatography/Fluorescence Detection in the Analysis of Phenols in Mainstream Cigarette Smoke. *Journal of Chromatography A*, 1141 90–97.

Mota L. N., Albuquerque F., Beltrame T. C., Chiavone-Filho O., Machulek A., Nascimento C., A., (2008). Advanced Oxidation Processes and their Application in the Petroleum Industry: A Review. *Brazilian Journal of Petroleum and Gas*. Vol. 2, No. 3, Pp. 122-142.

Munter R., (2001). Advanced Oxidation Processes – Current Status and Prospects. *Proc. Estonian Acad. Sci. Chem*. 50, 2, 59–80.

Murakami T. and Fujishima A., (2010). Expanding Industrialization of Photocatalysts. Available online from: https://sangakukan.jp/journal/journal_contents/2010/06/articles/1006-03-2/1006-03-2_earticle.html. [Accessed on 13/06/16]

Myhre, L.P., Bausant, T., Sundt, R., Sanni, S., Vabø, R., Skjoldal, H.R., Klungsøyr, J., (2004). Risk Assessment of Reproductive Effects of Alkyl Phenols in Produced Water on Fish Stocks in the North Sea, RF-Akvamiljø Report AM-2004/018.

NASA (2007). Electromagnetic Spectrum. Available from: http://science.hq.nasa.gov/kids/imagers/ems/waves3.html [Accessed online on 19th July 2016].

Nauman, E. B., (2002). *Chemical Reactor Design, Optimization, and Scale up*. McGraw-Hill, US.

Nave Rod (2015). Absorption and Emission. Available from: http://hyperphysics.phy-astr.gsu.edu/hbase/mod5.html [Accessed on 12th Jan 2017].

Neff J., Lee K., DeBlois E., (2011). Produced Water: Overview of Composition, Fates and Effects. Accessed online from: https://www.researchgate.net/publication/225911658 . [Accessed on 19th January 2017].

Noh J. S., and Schwartz J. A., (1989). Estimation of the Point Of Zero Charge of Simple Oxides by Mass Titration. *J. Colloid Interface Sci.,* 130 (1), pp. 157–164.

Norsk olje and Gass Environmental Report (2015). Available from: https://www.norskoljeoggass.no/Global/2015%20dokumenter/Environmental%20report%202015.pdf. [Accessed on 15th January 2017].

Ohama, Y. and Van Gemert, D. eds., (2011). *Application of titanium dioxide photocatalysis to construction materials: state-of-the-art report of the RILEM technical committee 194-TDP* (Vol. 5). Springer Science & Business Media.

Oil and Gas Producers, (2011). Aromatics in Produced Water; Occurrence, Fates, Effect and Treatments. *Report no 1.20/324.*

Oil and Gas Producers, (2005). Fate and Effects of Naturally Occurring Substances in Produced Water on the Marine Environment. Report no. 364. Available from. http://www.ogp.org.uk/pubs/364.pdf (Accessed on 19th February 2013).

OSPAR (2010). Alkylphenols. Quality Status Report. *Status and trend in marine chemical pollution.* Accessed from: http://onlinelibrary.wiley.com/doi/10.1002/0471238961.0112112512151805.a01.pub2/full. [Accessed on 20th January 2017].

Owens, N. and Lee, D.W., (2007).The Use of Micro Bubble Flotation Technology in Secondary & Tertiary Produced Water Treatment - A Technical Comparison With Other Separation Technologies. *TUV NEL, 5th Produced Water Workshop Aberdeen, Scotland*.

Pace, N. C., Vajdos F., Fee L., Grimsley G. and Gray T., (1995). How to Measure and Predict the Molar Absorption Coefficient of a Protein. *Protein Sci.* 4:2411-23.

Palacio M., Villabrille p., Romanelli G., Vázquez P. and Cáceres C., (2009). Eco-friendly Liquid Phase Oxidation With Hydrogen Peroxide Of 2,6-Dimethylphenol To 2,6-Dimethyl-1,4-Benzoquinone Catalyzed By Tio_2–Ceo_2 Mixed Xerogels. *Applied Catalysis A*: General Volume 359, Issues 1–2, 15 May 2009, Pages 62–68.

Park, S.H., Kim, S.J., Seo, S.G. and Jung, S.C., (2010). Assessment of microwave/UV/O 3 in the photo-catalytic degradation of bromothymol blue in aqueous nano TiO 2 particles dispersions. *Nanoscale research letters*, *5*(10), p.1627.

Parsons S., (2004). Advanced Oxidation Processes for Water and Wastewater Treatment IWA publishing London.

Pelaez, M., Nolan N., Pillai S., Seery M., and Falaras P., (2012). A Review on the Visible Light Active Titanium Dioxide Photocatalysts for Environmental Applications. *Applied Catalysis B: Environmental*, vol. 125, pp. 331– 349.

Peña C. R.., Silva V. O., Quina F. H., Bertotti M., (2012). Hydrogen Peroxide Monitoring in Fenton Reaction by Using a Ruthenium Oxide Hexacyanoferrate/Multiwalled Carbon Nanotubes modified electrode. *Journal of Electroanalytical chemistry*. V686 Pp1-6.

Perfumo, A., Banat, I.M., Marchant, R. and Vezzulli, L., (2007). Thermally Enhanced Approaches for Bioremediation of Hydrocarbon-Contaminated Soils. Chemosphere 66, 179–184.

Petri B. G., Watts J. R., Teel L. A., Huling S. G. and Brown R. A., (2011). Fundamentals of ISCO Using Hydrogen Peroxide.

Petrowiki, (2013). Oil Emulsions. Available from: http://petrowiki.org/Oil_emulsions [Accessed on 22th March 2017]

Pham L. A, Doyle M. F., and Sedlak L. D., (2012). Kinetics and efficiency of H_2O_2 Activation by Iron-containing Minerals and Aquifer Materials. *Water Research 46* Pp. 6454- 6462

Phillips, R. and Phillips, R., 1983. *Sources and Applications of Ultraviolet Radiation* (No. 544.52/. 54 PHI).

Pierce Biotechnology (2002). Extinction Coefficients: A Guide to Understanding Extinction Coefficient with Emphasis on Spectrophotometric Determination of Protein Concentration. *Technical Resource.*

Pignatello, J.J. and Huang, L.Q., (1993). Degradation of Polychlorinated Dibenzo-p-dioxin and Dibenzofuran Contaminants in 2, 4, 5-T by Photoassisted Iron-Catalyzed Hydrogen Peroxide. *Water research*, *27*(12), pp.1731-1736.

Pignatello, J.J., Oliveros E. & Mackay A., (2006). Advanced Oxidation Processes for Organic Contaminant Destruction Based on the Fenton Reaction and Related Chemistry.

Pozdnyakov. I. P.; Glebov, E. M.; Plyusnin, V. F.; Grivin, V. P.; Ivanov, Y. V.; Vorobyev, D. Y. & Bazhin, N. M., (2000). Mechanism of $Fe(OH)^{2+}(aq)$ photolysis in aqueous solution. *Pure and Applied Chemistry*, Vol. 72, No. 11, pp. 2187-2197, *Critical Reviews in Environmental Science & Technology*, Vol. 36, No. 1, pp. 1-84.

Ragheb, M., (2018). Fresh Water Augmentation. Available online from: http://mragheb.com/NPRE%20402%20ME%20405%20Nuclear%20Power%20Engineering/Fresh%20Water%20Augmentation.pdf. [Accessed on 20/03/18].

Rashid, S. et al., (2014). Flotation, Filtration, and Adsorption: Pilot Trials for Oilfield Produced-Water Treatment.Society of Petroleum Engineers Vol. 3:2.

Ray A. K., (1999). Design, modelling and experimentation of a new large-scale photocatalytic reactor for water treatment. *Chemical Engineering Science 54* 3113-3125.

Ray A. K. and Beenackers, A. A. C. M., (1998). Development of a New Photocatalytic Reactor for Water Purification. *Catalysis Today*, 40, 73-83.

Ray, A.K. and Beenackers, A.A.C.M., (1996). A photocatalytic Reactor Suitable for Water Purification as well as a Process for the Purification of Wastewater. European Patent 96200942.9-2104 .

REIS, J. C., (1996). Environmental Control in Petroleum Engineering, Houston, Texas, Gulf Publishing.

Remya, N. and Lin, J.G., (2012). Current status of microwave application in wastewater treatment—A review, Chem. Eng. J. Vol. 166 pp. 797–813.

Rice, C.A. and Nuccio, V., (2000). Water produced with coal-bed methane. *US Geological Survey Fact Sheet FS–156–00*, *2*.

Roberts, P.V., Munz, C., and Daendliker P., (1984). Modelling Volatile Organic Solute Removal by Surface and Bubble Aeration, *J. Water Pollut. Control Fed*., Vol 56,157-163.

Rodríguez, M., (2003). *Fenton and UV-vis based advanced oxidation processes in wastewater treatment: Degradation, mineralization and biodegradability enhancement*. Universitat de Barcelona.

Røe, T. I. and Johnsen, S., (1996). Discharges of Produced Water to the North Sea; Effects in the Water Column. Produced Water 2. Environmental Issues and Mitigation Technologies. M. Reed and S. Johnsen. New York, USA, Plenum Press: 13-25.

Roig B., Gonzalez C. and Thomas O., (2003). Monitoring of Phenol Degradation by Ultraviolet Spectroscopy. *Spectrochimica Acta Part A* 59 Pp303-307.

Rosen A., (2014) Reactor Design. Available from: http://sites.tufts.edu/andrewrosen/files/2013/09/reactor_design_guide1.pdf. [Accessed on 23rd July 2017].

Saillard, R., Poux, M., Berlan, J. and Audhuy-Peaudecerf, M., (1995). Microwave heating of organic solvents: thermal effects and field modelling. *Tetrahedron*, *51*(14), pp.4033-4042.

Salgado P., Melin V., Contreras D., Moreno Y. and Mansilla H., (2013). Fenton Reaction Driven by Iron Ligands. *J. Chil. Chem. Soc*. 58 (4) Pp 2097.

Schalk, S., Adam, V., Arnold, E., Brieden, K., Voronov, A. and Witzke, H.D., (2005). UV-Lamps for disinfection and advanced oxidation–lamp types, technologies and applications. *IUVA news*, *8*(1), pp.32-37.

Scurtu T. C., (2009). Treatment of Produced Water: Targeting Dissolved Compounds to meet a zero Harmful Discharge in Oil and Gas Production. *Thesis for the degree of Doctor of Science and Technology, Department of Hydraulic and Environmental Engineering. Pp 27-30.*

Shawkat M. A, Carraher C. E., and Harvey P. D., (2010). Introduction to Photophysics and Photochemistry. *Macro molecules containing metals and metal-like elements* Vol. 10. Pp 3-5. John Wiley and Sons Inc.

Sheldon M. T., Mistrik R., and Croleya T. R., (2009). Determination of Ion Structures in Structurally Related Compounds Using Precursor Ion Fingerprinting. *J Am. Soc. Mass Spectrum* V. 20, Pp370–376.

Shimadzu, (2016). Introduction to LCMS. Accessed online from: http://www.shimadzu.com/an/hplc/support/lib/lctalk/47/47intro.html [Accessed on 8th January 2017).

Shrivastava A and Gupta V. B., (2011). Methods for the Determination of Limit of Detection and Limit of Quantitation of the Analytical Methods. *Chron Young Sci*; 2:21-5 Pp21.

Siegrist, R.L., Crimi, M. and Simpkin, T.J. eds., (2011). *In-situ Chemical Oxidation for Groundwater Remediation* (Vol. 3). Springer Science & Business Media.

Skoog D., West D. and Holler J., (1992). Fundamentals of Analytical Chemistry, Sixth Edition. Sander's College Publishing New York.

Spivey, J. J., Roberts, G.W., Davis, B. H., (2001). *Catalyst Deactivation 2001 (Studies in Surface Science and Catalysis*; *Elsevier: Amsterdam, the Netherlands.* Volume 139. Pp271-278.

Stasinakis, A. S., (2008). Use of Selected Advanced Oxidation Processes (AOPs) for Wastewater Treatment- A Mini Review. In: Global NEST journal 10, 376-385.

Stefan, M. I., ed., (2004). Advanced Oxidation Processes for Water and Wastewater Treatment, IWA, London.

Stein, S. E., (1994). Estimating Probabilities of Correct Identification from Results of Mass Spectral Library Searches. *J. Am. Soc. Mass Spectrom.* V. *5,* Pp 316–323.

Stephenson M. T., (1992). Components of Produced Water: A Compilation of Industry Studies. *Journal of Petroleum Technology* 44(5):548-603 ·

Strauss C. R. and Trainor R. W., (1995). Developments in Microwave-Assisted Organic Chemistry," *Australian Journal of Chemistry*, Vol. 48, No. 10, pp. 1665-1692.

Stroud J.L. Paton G. I., and Semple K.T., (2007). Microbe-aliphatic Hydrocarbon Interactions in Soil: Implications for Biodegradation and Bioremediation. *Journal of applied Microbiology*. 1364-5072.

Stuglik Z. and Zagorski Z., (1980). Pulse Radiolysis of Neutral iron (ii) Solutions: Oxidation of Ferrous Ions by OH Radicals. *Radiat. Phys. Chem.* Vol. 17, pp. 229-233.

Stumm, W., (1964). Chemistry of Natural Waters in Relation to Water Quality. In *Symposium on Environmental Measurements. US Public Health Service Publ* (p. 299).

Sule M. N., (2013). Understanding Salt and Contaminant Removal by a Pervaporative Treatment Process. *Thesis submitted for the degree of Doctor of Philosophy of Imperial College London.*

Sumi L., (2005). Oil and Gas Accountability Project. Presentation at the 2005 people's oil and Gas Summit Farmington, New Mexico.

Sun J. H., Wang G. L., Chai Y., Zhang G., Li, J. and Feng, J. L., (2009). Distribution of Polycyclic Aromatic Hydrocarbons (PAHs) in Henan Reach of the Yellow River, Middle China. *Ecotoxicology and Environmental Safety*, 72(5): 1614-1624.

Sun, Y. and Pignatello, J.J., (1993). Photochemical reactions involved in the total mineralization of 2, 4-D by iron (3+)/hydrogen peroxide/UV. *Environmental science & technology*, *27*(2), pp.304-310.

Szulbinski, W.S., (2000). Electroreduction of Dioxygen Catalyzed by Ferric Carboxymethylene-cyclam Complex. *Polish Journal of Chemistry*, *74*(8), pp.1163-1176.

Tamimi, M., Qourzal, S., Barka, N., Assabbane, A., & Ait-Ichou, Y., (2008). Methomyl Degradation in Aqueous Solutions by Fenton's Reagent and the Photo-Fenton System. *Separation and Purification Technology, 61*(1), 103-108.

Tarr M. A., (2003). In Chemical Degradation Methods for Wastes and Pollutants: Environmental and Industrial Applications, Marcel Dekker Inc, New York.

Tellez, G.T., Nirmalakhandan, N. and Gardea-Torresdey, J.L., (2002). Performance Evaluation of an Activated Sludge System for Removing Petroleum Hydrocarbons from Oilfield Produced Water. *Advances in Environmental Research*, *6*(4), pp.455-470.

Terrens, G.W. and R.D. Tait., (1996). Monitoring Ocean Concentrations of Aromatic Hydrocarbons from Produced Formation Water Discharges to Bass Strait, Australia. SPE

36033. Pages 739-747 In: Proceedings of the International Conference on Health, Safety & Environment. Society of Petroleum Engineers, Richardson, TX.

Thomas K. V., Langford K., Peterson K., Smith J., and Tollefsen K. E., (2009). Effect-Directed Identification of Naphthenic Acids As Important in- Vitro Xeno-Estrogens and Anti-Androgens in North Sea Offshore Produced Water Discharge. *Environ. Sci. Technol*. Vol 43. Pp 8066-8071.

Tiangyie, G., (2008). Synthesis, Chemical Characterization and Scale Up of a Heterogeneous Catalyst for the Oxidation of Organic Pollutants in Wastewater. *PhD thesis*. DE Montfort University, Leicester England.

Toet S., Van Logtestijn, Richard S., Kampf R., Schreijer M., Verhoeven j., (2005). The Effect of Hydraulic Retention Time on the Removal of Pollutants From Sewage Treatment Plant Effluent in a Surface-Flow Wetland System. *Society of Wetland Scientists.* Vol. 25 (2), pp 375–391.

Tong, L., Zheng, X.L., Li, M. and Hu, Z.F., (2008). Volatilization Behaviour of BTEX on Different Underlying Materials. *Huan jing ke xue= Huanjing kexue*, *29*(7), pp.2058-2062.

Torrades, F., Pérez, M., Mansilla, H.D., Peral, J., (2003). Experimental Design of Fenton and Photo-Fenton Reactions for the Treatment of Cellulose Bleaching Effluents. *Chemosphere*, Vol. 53, pp. 1211–1220.

Truong, K.N. and Blackburn J.W. (1984). The Stripping of Organic Chemicals in Biological Treatment Processes. *Environ. Prog*., Vol 3, No 3,143-152.

Turner, R.C. and Miles, K.E., (1957). The Ultraviolet Absorption Spectra of the Ferric Ion and its First Hydrolysis Product in Aqueous Solutions. *Canadian Journal of Chemistry*, *35*(9), pp.1002-1009.

UKPOHOR, T. O., (2001). Produced Water: Environmental Issues/ Technological Solution Of The Nigeria Depletion Era. *SPE Annual Technical Conference and Exhibition, 30 September-3 October 2001, New Orleans, Louisiana.*

UNESCO (2013). UN Water World Water day (2013). Available from: [http://www.unwater.org/water-cooperation-2013/water-cooperation/facts-and-figures/en/. [Accessed on 20th July 2016].

Upreti D. P., Chi T. G., Huddresman K. and Smail I., (2016). Field trial of an ion exchange based metal removal technology in the treatment of mine waters. Available online from: https://www.dora.dmu.ac.uk/xmlui/handle/2086/12271. Accessed 12/06/17

US Energy Information Administration (2016). Shale in the United States. Available from: https://www.eia.gov/energy_in_brief/article/shale_in_the_united_states.cfm. [Accessed on 17th January 2017].

USP Technologies (2016). Ultraviolet Absorption Spectrum. Available from: http://www.h2o2.com/technical-library/physical-chemical-properties/radiation-properties/default.aspx?pid=65 [Accessed on 7th October 2016.

Utvik, T.I.R., Hasle, J.R., (2002). Recent Knowledge about Produced Water Composition, and the Contribution from Different Chemicals to Risk of Harmful Environmental Effects. SPE Paper SPE 73999. *Presented at the 2002 HSE Conference in Kuala Lumpur, Malaysia, 20–22 March 2002.*

Veil J., (2015). New Information on Produced Water Volumes and Management Practices. *22nd International Petroleum Environmental Conference Denver, CO USA November 17-19.*

Veil J., Puder M., Elcock D., Redweik J., (2004). A White Paper Describing Produced Water From Production of Crude Oil, Natural Gas and Coal Bed Methane. *Argon national library Pp* 3.

Vitkovskaya R., Rumynskaya I., Romanova E., Tereshchenko L., (2003). Fibre Catalyst from Modified Polyacrylonitrile Fibres. *Fibre Chemistry*, Vol. 35, (3), Pp. 202–207.

Vyrides, I. and Stuckey, D.C., (2009). A Modified Method for the Determination of Chemical Oxygen Demand (COD) for Samples with High Salinity and Low Organics. *Bioresource technology*, *100*(2), pp.979-982.

Pinheiro, R. and Wagner, G., (2001). *Upgrading Water Treatment Plants*. CRC Press.

Wadley, S. and Waite, T.D., (2004). Fenton Processes in Water and Wastewater treatment. In Advanced Oxidation Processes in Water and Wastewater Treatment, S. Parsons (Eds), IWA Press.

Walling Cheves (1975). Fenton's reagent Revisited. *Acc. Chem. Res. 1975 8 (4)* Pp130.

Wang X., Goual L., Colberg P., (2012). Characterization and Treatment of Dissolve Organic Matter from Oil field Produced Waters. *Journal of Hazardous Materials. Elsevier* Pp 164.

Watts, R. J., Udell, M. D., and Monsen Robert, M. M., (1993). Use of Iron Minerals in Optimizing the Peroxide Treatment of Contaminated Soils. *Water Environ. Res*. 65, 839–844.

Watts, R. J., Foget, M.K., Kong, S. H., and Teel, A. L., (1999). Hydrogen Peroxide Decomposition in Model Subsurface Systems. *J. Hazardous Materials* 69, 229–243. Willet K. and Hites (2000). Chemical Actinometry: Using 0-Nitrobenzaldehyde to measure Light Intensity in photochemical Experiments. *Journal of chemical Education* V77 No 7.

Yang Bai-Juan, Jiang F., Xu X., Chen J., and Frank S. C., (2007). Determination of Alkylphenols in Water by Solid Phase Extraction, With On-column Derivitizaiton Coupled with Gas Chromatography-Mass Spectrometry. *Chinese Journal of Analytical chemistry*, Volume 35 (5) Pp633.

Yang M., (2011). Measurement of Oil in Produced Water in Produced Water: Environmental risks and Advances in mitigation Technologies. *Springer Science* xviii. P. 608.

Yang M., (2006). Produced water – Best Management Practices; Oil in Produced Water Analysis and Monitoring in the North Sea. *Society of petroleum Engineers*. Presentation at SPE annual Technical conference and exhibition held in San Antonio, Texas.

Yamano T., Schimizu M. and Noda T. (2004). Allergenicity Evaluation of Bioban CS-1135 in Experimental Animals: Contact Dermatitis. *PubMed* 50: 339.

Yatmaz H., (1993). Photocatalysis of Organic Effluents. *Thesis submitted for the degree of Doctor of Philosophy in the Faculty of Engineering of the University of Newcastle upon Tyne.*

Yatmaz H., Wallis C., Howarth C., (2000). The spinning disc reactor studies on a novel TiO2 photocatalytic reactor. *Chemosphere 42* 397- 403.

Yazici E. Y. and Deveci H., (2010). Factors Affecting the Decomposition of Hydrogen Peroxide. Proceedings of the Xiith International Mineral Processing Symposium Cappadocia-Nevsehir Turkey.

Yue P.L., (1985). Introduction to the Modelling and Design of Photoreactors, *Photoelectrochemistry. Photocatalysis and Photoreactors*, M. Schiavello, Ed.; Reidel Publishing.

Zazo J., Cassas J., Mohedano A., Gilarranz M., and Rodriaguez J., (2005). Chemical Pathway and Kinetics of Phenol Oxidation by Fenton's Reagent. *Environ. Sci. Technol*. Vol. 39, Pp. 9295-9302.

Zhang H., Choi H.J., Huang C.P., (2005). Optimization of Fenton process for the treatment of landfill leachate, *Journal of Hazardous Materials*, 125(1-3), 166-174.